Détermination des paléo-taux d'érosion par l'utilisation des isotopes cosmogéniques. Cas de la transition pliocène-pleistocène

Nicolas Puchol

THÈSE

présentée à

L'UNIVERSITÉ DE LORRAINE

(École doctorale RP2E)

pour l'obtention du grade de

Docteur, spécialité Géosciences

par

Nicolas PUCHOL

Détermination des paléo-taux d'érosion par l'utilisation des isotopes cosmogéniques. Cas de la transition Pliocène-Pleistocène.

Directeur : *Raphaël PIK*
Co-directeur : *Pierre-Henri BLARD*
Co-encadrant : *Julien CHARREAU*

Soutenue le 6 décembre 2013
Devant la commission d'examen formée de :

M. *Peter MOLNAR* (Professeur, University of Colorado, Boulder, USA), **Rapporteur**

M. *Peter VAN DER BEEK* (Professeur, Université Joseph Fourrier, Grenoble), **Rapporteur**

M. *Didier BOURLÈS* (Professeur, Université Aix-Marseille), **Examinateur**

M. *Vincent GODARD* (Maître de Conférences, Université Aix-Marseille), **Examinateur**

M. *Jérôme LAVÉ* (Directeur de recherches, CRPG, Nancy), **Invité**

Résumé

Les processus complexes et intriqués liant érosion, climat et tectonique à la surface de la Terre sont encore sujets à de riches controverses. Leur meilleur compréhension nécessite notamment le développement de méthodes permettant la quantification fiable de taux d'érosion à des échelles temporelles et spatiales variées. En particulier, les derniers ~10 Ma ont vu la Terre affectée par des changements climatiques majeurs, que certains auteurs ont associés à une apparente accélération mondiale des taux d'érosion. La réalité de cette accélération fait cependant l'objet d'un intense débat. L'analyse dans des dépôts anciens des isotopes cosmogéniques in-situ, déjà largement employés dans les sédiments de rivières actuelles, a le potentiel de fournir des enregistrements haute résolution, sur ces échelles de temps, de taux de dénudations intégrés sur des bassins versant entiers.

Nous avons tout d'abord testé des points techniques spécifiques des isotopes cosmogéniques dans deux zones cibles: l'Himalaya central et les Plateaux Ethiopiens. Ces deux études confirment que l'emploi des isotopes cosmogéniques dans ces zones, sous réserve de respecter plusieurs points de prudence, reste valide et extensible à des sédiments anciens.

Nous avons ensuite étendu avec succès cette méthode à des sédiments des piedmonts du Tian-Shan (Chine) et de l'Himalaya (collines Siwaliks, Népal). Ces deux zones sont au coeur de débats sur l'évolution des relations climat/érosion/tectonique depuis ~10 Ma.
Quatre sections au Tian-Shan, couvrant ~9 Ma, et une large étendue spatiale autour de cette chaîne, ne montrent pas de brusque accélération de l'érosion il y a ~3-5 Ma. Au contraire, nous observons à l'échelle régionale une augmentation progressive (× 4 entre 9 et 4 Ma) puis une stabilisation entre 4 Ma et l'actuel. Ces résultats suggèrent une influence limitée des cycles glaciaires quaternaires sur les taux d'érosion dans cette zone.
Un enregistrement dans les sédiments himalayens ne montre également pas d'augmentation significative de l'érosion depuis ~6.5 Ma. Il est en revanche probablement le témoin de réorganisation des systèmes de drainages et d'évolutions tectoniques dans cette région.

Avec ces études, nous avons ainsi pu produire pour la première fois des enregistrements haute résolution de taux d'érosion depuis ~10 Ma, grâce aux isotopes cosmogéniques. Cette méthode étant potentiellement applicable dans de nombreux contextes géologiques et climatiques, elle permettra indubitablement des avancées importantes dans la compréhension des processus de surface actuels et passés.

Abstract

The complex and intricate processes linking erosion, climate and tectonics still are the matter of extensive controversies. A better comprehension of these processes notably require reliable estimates of erosion rates evolution upon various spatial and temporal scales. In particular, throughout the last ~10 Myr, the Earth's surface has undergone major climatic changes, which some authors have associated to a dramatic increase in global erosion rates. Nevertheless, the reality of this increase has since been severely questioned. In-situ cosmogenic nuclides analysis in ancient sediment could potentially provide high-resolution records of denudation rates, integrated over whole drainage basins, and on several million-year time scales.

We first tested specific technical issues of cosmogenic isotopes in two target areas: Central Himalaya and Ethiopian Plateaus. These two studies have confirmed that the use of cosmogenic nuclides, if carried out properly, are valid and extensible to ancient sediments.

We then successfully extended this method to sediments from the Tianshan (China), and the Himalayas (Nepal) piedmonts. These two areas are at the core of ongoing debates on climate-erosion-tectonics relationships since ~10 Ma.
Four sections in the Tianshan, covering ~9 Myr and a broad spatial extent around this range, do not display a brutal increase in denudation at 3-5 Ma. On the other hand, they show at the regional scale a progressive increase (×4 between 4-9 Ma) and a subsequent stabilization since ~4 Ma. These results suggest a limited influence of Quaternary glaciations on erosion in this region.
One section in the Himalayan piedmont (Siwaliks hills), neither display any significant increase since ~6.5 Ma that would be link to a major climatic shift. It has nevertheless probably recorded reorganizations of the drainage system and tectonics evolutions in this region.

With these studies, we were able to produce the first cosmogenic nuclides-based high resolution records of denudation rates over 10 Myr. This method being potentially applicable in many geological and climatic settings, it will indubitably allow further advances in our understanding of past and present surface processes.

Organisation de ce manuscrit

Ce manuscrit comporte deux chapitres introductifs, trois chapitres présentant les principaux résultats de cette thèse, comportant chacun un court paragraphe introductif, une conclusion générale, et trois annexes.
Les chapitres introductifs généraux, les paragraphes introductifs et la conclusion partagent une arborescence et des références bibliographiques communes, répertoriées en fin de manuscrit principal. Les trois chapitres centraux, écrits en anglais, sont organisés sous forme d'articles scientifiques, soumis à des revues internationales, en voie de soumission, ou en cours de préparation. Ces articles peuvent être abordés indépendamment du reste du manuscrit, et ont leurs référence bibliographiques et leurs arborescences propres.

Note to the Anglophone readers :

Organization of this manuscript

This manuscript includes two introductory chapters, three chapters compiling the main results of this PhD, a general conclusion, and trois annexes.

The general methodology is treated in French in the second chapter, but is also largely addressed in English in the supplementary information provided within Chapter 4
The three central chapters are written in English language, under the form of scientific papers, submitted or to be submitted to international journals. These papers can be addressed independently of the rest of the manuscript, and each has got its own bibliography and contents table. Since the short forewords of these papers are also in French, I will summarize them here :

Chapter 3 is constituted of two technical studies. These studies were originally designed at the beginning of my works to address several potential complications of cosmogenic nuclides measurement in two areas we targeted then. In central Nepal, we were concerned about the potential influence of dominant landslides processes on the cosmogenic ^{10}Be signal. In Ethiopia, we wanted to investigate the influence of the magmatic ^{3}He over the cosmogenic ^{3}He signal.

Chapter 4 and 5 are "the real deal" of this manuscript. They present paleo-denudation rates records from two important areas regarding ongoing debates on climate-tectonics-erosion interactions : the Tianshan range and the Himalayas. The Tianshan (chapter 4) is the first area where we were able to successfully derive paleo-denudation rates from cosmogenic nuclides. Our survey there is more fully developed. In the Himalayas (chapter 5), we successfully analyzed only one sedimentary section yet.

Remerciements

Voici donc la section qui sera sans doute la plus lue de ce manuscrit... Malheureusement, je ne peux garantir avoir pensé à toutes celles et ceux qui auraient mérité y avoir leur place, et je m'en excuse d'avance.
Merci donc à toutes celles et ceux qui m'auront aidé d'une manière ou d'une autre à aller au bout de ces quatre ans et de ce manuscrit. Et en particulier...
Le CRPG, Julien, Raph, Jérôme, Maarten, Christian, Pete, Bouch', Zim', Manu, Le bureau 304 (Camille, Evelyn). Le STEVAL (Bob, Jean-Marie, Fred). Le CEREGE, Fred, Laetitia, Didier, Régis, Georges, Karim
Sur le(s) terrain(s) : Ananta, Shengli, Dimitri, Guillaume, Flo.
Dans la vraie vie : Pauline, Nico, l'OSUL, les Wise Dudes, mes amis, ma famille.

P.-H., qui m'a encadré avec tant de passion qu'il aura presque réussi à me la transmettre.

Table des matières

(in blue color: Sections in English)

L'histoire de la Terre se compose, d'une part, de données fournies par l'expérience, et, de l'autre, de raisonnements fondés sur ces données. L'essentiel pour la science ne consiste pas à déterminer ce que la Terre a été il y a un million d'années (et en fait d'années on peut se donner libre carrière), mais à déterminer ce qu'elle est telle qu'elle est devant nous : il consiste, en d'autres termes, à déterminer la connexion systématique de ces diverses formations. C'est, sans doute, une science où l'expérience a une large part, et tout ne saurait être ramené à la notion dans ce cadavre, car l'accident y joue son rôle.

G. W. F. Hegel,

Encyclopédie des Sciences Philosophiques (II, Philosophie de la Nature), 1830

Chapitre 1
Introduction

1.1 Mais en fait, ta thèse, à quoi sert-elle ?

Comme ce titre, pas si provocateur que ça, l'indique, on ne trouvera pas dans cette section §1.1 une revue détaillée et exhaustive des étroites relations reliant les enveloppes fluides de la Terre, la construction des reliefs, et les mouvements tectoniques. En revanche, puisque ce titre est la question que j'aurai peut-être le plus entendue ces quatre dernières années, je me suis attaché à traiter le début de cette introduction de la manière la plus didactique possible, afin de tenter d'éclairer celles et ceux, y compris non spécialistes voire non scientifiques, qui se la seront un jour posée. J'en fais partie.

1.1.1 Altération/érosion/dénudation

Le relief des continents est contrôlé par un équilibre entre construction, par les grands mouvements tectoniques nés de la machinerie interne terrestre, et destruction, par les agents de sa machinerie externe. Si ce qu'on appelle l'*érosion* peut, au premier abord, paraître bien se concevoir, cette notion est en fait un peu plus subtile. Il me semble donc important de préciser ce qu'il faudra entendre ici derrière ces trois concepts d'altération, érosion et dénudation.

1.1.1.1 L'altération

La première étape de la destruction des reliefs peut en fait être plus formellement appelée *altération*. Il s'agit de l'ensemble des processus qui transforment ou détruisent la structure d'une roche et ses constituants, quand celle-ci approche suffisamment de la surface. On peut distinguer deux grande famille de processus d'altération, même si ceux-ci sont très intimement liés (FIG. 1.1) (e.g. Gabet, 2007; Gabet & Mudd, 2009; Dixon *et al.*, 2009) :

D'une part, l'altération chimique. Il s'agit de la transformation de minéraux, instables dans les conditions de température, d'humidité, de taux d'oxygène ou d'acidité de la surface, en d'autre minéraux, et de la dissolution d'éléments les constituant.

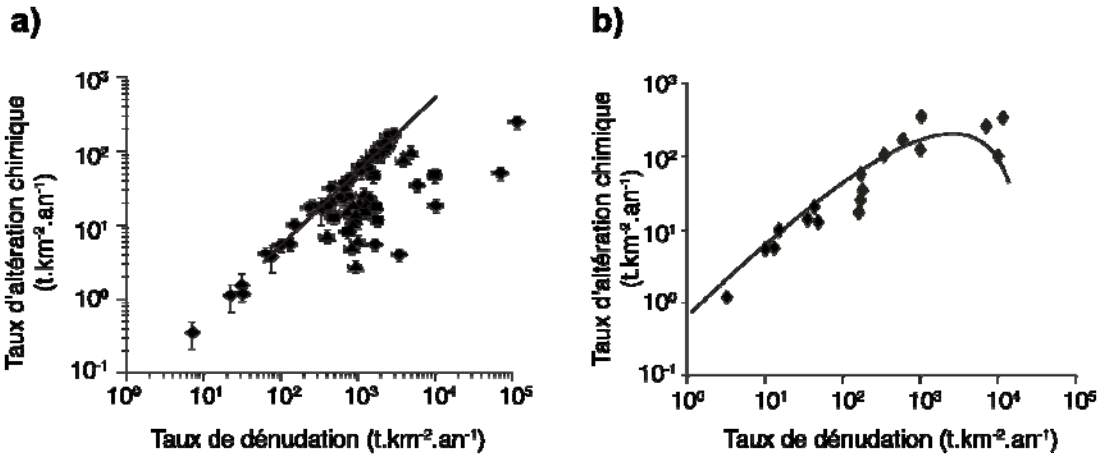

FIG. 1.1 - *Couplage entre altération chimique et dénudation totale, modèles (courbes noires) et comparaison avec des données empiriques. a) Dixon et al, 2009; b) Gabet & Mudd, 2009.*

D'autre part, l'altération physique. Par exemple, les cycles de température jour/nuit et hiver/été, ou encore la création de minéraux secondaires issus de l'altération chimique, peuvent agrandir progressivement, par dilatation et rétractation, les défauts dans les jointures entre grains. Les cycles de gel/dégel de l'eau d'infiltration, les animaux fouisseurs et les racines des plantes peuvent également fracturer physiquement les roches.

1.1.1.2 L'érosion

L'érosion en elle même consiste en la mobilisation des produits de l'altération, et leur transport vers une altitude plus basse. Le principal agent de l'érosion à la surface de la Terre est l'eau liquide. La capacité d'érosion d'un ruissellement, d'un ruisseau, une rivière, un fleuve... est un équilibre entre la puissance de son flux, due à la pente du relief et à la quantité d'eau, et la quantité de matière à transporter. L'eau solide, sous forme de glaciers, est également un puissant agent d'érosion. Dans les régions les plus arides ou pour les particules les plus fines, le vent peut aussi en être un agent non négligeable. Enfin, pour les reliefs les plus pentus, les roches peuvent subir une érosion par mouvements de masses, comme les glissements de terrains et les éboulis.

1.1.1.3 La dénudation

La dénudation est la quantité totale de matière qui est enlevée de la surface de la crôute terrestre. Il s'agit donc de la somme de la matière retirée par l'érosion et des éléments dissous ou

évaporés lors de l'altération chimique. C'est cette notion que j'utiliserai préférentiellement dans ce manuscrit, car ce sont les taux de dénudation qui sont enregistrés par les isotopes cosmogéniques, qui furent l'outil de base de mon travail, et que j'introduis plus bas (§1.3).

Il existe des liens particulièrement intriqués entre la dénudation des reliefs, la géodynamique (c'est à dire les mouvements des roches entre elles, comme par exemple la convergence entre plaques tectoniques, ou la relaxation des reliefs sous leur propre poids), et le climat (FIG. 1.2). Je vais rapidement détailler ces influences mutuelles dans les paragraphes suivants. On trouvera plus de références bibliographiques par exemple dans Champagnac *et al.*, 2012.

1.1.2 Les relations climat /géodynamique /dénudation

1.1.2.1 Influences du climat sur l'érosion

Instinctivement, le premier lien qui vient à l'esprit est l'influence du climat sur la dénudation. Des températures plus élevées peuvent favoriser les taux d'altération chimique des minéraux (Dixon *et al.*, 2009), tandis que des températures plus basses peuvent favoriser l'apparition de glaciers. Ces derniers sont de puissants agents érosifs, et favorisent la formation de profondes et étroites vallées (Valla *et al.*, 2010; Sternai *et al.*, 2012; Pedersen & Egholm, 2013). Pour les plus hauts reliefs, ils peuvent ainsi limiter l'altitude des montagnes en agissant comme une "scie sauteuse" sur ces sommet englacés (Egholm *et al.*, 2009) (FIG. 1.3).

Cependant, sur la totalité de leur bassin versant et sur le long terme, ils ne sont probablement pas des agents plus puissants que les rivières (Koppes & Montgomery, 2009) (FIG. 1.3). Dans certains cas où leur glace flue particulièrement lentement (basses températures), ils peuvent même agir comme une protection pour les roches sous-jacentes (Thomson *et al.*, 2010).

Les précipitations (tant leur quantité que leur distribution annuelle, continues ou très épisodiques) peuvent avoir dans certaines régions un contrôle important sur l'érosion (e.g. Thiede *et al.*, 2004), en fournissant aux rivières l'énergie nécessaire au transport des sédiments. Cependant, de manière contre-intuitive, elles n'ont, à l'échelle globale, qu'un rôle secondaire (e.g. Riebe *et al.*, 2001b; Burbank *et al.*, 2003; Finnegan *et al.*, 2008; Binnie *et al.*, 2010; Henck *et al.*, 2011; Portenga & Bierman, 2011) ou plutôt non déconnectable des autres forçages (FIG. 1.4) (Molnar, 2009; Champagnac *et al.*, 2012).

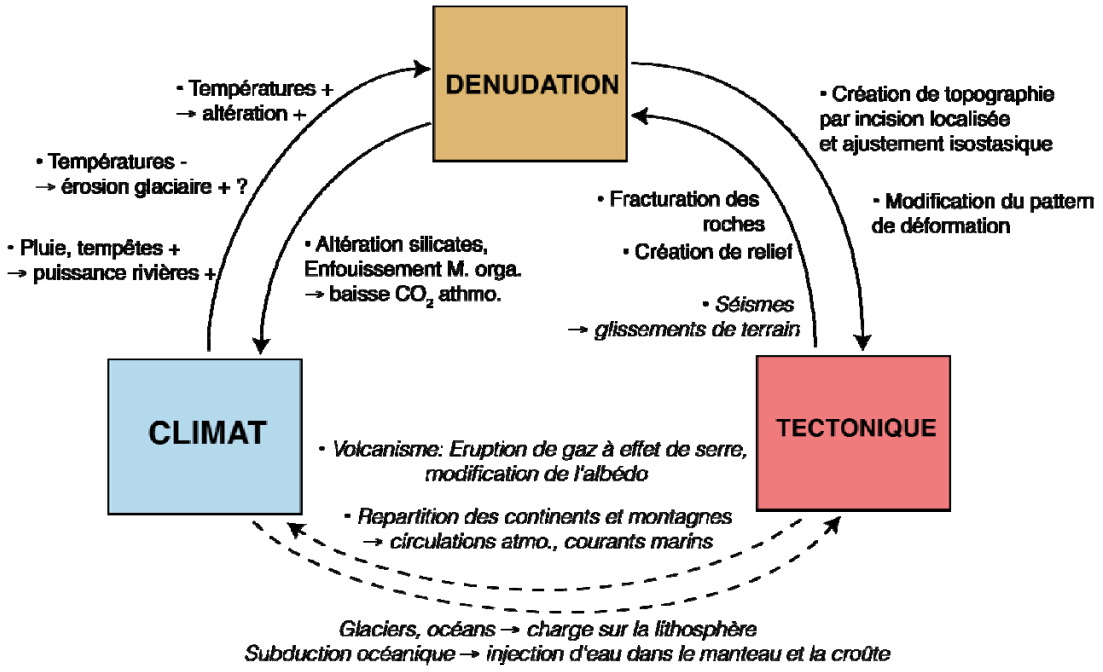

FIG. 1.2 - ***Schéma des influences entre dénudation, climat et tectonique.***
Les influences en italique ne seront pas traitées, car changeant sur des échelles de temps inappropriées à nos travaux, ou étant secondaires.

1.1.2.2 Influence de la dénudation sur le climat

De manière plus surprenante, la dénudation exerce en retour un contrôle important sur le climat global de la Terre, car elle joue le rôle d'une pompe à CO2 atmosphérique à l'échelle des temps géologiques.

D'une part, l'altération des silicates, suivie de la précipitation de carbonates dans l'océan, a pour bilan net la consommation de CO_2 atmosphérique (Ebelmen, 1845; Berner *et al.*, 1983).

D'autre part, les flux de sédiments détritiques comprennent une part de matière organique, qui se retrouve enfouie avec eux, et ainsi à l'abri de l'oxydation dans les sédiments océaniques (France-Lanord & Derry, 1997; Galy *et al.*, 2007).

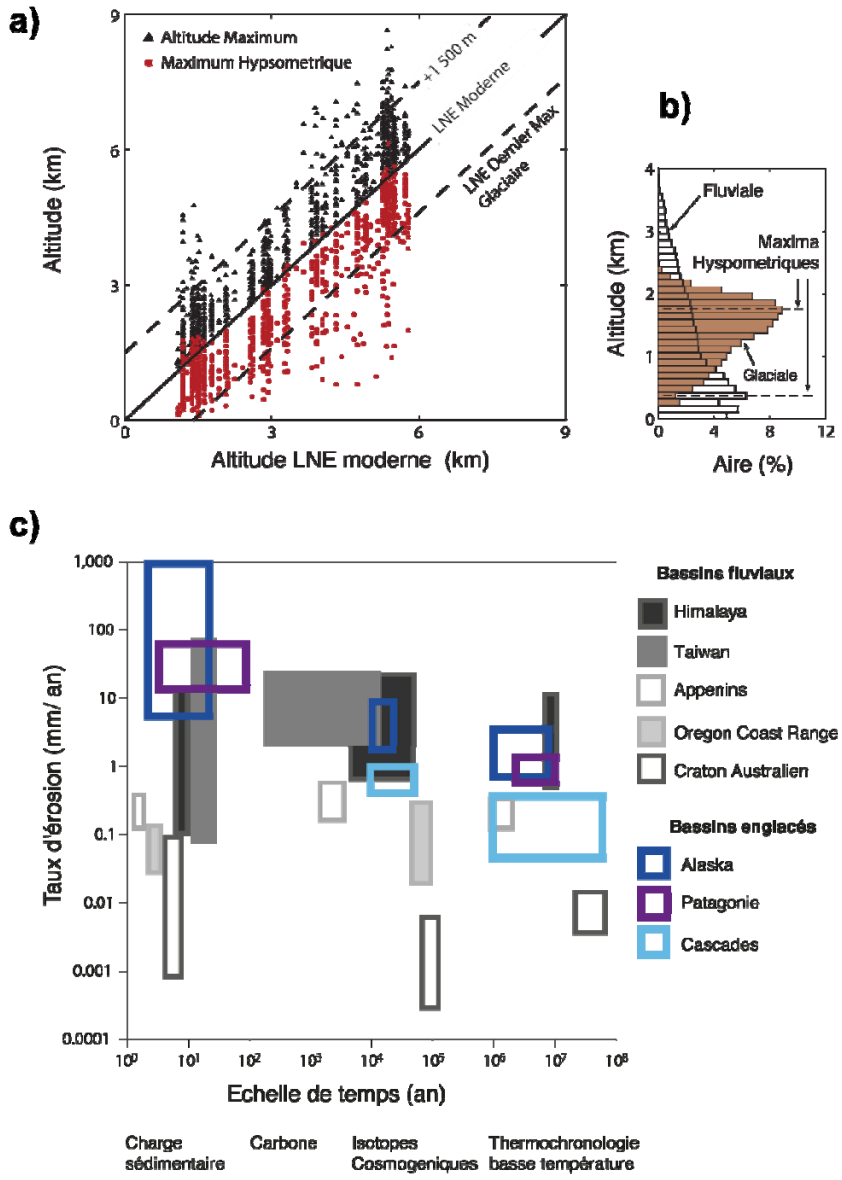

FIG. 1.3 - *L'érosion glaciaire: agent majeur ou influence limitée?* *a) Corrélation entre ligne de neiges éternelles (LNE) et altitudes des reliefs mondiaux, montrant l'effet des glaciers comme "rabots" limitant l'élévation des montagnes (Hegholm et al. 2009); b) Hypsométries caractéristiques d'un bassin englacé et fluvial (Hegholm et al. 2009); c) Comparaison de taux de dénudations sur plusieurs échelles de temps et plusieurs chaînes du monde. L'érosion glaciaire, si elle est capable de contrôler la topographie et l'hypsométrie d'un bassin, ne semble en revanche pas plus efficace que l'érosion fluviale, en moyenne, sur de longues échelles de temps et spatiales (Koppes et Montgomery, 2009).*

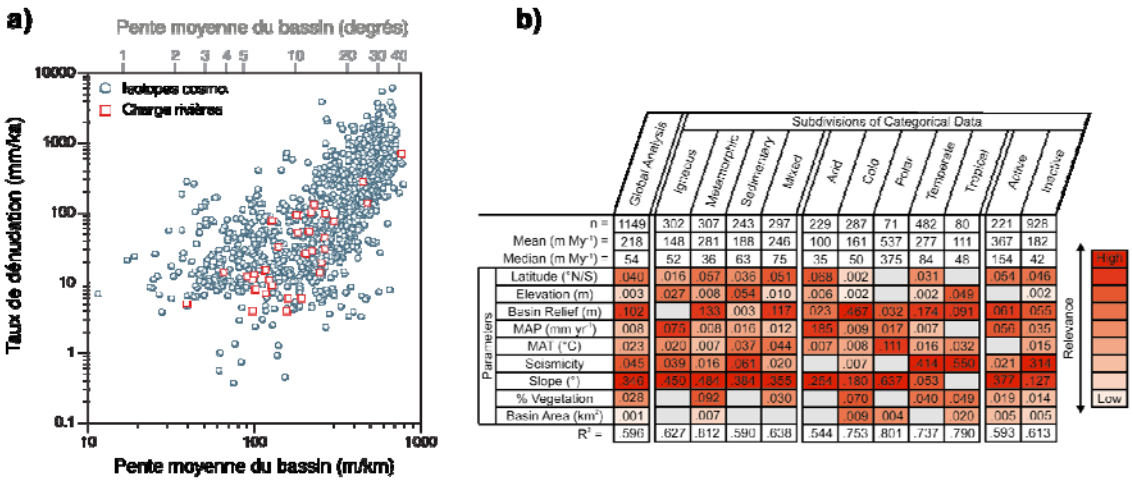

FIG. 1.4 - *Relations entre taux de dénudation, pente moyenne du bassin, et autres facteurs climatiques et morphologiques. a) Compilation de taux de dénudation par isotopes cosmogéniques et charges sédimentaires (d'après Willenbring et al. 2013). b) Coefficients de covariance entre dénudation (isotopes cosmogéniques, jeu de donnés similaire à Willenbring et al. 2013) et différents facteurs, classés par lithologie dominante du bassin et contexte climatique. MAP : précipitations moyennes annuelles, MAT : Température moyenne annuelle (tiré de Portenga & Bierman, 2011).*

1.1.2.3 Influence de la tectonique sur la dénudation

La tectonique a un double effet sur la dénudation. Premièrement, ce sont les mouvements tectoniques qui créent des montagnes à dénuder. Ce truisme n'est en fait pas qu'une lapalissade. En effet, à l'échelle globale, on observe que les taux de dénudation sont, en premier lieu, grossièrement corrélés aux pentes moyennes des bassins versant (von Blanckenburg, 2005; Portenga & Bierman, 2011; Willenbring *et al.*, 2013). Deuxièmement, la tectonique peut fracturer des unités rocheuses par des réseaux de failles, ce qui améliore leur érodabilité.

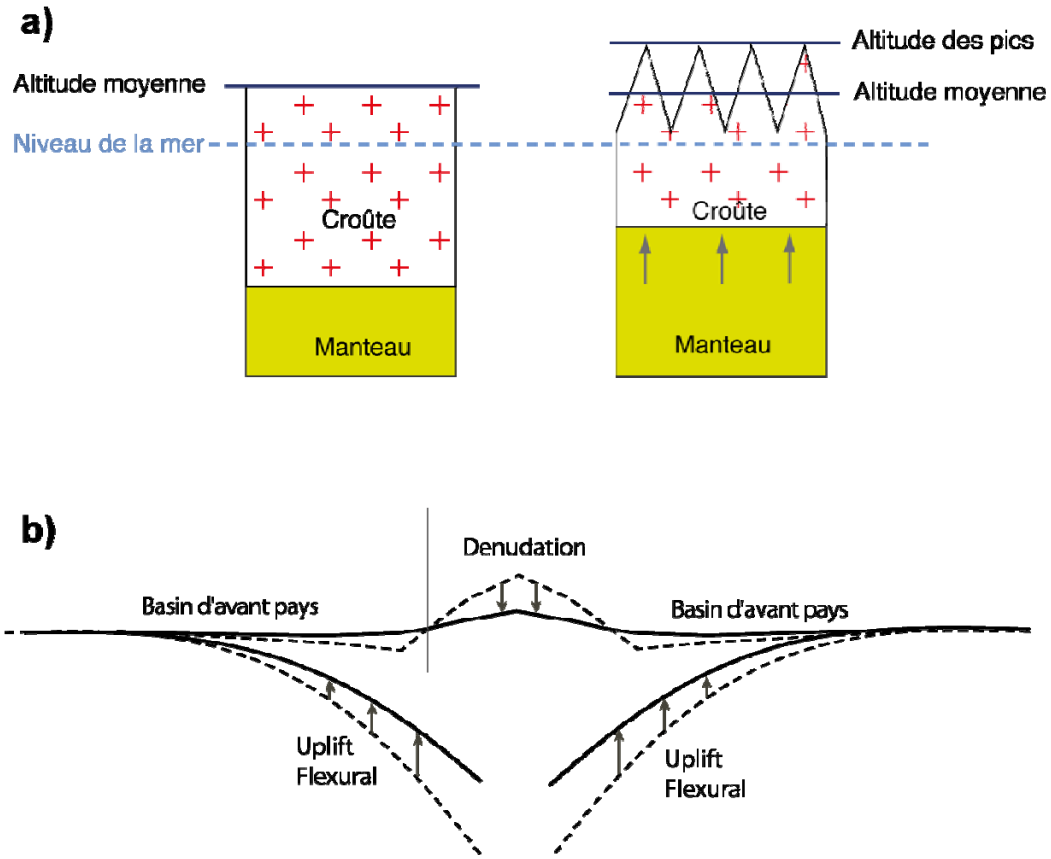

FIG. 1.5 - *Effet de la dénudation sur la topographie par isostasie. a) Création de relief (différence entre sommet et vallées) par incision localisée. b) Soulèvement des bassins d'avant-pays par diminution de la charge de l'orogène (Figures d'après Willet 2010).*

1.1.2.4 Influence de la dénudation sur la tectonique

Encore une fois, de manière contre-intuitive, la dénudation joue en retour un rôle important sur la tectonique. C'est une des découvertes majeures en sciences de la Terre de ces vingt dernières années.

La croûte continentale est plus légère que le manteau terrestre sous-jacent. Aussi, tel un glaçon dans un verre d'eau, la dénudation de la surface de cette croûte va provoquer une remontée de celle-ci pour revenir à son point d'équilibre, ce que l'on appelle l'isostasie. Si l'on dénude préférentiellement les reliefs au niveau des vallées, les pics et crêtes avoisinant peuvent ainsi en moyenne, paradoxalement, gagner en altitude (FIG. 1.5) (Molnar & England, 1990; Champagnac *et al.*, 2007).

De manière encore plus surprenante, la dénudation, surtout si elle est particulièrement focalisée sur une partie de la chaîne de montagnes, comme c'est le cas dans les Andes ou en Himalaya, peut même activement redistribuer les champs de déformation et de contraintes physiques dans la croûte (Willett, 1999; Whipple & Meade, 2006; Berger *et al.*, 2008; Whipple, 2009).

1.1.2.5 Autres relations

Il est à noter que d'autres relations directes existent entre la tectonique et le climat, mais que nous ne traiterons pas en détail. Notamment, la tectonique, par l'élévation des reliefs ou la position des continents, crée des barrières pour les masses d'air ou les courants océaniques qui peuvent réorganiser le climat global.

1.1.3 Les Grandes évolutions climatiques de la fin du Cénozoïque

Reconstituer les évolutions climatiques globales en terme de températures, précipitations, ou saisonnalité s'avère particulièrement complexe et n'est pas le sujet de cette thèse. Par simplification, nous allons considérer principalement ici les évolutions de la température de surface. En effet la paléo-température est certainement la variable climatique la mieux contrainte sur ces longues échelles de temps. La température moyenne à moyen terme de la surface du globe est au premier ordre corrélée à la température du fond des océans. Celle-ci, dans le passé, peut être reconstituée par l'étude des isotopes de l'oxygène dans les fossiles de coquilles de foraminifères benthiques, des micro-organismes vivant au fond des océans et construisant une coquille (le *test)* carbonatée. En compilant ces enregistrements à partir de différentes carottes forées dans les sédiments océaniques, il est ainsi possible de reconstituer l'évolution de la température moyenne du globe (FIG. 1.5).

Le Cénozoïque, également appelé ère Tertiaire, est l'ère géologique courant de ~65 Ma jusqu'à aujourd'hui. Les relations complexes entre le climat, la tectonique et la dénudation ont été déterminantes dans l'évolution de la surface de la Terre sur cette période. En particulier, la concomitance de deux évènements majeurs ont tôt attiré l'attention des chercheurs : en effet, alors que la fermeture de l'ancien Océan Téthys a été suivie par l'orogenèse alpine et himalayenne, puis la surrection du plateau du Tibet depuis ~45 Ma, il s'est produit en parallèle un refroidissement quasi continu depuis le début de l'Eocène (~55 Ma).

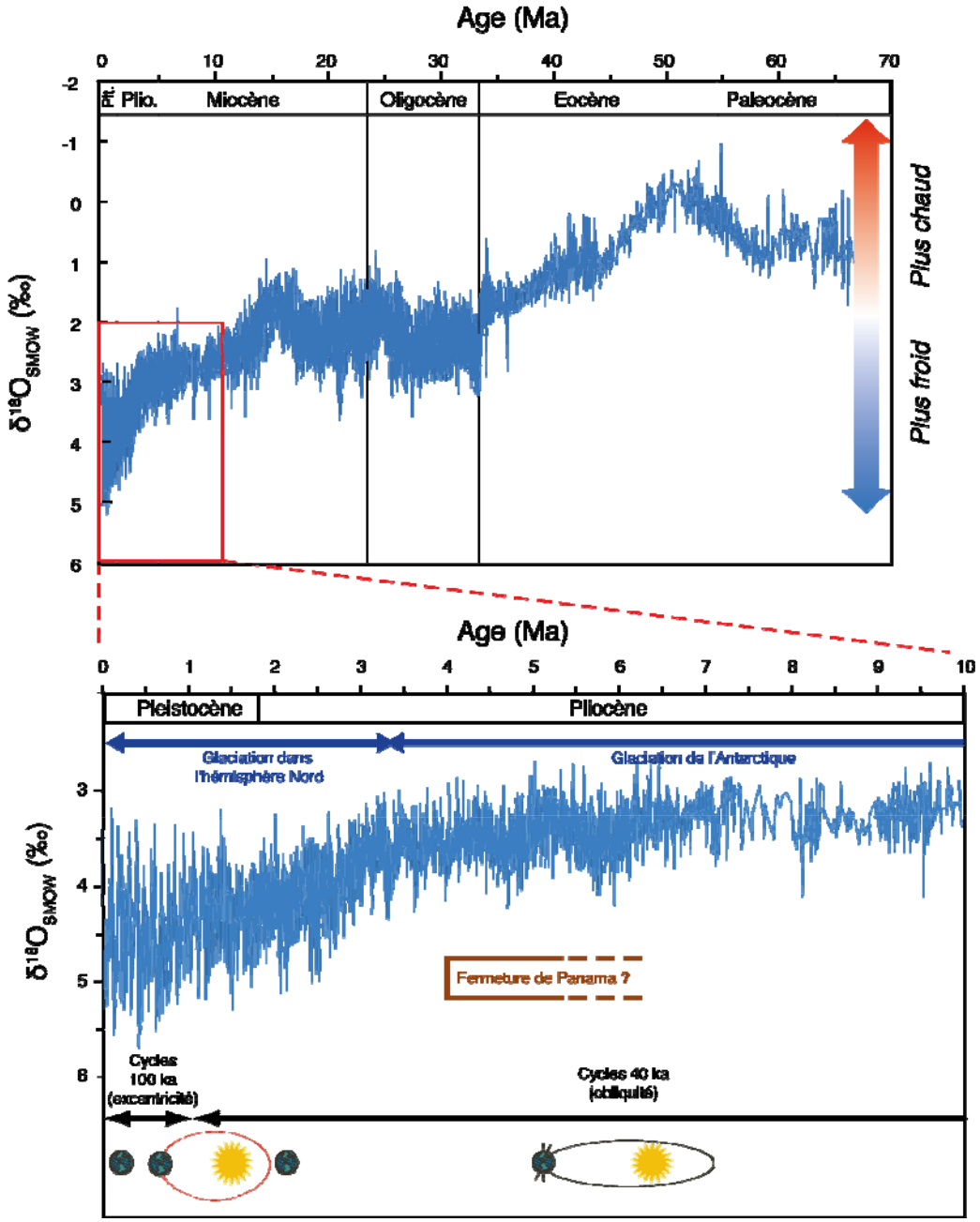

FIG. 1.6 - *Compilation global du $\delta^{18}O$ dans les foraminifères benthiques, comme proxy de la température des océans* (Zachos 2001). *Haut : depuis 70 Ma; Bas : zoom sur les 10 derniers Ma. On remarque une intensification du refroidissement vers ~3Ma, synchrone du développement des glaciations dans l'hémisphère Nord. La fermeture du passage de Panama et la mise en place de la circulation thermohaline a été proposée comme précurseur de ce refroidissement. Par ailleurs, il y a 0.9 Ma, les cycles climatiques deviennent dominés par la période de 100 ka associée à l'excentricité de l'orbite terrestre.*

Cette concomitance a ainsi conduit plusieurs chercheurs à proposer que le refroidissement cénozoïque a été engendré par la surrection himalayenne, notamment par la consommation de CO_2 atmosphérique qu'elle a induit (§1.1.2.2) (Raymo & Ruddiman, 1992; Galy *et al.*, 2007). Le refroidissement ainsi induit aurait, par l'apparition de glaciers, encore augmenté la dénudation des montagnes et la topographie (Molnar & England, 1990).

Ici, nous allons nous focaliser sur les dix derniers millions d'années. Il s'agit probablement de la période la plus froide de l'histoire de la Terre depuis ~250 Ma (Royer *et al.*, 2007). Cette période est marquée par deux évolutions majeures du climat (e.g. Zachos *et al.*, 2001, et références incluses).

Tout d'abord, elle voit une diminution progressive des températures moyennes à partir de 6 Ma (FIG 1.6) : Pendant cette période, les calottes glaciaires finissent de se développer sur tout le continent Antarctique et deviennent permanentes. Vers 4 Ma, le passage de Panama finit de se refermer, isolant l'Atlantique du Pacifique et modifiant de manière probablement importante le système de circulation océanique mondial, qui a un rôle majeur dans la redistribution de la chaleur tropicale. Cette théorie est cependant débattue (Molnar, 2008). La chute des température s'accélère à partir de 3.2 Ma. Cette époque concorde avec l'augmentation significative de la taille des calottes polaires de l'hémisphère nord (groenlandaise, laurentide, sibérienne) (FIG. 1.6, bas).

Ensuite, une évolution majeure s'est produite dans la cyclicité du climat. Jusqu'à ~0.9 Ma, le climat répondait en phase avec les cycles d'obliquité de l'axe Terre (période de 40 ka) et dans une moindre mesure de précession des équinoxes (période de 22 ka). Depuis 0.9 Ma en revanche, ce sont les cycles d'excentricité de l'orbite terrestre autour du soleil qui dominent largement le climat, avec une grande amplitude entre périodes glaciaires et interglaciaires. D'après les données de paléo-température issues des forages dans les calottes antarctiques, ces amplitudes sont d'environ 10 °C entre les maxima glaciaires et les interglaciaires des cycles de 100 ka (FIG. 1.6, bas). L'amplitude énergétique induite par les cycles d'excentricité de période 100 ka étant insuffisante pour causer un tel écart de température, des mécanismes internes d'amplification (albédo des calottes et cycle court terme du carbone) doivent jouer un rôle majeur dans le contrôle de ces cycles quaternaires de 100 ka.

Le climat global sur de longues échelles de temps et la tectonique sont intimement liés par la dénudation (somme de l'érosion physique et de l'altération chimique), selon des mécanismes complexes et très débattus. Or, la Terre a, au cours de son histoire, et en particulier sur les derniers millions d'années, enduré des évolutions climatiques et tectoniques majeures. Il est donc essentiel pour comprendre ces mécanisme de pouvoir reconstituer de manière fiable et précise l'évolution des taux de dénudations globaux sur ces échelles de temps.

1.2 Quelle évolution de la dénudation globale durant le Cénozoïque?

Dans cette section, je rentrerai plus franchement dans le vif du sujet, mais j'invite les éventuels courageux lecteurs non spécialistes à ne pas se laisser impressionner par le jargon.

1.2.1 Evolution des flux sédimentaires mondiaux et variabilité climatique.

En l'absence d'autres méthodes permettant de déterminer les taux de dénudation du passé, ce sont pendant longtemps les taux d'accumulation sédimentaires qui ont été utilisés comme leur meilleur enregistrement.

La datation de carottes marines a révélé dans les années 1980 une augmentation très importante et globale des taux d'accumulation sédimentaires dans l'océan profond depuis ~40 Ma (FIG. 1.7 a) (Hay *et al.*, 1988). Toutefois, cette augmentation apparente résulte essentiellement de deux phénomènes : Tout d'abord, la subduction de la croûte océanique fait qu'une partie des sédiments anciens, grandissant linéairement avec l'âge, a disparu (Parsons, 1982). Ensuite et surtout, les baisses du niveau des océans associées aux cycles glaciaires de la fin du Cénozoïque ont provoqué la reprise des sédiments déposés sur les marges continentales (Hay *et al.*, 1988).

Cependant, à l'échelle globale, de nombreux bassins continentaux ou cônes sédimentaires déposés sur les marges continentales enregistrent également des augmentations spectaculaires sur les 2-5 derniers millions d'années. Ces taux d'accumulation ont été compilés par Zhang *et al.*, (2001) et Molnar (2004) (FIG. 1.7). Ces auteurs remarquèrent que cette hausse spectaculaire n'était associée à aucune accélération mondiale connue de la tectonique des plaques. Ainsi, le seul candidat recevable pour expliquer une hausse mondiale de l'érosion qui *aurait* mené à cette hausse des taux d'accumulation sédimentaire serait un changement climatique.

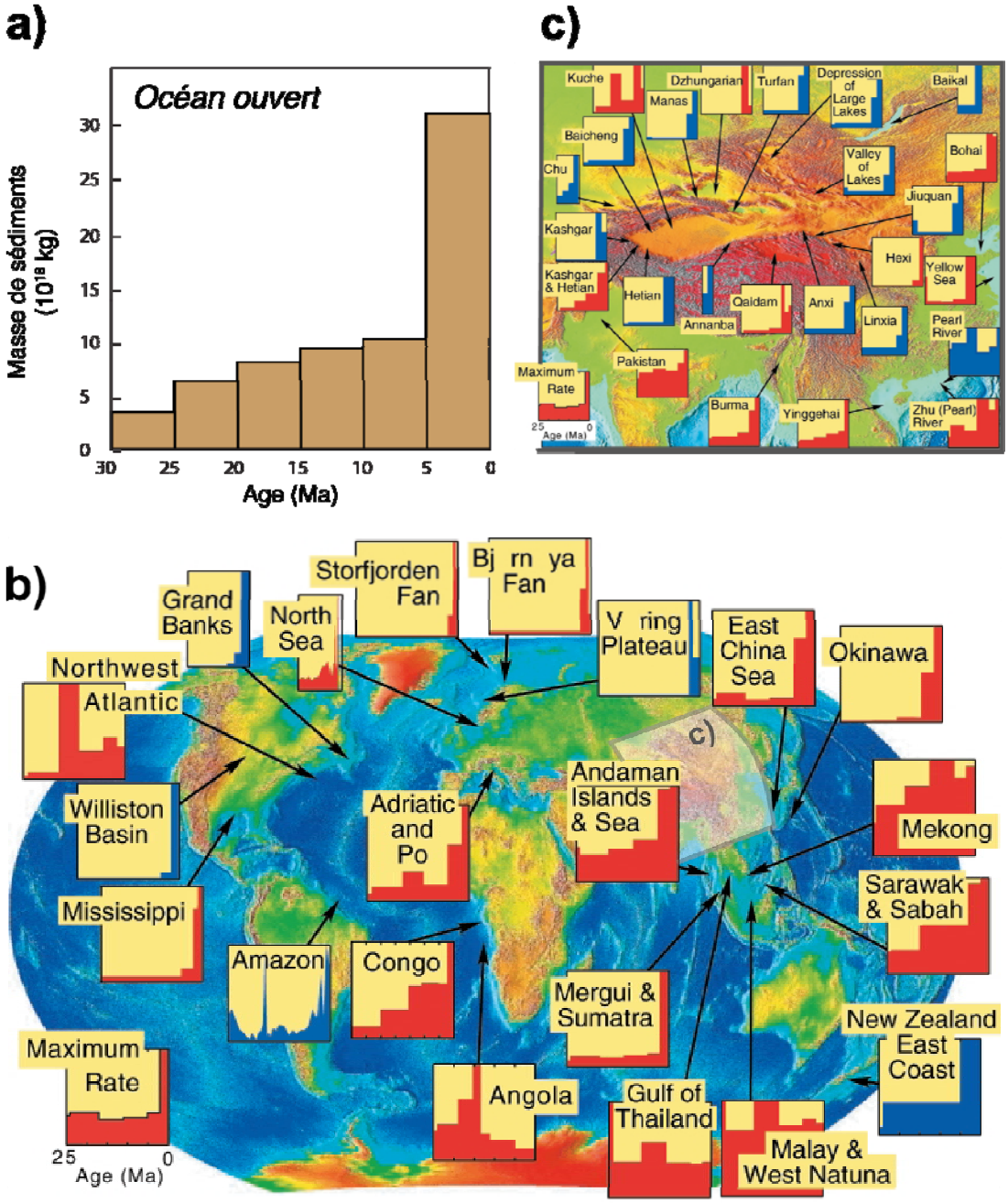

FIG. 11.7 - *Compilation des taux d'accumulation sédimentaire durant le Néogène. a) Sédiments terrigènes, océan ouvert (Hay 1988). b) Taux d'accumulation normalisés au maximum de l'enregistrement, sédiments de plateforme et continentaux. Bleu : section 1D, Rouge : estimation de volumes (mais souvent à partir de profils 1D). c) Zoom sur l'Asie centrale. Figures b) et c) tirées de Molnar, 2004.*

Une explication "traditionnelle" eut été d'invoquer l'effet de la mise en place des glaciers (§1.1.2.1). Or, certains de ces bassins se situent dans des zones tropicales n'ayant jamais été englacées. Ces auteurs proposèrent donc plutôt comme cause une variabilité accrue du climat, tant en amplitude qu'en fréquence, oscillant entre périodes froides et sèches et périodes humides et chaudes, menant les reliefs à un état de déséquilibre permanent avec le climat, état engendrant une augmentation de l'érosion.

1.2.2 Un paradigme largement remis en cause.

Malgré la prudence initialement affichée par ces auteurs dans leurs articles (Molnar, 2004), ce paradigme d'une augmentation globale de l'érosion depuis 2-5 Ma, a largement été relayé pendant les années 2000. Cependant, plusieurs études récentes l'ont remis en cause.

1.2.2.1 Biais des reconstitutions de taux d'accumulation

Reconstituer des taux d'accumulations fiables s'avère souvent ardu, et il est d'autant plus hasardeux de les relier à des variations de taux d'érosion.

La plupart des taux d'accumulations compilés par Zhang *et al.* (2001) et Molnar (2004) ont été calculés à partir d'enregistrements 1D. Or, la géométrie des dépôts peut varier significativement, notamment par la migration des dépôcentres, la géométrie du bassin sédimentaire ou sa vitesse de subsidence. Ainsi, extrapoler des variations de taux d'érosion à partir de quelques enregistrements 1D dans un bassin a peu de sens (Métivier, 2002). Le moyen le plus fiable d'estimer des volumes sédimentaires reste donc l'extrapolation de profils sismiques 2D, cette méthode étant très coûteuse. Le cône du Bengale illustre bien ce problème, même si (Zhang *et al.*, 2001) et (Molnar, 2004) ne le prenaient pas en compte dans leurs études : Les taux de sédimentation déduits d'après des forages 1D (Métivier *et al.*, 1999) et des profils sismiques 2D (Clift, 2006) s'avèrent en contradiction. Dans cette région, les très larges plaines alluviales en amont de ces dépôts, comme la plaine du Gange, ajoutent encore à la difficulté d'interprétation de ces résultats, en agissant comme des zones tampons pour le transport sédimentaire (Métivier & Gaudemer, 1999). Ensuite, pour une même zone de dépôt, c'est la source des sédiments qui peut elle-même avoir varié, avec des cônes de différentes rivières se recouvrant les uns les autres, comme dans le cas du Golf du Mexique (Galloway *et al.*, 2011).
Enfin, il faut également noter que de nombreux enregistrements reportés par exemple par Zhang *et al.* (2001) et Molnar (2004) ne prennent pas en compte la compaction sédimentaire, qui réduit la porosité et donc la masse volumique des sédiments les plus vieux et profonds.

Un autre problème inévitable des enregistrements sédimentaires est leur plus grande probabilité de comporter des lacunes lorsque leur âge augmente. Ainsi, plus les sédiments sont anciens, plus les taux d'accumulation vont avoir tendance à être moyennés sur des périodes longues et ayant de chances de comporter des lacunes (Schumer & Jerolmack, 2009). Ceci a pour effet une augmentation artificielle exponentielle des taux d'accumulation vers les périodes récentes (Schumer & Jerolmack, 2009; Schumer *et al.*, 2011). Cet effet est parfois appelé "effet Sadler", du nom de l'auteur ayant le premier alerté sur cet artefact (Sadler, 1981; Sadler, 1999).

En plus de ces biais inhérents, des raisons de douter de ces taux d'accumulation sédimentaire sont apparues avec de nouvelles données dans plusieurs zones du monde, remettant en cause largement la théorie d'une augmentation mondiale des taux d'érosion.

Dans les Alpes, la principale compilation de volumes sédimentaires était au début des années 2000 celle de Kuhlemann *et al.* (2001; 2002). Si des auteurs ont utilisé cette estimation pour expliquer une partie du soulèvement actuel des Alpes (Champagnac *et al.,* 2007), les données de thermochronologie basse température ont cependant mené à des interprétations contradictoires (Willett, 2010). Ainsi, les thermochronomètres *in-situ* montrent soit une forte augmentation de relief, potentiellement liée au creusement des vallées glaciaires (Valla *et al.*, 2010), soit un relief stable (Reverman *et al.*, 2012), selon les zones. La thermochronologie détritique, enregistrant les taux de dénudation moyens intégrés sur les bassins versants entiers, n'observe pas d'augmentation plio-pleistocène (Glotzbach *et al.*, 2011).

Une autre zone importante est l'Afrique de l'ouest, puisque cette zone n'a jamais été englacée et pourrait donc être témoin d'une hausse de la dénudation liée à l'instabilité du climat. Or, les enregistrements sédimentaires entre le Congo, l'Angola (pourtant proche) et le fleuve Orange sont contradictoires (Lavier *et al.*, 2001). Leurs variations sont largement imputables à des processus tectoniques de soulèvement des marges ouest-africaines (Seranne & Anka, 2005).

Enfin, une des zones clefs pour l'étude de l'évolution des taux de dénudation est l'Asie centrale (FIG. 1.6 c)(Molnar, 2004). En effet, cette large zone est endoréique et donc isolée d'une éventuelle influence des variations eustatiques, et inclut une grande partie des enregistrements compilés par (Zhang *et al.*, 2001) et (Molnar, 2004). Cependant, ces enregistrements et compilations de volumes sédimentaires (Metivier & Gaudemer, 1997; Metivier *et al.*, 1999), jusqu'au développement récent de la magnétostratigraphie dans cette région, étaient fondées sur des datations très incertaines. Notamment, l'apparition de la formation Xiyu, un épais niveau conglomératique, présente au sommet des sections tout autour des bassins d'Asie centrale (Junggar et Tarim), était systématiquement datés à ~2 Ma. Or, les études magnétostratigraphiques ont montré depuis que cette formation est diachrone, avec un âge

compris entre 15 et 1.5 Ma selon les zones. La formation Xiyu correspond en fait à une progradation sédimentaire ayant une cause tectonique (e.g. Charreau *et al.*, 2005; Charreau *et al.*, 2006; Charreau *et al.*, 2009a; Charreau *et al.*, 2009b).

Enfin, toutes ces reconstructions basées sur des sédiments détritiques ne permettent pas de remonter à une autre composante importante de la dénudation : l'altération chimique. Les proxy chimiques de cette altération sont pourtant eux aussi contradictoires. L'utilisation du rapport $^{87}Sr/^{86}Sr$ des océans, jusqu'alors couramment invoqué comme proxy de l'altération continentale au cours du Cénozoïque, est contestée, du fait de la forte dépendance de son taux de dissolution aux températures atmosphériques et à la concentration dans les roches mères (Kashiwagi *et al.*, 2008). Le rapport $^{87}Sr/^{86}Sr$ des océans peut aussi être modifié par un changement de la nature et de l'âge des roches sources altérées. Ce n'est donc pas un traceur univoque de l'intensité de l'altération. Un autre proxy, le rapport $^{10}Be/^{9}Be$ de l'océan, montre des flux d'altération relativement stables depuis ~10 Ma (Willenbring & von Blanckenburg, 2010). Au contraire, le $\delta^{7}Li$ marin enregistré par les foraminifères planctoniques semble montrer une augmentation très rapide de l'altération entre 6 et 18 Ma, suivie d'une relative stabilité depuis 6 Ma (Misra & Froelich, 2012). En tout état de cause, il n'est pas impossible d'imaginer que dans des conditions climatiques différentes de l'actuel, ou dans des phases de transition d'un état d'équilibre à un autre, érosion physique et altération chimique se retrouvent interconnectées différemment d'aujourd'hui.

Ainsi, la compilation de taux d'accumulation sédimentaire est une méthode affectée par des biais importants quand elle est utilisée pour remonter aux taux de dénudation du passé, comme l'ont montré études théoriques et nouvelles données contradictoires. De plus, ils n'incluent pas dans leur bilan l'altération chimique.

1.3 Apport potentiel des isotopes cosmogéniques

1.3.1 Application des isotopes cosmogénique dans l'actuel

J'introduis brièvement ici l'utilisation des isotopes cosmogéniques pour la détermination de taux de dénudation, dans l'actuel. Pour une description complète des isotopes cosmogéniques et de leurs utilisations en sciences de la Terre, on pourra chaudement recommander l'ouvrage de T. Dunai (2010).

1.3.1.1 Production des isotopes cosmogéniques *in-situ*

Les isotopes dits cosmogéniques sont les éléments créés par la cascade de réactions engendrées dans l'atmosphère terrestre par le rayonnement cosmique. Ce rayonnement n'est en fait pas à proprement parler une onde magnétique mais un flux de particules de haute énergie, essentiellement de protons et de particules α (e.g. Gosse & Phillips, 2001). Ces particules vont réagir avec les atomes des enveloppes terrestres, et produire de nouveaux noyaux plus légers, par réaction de spallation (destruction du noyau par la particule incidente), ainsi que des muons, protons, et neutrons de différentes énergies. C'est ce flux secondaire qui, en réagissant à son tour avec les atomes des enveloppes terrestres, va produire les isotopes dit cosmogéniques (FIG. 1.8)

Si la très grande majorité de ces réactions a lieu dans l'atmosphère, une partie de flux secondaire atteint la surface terrestre. La majeure partie de ce flux est atténuée exponentiellement dans les roches de surface (Eq. 1.1), mais produit dans celles-ci des isotopes cosmogéniques, selon trois mécanismes principaux: la spallation, par les neutrons de haute énergie (la majeure partie de la production en surface, mais rapidement atténuée avec la profondeur), la capture muonique (plus faible production mais plus pénétrative en profondeur) (FIG. 1.8), et la capture neutronique, négligeable dans notre cas. Le taux de production P (at.g^{-1}.an^{-1}) d'un isotope cosmogénique donné à une profondeur z peut ainsi s'écrire:

$$P(z) = \sum_i P_i(0)\, e^{-z\rho/\Lambda_i} \tag{1.1}$$

Avec ρ la masse volumique de la roche mère (g.cm^{-3}), Λ la longueur caractéristique d'atténuation (g.cm^{-2}), et i indice désignant les différents mécanismes de production (spallation, captures muoniques...).

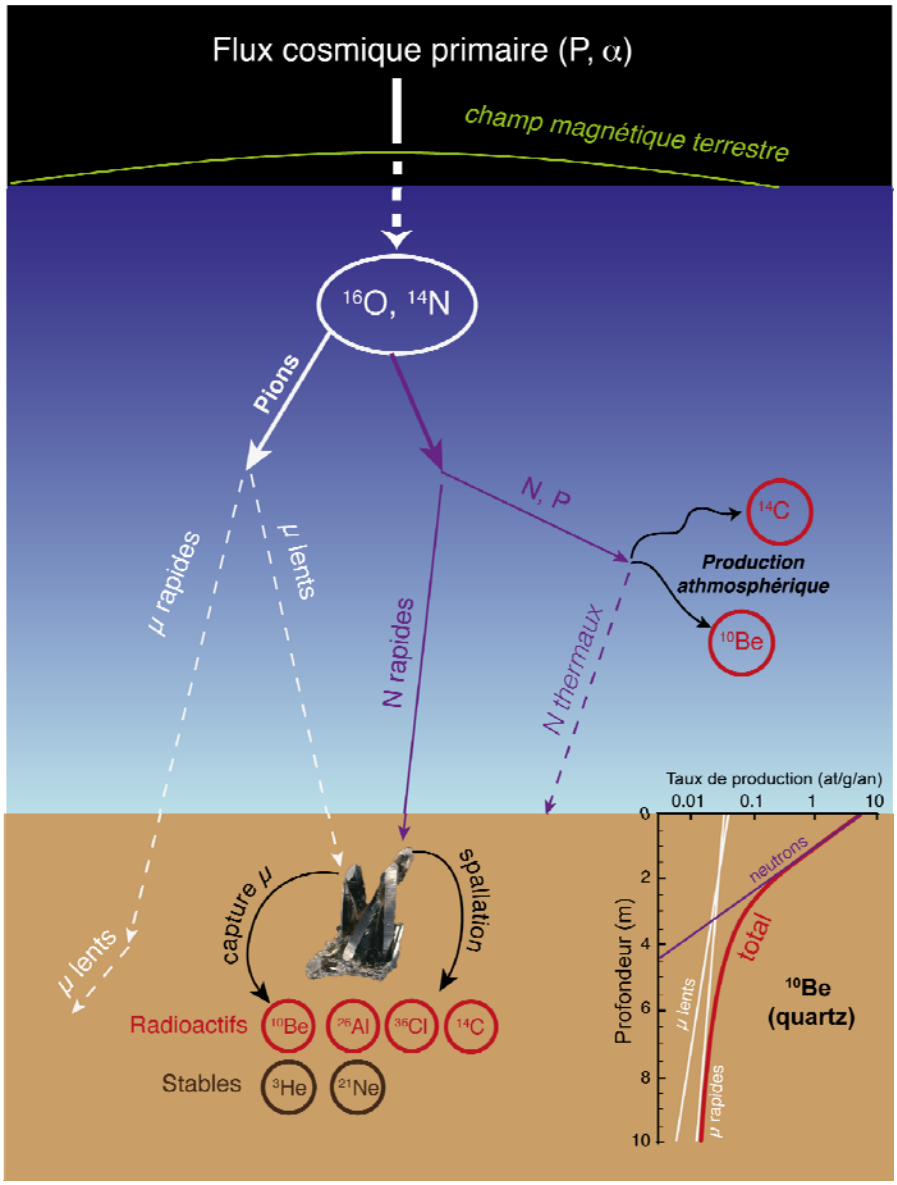

FIG. 1.8 - *Schéma de la cascade de réactions menant du flux cosmique primaire à la production d'isotopes cosmogéniques in-situ. Le flux est fortement absorbé par l'atmosphère et dévié par le champ magnétique terrestre, en fonction de la latitude. Il réagit avec les atomes de l'atmosphère, créant une gamme de particules secondaires (N: neutrons, P: protons, μ: muons). Dans la surface, le taux de production par les différentes réactions de production cosmogénique décroît exponentiellement, avec des longueurs caractéristiques différentes. Ici, on a représenté les taux de production pour le ^{10}Be dans le quartz, mais les longueurs d'atténuation (profondeur nécessaire pour que le flux décroisse de 63%) seraient similaires pour d'autre minéraux et/ou isotopes (Eq. 1.1).*

1.3.1.2 Utilisation pour la détermination de taux de dénudation

La concentration en isotopes cosmogéniques de la surface d'une roche ou d'un sol est directement reliée à son temps d'exposition, au taux de dénudation qu'elle subit, et au taux de production en isotopes cosmogénique à cet endroit donné (Lal, 1991).

Pour une concentration initiale nulle, la concentration C d'une surface exposée subissant un taux de dénudation constant ε pendant un temps t est décrite par :

(1.2)

$$C(t) = \sum_i \frac{P_i(0)}{\lambda + \rho\varepsilon/\Lambda_i}\left(1 - e^{-t(\lambda+\rho\varepsilon/\Lambda_i)}\right)$$

Avec λ (an^{-1}) la constante de désintégration, si l'isotope considéré est instable.

Si la surface est exposée suffisamment longtemps avec le même taux de dénudation, sa concentration atteint un état d'équilibre directement dépendant de ce taux de dénudation (plateaux sur la FIG. 1.9 a). Autrement dit, pour $t >> 1/(\lambda + \rho\varepsilon/\Lambda_i)$:

(1.3)

$$C(t) = \sum_i \frac{P_i(0)}{\lambda + \rho\varepsilon/\Lambda_i}$$

De manière remarquable, les concentrations en isotopes cosmogéniques peuvent aussi permettre de calculer le taux de dénudation moyen d'un bassin versant entier. Il serait en effet bien trop fastidieux d'échantillonner des centaines de surfaces dans tout un bassin. En revanche, le sable transporté par la rivière à l'exutoire de ce bassin est constitué de grains de sable provenant de tout le bassin versant. Dans les cas où $\lambda << \rho\,\varepsilon/\Lambda$ (i.e., pour le ^{10}Be par exemple, $\varepsilon >>$ 0.3 $m.Ma^{-1}$, condition très largement observée à la surface terrestre), on peut montrer que la concentration totale $\overline{C}$ de ce sable est directement reliée au taux d'érosion moyen $\overline{\varepsilon}$ de ce bassin versant et à son taux de production moyen en isotopes cosmogéniques $\overline{P}_i(0)$ (voir aussi FIG. 2.1) (Brown *et al.*, 1995; Granger *et al.*, 1996) :

(1.4)

$$\overline{C}(t) = \sum_i \frac{\overline{P}_i(0)}{\rho\overline{\varepsilon}/\Lambda_i}$$

Cependant, cette équation ne reste valable que si certaines conditions sont vérifiées :

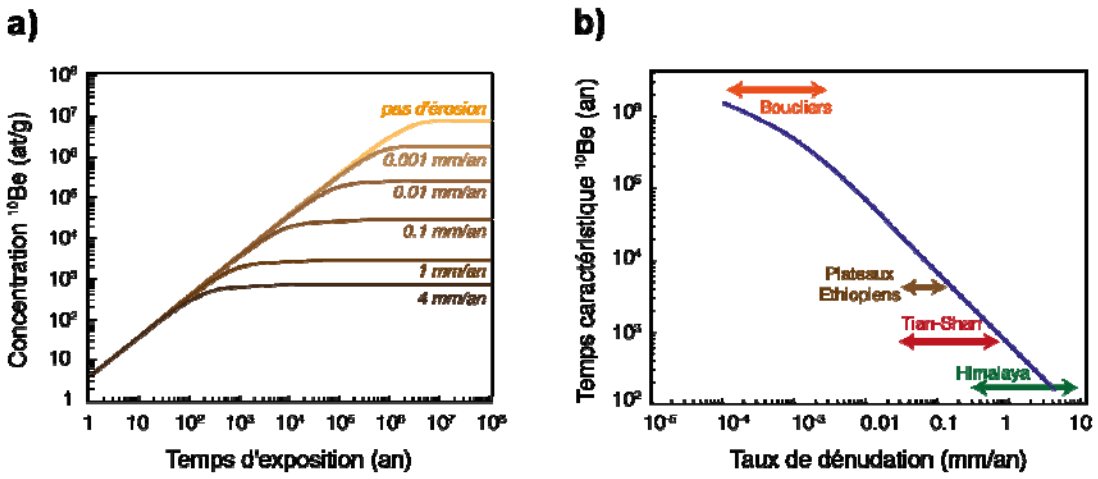

FIG. 1.9 - *Notion de temps d'équilibre des taux de dénudation dérivés des isotopes cosmogéniques. a) Surface partant d'une concentration nulle exposées à différents taux de dénudation. Si ce taux reste constant, la concentration atteint un plateau au bout d'un temps lui-même fonction de ce taux. J'ai pris ici le cas du ^{10}Be dans le quartz, au niveau de la mer et à une haute latitude, mais ces courbes seraient qualitativement les mêmes pour d'autres minéraux cibles et isotopes radioactifs. b) Temps caractéristique de lissage du taux de dénudation par les isotopes cosmogéniques (courbe bleu). J'ai également représenté les gammes d'érosions rencontrées dans les zones abordées pendant cette thèse, et un taux représentatifs des boucliers continentaux.*

(i) Le taux de dénudation est supposé constant sur l'échelle de temps caractéristique nécessaire pour éroder l'épaisseur d'atténuation du taux de production, dépendant de la densité de la roche mais typiquement ~0.6 m (FIG. 1.8) (e.g. Niemi et al., 2005; Yanites et al., 2009);

(ii) Le minéral sur lequel sont menées les analyses doit être présent en proportion équivalent dans tout le bassin versant.

(iii) La granulométrie du minéral étudié doit être équivalente dans tous le bassin versant, et la granulométrie étudiée du sable de rivière doit être représentative de toutes les unités de ce bassin (e.g. Codilean *et al.*, 2012);

(iv) La perte de masse par altération en profondeur doit rester faible (e.g. Riebe *et al.*, 2001a);

(v) Le temps de transfert du sédiment dans le bassin doit être assez rapide pour éviter à la fois une réexposition au rayonnement cosmique et une décroissance radioactive pour les isotopes cosmogéniques instables (^{14}C, ^{10}Be, ^{26}Al, ^{36}Cl).

Dans la plupart des environnements, ces conditions ne sont pas toutes parfaitement vérifiées. En particulier, nous avons exploré les conditions (i) et (iii) dans deux contextes géologiques très différents, de manière préliminaire à l'extension de cette méthode pour des sédiments anciens de ces régions. Ce travail a donné lieu à la soumission pour publication de deux articles, formant le chapitre 3 de ce manuscrit.

Il faut également noter que le taux de production moyen dans le bassin versant peut être entaché d'incertitudes, liées notamment aux modèles d'évolution de ces taux de production avec l'altitude et la latitude (e.g. Lal, 1991; Stone, 2000; Dunai, 2001; Desilets et Zreda, 2003; Lifton *et al.*, 2008), l'écrantage partiel par la topographie (e.g. Dunne *et al.*, 1999; Norton and Vanacker, 2009), ou l'effet des couvertures neigeuses (e.g. Schildgen *et al.*, 2005; Delunel *et al.*, 2013).

Malgré ces limitations, l'étude des isotopes cosmogéniques dans les sédiments de rivière a permis depuis une vingtaine d'année de fournir des estimations de taux de dénudation moyens sur des échelles de temps hors de portée d'autres méthodes. Les nombreuses études ont ainsi amené des informations cruciales sur la compréhension des relation tectonique/érosion/climat dans l'actuel (voir par exemple les compilations de Portenga & Bierman (2011) et Willenbring *et al.* (2013), FIG. 1.3). Il s'agit également d'une méthode extrêmement simple à appliquer, puisqu'elle ne nécessite que l'analyse de quelques aliquotes de sables de rivière (à comparer par exemple avec les études basées sur la charge sédimentaire et dissoute, nécessitant un suivi sur de nombreuses années).

1.3.2 Application dans l'ancien : potentiels et limites?

Une des propriétés remarquables des isotopes cosmogéniques est de lisser les variations de taux de dénudation sur des temps caractéristiques hors de portée d'autres méthodes (FIG. 1.9). Ainsi, pour les taux de dénudation rencontrés communément sur Terre, ce temps caractéristique va d'environ 200 ans (taux de dénudation >3 $mm.a^{-1}$) à 500 000 ans (taux < 10^{-3} $mm.a^{-1}$). Cette propriété permet d'éviter les variations saisonnières ou annuelles qui affectent notamment les mesures de charges sédimentaires. Pour les taux de dénudation modérés, elle permet même de lisser des éventuelles variations de dénudation dues aux cycles climatiques millénaires (Schaller & Ehlers, 2006). A l'inverse, ces temps typiques permettent une meilleure résolution que les thermochronomètres basse température. Par exemple, les traces de fissions sur apatites ou les âges (U-Th)/^{4}He, avec des températures de fermeture de 70-100°C, et dans le cas d'orogènes à forts taux de dénudation, n'autorisent une résolution temporelle que de l'ordre du million d'années (e.g. Braun, 2002; Ehlers & Farley, 2003). La thermochronologie très basse

température (30°C) par OSL (Optically Stimulated Luminescence), développée récemment, offre toutefois des résultats prometteurs et des fenêtres temporelles intermédiaires entre les isotopes cosmogéniques et les thermochronomètres traditionnels (Herman *et al.*, 2010). Toutefois, ces méthodes restent très dépendantes du modèle de refroidissement choisi. Par ailleurs, à l'exception de la thermochronologie dans des minéraux détritiques, elles fournissent des taux d'exhumation locaux et non intégrés sur des bassins versants entiers.

Les isotopes cosmogéniques ayant montré leur efficacité pour déterminer des taux de dénudation dans l'actuel, l'idée est rapidement venue d'étendre cette même méthode à des sédiments anciens (e.g. Shaller *et al.*, 2001; von Blanckenburg, 2005; Blard *et al.*, 2006; Dunai, 2010). Cependant, plusieurs limites théoriques et difficultés ont jusqu'à présent réfréné (ou poussé à l'autocensure?) les chercheurs dans cette tentative.

L'isotope cosmogénique de loin le plus utilisé pour dériver des taux d'érosions est le ^{10}Be. Il combine en effet plusieurs avantages cruciaux: (i) Il est retenu dans le quartz, seul minéral présent dans presque toutes les formations géologiques continentales, contrairement par exemple à l'^{3}He (Trull *et al.*, 1991)); (ii) Il est *relativement* facile à extraire des minéraux, contrairement au ^{14}C; (iii) Il n'a qu'un seul autre isotope, le ^{9}Be, souvent présent sous forme de traces dans le quartz, contrairement par exemple au ^{26}Al, dont l'isotopes majeur ^{27}Al est présent en grandes quantités; (iv) Le ^{10}Be ne provient que de la production cosmogénique, et le ^{10}Be atmosphérique adsorbé sur les grains est aisément éliminable, contrairement au ^{21}Ne et ^{3}He qui peuvent provenir de nombreuses autres sources. Ces derniers, de par leur stabilité, peuvent en effet avoir été produits par d'autres mécanismes (production radiogénique) sur de très longues périodes, en quantité écrasant totalement le signal cosmogénique ou rendant peu fiable sa détermination. Dans le cas du ^{3}He, cette problématique sera traitée dans l'article inséré au chapitre 3, avec un cas d'étude appliqué à l'érosion des trapps basaltiques du plateau éthiopien.

Le ^{10}Be, cependant, est instable, et se désintègre avec une demi-vie de 1.39 Ma (constante de désintégration $\lambda = 4.997 \times 10^{-7}$ an^{-1}, Chmeleff *et al.*, 2010; Korschinek *et al.*, 2010). Ainsi, une barrière de l'âge semble se dresser : pour des sédiments vieux de plusieurs millions d'années, le ^{10}Be aura trop décru pour être détectable par Spectrométrie par Accélération de Masse (AMS), en particulier pour des taux de dénudation élevés engendrant des concentrations initiales faibles (FIG. 2.4).

Un autre problème potentiel est l'évolution de la topographie du bassin versant. En effet, le taux de production moyen est très dépendant de son altitude (Lal, 1991; Stone, 2000), et celle ci peut avoir significativement varié sur plusieurs millions d'années. Enfin, sur des échelles de temps

aussi longues, il devient difficile d'estimer une éventuelle reprise de ses propres sédiments par la rivière ("cannibalisme") ou de multiples épisodes de dépôt pouvant fausser le signal cosmogénique.

Jusqu'à très récemment, les rares publications de données de paléo-taux de dénudation a partir d'isotopes cosmogéniques était en fait basées sur des couples d'isotopes cosmogéniques, notamment le rapport $^{10}Be/^{26}Al$ (Granger *et al.*, 2001; Schaller *et al.*, 2002; Schaller *et al.*, 2004; Balco & Stone, 2005; Hu *et al.*, 2011; Matmon *et al.*, 2012). Ces derniers ayant un rapport de production constant lors de l'érosion et des constantes de décroissance différente, leur rapport dans un sédiment permet de dater l'âge de son d'enfouissement (voir §2.1.2). Or cette méthode cumule plusieurs inconvénients :

(i) Le ^{26}Al a une demi-vie encore plus faible que le ^{10}Be (0.708 Ma), ce qui limite encore les ages maximaux atteignables;

(ii) Le cumul des erreurs sur les mesures de ^{10}Be et d'^{26}Al, et sur la constante radioactive du ^{26}Al, mal contrainte (Nishiizumi, 2004), mène à de larges incertitudes sur ces taux de dénudation;

(iii) En l'absence de datation indépendante, il est impossible d'estimer un éventuel cannibalisme ou une histoire pré-dépôt complexe (Hu *et al.*, 2011; Matmon *et al.*, 2012);

(iv) Souvent menés sur des terrasses alluviales (Schaller *et al.*, 2002; Schaller *et al.*, 2004; Balco & Stone, 2005; Matmon *et al.*, 2012) ou dans des cavernes (Granger *et al.*, 2001; Hu *et al.*, 2011; Refsnider, 2011), ces enregistrements sont discrets et non continus et haute résolution, ce qui est nécessaire pour pouvoir suivre une éventuelle réponse de l'érosion à un changement climatique majeur. Aussi, jusqu'à présent, seules les études de Schaller *et al.* (2002, 2004) ont été clairement axées vers l'étude de la réponse de la dénudation aux cycles glaciaires, mais seulement pour les derniers 1.2 Ma, et seul Refsnider (2010) est remonté jusqu'à 5 Ma, mais avec un enregistrement de seulement 5 points, et un bassin versant extrêmement petit (quelques km^2).

L'intérêt théorique de l'application des isotopes cosmogéniques à des enregistrements sédimentaires continus anciens est énorme. Cependant, à cause des difficultés pratiques de cette méthode et surtout de sa relative nouveauté, aucune étude n'avait, au début de cette thèse, tenté de l'appliquer à l'étude de l'évolution des taux de dénudation depuis ~10 Ma, matière à un intense débat.

Dans le chapitre suivant, je détaillerai de manière générale les obstacles techniques et théoriques à surmonter pour aboutir à ces résultats.

Unité

Il y a quelque chose de dense, uni, déposé au fond,
répétant son chiffre, son signe identique.
Les pierres ont touché le temps, c'est évident,
une odeur d'âge émane de leur fine matière,
et de l'eau qu'amène la mer et du sel et du rêve.

Une même chose m'entoure, un seul mouvement :
le poids du minéral, la lumière de la peau,
unis au son du même vocable : noche
l'encre des blés, de l'ivoire, des sanglots,
des choses en cuir, en bois, en laine,
vieillies, décaties, uniformes,
se dressent autour de moi telles des parois.

Je travaille sourdement, tournant sur moi-même,
comme le corbeau sur la mort, le corbeau de deuil.
Je réfléchis, isolé au milieu de longues saisons,
central, cerné de géographie silencieuse :
une température partielle tombe du ciel,
un empire extrême d'unités confuses
s'assemble en m'entourant.

P. Neruda,
Résidence sur la Terre.

Chapitre 2
Isotopes cosmogéniques, de l'actuel à l'ancien.

2.1 Principes théoriques

L'idée de base de l'extension des isotopes cosmogéniques dans des sédiments anciens est simple : si l'analyse d'un sable de rivière actuel permet de calculer le taux de dénudation moyen de son bassin versant, il doit également être possible d'appliquer la même méthode à des sables anciens, enfouis depuis plusieurs milliers ou millions d'années, et mis ensuite à notre disposition par le couple tectonique-érosion, les constructions humaines, ou des forages. Toutefois, plusieurs corrections et points de prudence primordiaux sont à respecter. Je vais ici décrire les grands principes de cette méthode, ainsi que ses limitations théoriques. Pour le détail particulier du traitement et de l'analyse des échantillons provenant des différentes zones ciblées, on se référera aux paragraphes méthodologiques de chaque article correspondant (Ethiopie et Népal central, Chapitre 3; Tianshan, Chapitre 4; Sud Népal, Chapitre 5).

2.1.1 Correction de l'enfouissement et du transport.

Contrairement à un sable de rivière actuel, le signal cosmogénique d'un paléo-sable peut largement évoluer après sa production sur les pentes du bassin versant (FIG 2.1).
En effet, les sédiments peuvent accumuler pendant leur long dépôt et jusqu'à la réexposition récente une quantité significative d'isotopes cosmogéniques (Eq. 2.1). Tout d'abord, cette accumulation indésirable peut se produire pendant l'enfouissement du sédiment, si celui-ci se déroule en une durée non négligeable devant le temps caractéristique durant lequel a été enregistré la dénudation. Ensuite, et même une fois le sédiment profondément enfoui et protégé du rayonnement neutronique, une très faible production, muonique, se poursuit, même à grandes profondeurs (>4 m). Celle-ci est souvent négligeable pour des sédiments récents.

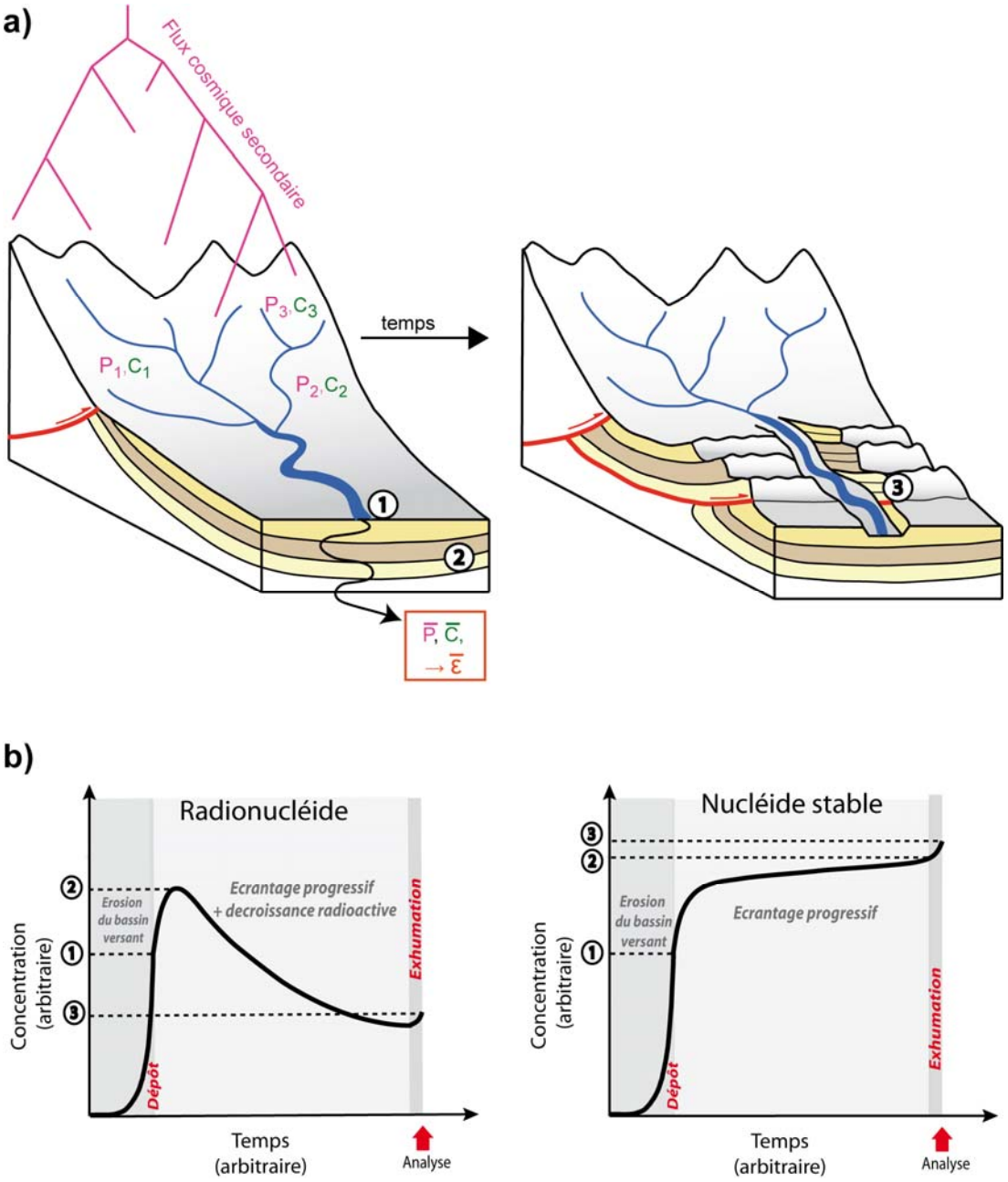

FIG. 2.1 - *a) Trajet du sédiment et b) évolution du signal cosmogénique au cours du temps. (1) Production initiale dans le bassin. La concentration moyenne* $\overline{C}$ *est reliée au taux de production moyen de ce bassin* $\overline{P}$ *et à son taux de dénudation moyen* $\overline{\varepsilon}$ *. (2) Enfouissement progressif et ré-accumulation, y compris à grande profondeur par réactions muoniques. (3) Exhumation (ici par exemple, exhumation tectonique) et analyse.*

En revanche, elle peut être relativement importante pour des temps d'enfouissement de plusieurs millions d'années, alors qu'en parallèle, dans le cas d'isotopes radioactifs comme le ^{26}Al et le ^{10}Be, le signal initial qui nous intéresse décroît drastiquement. Cette production post-dépôt est décrite par :

(2.1)

$$C_{enf} = \sum_i \left[\frac{(P_{enf})_i}{\lambda - A\rho_s/\Lambda_i} \left(e^{-tA\rho_s/\Lambda_i} - e^{-\lambda t} \right) \right]$$

(Braucher *et al.*, 2000)

Avec P_{enf} le taux de production de surface au point de dépôt A le taux d'accumulation, ρ_s la masse volumique du sédiment, et t l'âge d'enfouissement (les autres constantes sont les mêmes qu'aux équations 1.1 et suivantes).

Comme on le voit, il est nécessaire de disposer d'une estimation indépendante de la vitesse d'accumulation A afin de corriger de C_{enf}. Pour la production spallogénique, très dominante en surface mais peu pénétrative en profondeur, il est préférable de considérer le taux d'accumulation des ~4 premiers mètres au dessus du sédiment. En revanche, pour les productions par les muons rapides et lents, pénétratives à grande profondeur, et si le taux d'accumulation varie fortement, il est préférable de considérer un taux d'accumulation moyen intégré sur toute la colonne sédimentaire.

Heureusement, cette production post-enfouissement tend à être relativement limitée par le fait que le dépôt se fait toujours à une altitude plus basse que celle de la zone en érosion. Or, les taux de production cosmogénique croissent exponentiellement avec l'altitude (Lal, 1991; Stone, 2000; Dunai, 2001; Desilets et Zreda, 2003; Lifton *et al.*, 2008). Ainsi, le taux de production dans le bassin est beaucoup plus élevé que dans la zone de transport (plaine alluviale) et de dépôt, ce qui tend à limiter cette correction.

2.1.2 Réexpositions et cannibalisme

D'autres complications dues aux dynamiques sédimentaires entre les zones de production et de dépôt final du sédiment peuvent sévèrement affecter le signal cosmogénique.

Comme pour les rivières actuelles, tout d'abord, cette concentration peut avoir évolué lors du transport entre la roche mère et le point de dépôt final, suite à plusieurs épisodes de dépôts puis de ré-incision par la rivière. Les données et modèles existants sont rassurants, et semblent montrer que cette contribution reste en général faible, même sur de longues distances

de transport, comme notamment la plaine du Gange (Lupker *et al.*, 2012) ou le bassin de l'Amazone (Wittmann *et al.*, 2009a; Wittmann *et al.*, 2009b; Wittmann *et al.*, 2011). Cependant, il reste préférable de tester cette potentielle modification du signal, pour des distances de transport longues ou des systèmes fluviatiles de faible dynamisme. On peut avoir recours dans ce cas à un modèle (Wittmann *et al.*, 2007; Lauer et Willenbring, 2010), et à des ages théoriques d'enfouissement fournis par des couples d'isotopes cosmogéniques radioactifs (voir ci dessous).

Sur de longues échelles de temps, il devient de plus en plus probable que le sédiment ait subi un ou plusieurs épisodes de re-érosion et dépôt en zone plus proximale, la rivière cannibalisant ses propres sédiments. D'une part, une re-exposition peut donner lieu à une re-accumulation d'isotopes cosmogéniques. D'autre part, et *a fortiori* dans le cas des isotopes stables, les anciens sédiments repris peuvent encore contenir une quantité non négligeable d'isotopes cosmogéniques provenant de leur première exposition, notamment quand une partie significative du bassin versant est constituée d'anciens sédiments maintenant soulevés (voir Chapitre 4 le cas de Siwaliks par exemple).

Enfin, si l'échantillonnage ne se fait pas sur un affleurement extrêmement récent anthropogénique (construction de route, carottage), sa dernière re-exposition peut avoir conduit à une re-accumulation d'isotopes cosmogéniques. Cette dernière est limitée par le fait qu'elle a lieu plus bas en altitude que la production initiale, mais, dans le cas d'isotopes radioactifs, elle est aggravée par le fait que la concentration initiale a décru depuis le dépôt des sédiments.

La meilleure solution pour pouvoir tester l'existence de tels biais, à défaut de les quantifier, est de comparer les ages d'enfouissement fournis par des couples d'isotopes cosmogéniques radioactifs avec les ages "réels" fournis par des méthodes de datation indépendantes (telle la magnétostratigraphie). Ces datations reposent sur le principe suivant : s'il est possible de mesurer de manière fiable le rapport $^{26}Al/^{10}Be$ actuel et la concentration absolue actuelle en ^{10}Be d'un sédiment, alors il est possible de mesurer le temps depuis lequel ce sédiment a été enfoui et isolé du rayonnement cosmique. En effet, le rapport de production initial (avant enfouissement) de deux isotopes cosmogéniques dans un minéral donné est calculable avec ces données, quel que soit le taux de dénudation : un échantillon exposé en surface à l'état stationnaire appartient nécessairement à une courbe ayant une forme caractéristique de crosse de hockey (FIG. 2.2). Après enfouissement et le quasi arrêt de la production, si ces deux isotopes ont des périodes de décroissance différentes, ce rapport va évoluer à mesure qu'un des deux isotopes disparaît plus vite que l'autre (FIG. 2.2) (Klein *et al.*, 1986; Lal, 1991; Granger et Muzikar, 2001; Balco et Rovey, 2008).

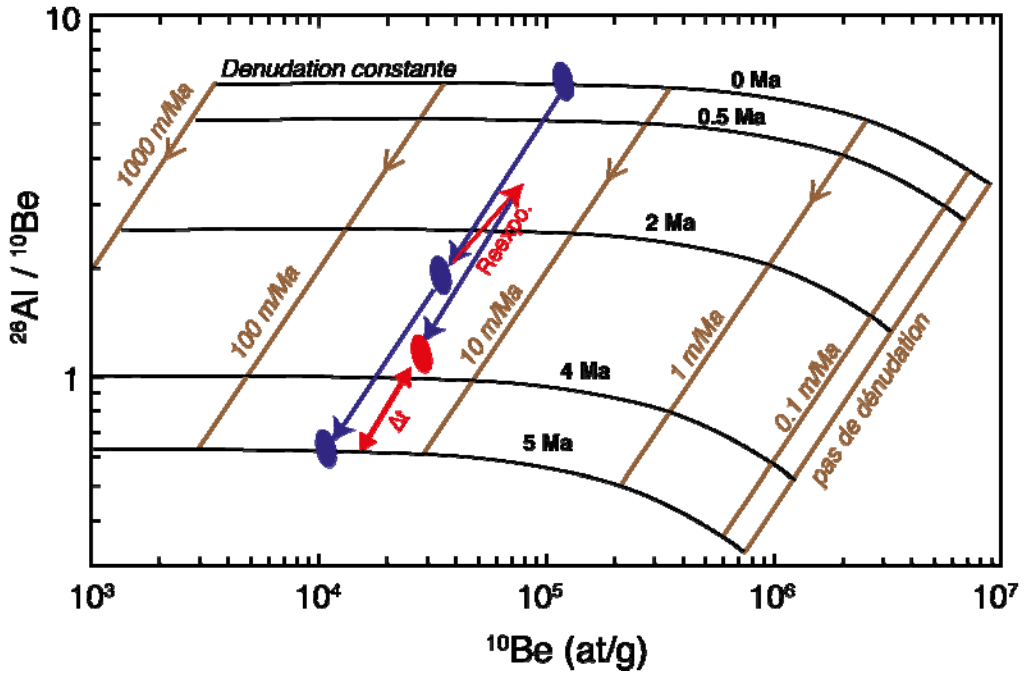

FIG. 2.2 - *Evolution dans l'espace $^{26}Al/^{10}Be$ vs. ^{10}Be d'un sable enfouis, produit avec un taux de dénudation stable dans le bassin versant originel. Dans le cas d'une réexposition, le rapport $^{26}Al/^{10}Be$ et la quantité de ^{10}Be vont être réalimentés. On observe donc dans l'échantillon actuel un "âge $^{26}Al/^{10}Be$" artificiellement plus jeune que l'âge réel du dépôt.*

Ainsi, en considérant les concentrations $C_A(t)$ et $C_B(t)$ en deux isotopes A et B, le rapport $R_{AB}(t) = C_A/C_B$ évolue avec le temps t selon :

(2.2)

$$R_{AB}(t) = \frac{C_A(t)}{C_B(t)} = \frac{C_A(0)e^{-t\lambda_A}}{C_B(0)e^{-t\lambda_B}} = R_{prod}\, e^{-t(\lambda_A-\lambda_B)}$$

Avec R_{prod} le rapport initial de production.

On peut ainsi remonter à l'âge d'enfouissement :

(2.3)

$$t = \frac{-\ln\left(R_{AB}/R_{prod}\right)}{\lambda_A - \lambda_B}$$

Un âge d'enfouissement significativement plus vieux que l'âge réel sera indicateur d'un cannibalisme d'anciens sédiments. Un âge d'enfouissement plus jeune sera synonyme d'épisodes de re-exposition entre le dépôt et l'échantillonnage (FIG. 2.2).
Encore une fois, on voit qu'une datation indépendante est primordiale.

2.1.3 Evolutions du bassin versant

Une autre incertitude majeure pouvant peser sur les paléo-taux de dénudation est celle concernant l'évolution du bassin versant, et notamment son hypsométrie, son réseau de drainage, et sa géologie.
Comme on l'a déjà évoqué, le taux de production est très dépendant de l'altitude. Or, sur des périodes de plusieurs millions d'années, l'altitude moyenne et la répartition des altitudes (hypsométrie) dans le bassin peuvent avoir significativement évolué.
D'autre part, dans le cas d'une réorganisation majeure d'un bassin versant, la comparaison des taux de dénudation au long de l'enregistrement peut ne plus être significatif : on peut imaginer qu'épisodiquement, dans la colonne stratigraphique, les sédiments n'aient été apportés que par un affluent local, ou au contraire que la rivière approvisionneuse ait été capturée par un plus gros affluent.
Les paléo-altimètres peuvent apporter des indices sur l'élévation des bassin versants , mais ces données sont souvent rares et sujets à de larges incertitudes (e.g. Clark, 2007). Dans le cas du Tian-Shan (Chapitre 4), nous nous sommes par exemple appuyés sur des enregistrements d'isotopes stables de l'oxygène et du carbone (Charreau *et al.*, 2012).
Enfin, des complications peuvent provenir de la géologie du bassin versant en fonction du minéral cible. En effet, comme je l'ai évoqué au Chapitre 1 §1.3.1, les proportions du minéral cible dans les roches du bassin versant doivent être homogènes pour produire un taux de dénudation qui soit réellement représentatif de la moyenne globale. Même si cette condition n'est pas parfaitement respectée, les isotopes cosmogéniques peuvent néanmoins être utilisés pour estimer des variations relatives de la dénudation des zones les plus productrices de ce minéral. En revanche, si le bassin versant évolue de manière à drainer alternativement des zones plus ou moins concentrées en ce minéral cible, cette comparaison devient hasardeuse. Dans le cas du quartz, ubiquiste dans la grande majorité des formations continentales, ce problème reste limité. Il peut cependant être important dans le cas de minéraux plus rarement présents dans les formations de surface (grenats, pyroxènes, olivines pour l'^{3}He par exemple). Les traceurs de sources géochimiques et/ou minéralogiques peuvent être utilisés comme indicateurs de telles évolutions.

2.1.4 Résolution du système, propagation d'erreurs

En additionnant toutes les sources de production d'isotopes cosmogéniques (Eq. 1.4, 2.1 et exposition récente), et dans le cas simple d'absence de re-exposition ou de cannibalisme, la concentration totale d'un paléo-sable d'âge *t* s'écrit :

(2.4)

$$C_{tot} = C_{recent} + \sum_i \left[\frac{\overline{P}_i}{\rho\bar{\varepsilon}/\Lambda_i} e^{-\lambda t} + \frac{(P_{enf})_i}{\lambda - A\rho_s/\Lambda_i} \left(e^{-tA\rho_s/\Lambda_i} - e^{-\lambda t} \right) \right]$$

Avec i indice décrivant les différents mécanismes de production, $\overline{P}_i$ (at.g^{-1}.a^{-1}) les taux de production par ces mécanismes, moyennés sur le bassin versant, $\bar{\varepsilon}$ (cm.a^{-1}) le paléo-taux de dénudation moyen du bassin versant, $(P_{enf})_i$ (at.g^{-1}.a^{-1}) les taux de production au lieu de déposition, A (cm.a^{-1}) le taux d'accumulation au moment du dépôt, ρ et ρ_s (g.cm^{-3}) les masses volumiques de la roche mère et du sédiment déposé, respectivement, λ (a^{-1}) la constante de désintégration de l'isotope considéré, Λ_i (g.cm^{-2}) les longueurs d'atténuation des différents mécanismes.

Ce système n'est pas solvable analytiquement pour ε si l'on ne néglige pas l'influence muonique, et dans le cas d'une érosion faible (λ non négligeable devant $\rho\varepsilon/\Lambda_i$). Le moyen le plus rigoureux est donc de passer par une résolution numérique.

Par ailleurs, chacun de ces paramètres est affecté par une incertitude qui n'est pas toujours négligeable et qu'il faut propager au résultat final. En pratique nous avons donc mis au point un code de propagation d'incertitudes qui réalisent des simulations de Monte-Carlo, avec tirage aléatoire de chacun de ces paramètres dans une distribution fixée. Le code résout ensuite numériquement l'équation (2.4), puis analyse la distribution des solutions. Le programme Matlab® utilisé à cette fin est fourni en Annexe de ce manuscrit.

2.2 Limites analytiques de l'extension aux anciennes séries sédimentaires

Outre ces limites liées aux contextes géologiques des bassins cibles, une autre barrière fondamentale est la limite de détection des isotopes cosmogéniques instables dans les sédiments les plus anciens. En effet, le radionucléide le plus couramment utilisé, le ^{10}Be, a une demi-vie de 1.39 Ma (Chmeleff *et al.*, 2010; Korschinek *et al.*, 2010). Si l'on cible des sédiments âgés de 10 Ma, le risque est de tomber sous la limite analytique de cet élément. Au début de cette thèse,

l'idée pour s'affranchir de ce problème de la "barrière de l'âge" était de non pas utiliser le ^{10}Be, mais plutôt de développer l'utilisation des isotopes cosmogoniques stables, ^{3}He et ^{21}Ne. Cependant, plusieurs problèmes nous repoussèrent finalement vers l'utilisation du ^{10}Be, assortie de certaines stratégies analytiques spécifiques.

2.2.1 Les isotopes cosmogéniques stables : potentiel et limitations

Le ^{3}He est non seulement stable, mais tant la préparation des échantillons que leur analyse sont bien plus aisées, et exposent à de moindres risques chimiques (voir ci dessous §1.2.4) que le ^{10}Be ou le ^{26}Al. Malheureusement, le ^{3}He cumule deux défauts qui rendent son utilisation impossible dans plusieurs contextes géologiques.

Tout d'abord, il n'est pas retenu quantitativement dans le quartz, minéral ubiquiste à la surface de la Terre (Trull *et al.*, 1991). Son taux de production n'est connu que dans des minéraux généralement rares, ou dont la présence est limitée à certaines parties du bassin versant : pyroxène et olivine (e.g. Kurz *et al.*, 1990; Cerling et Craig, 1994; Goehring *et al.*, 2010), apatite, zircon, grenat, disthène, biotite (e.g. Gayer *et al.*, 2004; Farley *et al.*, 2006; Amidon *et al.*, 2008; Amidon *et al.*, 2009; Amidon et Farley, 2010; Amidon et Farley, 2012). Mis à part dans les olivines et pyroxènes, ces taux sont par ailleurs généralement mal contraints, et des variations inexpliquées avec l'altitude ont été décrites localement (Gayer *et al.*, 2004; Amidon *et al.*, 2008). Ainsi, l'utilisation du ^{3}He comme traceur de paléo-taux de dénudation ne peut se faire que dans les bassins où la géologie dispose d'une répartition suffisamment homogène d'un de ces minéraux.

Ensuite, l'hélium présent dans ces minéraux provient de multiples sources (voir chapitre 3, article 2). En particulier, une quantité parfois non négligeable du ^{3}He provient du manteau, et est présent dans les minéraux sous forme d'inclusions fluides. Pour les minéraux particulièrement anciens (>> 1 Ma), ou concentrés en U et Th (> 10 ppm), la correction "traditionnelle" (Kurz, 1986, voir Chapitre 3 article 2) de cette composante est compliquée par les concentrations importantes en ^{4}He radiogénique (Blard et Farley, 2008).

Enfin, comme on l'a vu, il peut être très utile de disposer d'un couple d'isotopes cosmogéniques, afin de contraindre une éventuelle re-exposition ou "cannibalisme" sédimentaire (§2.1.2). Or, les méthodes d'analyse et surtout les taux de production du ^{10}Be et du ^{26}Al dans les minéraux retenant le ^{3}He (notamment olivines et pyroxènes) sont soit mal, soit non connus (Nishiizumi *et al.*, 1990; Seidl *et al.*, 1997; Ivy-Ochs *et al.*, 1998; Blard *et al.*, 2008)

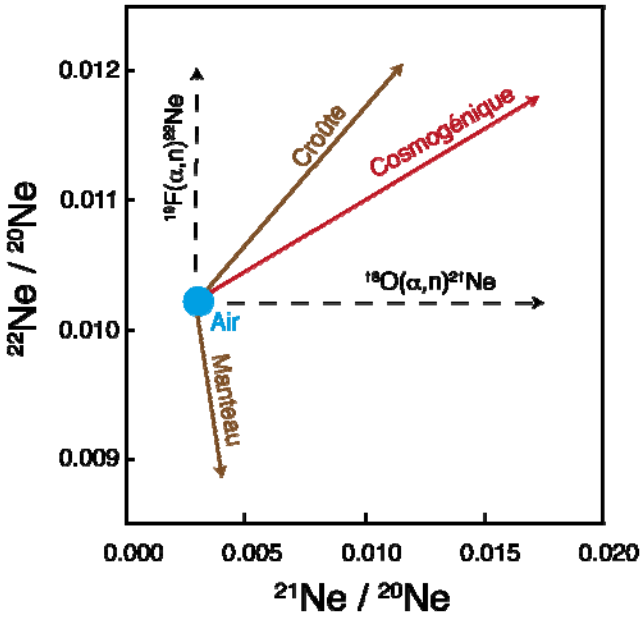

FIG. 2.3 - *Diagramme tri-isotopique du Néon, avec les droites de mélanges des différentes composantes communément rencontrées en milieu naturel (Niedermann et al., 1994). Pour les concentration trop faibles en ^{21}Ne et ^{22}Ne cosmogéniques (basses altitudes et taux de dénudation élevés), ceux-ci ne peuvent être résolus des composantes atmosphérique et crustale.*

Les ^{21}Ne et ^{22}Ne, en revanche, sont retenus dans le quartz, et leur taux de production bien documenté (e.g. Niedermann, 2000; Kober *et al.*, 2005). En théorie, ces isotopes sont donc bien adaptés à la détermination de paléotaux de dénudation (Libarkin *et al.*, 2002). Cependant, comme pour le ^{3}He, ces isotopes ont de nombreuses sources autres que cosmogéniques, notamment l'atmosphère, certaines réactions de particules alpha sur des noyaux d'oxygène et de fer (Niedermann *et al.*, 1994; Niedermann, 2002). Ces sources peuvent être identifées et quantifées dans un diagramme de mélange à trois isotopes (FIG. 2.3). Cependant, comme on le constate sur un tel diagramme, la distinction entre ces sources nécessite une concentration suffisante en ^{21}Ne et ^{22}Ne cosmogéniques. Ces isotopes souffrent donc eux aussi d'une limite de détection assez élevée (10^5 à 10^6 at.g^{-1}) et ils ne peuvent donc être utilisés que pour des taux de dénudation très faibles (<50 m.Ma^{-1} pour un bassin de 2000 m d'altitude moyenne, Blard *et al.*, 2006)

Isotope	Avantages	Inconvénients
^{3}He	• Stable • Facile et économique à mesurer	• Non retenu dans le quartz • Autres sources d'Hélium compliquent la mesure de la composante cosmogénique pour $\varepsilon > 0.1$ mm.yr^{-1} (voir Ch. 3)
$^{21}Ne/^{22}Ne$	• Stable • Facile et économique à mesurer • Retenu dans le quartz	• Autres sources de Ne à corriger • Utilisable uniquement pour très faible taux de dénudation et/ou très hautes altitudes (<50 m.Ma^{-1} à 2000m par exemple)
^{10}Be, ^{26}Al	• Retenu dans le quartz • Une seule composante, cosmogénique.	• Instables ($t_{1/2}$ =1.39 et 0.7 Ma respectivement) • Préparations et analyses longues, dangereuses, et coûteuse.
Autres isotopes (^{36}Cl, ^{14}C)	-	• Période de décroissances trop courtes pour remonter à plusieurs Ma.

FIG. 2.4 - *Comparaison des avantages et inconvénient des isotopes potentiellement utilisables pour dériver des paléo-taux de dénudation*

Ainsi, malgré leur relative simplicité d'analyse, et bien qu'ils permettent potentiellement de remonter à de très anciens taux de dénudation, les isotopes cosmogéniques stables ne restent applicables que dans quelques contextes particuliers : bassin intégralement dominé par des roches mafiques, ou très faibles taux de dénudation.

2.2.2 Limite actuelle de détection du ^{10}Be

Lors de cette thèse, l'isotope qui a fourni les meilleurs résultats reste le ^{10}Be, car, comme on l'a vu, il s'agit du mieux adapté à la majorité des contextes géologiques. Nous ne traiterons pas ici des autres isotopes cosmogéniques potentiellement utilisables dans le quartz, car ceux-ci ont des périodes de décroissance inadaptées aux échelles de temps visées ici ($t_{1/2}$ = 710 ka pour le ^{26}Al et 5.7 ka pour le ^{14}C).

2.2.2.1 Procédure d'extraction et d'analyse du ^{10}Be

La procédure d'extraction et de mesure du ^{10}Be cosmogénique est la suivante :

1 - Isolement de quartz pur à partir du sable brut par des méthodes physiques (séparation magnétique, flottation, liqueurs denses) et chimiques (dissolution séquentielle dans H_2SiF_6).

2 - Décontamination du ^{10}Be atmosphérique, adsorbé en très grandes quantités sur les grains, par lessivage à l'acide fluorhydrique HF (Brown *et al.*, 1991; Kohl et Nishiizumi, 1992)

3 - Ajout d'entraîneur (*spike*) ^{9}Be de concentration précisément connue et dissolution des grains dans HF concentré.

4 - Evaporation des fluorures (BF_3, SiF_4...) et dissolution en milieu acide.

5 - Précipitation alcaline de BeOH à pH ~9

6 - Redissolution en milieu acide et séparations du bore et autres cations par colonnes chromatographiques.

7 - Oxydation du Be en milieu nitrique (HNO_3), puis par l'oxygène athmosphérique dans un four haute température.

8 - Cathodage du BeO pour analyse au Spectromètre de Masse par Accélération (AMS). Le recours à ce type de spectrométrie très haute énergie est nécessaire pour résoudre le ^{10}Be de son ultra dominant isomasse ^{10}B.

En supposant la concentration en ^{9}Be dans l'échantillons nulle (voir ci dessous §2.2.3), la quantité absolue de ^{10}Be dans l'échantillon est alors donnée par :

(2.5)

$$^{10}Be_{echant} = \left[\left(\frac{^{10}Be}{^{9}Be} \right)_{echant} - \left(\frac{^{10}Be}{^{9}Be} \right)_{blanc} \right] \times m_{spike} \times \left[^{9}Be \right]_{spike}$$

2.2.2.2 Limites d'analyse du ^{10}Be

La limite de détection du ^{10}Be est donc contrôlée par une chaîne de trois facteurs, dont la solidité est celle de son maillon le plus faible :

- Le blanc machine du rapport $^{10}Be/^{9}Be$ de l'AMS.

A l'AMS ASTER (Accélérateur pour les Sciences de la Terre et les Risques), au CEREGE, Aix-en-Provence, où nous avons réalisé l'intégralité de nos analyses, le rapport isotopique $^{10}Be/^{9}Be$ du blanc machine fut pour toutes nos sessions d'analyse compris entre 0.2 et 1.3×10^{-15}.

Date mesure	Total coups 10Be	10Be/9Be	1σ 10Be/9Be (%)
CRPG			
23/01/2013	12	**1.42E-15**	29
12/4/2013	9	**1.10E-15**	33
12/04/2013	8	**9.84E-16**	35
18/04/2013	13	**1.15E-15**	28
	Moyenne*	**1.14E-15**	**0.175E-15**
CEREGE			
11/5/2011	23	**5.71E-15**	21
29/6/2011	8	**2.38E-15**	35
28/11/2011	4	**2.12E-15**	50
28/11/2011	4	**1.05E-15**	50
28/11/2011	7	**1.92E-15**	38
29/11/2011	5	**9.46E-16**	45
5/12/2011	21	**1.26E-15**	25
17/3/2012	7	**2.75E-15**	38
	Moyenne*	**1.49E-15**	**0.39E-15**

Table 2.1 - *Blancs (chimie +entraîneur) des séries analysées lors de cette thèse (entre 8 et 10 échantillons par séries). *Moyennes pondérées par l'incertitude.*

- **Le rapport ^{10}Be/ ^{9}Be de l'entraîneur (ou *spike*).** Le rapport des entraîneurs Be commerciaux est, en général, de ~10^{-14} (S. Merchel, communication personnelle). Ainsi, baisser la limite de détection jusqu'aux niveaux requis pour l'analyse de paléo-taux de dénudation vieux de plusieurs millions d'années requiert d'avoir recours à des entraîneurs alternatifs. Le CEREGE a ainsi, pour les échantillons les moins concentrés, préparé son propre entraîneur, fabriqué à partir de minéraux de phénakites (Be_2SiO_4) provenant d'une mine creusée à plusieurs centaines de mètres sous la surface, et donc préservés de la production de ^{10}Be *in-situ*. L'entraîneur utilisé au CEREGE possède un rapport ^{10}Be/^{9}Be <2 ×10^{-15}. J'ai également produit au CRPG notre propre entraîneur, à partir d'une autre phénakite brésilienne. Celui-ci a un rapport <4×10^{-16}, ce qui en fait un excellent choix pour des mesures de concentrations très basses.

- Le blanc de la préparation chimique (contamination par du ^{10}Be atmosphérique du laboratoire ou présent dans les réactifs utilisés). Les blancs de chimie + entraîneurs des différentes séries d'échantillons analysés pendant cette thèse sont reportés Table 2.1. On constate que le blanc total est en moyenne de 1.1 ×10^{-15} au CRPG et 1.5 ×10^{-15} au CEREGE, ce qui est à peine 2 fois supérieur au rapport de l'entraîneur. Cela signifie que le blanc de Be

apporté par les réactifs chimiques est du même ordre de grandeur que celui de l'entraîneur (~5 × 10^{-16}).

Afin d'augmenter relativement le rapport $^{10}Be/^{9}Be$ mesuré dans l'échantillon, il peut être tentant de baisser la quantité d'entraîneur (donc essentiellement de ^{9}Be) introduit. Toutefois, en dessous de ~0.3 mg de Be introduit, il devient très difficile de recueillir assez d'oxyde de Be final, ce qui provoque une baisse drastique de l'intensité du faisceau de ^{10}Be dans l'AMS. Il semble donc nécessaire de se borner à cette limite.

2.2.3 Repousser les limites

Afin d'augmenter la quantité de ^{10}Be mesurable, il peut être tentant d'augmenter tout simplement la quantité de quartz dissout. Cette méthode est efficace, mais l'expérience accumulée lors de cette thèse a montré qu'elle s'avère contreproductive au delà d'environ 150 g de quartz :

- Tout d'abord, obtenir de grandes quantités de quartz nécessite de traiter de plus grandes quantités de sable brut (pour le Tianshan par exemple, ~3 kg de sable pour obtenir 150 g de quartz de granulométrie 150-800 μm). Cela signifie, outre des coûts de transports non négligeables, de consommer plusieurs litres d'acides pour la purification et la dissolution totale (synonymes de coûts, et de risques importants pour le manipulateur).
- Le quartz n'est jamais totalement pur. Quelques minéraux accessoires peuvent subsister, et des éléments autres que Si et O peuvent être contenus sous forme de traces. Lors de l'étape (4) de la chimie (voir ci-dessus), ces cations vont avoir tendance à former des fluorures (notamment CaF_2 et MgF_2). Or, ceux-ci sont très insolubles, et peuvent séquestrer le Be, réduisant drastiquement le rendement de la procédure. Par ailleurs, ces cations peuvent également saturer les colonnes chromatographiques (étape 6).
- Le ^{9}Be naturel, en général négligeable dans du quartz correctement purifié, pour de faibles masses d'échantillons (<50 g), peut devenir significatif face au ^{9}Be introduit par l'entraîneur et fausser l'équation 2.5.

Ainsi, la méthode consistant à simplement augmenter la quantité de quartz analysé, que nous avons tenu à utiliser au début de cette thèse (avec par exemple des quantités allant jusqu'à 300g de quartz...) s'avère difficile et même contre-productive. Cette limite de taille d'échantillon reste cependant dépendante du budget, de la procédure et de l'équipement analytique utilisé dans chaque laboratoire. Dans notre cas, des complications lors de la chimie, en particulier à l'étape d'évaporation, ont été constatées à partir de ~150 g de quartz.

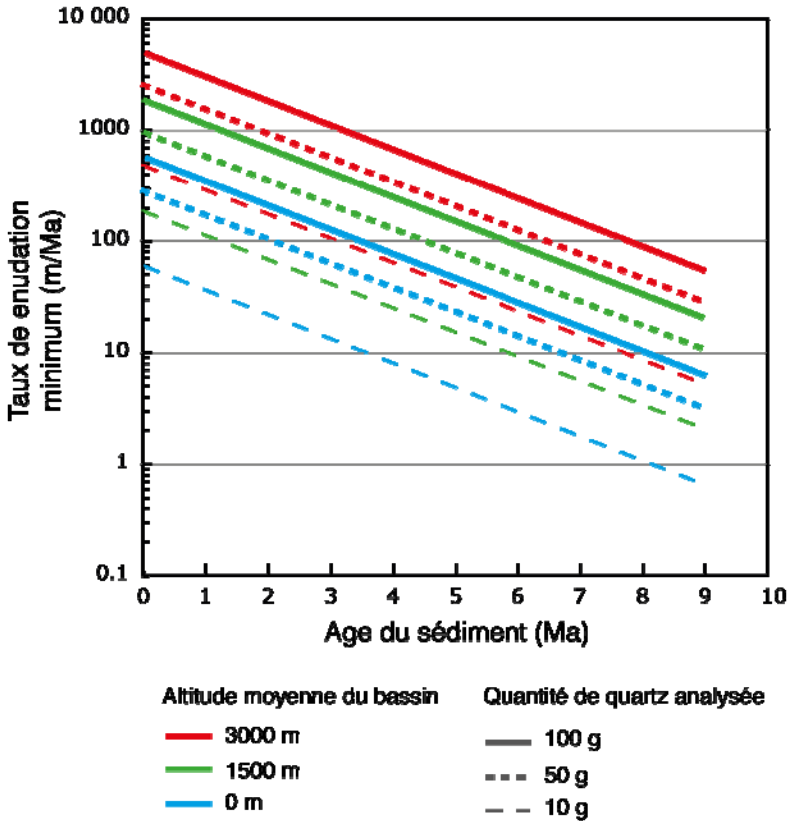

FIG. 2.5 - *Taux de dénudation minimum mesurables par le ^{10}Be, en fonction de l'âge du sédiment, pour différentes altitudes moyennes de bassin versant (ici pour une latitude de 45°), et différentes masses d'échantillon. On suppose un rapport ^{10}Be/^{9}Be de blanc de chimie+entraîneur de ~2 ×10^{-15}, un ajout (minimal) de 0.3 mg de ^{9}Be (i.e. 2 ×10^{19} atomes), et un rapport signal/blanc de 10.*

La meilleure méthode pour encore repousser la limite de détection du ^{10}Be à l'avenir restera probablement d'améliorer le blanc analytique et les rendements de la spectrométrie de masse par accélération.

2.3 Synthèse : le candidat idéal

Le contexte géologique parfait à l'enregistrement de paléo-taux de dénudation grâce aux isotopes cosmogéniques serait donc (en plus de toutes les conditions également requises dans l'actuel (voir §1.3.1) :

- Un bassin versant le plus élevé en altitude, et un taux de dénudation le plus faible afin d'assurer une forte concentration initiale.
- Des traceurs de sources potentiels (minéralogiques, géochimiques) au sein de ce bassin versant.
- Un bassin versant dont la topographie n'a pas varié significativement, ou dont on peut quantifier précisément les évolutions hypsométriques
- Une zone de dépôt la plus basse en altitude, et un taux d'enfouissement très rapide afin de minimiser la concentration post-dépôt.
- Une réexposition récente très limitée (incision très rapide dans une gorge, affleurement anthropogénique)
- Une série sédimentaire continue.
- Une datation haute résolution, précise et indépendante, de la série sédimentaire.

Dans l'idéal, on pourra même ajouter : un bassin versant comprenant de manière homogène des minéraux mafiques jeunes (moins de quelques millions d'années), ou soumis à un taux de dénudation extrêmement faible, afin de pouvoir utiliser les isotopes cosmogéniques stables (^{3}He et ^{21}Ne).

Chant d'Ombre

(...)

Me faudra-t-il lâcher les tempêtes de toutes les cavernes magiques du désert ?

Rassembler les sables aux quatre coins du ciel vide, en une ferveur immense de sauterelle ?

Puis dans un silence immémorial, le travail du froid apocalyptique ?

Glissent déjà tes paroles confuses de femme, comme des plaintes d'heureuse détresse, on ne sait

Et les pierres, brusque et faible chute, vont prendre le fracas des cataractes.

(...)

Léopold Sédar Senghor,

Chants d'Ombre

Chapitre 3
Questions(s) de granulométrie.

Vouloir étendre l'utilisation des isotopes cosmogéniques à d'anciennes séries sédimentaires, avec toutes les incertitudes supplémentaires afférentes, requiert *a fortiori* d'en contraindre les limites dans les sédiments modernes. Or, comme évoqué précédemment (§1.3), les contextes géologiques d'études remplissent souvent de manière satisfaisante les conditions requises à cette méthode, mais jamais parfaitement.

Dès le début de cette thèse, il fut clair qu'une partie de mon travail devrait être mené sur les bassins versant actuels des zones cibles, afin de tester la sensibilité des taux de dénudation dérivés des isotopes cosmogéniques à plusieurs complexités locales. Plus prosaïquement, ces études débutèrent au tout début de ma thèse, à l'occasion des premières expéditions sur le terrain, une période d'encore prospection quand à la face par laquelle attaquer le coeur de mon sujet. Aussi, ces deux études, que l'on peut qualifier de techniques, peuvent de prime abord sembler secondaires à l'économie de ce manuscrit. Il est même à craindre qu'elles paraissent rébarbative pour les non-spécialistes des isotopes cosmogéniques. Néanmoins, elles proposent des avancées et des points de prudence à respecter pour leur utilisation, dans deux contextes très différents : l'Himalaya central et les plateaux basaltiques Ethiopiens. Elles auront, du reste, permis de me familiariser avec ces zones et la "cuisine" cosmogénique.

Le premier article présenté traite de la dépendance de la concentration en ^{10}Be à la granulométrie étudiée, dans le cas d'un bassin versant Himalayen dominé par d'actifs glissements de terrain. Il fut motivé par un certain nombre d'articles de la littérature ayant alors montré l'influence potentiellement importante des mouvements de masses épisodiques sur le signal cosmogéniques (Brown *et al.* 1995; Niemi *et al.* 2005; Yanites *et al.* 2009), voir même de l'utilisation de leur signal particulier pour quantifier les provenance de sédiments (Belmont *et al.*, 2007).

Le second traite de l'influence de l'hélium magmatique dans la mesure de l'hélium cosmogénique, en fonction de la granulométrie étudiée, dans deux rivières éthiopiennes. Cette étude est le prolongement d'un travail débuté lors de mon master. Il fut motivé par l'apparente variabilité inter-aliquots du ^{3}He cosmogénique mesurée dans des rivières éthiopiennes (Pik *et al*, en préparation), et alors que cet isotope stable et les dépôts sédimentaires de l'Afar semblaient des cibles de choix pour l'étude de paléo-taux de dénudation.

Cosmogenic ^{10}Be grain size-dependent concentration and erosion dynamics of a landslide-dominated Himalayan watershed

(Submitted to Geomorphology)

Nicolas Puchol[1], Jérôme Lavé[1], Maarten Lupker[1,2], Florian Gallo[1], Pierre-Henri Blard[1], Christian France-Lanord[1], ASTER Team[3,+]*

[1]Université de Lorraine - CNRS, CRPG, 15 rue Notre-Dame des pauvres, 54500 Vandoeuvre-lès-Nancy, France

[2]ETH, Inst. f. Geochemie und Petrologie, Clausiusstrasse 25, 8092 Zurich, Switzerland

[3]Université Aix-Marseille, CNRS-IRD-Collège de France, UM 34 CEREGE, Technopôle de l'Environnement Arbois-Méditerranée, BP80, 13545 Aix-en-Provence, France

[+]Maurice Arnold, Georges Aumaître, Didier L Bourlès, Karim Keddadouche.

*Corresponding author: puchol@crpg.cnrs-nancy.fr, +33 3 83 59 42 11

(other authors: jlave@crpg.cnrs-nancy.fr, maarten.lupker@erdw.ethz.ch, fgallo@crpg.cnrs-nancy.fr, blard@crpg.cnrs-nancy.fr, cfl@crpg.cnrs-nancy.fr, aster@cerege.fr)

Contents of this paper

Abstract

To document recent or Late Quaternary erosion rates at the scale of a small watershed, as well as of a whole range, the use of in-situ terrestrial cosmogenic nuclides (TCN) in river sediments, such as ^{10}Be, has been generalized during the past decades. In mountainous settings, however, landslides have been recognized to potentially induce a twofold complication on the cosmogenic nuclides budget. First, they may episodically deliver large amounts of sediments with low TCN concentration to the river channel. Second, they may generate a grain-size-concentration dependence in said sediments. However, studies exploring such grain-size dependences in landslide-dominated areas have led to various conclusions and the underlying mechanisms are still poorly understood. We focused the present study on the Khudi Khola river basin, a small drainage basin of the central Himalayas. This area has steep slopes, heavy rainfall, and high sediment production rates. Importantly, the watershed displays a large active landsliding area.

We analyzed in-situ ^{10}Be in various grain sizes, ranging from 75 μm up to ~ 4cm in sediments from five locations: upstream, downstream, and in the small tributaries draining the landslides. In all sampling locations, including upstream of the landslides, the finest grains (75-250 μm) are between 2 and 4 times more concentrated in ^{10}Be than the biggest clasts (>4.7 mm).

We develop a numerical model of a slope including a low background soil erosion and episodic large mass-wasting denudation. We then implement in this model an average grain-size coarsening with soil depth. This simulation shows that a scenario where landslides deliver to the channel coarse grains, less concentrated in TCN, from deeper provenance, is compatible with the data available for this valley. Best-fit estimates of the model parameters suggest a recurrence times for a major landslide on the same slope of 3000 up to 9000 years, and a long-term average landslide denudation rates of 1.7-4.7 mm.yr^{-1}.

The fact that the TCN concentration anti-correlation to the grain-size is also observed directly upstream and 5 km downstream of the landsliding area suggests that almost all of the sediment carried by the river derives from ancient landslides while almost no erosion occurs from soil-mantled slopes.

Despite these complications, denudation rates directly derived from the TCN concentrations, from our model and from previously published data are in the same

order of magnitude, around ~ 2mm.yr^{-1}. On the other hand, a variability of a factor 3 remains between these various surveys, depending on the location and the year of sampling. Thus, although TCN-derived average denudation rates appear to somehow remain robust, even in fast-eroding terrains dominated by landslides, great caution is required for the application of quantitative studies in such settings.

1 Introduction

To document recent or Late Quaternary denudation rates at the scale of a small watershed, as well as of a whole mountain range, the use of terrestrial cosmogenic nuclides (TCN), such as ^{10}Be in fluvial sediments, has been generalized during the past decade.

TCN are produced by the secondary cosmic flux in the top uppermost meters of the Earth's surface, at a rate decreasing exponentially with depth. When a surface undergoes a steady and continuous denudation by physical and chemical weathering, the concentration of a given cosmogenic nuclide in this surface can be directly linked to its denudation rate (Lal, 1991).

A river-sand, sampled at the outlet point of a watershed integrates sediments from the entire watershed. Under the assumptions of fast denudation relative to the radioactive decay of the considered nuclide, steady denudation for a long period of time, homogeneous lithology with respect to the analyzed mineralogy, proper mixing and fast transfer of the sediments through the catchment, the average concentration of cosmogenic nuclides in the river sand is directly linked to the average denudation rate of the whole upstream watershed (Brown *et al.*, 1995; Granger *et al.*, 1996). Thus, one can theoretically calculate a basin-averaged denudation rate from a single analysis of cosmogenic nuclide concentration in river sediments. An interesting property of cosmogenic nuclides is that so-derived denudation rates are averaged on the time scale needed for the analyzed mineral grain to travel thought the uppermost ~1m of the surface (~10^2 years, for very fast denudation rates in the order of mm/yr, up to 10^5 years for very slow denudation rates in the order of m/Myr), thus avoiding daily and seasonal fluctuations, or even the influence of short Milankovitch climatic cycles in the case of low denudation rates (von Blanckenburg, 2005; Schaller and Ehlers, 2006).

Although all of these geological limitations are rarely totally fulfilled in natural settings, this method at least provides an order of magnitude estimate of denudation rates on time scales, and with a precision, inaccessible to other complementary techniques such as sediment gauging and budgeting, or low temperature termochronometry.

In steep mountainous settings, additional complexity arises: one of the major limitation to the technique is coming from mass wasting and landsliding erosional processes, that usually represent a significant part, or even the totality, of the material delivered to the channels (Hovius *et al.*, 1997). In the absence of major landslide activations, slowly weathering and eroding hillslopes provide a TCN-enriched material to the fluvial network. Conversely, periods of deep-seated landslide activation, either storm- or earthquake-triggered, deliver large amounts of sediments from depths below the attenuation length of cosmogenic nuclides production (> 1 - 10 m) and therefore devoid of TCN, in other words with low average TCN concentration. As a consequence, fluvial sediments at the outlet of a small watershed are presumed to present large temporal variations of their cosmogenic nuclide content. These effects can preclude the use of the method in areas dominated by landslides or could on average lead to significant underestimation of the "long term" denudation rates because of the rareness of the large landslides events, unless the catchment area is large enough to produce river sands averaging these stochastic events (Niemi *et al.*, 2005; Reinhardt *et al.*, 2007; Yanites *et al.*, 2009).

Moreover, in these landslide-dominated settings, another complexity need to be considered: it has been indeed proposed that the deeper material produced by landslides, which is less concentrated in TCN, is on average coarser than that of the shallow material, because it is derived from fresher and less weathered or fragmented bedrock or saprock (Brown *et al.*, 1995). If so, landslides can produce sediments with variable TCN concentration depending on the analyzed grain size (Brown *et al.*, 1995; Belmont *et al.*, 2007; Aguilar *et al.*, 2013). This TCN size-dependent concentration in clasts of landslide-dominated watersheds, while preventing accurate estimation of average denudation rates if not accounted for, could on the other hand be used to constrain sediment mixing or erosion dynamics in the drainage area (Belmont *et al.*, 2007). While TCN concentrations have been observed to depend on grain size in a small hilly watershed of Puerto Rico and interpreted in terms of landslide and clast size increase with depth below surface (Brown *et al.*, 1995), this relationship has however not been observed in all landslide-dominated landscapes (Clapp *et al.*, 2002; Safran *et al.*, 2005; Kober *et al.*, 2012) .

Nevertheless, in most papers, the influence of grain size on the TCN concentration has been tested on only a few grain size fractions, usually, a generic coarse sand (200-1000 μm, which is the most frequently used fraction for deriving basin average denudation rates) and pebbles (> several centimeters). To our knowledge, only Brown *et al.* (1995) and Clapp *et al.* (2002) have explored a larger spectrum of grain sizes. Yet, systematic differences in concentration between grain sizes routinely used in TCN studies could be an important issue.

Most studies consider the same size ranges, by habit or for their abundance and ease of preparation.

In this study, we analyzed 6 to 7 fractions of sediments (ranging from 150 μm up to >4.7 mm) from various locations of a small watershed of the central Himalayas. This approach is partly similar to the one tested by Clapp *et al.* (2002). However, this previous study was carried in an arid, low erosional environment. The present study is focused on a zone with steep slopes, heavy monsoon rainfall, high denudation rates, and importantly affected by active landslides. It offers the opportunity to directly test their role on TCN concentration by sampling several locations: upstream, just below an active major landsliding area, or further downstream.

By this approach, we intend to constrain both the influence of this active landslide on the average cosmogenic signal and its dependence on the grain size. After a qualitative discussion of the results, we present a model of erosion by landslide stripping and explore the possibility to use TCN size dependency to understand sediment dynamics on hillslope and during transport, as previously pioneered by Belmont *et al.* (2007) or Aguilar *et al.* (2013). We finally compare our results with previously published denudation rates in this area obtained by various methods and discuss the validity of TCN-derived average denudation rates in such humid, active, steep slope environments.

2 Setting

2.1 Geological and geomorphologic setting

The Khudi Khola valley is located southeast to the Annapurna massif, in central Nepal (Fig 1) along the southern front of the High Himalaya. The Khudi Khola is an affluent of the Marsyandi River (Fig 1), which itself drains into the Narayani river.

The Himalayan Main Central Thrust (MCT) crosses the southern part of the Khudi Valley. It separates schists, black shales and marbles of the upper sequence of the Lesser Himalaya series in the south, from quartzo-pelitic gneisses of the high Himalayas series in the North (Colchen M., 1986).

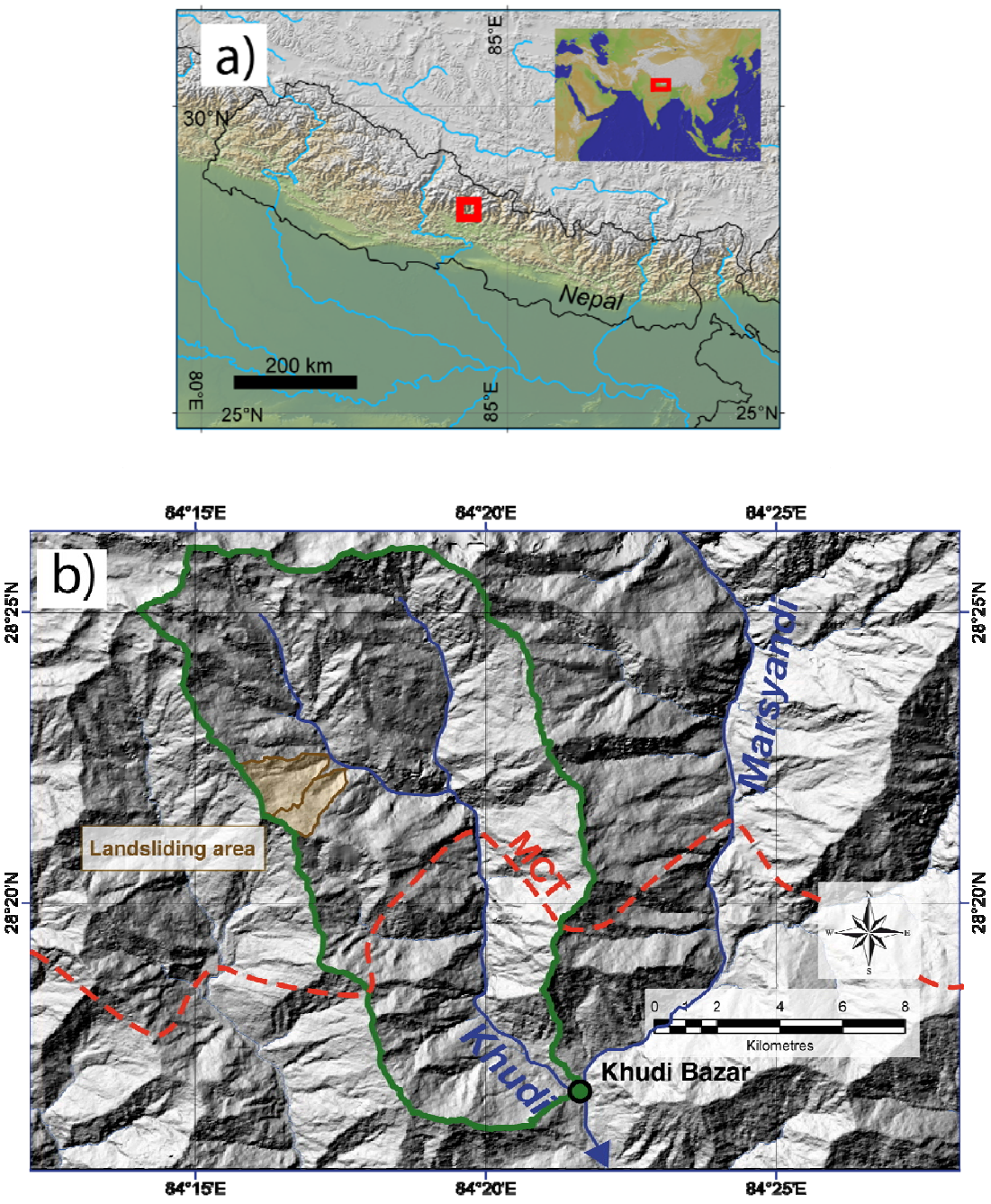

Fig. 1 - Geographic setting. *a) Relief map and Location of the study area. b) Zoom on the Khudi basin, based on a shaded SRTM digital elevation model. The Khudi watershed is delimited in green. The approximate trace of the Main Central Thrust, represented in red, separates black shales of the lesser Himalaya series in the south, from quartzo-pelitic gneisses of the high Himalayas series in the North. The two landslides areas are shaded in light brown.*

This region is marked by a gradient of heavy precipitation, increasing from south to north with intense monsoon rainfalls peaking at >3 m.yr^{-1} (Putkonen, 2004), by steep slopes, active micro-seismic activity all along the High Himalaya southern front (Ni and Barazangi, 1984; Pandey *et al.*, 1995), and by strong ground shaking by major earthquakes (Mw > 8) probably every hundred to thousand years (Lave and Avouac, 2000; Lave *et al.*, 2005). As a consequence, denudation rates of this region are ones of the highest of the Himalayas. The whole Narayani basin erodes at an average rate of 1.7 ± 0.4 mm.yr^{-1} (Lupker *et al.*, 2012). Moreover, in this basin, the southern front of the High Himalayas, where the Khudi valley is located, is expected to erode at rates roughly two times higher than that average (Lave and Avouac, 2001). TCN-derived denudation rates (Niemi *et al.*, 2005; Godard *et al.*, 2012) as well as suspended load flux measurements over a period of 4 yrs (Gabet *et al.*, 2008) at the outlet of the Khudi watershed confirm the high erosional activity at rates between 2 and 3.5 mm.yr^{-1}. This erosional activity seems to have been prevalent during the Quaternary with mean denudation rate of the Khudi basin of 2 to 4 mm.yr^{-1} (Blythe *et al.*, 2007; Whipp *et al.*, 2007).

Along with this sustained denudation, the Khudi valley is particularly well suited to document erosional dynamics of the southern front of the High Himalaya: the impact of anthropogenic activity has remained limited to the southern and lowest part of the catchment, its upper crests are presently not glaciated, and older glacial morphology and sediments cover a very limited surface of the basin, at its extreme north and north-west (Pratt-Sitaula *et al.*, 2011).

2.2 Recent landslide and erosional dynamic

In this part of the Himalayas, physical erosion is presumably dominated by episodic mass wasting processes such as landslides and debris flows (Gabet *et al.*, 2004). The Khudi valley features a major active landsliding area composed of two active landslides covering ~0.2 km^2 for the northern one (Fig. 2a and b) and ~0.5 km^2 for the southern one, and located between 2500 and 2900m a.s.l. Recent activity of the southern one (i.e. since the beginning of this survey in 2009) is expressed by upward and lateral recession of the landslide rims through collapse of 5 to 50 m wide slices towards the bottom of the landslide talweg (Fig. 2a, c and d). This observation is confirmed by satellite images and automatic cameras monitoring the daily evolution of the southern landslide. This monitoring indicates that, during the monsoon months, the landslides rims collapse and progressively creep toward the talweg and that, during heavy rainfall events, an ephemeral stream washes out and transfers those loose sediments further downstream toward the Khudi River.

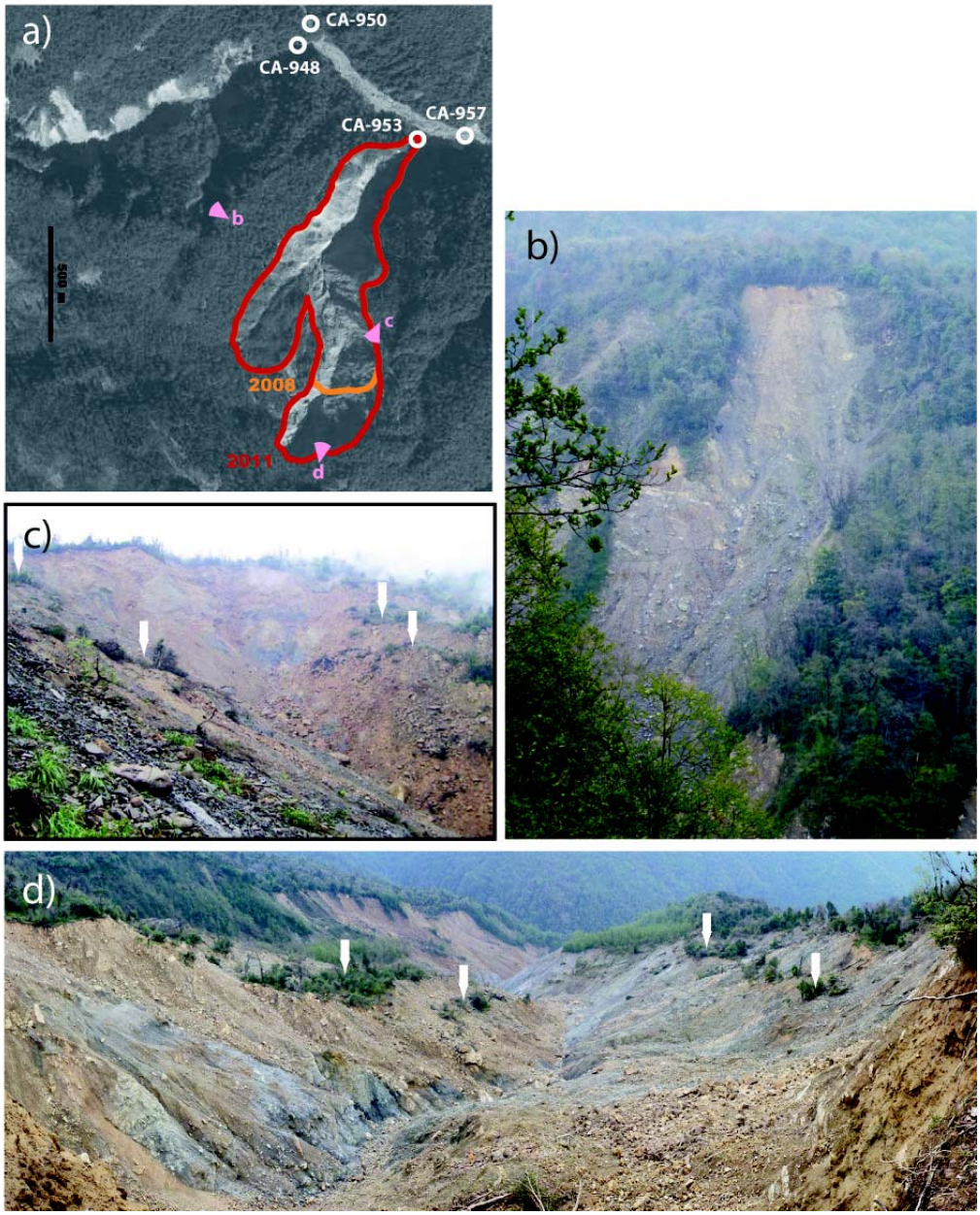

Fig. 2 - Western Khudi landslides. a*) Evolution of the southern landsliding area from satellite images between 2008 and 2011, including sampling points (circles) and viewpoints (pink slice of pie) for pictures of the major scar of the northern landslide zone (b), and of the southern landslide, as seen toward its top (c) or its bottom (d). On the pictures of the southern landslide, white arrows indicate slices, still vegetated at their summit, that were detached from the landslide rims and progressively slide and migrate toward the landslide talweg bottom.*

Such transport in Khudi River is not instantaneous but potentially delayed by temporary sediment storage since, as observed on Fig.2a, the channel just downstream the confluence of the Khudi with the landslide (i.e. below sample CA-950) suddenly enlarges due to sediment accumulation..

This deposition zone, which corresponds from field observations to a deposit of mostly metric boulders, displays variable channel width from 10m in narrow gorge sections up to 100m in more open valley reaches. Satellite image observation indicates that this storage has been present and stable for at least a decade. We suspect this zone to presently buffer the transport of metric or sub-metric boulders, whereas it would almost act as a bypass for the finest load (silt, sand, and gravels).

Finally, camera monitoring and direct observations during pre- or monsoon storm events indicate that the small streams draining the landslide, as well as the Khudi River in its downstream part, carry very frequently large load of suspended sediments, while tributaries draining sub-basins devoid of major landslide carry almost only clear water. We therefore strongly suspect that most of the fine sediments carried by the Khudi River come from the two landslides area. Observation of the present channel enlargement just downstream the landslides area, as described above, as well as the overwhelming dominance of gneissic pebbles relative to the Lesser Himalayas ones, in the downstream part of the Khudi, indicate that our inference of a dominant landslide source could also be applied for bedload.

2.3 Sampling

In order to document the TCN signal from these two active landslides and to compare it with the signal of wider and more integrative reaches, we sampled sands and gravels from 5 locations (Fig 2a):

- in the river bed 100 m upstream from the northern landslide (CA-950),
- in the small tributary draining the northern landslide (Fig. 2b), at its outlet point, ~50 m from its confluence with the Khudi river (CA-948),
- in the small tributary draining the southern landslide (Fig. 2c and d), at its outlet point, ~20 m from its confluence with the Khudi river (CA-953),
- in the river bed, 300 m downstream the southern landslide (CA-957),
- 5 km downstream the landsliding area, also downstream the confluence with the northeastern main tributary of the Khudi, near the Probi village (CA-964).

Each bulk sample consists of ~2 kg of unsorted sands, with maximum clasts size of ~4 cm.

All of our sampling points are associated to sub-basins that drain north of the MCT, i.e. only in the HH gneissic zone (sampling point of CA-964 drains however ~1% of upper LH units), which ensures a relatively uniform quartz content of the source bed rocks.

3 Methods and results

3.1 Samples treatment and ^{10}Be measurements

River and landslide bulk sands and pebbles were first sieved under water flux and vibrations into 6 granulometric fractions: 75-250 μm, 250-500 μm, 500-1000 μm, 1-2 mm, 2-4.7 mm and >4.7mm. One sample (CA-964) was further sieved into a 75-150 μm and a 150-250 μm fraction. Fractions >1 mm in size had to be crushed to release individual quartz minerals. The crushing products were sieved in two fractions (100-250 μm and 250-1000μm) in order to facilitate minerals separations and purification for further Be ion exchange chemistry (see bellow). Minerals with a low magnetic susceptibility (essentially quartz, feldspar, kyanite and muscovite) were isolated with a magnetic separator.

Then, quartz and kyanite were isolated from most feldspar and muscovite by froth flotation. Remaining feldspar and muscovite in the quartz-enriched fraction were dissolved sequentially in hexafluorosilicic and hydrochloric acid (H_2SiF_6 + HCl). After this step, samples were composed of almost pure quartz, except a few kyanite minerals (<1% mass.). Any remaining atmospheric ^{10}Be was removed by three sequential leachings in concentrated hydrofluoric (HF) acid in stoichiometric amount so as to remove ~10% of the total quartz weight at each of the three steps (Brown *et al.*, 1991).

Purified quartz was dissolved in concentrated HF, after addition of 101 mg of an in-house 3.025 10^{-3} g/g ^{9}Be carrier solution (Merchel *et al.*, 2008). It has to be noted that, while quartz dissolutions were completed, kyanite minerals were not dissolved in the concentrated HF, and removed after decantation. Beryllium was then separated by anion and cation exchange chromatographic columns, and alkaline precipitations.

Purified BeO targets were analyzed at the French national Accelerator Mass Spectrometer (AMS) facility ASTER, located at CEREGE (Aix-en-Provence, France). ^{10}Be/^{9}Be ratios were normalized to the NIST SRM 4325 standard, which ^{10}Be/^{9}Be value is (2.79 ± 0.03) ×10^{-11} (Nishiizumi *et al.*, 2007)

Analytical blank ratios were (2.5 ± 0.7) ×10^{-15} for the first analysis session (granulometric fractions <1mm) and (5.7 ± 1.2) ×10^{-15} for the second one.

3.2 ^{10}Be Results

For all five samples (Table 1 and Fig 3a), there is a clear dependency of the ^{10}Be concentration on the clasts size. Small fractions (>0.5 mm) are systematically between two and three times more concentrated than the coarser ones (>2 mm), except for sample CA-948 from the northern landslide, for which the 2-4.7 mm fraction displays a surprisingly high ^{10}Be concentration compared to the adjacent size fraction 1-2 mm. For this aliquot, we presumably suspect a chemical contamination in the lab, a procedure mistake, or a "nugget effect" from one or several extremely concentrated grains in this sample. Unfortunately there was not sufficient material left to duplicate the analysis in this size fraction, and to try to confirm or not this seemingly abnormal value. In the following, we will not take into account this sample in the discussions even if we kept it for calculation of Section 4.2.

Besides the grain-size-concentration negative relationship, a striking result is that the river sand displays the same size-concentration relationship wherever they are sampled just downstream active landslides (CA-948, CA-953 or CA-957), from sub-basin *a priori* exempt of deep-seated landslide (CA-950) or from further downstream (CA-964). ^{10}Be concentration results confirm also a clear dominance in Khudi sediments of the landslides material at least just downstream the landslide area (CA-957): using the raw ^{10}Be concentrations as a classical geochemical mixing tracer between the 3 contributing end-members represented by CA-950, CA-948 and CA-953 (Fig. 2a), the mass balance indicates that almost all the sand sampled in CA-957 is coming from the landslides sources. In the following section, we will assume such a close landslide provenance for CA-957 sediments.

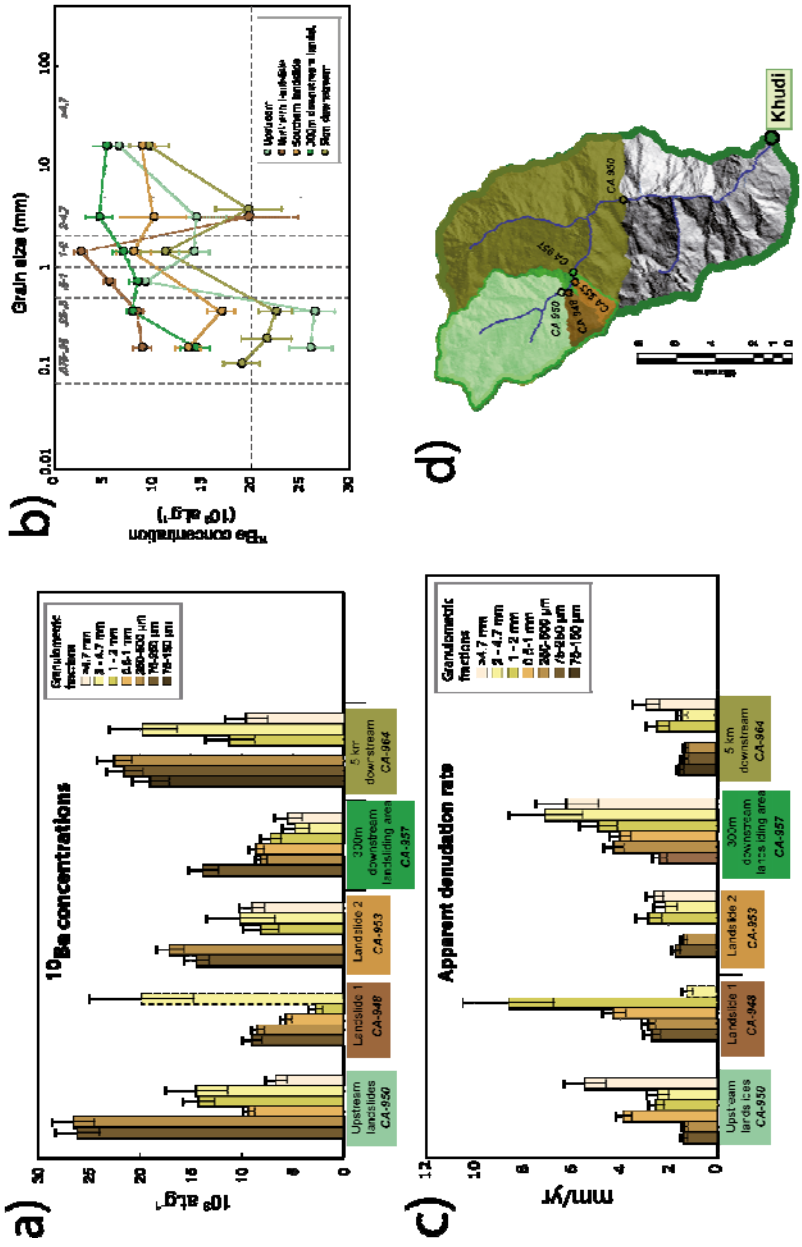

Fig. 3 - ^{10}Be Concentrations and derived denudation rates. *a) ^{10}Be concentrations (in 10^3 at.g^{-1}) sorted by clasts size and location. b) Calculated average denudation rates (mm.yr^{-1}), derived from the ^{10}Be concentrations, sorted by grain size fractions and location. c) Location of the sampling points and associated drainage basins. The color code for each zone is the same in all these figures. The 2-4.7 mm sample of the northern landslide (CA-948) is represented in doted lines because it displays an apparent anomalous high concentration, potentially resulting from a "nugget effect" induced by several very concentrated clasts*

Sample	Location coordinate (decimal deg.)	Drainage Basin Area (km2)	Average 10Be Production Rate (at.g-1.yr-1)	Grain Size (mm)	Analyzed Quartz Mass (g)	10Be (10^3 at.g-1)	1σ	Theoretical Denudation rate (mm.yr-1)	1σ
Upstream Landslide CA-950	N 28.37559 E 84.28865	27.6	37.7	0.072-0.25	32.2	26.1	2.2	1.4	0.1
				0.25-0.5	132.3	26.5	2.1	1.3	0.1
				0.5-1	355.3	9.2	0.6	3.8	0.3
				1-2	54.3	14.2	1.5	2.5	0.3
				2-4.7	43.4	14.4	3.1	2.4	0.5
				>4.7	62.6	6.6	1.1	5.4	0.9
Northern Landslide CA-948	N 28.37474 E 84.2887	2.9	24.8	0.075-250	26.7	8.9	0.9	2.6	0.3
				0.25-0.5	63.8	8.4	0.7	2.8	0.3
				0.5-1	87.7	5.6	0.5	4.2	0.5
				1-2	32.3	2.7	0.7	8.5	1.9
				*2-4.7**	*26.1*	*19.7*	*5.1*	*1.2*	*0.2*
Southern Lansdlide CA-953	N 28.37177 E 84.29403	1.8	23.8	0.075-250	48.6	13.6	1.2	1.6	0.2
				0.25-0.5	44.2	17.0	1.4	1.3	0.1
				1-2	24.5	8.0	1.8	2.8	0.5
				2-4.7	44.3	10.1	3.4	2.1	0.5
				> 4.7	134.4	8.9	1.2	2.5	0.4
Downstream Landslides CA-957	N 28.3713 E 84.29591	33.2	35.3	0.075-250	29.2	14.4	1.5	2.3	0.3
				0.25-0.5	67.7	7.9	0.6	4.2	0.4
				0.5-1	62.2	8.4	0.8	3.9	0.4
				1-2	33.7	7.0	1.0	4.8	0.8
				2-4.7	34.3	4.6	1.4	7.0	1.5
				>4.7	146.6	5.3	1.4	6.1	1.3
Downstream Probi CA-964	N 28.33483 E 84.3448	83.6	28.7	0.075-0.15	11.2	19.0	1.8	1.4	0.2
				0.15-0.25	50.1	21.6	2.6	1.3	0.2
				0.25-0.5	105.4	22.5	1.7	1.2	0.1
				1-2	28.0	11.3	2.5	2.4	0.5
				2-4.7	22.4	19.7	3.4	1.4	0.2
				>4.7	73.2	9.6	2.0	2.8	0.5

Table 1 - Analytical results and sample info. *The sample locations can be spotted on the figure 4c. All the uncertainties are at 1σ*

** The 2-4.7mm sample of the southern landslide displays an abnormally high 10Be concentration. This can be due to a chemical pollution of the sample or the "nugget effect" of one or several very highly concentrated grains in this sample.*

4 Regolith stripping model and sediment size-dependent TCN concentration

The dependence of the ^{10}Be concentration on the clasts size, observed below the two small basins affected by the active landslides (CA-948, CA-953 and CA-957), lines up with previous observations made by Brown *et al.* (1995) in similar, but less steep, terrain.

(Brown *et al.*, 1995) suggested a role of the landslides and of the vertical size grading in the regolith to explain their data: the deeper material carried to the river by landslides would have a low concentration in TCN because of the exponential decrease of their production rate with depth, and would be on average coarser because it comes from less weathered and disaggregated rocks. With such a mechanism, the ~3 ratio observed between the 75-250 μm and the 1-2 mm fractions in the northern landslide would represent an apparent depth provenance difference of ~0.7 m, if all the medium size sand (75-250 μm) and the gravel size (>2 μm) would be exclusively coming from the top soil and this deeper level, respectively. This depth difference would fall to ~0.3 m for the Southern landslide.

Field observations indicate that the slices that detached during the past 4 years from the southern landslide rim are at least 10 m-deep. To explore more quantitatively size segregation effect, we consider in the following a simplified model that accounts for mixing of the whole column of material that slides down the bottom of the landslides area.

4.1 Landslide and grain size vertical grading model

4.1.1 Landslide depth and recurrence time model

Because most of our observations have been made on the southern landslide, in the following we consider it as our reference to build our model. During the last 4 years, erosion was carried on by the progressive upward retreat of the margins of the landslide lips, through collapses of slices of a z_c thickness from the top or lateral rims (Fig. 2c, 2d and 4a). After collapse on the flanks of the landslide, either rapid or progressive during monsoon, the sediments are transported during the major precipitation events of the monsoon season by ephemeral streams in the talweg of the landslide, and then further downstream by the Khudi River.

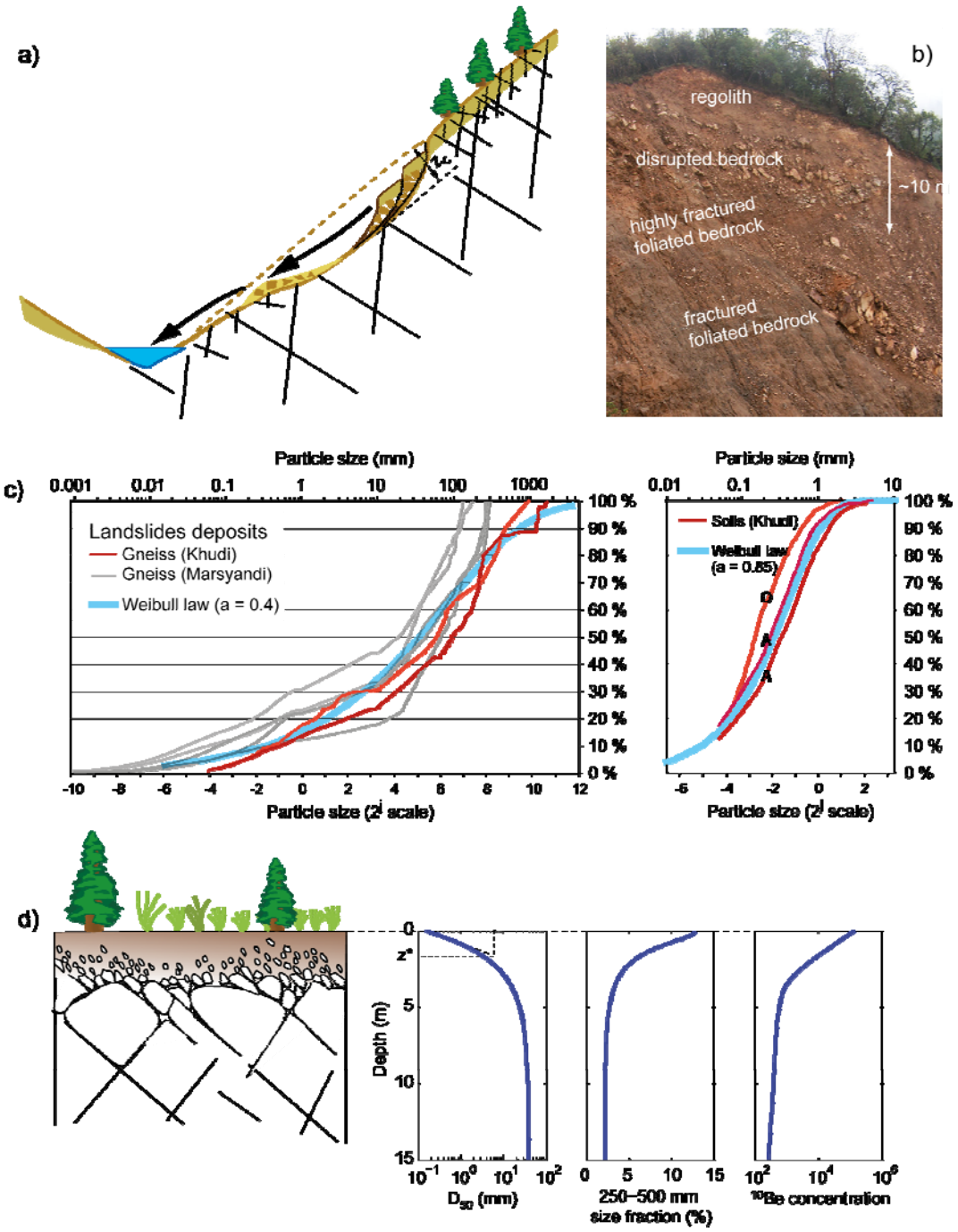

(caption on the next page)

Fig. 4 (previous page) - Landslide evolution, landslide material characteristics, and model.

a) *Schematic cross-section of the landsliding hillslope with thickness z_c.*

b) *Picture of the upper rim of the southern landslide that exposed the change of texture with depth. The foliation and structure of the lower bedrock seems preserved but the bedrock is densely fractured and already partly weathered so that it collapse produces significant fraction of medium and small particles..*

c) *Particle size cumulated distribution of the landslide deposits material from landslide occurring in Himalayan gneisses (left) and of the soil material (O = textural layer O in a soil profile along the western Khudi crest; A = textural layers A or B in soil profile exposed at the rim of the southern landslide) .*

d) *Typical profiles in the model of the evolution with depth of the median size material once collapsed from the rim (i.e. ready to be exported into the landslide talweg), of the size fraction 250-500μm proportion, and the cosmogenic concentration (Note that in the particular case of a uniform α, the median size, D_{50}, of the fragments follows the same variation with depth as Δ).*

During this latter process, the sediments are presumed to be well homogenized and the mean concentration in cosmogenic nuclide reflects the average concentration over the slice thickness z_c.

For a homogeneous particle size distribution with depth in the soil, regolith and shallow bedrock, this average concentration writes:

(1)

$$\overline{C}(z_c,t_0)=\frac{1}{z_c}\int_0^{z_c}\sum_k \frac{P_k}{\varepsilon_0\frac{\rho}{\Lambda_k}+\lambda}e^{-\frac{\rho}{\Lambda_k}z}\left(1-e^{-(\varepsilon_0\frac{\rho}{\Lambda_k}+\lambda)t_0}\right)dz$$

i.e.

$$\overline{C}(z_c,t_0)=\sum_k \frac{P_k}{\varepsilon_0\frac{\rho}{\Lambda_k}+\lambda}\left(1-e^{-(\varepsilon_0\frac{\rho}{\Lambda_k}+\lambda)t_0}\right)\frac{1}{z_c}\frac{\Lambda_k}{\rho}\left(1-e^{-\frac{\rho}{\Lambda_k}z_c}\right),$$

Where P_k are the surface local production rates by spallation, slow muons capture and fast muon radiations (at.g^{-1}.yr^{-1}), ρ the density of the bedrock (2.65 g.cm^{-3}), Λ_k are the typical attenuation mass for neutrons, fast and slow muons ($\Lambda_n \sim 160$, $\Lambda_{sm} \sim 1500$, $\Lambda_{fm} \sim 4500$ g.cm^{-2})(Braucher *et al.*, 2003; Braucher *et al.*, 2011), λ is the ^{10}Be decay constant (4.997×10^{-7} yr^{-1}) (Chmeleff *et al.*, 2010; Korschinek *et al.*, 2010), and where ε_0 represents the mean background denudation rate of the hillslope surface in absence of landslide, e.g. due to weathering, biological activity and soil entrainment by surface runoff, and where t_0 is the time since the last major landslide event which would be supposed having removed a large thickness of rock and reset the concentration on that hillslope surface. In the Khudi valley, measurements on material from crests surface, hillslope and low order channels suggest that this background denudation rate ranges between $\varepsilon_0 \approx 0.03$ mm/yr (bedrock outcrops on crests) and $\varepsilon_0 = 0.15 \pm 0.10$ mm/yr (low order channels) (Niemi *et al.*, 2005). The lowest value would in particular line up with average chemical weathering rate at the scale of the whole Khudi valley (France Lanord *et al.*, 2013).

As observed on Fig. 5a displaying the solutions of equation (1) for ε_0 ranging between 0 and 0.25 mm.yr^{-1}, there are infinite pairs of solutions (t_0, z_c) that permit to account for an average concentration of 6.1×10^3 atoms.gr^{-1} below the landslide area (CA-957). For very low background denudation rates, i.e. when denudation rate ε_0 and/or t_0 are low enough to prevent attainment of a TCN steady state, the solutions family displays a nearly linear relationship according to :

(2)

$$\overline{C}(z_c, t_0) \approx \left(\sum_k \frac{\Lambda_k P_k}{\rho} \right) . \frac{t_0}{z_c} \quad .$$

If we consider, from field observations, that the average slices thickness ranges between 10 and 30 m, we can estimate an average time lag of 15 to 30 ka between two major landslide events, for low background denudation rates. In contrast, large stripping depth are incompatible with background denudation rates larger than 0.2-0.3 mm.yr^{-1} or require unrealistically long period without landslide of several hundreds of thousands years (Fig. 5a).

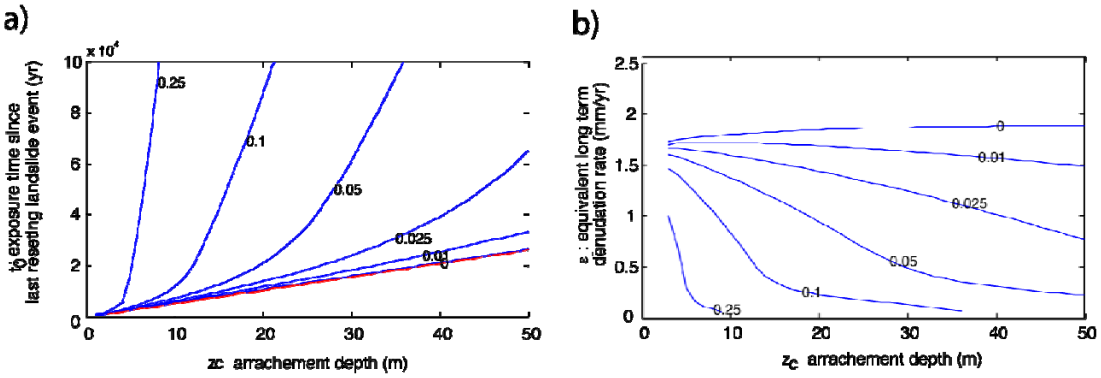

Fig. 5 - ***a)*** *Curves of possible solutions (z_c,t_0) that can account for the ^{10}Be cosmogenic mean concentration (average of the different grain size) of sample CA-957 for different values of the background hillslope erosion rate, ε_0 (numbers between 0 and 0.25 mm/yr).* ***b)*** *same as a), but represented in the (z_c,ε_L) space, with ε_L the equivalent long term denudation rate.*

On the other hand, if the exposure duration t_0 is assumed as a first order proxy of the return time between two landslides of same magnitude, we can define a mean denudation rate since the last local surface-resetting event:

(3)

$$\varepsilon_L \approx \frac{z_c}{t_0} + \varepsilon_0 .$$

For very low background denudation rates, and a given measured concentration in the mixed sediment, this long-term denudation rate is independent of the stripping depth z_c (Fig. 5b).

However, for $\varepsilon_0 > 0.01$ mm.yr^{-1}, the higher the background denudation rate, the lower the concentration at surface and at depth, and the longer the required exposure time to account for the depth-averaged concentration. Consequently, the equivalent long-term denudation rate ε_L calculated from a given concentration will significantly decrease for large background denudation rate.

4.1.2 Grain-size distribution model

If we now consider a vertical gradient of particle size distribution in the regolith and shallow bedrock, equation (1) can be re-casted for each grain size range according to :

(4)

$$\overline{C}_{[D_i;D_{i+1}]}(z_c,t_0,\varepsilon_0)=\frac{1}{\int_0^z\left(F_z(D_{i+1})-F_z(D_i)\right)dz}\int_0^z\left(F_z(D_{i+1})-F_z(D_i)\right)\sum_k\frac{P_k}{\varepsilon_0\frac{\rho}{\Lambda_k}+\lambda}e^{-\frac{\rho}{\Lambda_k}z}\left(1-e^{-(\varepsilon_0\frac{\rho}{\Lambda_k}+\lambda)t_0}\right)dz$$

with D the grain diameters, F_z the cumulative distribution of fragment size in the regolith profile at a depth z.

In absence of any detailed study on the grain size evolution in a vertical profile, we adopted a simplified model. Following previous studies on landslide deposits (e.g. McSaveney, 2002; Strom and Pernik, 2006), we first assume that the size distribution follows a Weibull distribution (Weibull, 1951):

(5)

$$F_{(\alpha,\Delta)}(D)=1-e^{-(D/\Delta)^{\alpha}}$$

Based on the grain-size of the landslide deposits in the Khudi southern landslide and in other parts of Nepal (Attal and Lavé, 2006), the empirical parameters α and Δ are observed to range in between 0.3 to 0.6 and 60 to 120 mm, respectively (Fig 4c). Sieving in upper soil sequences along Khudi crests or hillslopes show size distributions that can be also roughly approximated by a Weibull distribution with $\alpha_{surface} \approx 0.85$ and $\Delta_{surface} \approx 0.3$-0.4 mm. To keep a parsimonious model, we consider in the following that the shape parameter α remains uniform with depth, with an intermediate value of 0.5, and that only the scale parameter Δ varies with depth following the relationship:

(6)

$$\varphi_{\Delta}(z)=\varphi_{\Delta_{surface}}+\varphi_{\Delta_{landslide}}\left(1-e^{-(z/z^*)}\right)$$

where φ corresponds to a grain size expressed in φ-scale such that $\Delta=2^{\varphi_{\Delta}}$, and with $\Delta_{surface}$ = 0.3 mm and $\Delta_{landslide}$ = 80 mm.

The choice of an exponential relationship permits to define a single free parameter, the critical distance z* for bedrock fragments to be converted in the regolith in sandy material by weathering. This relationship is however likely to be a simplification, and could be viewed as the expression of the exponential decay in weathering efficiency with depth.

Combining equations (4), (5) and (6), we compute the mean ^{10}Be concentrations as a function of the grain size fractions for variable (t_0, z*) values and test the best fitting solutions that permit to reproduce the data below the landslide areas (Fig. 6 and 7).

4.2 Application of the model to TCN measurements downstream the landslide areas.

Based on our observations of the southern landslide, on Niemi *et al*'s (2005) results on crest denudation rate, and on our dissolved flux estimate (France-Lanord *et al.*, 2013), we assume at first that z_c = 15 m and ε_0 = 0.025 mm.yr^{-1}.

The critical distance of grain size reduction z* varies, however, between the samples: it is maximum for the northern landslide with z* ≈ 3-4 m (but any value larger than 0.7 m and lower than 50m would almost equally fit), minimum for the southern landslide with z* = $0.17\ ^{+0.17}/_{-0.08}$ m, and intermediate for the downstream sample (CA-957), which receives the contribution of both landslide areas, with z* = $0.45\ ^{+1.5}/_{-0.25}$ m.

Those values are obviously linearly linked to the depth attenuation of TCN production, in particular the spallogenic component. Consequently, decreasing the soil and regolith density will increase this optimum critical distance z*.

One of the striking results when introducing grain size reduction toward the surface is for the optimal solution to provide exposure times reduced by a factor 2 up to 3, when compared to the solution without size reduction (Fig. 5 and red dot on Fig. 6). Increasing the proportion of sand coming from the enriched surface layers, thus reducing the dilution by TCN-depleted deep layers, permits indeed to account for measured TCN concentration with lower exposure durations. The exposure duration t_0 for the best-fitting solution reaches 3200, 4100 and 9200 yrs for CA-948, CA-957 and CA-953, respectively. As another consequence, the equivalent landslide denudation rate ε_L (Eq. 3) will increase by a similar factor of 2 up to 3, reaching 4.7, 3.7 and 1.7 mm.yr^1, respectively (blue diamonds on Fig. 8).

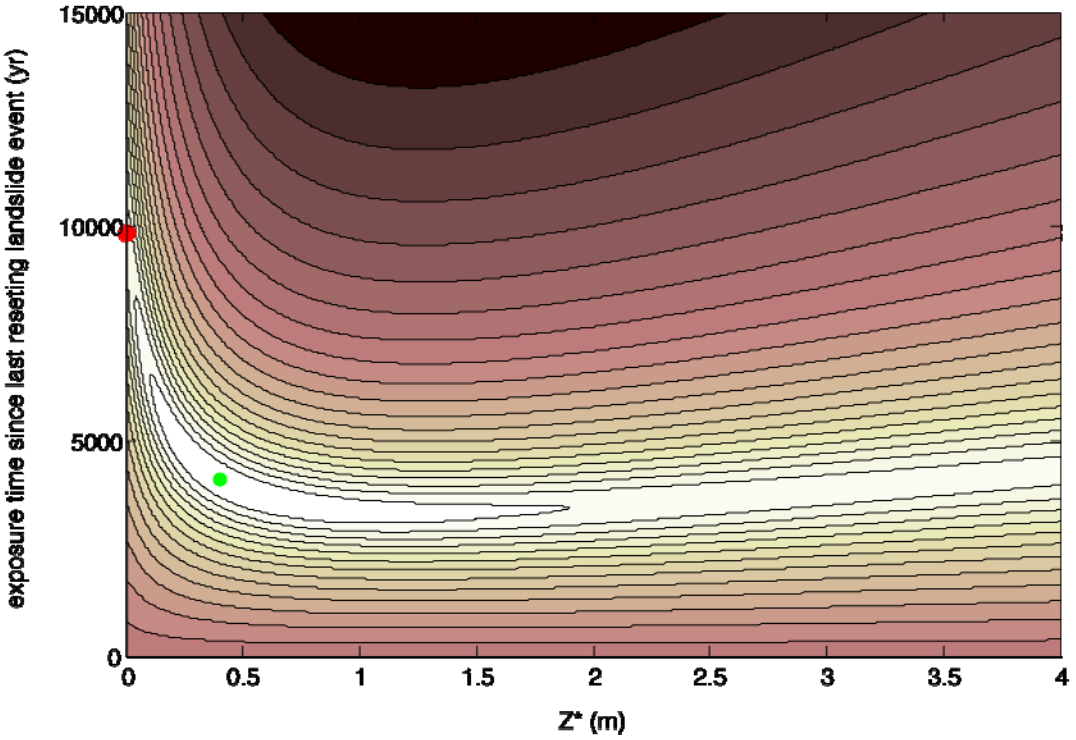

Fig. 6 - *Misfit value (sum of the square differences between model and data weighted by data uncertainties, log scale) between the ^{10}Be cosmogenic concentrations for different grain size intervals of sample CA-957 (downstream the two landslide) and the simplified model as a function of the characteristic depth of grain size increase, z*, and of the hillslope exposure duration, t_0, since the previous surface resetting landslide event. The red dot corresponds to best fitting exposure time t_0 in absence of depth-dependent size grading: introduction of depth heterogeneity in grain size distribution decreases by a factor >2 this exposure duration.*

4.3 Model sensitivity

Because the choice of the different parameters is difficult to constrain, we explored the sensitivity of the model to these parameters.

As for the vertically uniform case study, the slide depth, z_c, and the background denudation rate, ε_0, have a direct impact on the exposure time t_0, and the equivalent landslide denudation rate ε_L, but in contrast they have almost no effect on z* estimate. In fact, the variable z* is only sensitive to the chosen value of the α parameter in Weibull's law, that directly impacts the relative proportions of fine and coarse sediments: a lower value of α, i.e. a more spread-out size distribution, increases the best-fitting value of z*.

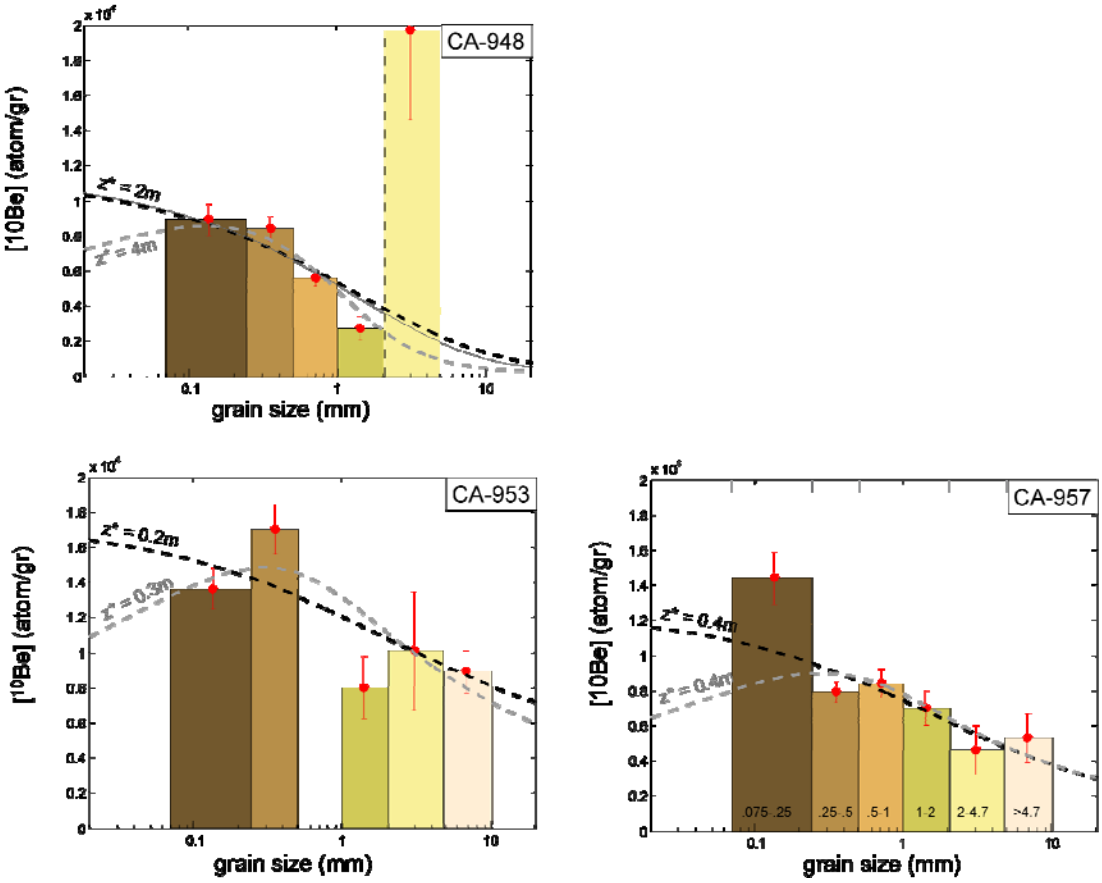

Fig. 7 - *^{10}Be concentrations sorted by clasts size and best fitting models. The continuous line correspond to a model for which parameter α is hold constant and equals to 0.5, whereas the gray line corresponds to a model in which α decreases exponentially from 0.85 close to the surface down to 0.45 at depth, following relation (6), i.e. evolving with the same parameter z* as log(Δ). Note that the apparently anomalous value for 2-4.7 mm of the sample CA-950 has been used during inversion but due to its large error bar its influence on the best fitting curve is rather limited.*

In all cases, the same general features of the $\chi 2$ map (Fig. 6) are observed, namely the banana shape of the optimal solutions, and the rapid decrease of t_0 compared to the case without grain size vertical grading.

In our last test, we also relaxed the hypothesis on α uniform and permitted it to vary between 0.85 close to the surface and 0.45 at depth using the same function as for φ (Eq. 6). Again, no significant change in the inversion results on z* was observed. It tends, however, to converge

toward lower exposure time, because a larger proportion of medium to coarse sand is in this case provided by the upper TCN-enriched soil layers. It concomitantly predicts a roll over of the concentration for the finest sand and silt fractions (gray lines on Fig. 7).

We did not test a different size-grading curve than Eq. 6. Although preliminary results on the grain-size measured into the soil sequence exposed at the landslide rim (Fig 4c) might suggest a roughly uniform size reduction in the first meter rather than a linear decrease with depth, we preferred keeping the model as parsimonious as possible and did not explore more complex undefined function depending on two or more parameters.

For similar reasons, in the model above, we also have implicitly assumed that quartz content was uniform, i.e. that quartz concentration was not enriched or depleted in a layer or/and in a size fraction compared to the initial bedrock content (Riebe *et al.*, 2001). We acknowledge, however, that future quantitative models will probably have to account for more realistic and elaborated grain size and quartz content vertical grading functions.

4.4 Model parameters and real world

Natural outcrops and auger sampling in several parts of the Khudi hillslopes generally show that the soil saprock interface is very deep (>3m), i.e. larger than our best-fitting z* estimates. More importantly, they show that in many places the soil/regolith is largely perturbed by mixing with coarse colluvium or mass movements deposits. If reworking on the hillslopes is a common process, then upper soil regolith could be enriched in large clasts and consequently the coarse sediment fraction could be more enriched in TCN than in our simplified end-member model.

Therefore, our model is not intended to give an exact reproduction of a natural setting but rather a simplified scheme to explain our data and a guide for future studies on this issue. The critical distance z* has not only to be considered as a quantitative estimate associated to an end-member model, but better as a minimum upward distance to weather >4.7 mm grains into <0.25 mm particles in the regolith and the soil, because of potential soil mixing and reworking on hillslopes.

5 Discussion

5.1 TCN size-dependency away from the active landslide areas

A striking result in the TCN measurements is that the river sediments upstream of the active landslides (CA-950) displays the same size-concentration relationship as the sub-basins affected by the deep seated landslides, although no major landslide (>1000 m^2) affects this upstream watershed. Similar observation can be done for the most downstream sample (CA-964) that integrates sediment coming from the whole upper half Khudi catchment.

To explain the size-concentration dependency, the landslide model described in Section 4 can be similarly applied to derive apparent (t_0, z*) values using their basin-average production rate (Table 1): best fitting couple of values (3500 yr, 1 m) and (8500 yr, 0.25 m) are obtained for upstream (CA-950) and downstream (CA-964) samples, respectively.

Although such values have to be considered with caution because we expect at the scale of a large watershed variable sources of sediments and mass wasting, they surprisingly fall within the range of values obtained below the landslides areas. The fact that size-concentration relationship in sediments is weakly sensitive to the slide depth z_c and does not depend on production rate could explain the coherence of z* all over the Khudi basin. In contrast, because of variable local production rates and surface concentration in a large watershed, the exposure time t_0 would have to be considered as only indicative.

If the landslide model applies also for the upper Khudi (CA-950), despite no major active landslide can be mapped, we propose that the material carried by the river might actually derive from ancient and currently un-active landslides. This implies that the input of sediments from background denudation is almost negligible, for example due to stabilizing vegetation cover. That implication would be consistent with our observation that stream water is clear even during monsoon along tributaries that do not drain landslides.

As regards the most downstream sample (CA-964), according to field observations, it is tempting to consider that most sediments come from the active landslides areas, and, in that case, it is straightforward to attribute the size-concentration dependency to the same process presumably occurring just downstream of the landslides. Adjunction of material derived from ancient and currently un-active landslides in the North-East sub-basin of the upper Khudi (Fig 1), and presenting similar signature as the upper North-West Khudi (CA-950) cannot however be excluded.

5.2 Alternative size-dependency and models

As discussed in the introduction, several previous studies have explored the TCN concentration as a function of the analyzed sediment size, with apparently no systematics (Codilean *et al.*, 2012). In a few settings with steep landscapes, no clear dependency or even a positive one has emerged (Clapp *et al.*, 2002; Safran *et al.*, 2005; Kober *et al.*, 2012). In other settings, a negative trend, as observed in Khudi basin, has been identified (Brown *et al.*, 1995; Belmont *et al.*, 2007; Aguilar *et al.*, 2013). The occurrence of this trend in landscapes a priori devoid of landslide like in the Appalachian Mountains (Matmon *et al.*, 2007) has fostered alternative models to explain clasts size-concentration relationship instead of the landslide-involving scenario as described in Section 4. We can therefore ask if alternative scenarios could also apply for the samples taken in Khudi away from the active landslides areas.

5.2.1 Sediment provenance and sediment attrition

Most of scenarios proposed in the literature suggest that sands and gravels could have distinct geographical provenances or could be associated to distinct processes acting at variable rates.

In the case of a negative concentration relation with grain size, as observed in Khudi, sand could come on average from higher elevation areas with higher productions rates whereas gravels could come from low elevation areas. As regards the northern sub-basin (CA-950), the average surface production rate of the drainage area is ~37 at.yr^{-1}.g^{-1} (Table 1), while the extreme production rates along the northern crests at ~4500 m and near the basin outlet at 2400 m are ~55 and ~17 at.yr^{-1}.g^{-1}, respectively. The difference in production rates of the two basin "extremities" reach a factor ~3 and, in theory, could explain ratios of 2 to 4 between TCN concentration of fine and coarse fractions if they would come each one from the two extremities of the basin.

Scenarios where the coarser grains could only come from the most downstream part of the watershed invoke attrition processes during fluvial transport, which would reduce most clasts coming from upstream (Carretier *et al.*, 2009; Carretier and Regard, 2011). Volumetric attrition rates for Himalayan gneisses are of the order of k = 1.4 ± 0.6 %.km^{-1}, with k the empirical pebble abrasion coefficient (Attal and Lave, 2006): over an average transport distance of L = 5km, the grain size reduction by attrition (k/3).L is of the order of ~2.5%. The transporting distances are therefore far insufficient to convert pebbles or gravels into sand size. In addition, it would remain unclear in this scenario why all the intermediate parts (with intermediate TCN production rates) of the basin would not contribute to the sand or gravel budget.

5.2.2 Glacial deposits

Alternatively (or concomitantly), the fine grains could also mostly come from glacial deposits (moraines) at high altitude. However, the cumulative granulometric distributions of morainic material in the Himalayas (Figure 5b in Attal and Lavé, 2006) display a gap in the sediment sizes between 0.05 and 1mm (φ = -4 to 0), i.e. just the measured fine fractions in our study, in contrast with landslide derived material. In absence of further measurements on morainic material in the upper Khudi, such explanation does not seem therefore appropriate.

5.2.3 Geomorphologic processes

Another mechanism, based on a scenario proposed by Aguilar *et al.* (2013), would be that most of the coarse clasts come from the landslides, and the finer ones from all of the basin, but without a depth provenance influence. Instead, it simply suggests that the landslides represent the part of the basin with the highest steepness, and hence the highest denudation rates and lower TCN concentrations.

Such scenario, proposed in a landscape eroding much more slowly, is hardly compatible with Himalayan denudation processes: it would require indeed that some specific points of the landscape would be eroded by several hundred meters in 100 kyrs while vast adjacent zones would be much less eroded: marked disequilibrium features would therefore appear in the watershed in contradiction with presently observed topography and slope map.

Finally, without fully discarding the above alternative models, we conclude from poor support to alternative scenario, and from the close similarity of the grain size-concentration patterns both upstream, near the landslides and downstream, that almost all of the sediments in the river derive from active or ancient landslide material, and probably very little from background soil erosion. As a matter of example, if we try to explain the apparent over-concentration in TCN of the two finest sandy fractions in CA-950 compared to the average size-concentration trend (Fig. 3) by adjunction of sand issued from background erosion at 0.025 $mm.yr^{-1}$, such contribution would be limited to ~1 % of the medium size (75 to 250 μm) sand budget.

5.3 Effect of the landslides on the apparent TCN-derived denudation rate

TCN measured in river sand are classically used to derive average denudation rates in the upper contributing area. For a surface undergoing a steady denudation ε since a time t_{eff} >> $1/(\lambda + \mu\varepsilon)$, the ^{10}Be concentration is :

(7)

$$C = \sum_k \frac{P_k}{\varepsilon \frac{\rho}{\Lambda_k} + \lambda}$$

(see Eq. 1 for the definition of the parameters)

In actively eroding settings like the Himalayas, $\varepsilon\rho/\Lambda_k < 1.73\times10^{-3} << \lambda$ and the equation (7) can be generalized for a whole catchment (Brown *et al.*, 1995; Granger *et al.*, 1996), so that a sediment exported from this catchment, of area *A*, has an average concentration $\overline{C}$ given by :

(8)

$$\overline{C} = \frac{1}{\overline{\varepsilon}_I} \iint_A \sum_k \frac{P_k(x)}{\varepsilon_{MS}(x)\rho/\Lambda_k} \varepsilon_I(x) d\vec{x}$$
$$= \frac{1}{\overline{\varepsilon}} \cdot \sum_k \frac{\overline{P_k}}{\rho/\Lambda_k}$$

With $\varepsilon_{MS}(x)$ the average local denudation rate at millennial scale, $\varepsilon_I(x)$ the instantaneous local denudation rate, $\overline{\varepsilon}$ the average denudation rate of the catchment and $\overline{P_k}$ the average production rates of neutrons, slow muons and fast muons. Note that the second simplified term of equation (2) is true only in case of steady denudation, i.e. $\varepsilon_{MS}(x) = \varepsilon_I(x)$ in any point of the landscape. In any case, apparent average denudation rates from TCN results using equation (2) can be derived (Table 1 and Fig.3; see details of calculation in Appendix) and we discuss their validity and interest in the following.

In the Khudi case, equation (8) is not applicable and would have to be replaced by Eq. (1) or (3) defined for a finite thickness of eroded material. The paradox in assuming $\varepsilon_{MS}(x) = \varepsilon_I(x)$ behind equation (8) is well illustrated by our watersheds affected by landslides. First, in the hillslope

affected by the active regressive erosion of the landslides, the instantaneous erosion rate ε_I reaches several meters per year, i.e 5 to 6 orders faster than the mean erosion rate at millennial scale ε_{MS}. Consequently, as mentioned in section 3.2., if we use TCN concentration as a mixing tracer for the sample CA-957 (downstream the two landslides area), and considering the different sediment end-members given by CA-950, 048 and 953, we would end up for the sediment CA-957 with a minimal proportion of material coming from the upper Khudi (CA-950), i.e close to 0 and in any case <30%. If we now derive the theoretical average sediment fluxes from the TCN results and equation (8), writing $F = A\bar{\varepsilon}$ with F the sediment volumetric flux, considering for example the 0.25-0.5 mm size fraction (using another grain size would not change the first order picture), we end up both with a theoretical flux from the upper Khudi 4 times higher than the flux coming from the landslides and a sum of these two contributions 3 times too low to account for the theoretical flux computed for the downstream sample CA-957. TCN-derived sediment fluxes derived from Eq. (8) are irreconcilable with mass budget.

In those setting dominated by landslides, it has been proposed that only long temporal volumetric averages or large spatial volumetric averages as provided by large watershed permit to converge toward relation (8) between TCN concentration in sand and mean denudation rate in the watershed (Niemi *et al.*, 2005; Yanites *et al.*, 2009).

However, this affirmation holds if there is no grain-size dependency. For each Khudi sample, the use of Eq. (8) leads to a denudation rate which depends on the analyzed grain-size in a inverse relation to the one for TCN concentration: gravel size fractions present higher denudation rates than medium sand fractions. There is no rationale to decide which size fraction is more representative of the mean denudation rate and we end up with a large indetermination of the problem.

In active landslide areas, as an alternative, we could use Eq. (2). However, large uncertainties would remain on the exact stripping depth in landslides (z_c), the background denudation rate (ε_0) and on how representative is the last cycle of landsliding of the long term landslide size and return period. It prevents to consider ε_L as a precise estimate, even if the size-dependent TCN concentration can be fully accounted by the use of a model like the one presented in Section 4, in contrast with Eq. (8).

5.4 Are TCN-derived denudation rates relevant in active mountainous settings?

5.4.1 Comparison with denudation rates at different time scales

Despite aforementioned difficulties for using Eq. (8) or Eq. (3) in actively eroding setting, we can compare apparent denudation rates derived from our samples with previous estimates. In order to compare with previous TCN-derived denudation rates from 250-1000 μm fraction (Niemi *et al.* 2005; Arjun Heimsath, personnal communication; Godard *et al.*, 2012), we will consider only our results for 250-500 and 500-1000 μm fractions, and these previously published results will be recalculated using the same method and TCN production rate as the one we have used (Appendix).

Surprisingly, our denudations rates $\overline{\varepsilon}$ range between 1.3 and 4.2 mm/yr, and bracket previous ^{10}Be derived denudation rate estimate of ~2.5 mm/yr (Niemi *et al.* 2005; Godard *et al.*, 2012), as well as very short term (Gabet *et al.*, 2008) or Quaternary rates (Fig. 8) (Blythe *et al.*, 2007; Whipp *et al.*, 2007). They under- or over-estimate those rates by only a factor 1.50 or less.

Moreover, the calculation of the equivalent landslide denudation rates ε_L derived from our best-fitting models also provide estimate in relatively good agreement with above TCN or independent values, despite being slightly higher.

5.4.2 Spatial and temporal variability at the scale of a small basin

By contrast, moving downstream, integrating over a larger watershed, a theoretical smoothing of stochastic inputs of sediments as proposed by Niemi *et al.* (2005); Binnie *et al.* (2006); Yanites *et al.* (2009); Kober *et al.* (2012) is not reflected by our data. Discrepancies with supposed basin average around 2-3 mm.yr^{-1} are as high for our downstream sample (CA-964) than for the upstream ones. For this later sample, we need to invoke either a significant input, in all grain sizes, from the North-East branch of the upper Khudi (despite most of this sub basin seems from satellite image exempt of major mass wasting source) or a rapid temporal variations (in between years or even large storms during the monsoon) of the TCN concentration in landslide-derived material, due to variable slices thickness and TCN signature along the rims of the landslides. This later explanation would suggest that the fluvial system across steep

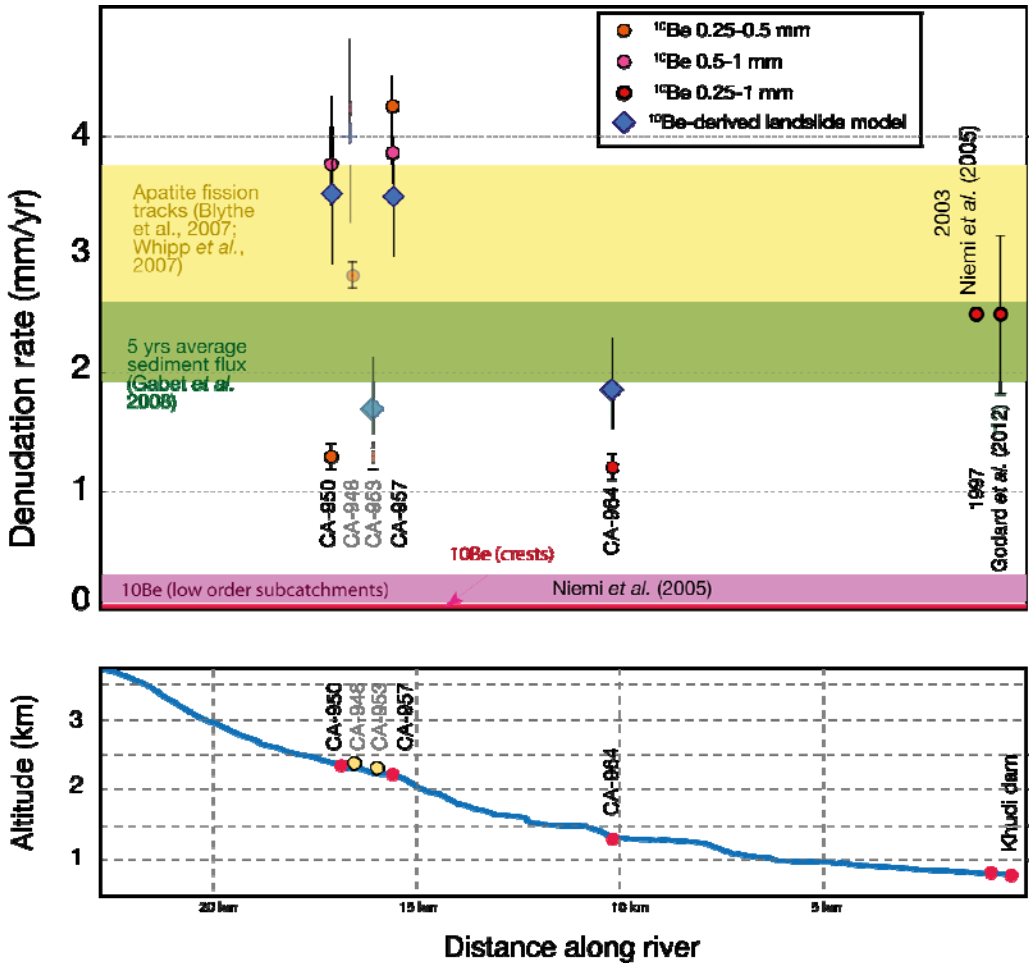

Fig. 8 - Downstream evolution of the TCN-derived denudation rates (in 250-1000 mm size fraction) as compared geologic and short term denudation rates. *In addition, we rescaled their results to new Sea Level High Latitude (SLHL) production rate of 3.9 atom/gr/yr instead of a value of 5.3 used by Niemi et al. (2005), 4.5 used by Godard et al. (2012). Note that no methodology (in particular about the analyzed grain size) is provided by Niemi et al.'s (2005) (reported from Arjun Heimsath's unpublished data), but probably correspond to 200-500 μm interval.*

mountains has a limited storage buffering capacity for sand and fine gravels: CA-964 was sampled in 2009, while Niemi et al.'s and Godard et al.'s sediments were sampled in 2003 and 1997, respectively. Such temporal variations, by a factor up to 3, has been observed in other places (e.g. Kober *et al.*, 2012), even for very large watersheds (~60,000 km2) (Lupker *et al.*, 2012), and could be a general propriety of mountainous fluvial/landscape systems.

5.4.3 Implication for the sediment dynamics in the Khudi valley

One of the most striking results, in sharp contrast with stochastic models predictions (Niemi *et al.*, 2005; Yanites *et al.*, 2009), is the similarity of the apparent denudation rates and long term denudation rate, both for the area actively eroded by the receding landslide, and for the upper Khudi which is in contrast not affected by active landslides.

In the landslide-affected areas, stochastic models would predict abnormally low TCN concentration in mixed landslide material in particular if the background denudation rate is higher than 0.1 mm/yr. We make the inverse observation, which requires very abnormal quiescence time since the previous surface resetting event (Fig. 5a) or/and very low background denudation rates ($\varepsilon_0 < 0.05$ mm/yr), in coherence with denudation rates reported by Niemi *et al.* (2005) along the Khudi basin ridge tops. We can also add that the vertical size grading in the regolith has a positive effect since the overrepresentation of the surface layers in the sandy fractions (i.e. the usually 250-1000 μm analyzed fraction for ^{10}Be) makes the analyzed TCN concentrations higher than the whole material depth average.

For the upper Khudi, devoid of active landslides, stochastic models would predict abnormally high TCN concentrations in river sands. As mentioned earlier in Section 5.2, the opposite observation requires that this input is dwarfed by sediments remobilized along the channels from ancient landslide deposits. The absence of sand with high ^{10}Be concentration coming from the background surface erosion could therefore suggest that such background erosion is mostly related to weathering and chemical denudation, and does not produce significant input of sandy material into the river system. As a consequence, in channels starved of fresh landslide input, minimal storage along the channels of sediment issued from older landslides (i.e. that were active few 10's to 100 yrs ago) would be sufficient to leave a low ^{10}Be concentration signature in the sandy material decades later.

To conclude these empirical considerations about the TCN-derived denudation rates in the Khudi basin, let us emphasize a good news and two bad ones.

For the good news, it seems that a series of factors (presumably a size grading in the regolith, very low sand input from background erosion in vegetated landscapes and channel sediment storage in channels) make the denudation rates closer to the average long term value than expected in such a landslide-dominated landscape. This would particularity maintain the use of TCN as a reliable tool to estimate long term denudation rates compared to the measurements of suspended load fluxes, since these estimates are quite sensitive for small watersheds to the occurrence or not of landslides. Such assertion seems confirmed in the High Himalayas since

TCN-derived denudation rates (Godard *et al.*, 2012) are of the same order of magnitude as long-term denudation rates of 2-4 $mm.yr^{-1}$ (Lave and Avouac, 2001; Burbank *et al.*, 2003) while most suspended load flux estimates (except for the Khudi basin) provide rates <1 mm/yr in the Marsyandi basin (Gabet *et al.*, 2008) or in central and West Nepal (Andermann *et al.*, 2012).

The bad news are twofold. First, stochasticity of the sediment inputs has still a probable impact and result in significant spatial and temporal variability. As a result, the TCN-derived denudation rates, based on medium to coarse sand size fractions, must be handled with caution and considered as first order estimates. In our case, they cannot provide long-term estimates with a precision better than a factor of ca. 2. Second, Niemi *et al.* (2005) have reported in Khudi basin very low TCN-derived denudation rate values in the low order drainage basins, so that a critical basin size exists under which the TCN averaging propriety of the fluvial system stops to be valid (Niemi *et al.*, 2005; Binnie *et al.*, 2006; Yanites *et al.*, 2009; Kober *et al.*, 2012). From CA-950 draining the upper Khudi, this critical size would be lower than 25 km^2, but a considerable work would be required to document this value, how it depends on the geomorphic and vegetation setting, and if this threshold is constant through time.

6 Conclusion

We sampled river sands from five locations of the small upper Khudi watershed, central Nepal: upstream, at the outlet of two major active landslides, directly downstream the landslides area, and 5 km downstream.

As reported in some other areas (Brown *et al.*, 1998; Belmont *et al.*, 2007; Aguilar *et al.*, 2013), the sand from the two landslides displays a negative correlation between clasts size and cosmogenic ^{10}Be concentration. Such a trend is well explained by size grading within the regolith and erosion by landslide (Brown *et al.*, 1995) and quantitatively corroborated by a simplified model.

In the future, more systematic TCN studies for various grain size studies below landslides areas, complemented by TCN signature of the hillslopes around these landslides confronted to more elaborated models, could help document the average grain size distribution and concentration content in soil/regolith profiles.

Surprisingly, TCN concentration anti-correlation to the grain-size is also observed directly upstream and 5 km downstream of the landsliding area. The most probable explanation is that almost all of the sediment carried by the river actually derives from ancient landslides, and almost no erosion occurs from soil-mantled slopes. This hypothesis is supported by ^{10}Be data

reported by Niemi *et al.* (2005), with very slow denudation rates reported on the crestal hillslopes compared to the basin-average denudation rate.
The data show that an uncompleted and probably seasonally-varying mixing occurs between the active landslides material and the river sediments. Thus, in our case of a small watershed controlled by stochastic mass wasting events, sediment budgeting attempts based on the size-concentration dependence, such as the ones developed by Belmont (2007) or Matmon (2003) , are precluded.

In light of our detailed review of grain size fractions commonly used in cosmogenic studies, comparison with other reported denudation rates in this area must be performed carefully. While the reported orders of magnitude are all coherent (around ~2 $mm.yr^{-1}$), even at very different time scales and with very different methods, a scatter of a factor up to 3 remains between cosmogenic studies depending on the chosen grain size, the location and the sampling date. Cosmogenic nuclides provide unique information and are an increasingly applied tool, but their use in such mountainous small basins must be done with caution.

Appendix: Mean apparent TCN-derived denudation rates calculation:

For all cosmogenic nuclide average production rates calculation we used a ASTER Digital Elevation Model (DEM) of a 15m horizontal resolution.

The reference production rate at sea level and high latitudes (SLHL) used is 3.9 ± 0.1 at.g^{-1}.yr^{-1} (Balco *et al.*, 2009).

In each cell of the DEM, we calculated the altitude and latitude correction factor for spallogenic, slow-muonic and fast-muonic productions following the scaling scheme of Stone (2000). We also corrected the production rate from local slope and topographic shielding by relief in a 15km radius following Dunne *et al.* (1999). We included in this topographic shielding a correction for grid resolution smoothing of the local topography following Norton and Vanacker (2009).

Equation (7) cannot be solved analytically. For the best precision and to avoid analytical simplifications, we solved equation (7) numerically, even if in this case of a very-high denudation setting, it could theoretically be simplified into equation (8) with very limited error.

To propagate uncertainties from the multiple input parameters of this equation, we used a Monte-Carlo simulation, with 10k draws in a normal distribution of each parameter.

Acknowledgements

We thank Ananta Gajurel (Tribhuvan University) and Etienne Dambrinne (INRA) for assistance on the field, the STEVAL Pilot Plant team for helping in mineral separations, and Frédéric Chauvet and Laetitia Leanni (CEREGE) for their help during chemical preparations. Didier Bourlès (CEREGE) kindly proof-read and helped to improve this manuscript. This research was founded by the ANR Blanche project "Calimero".

References for this paper

Aguilar, G., Carretier, S., Regard, V., Vassallo, R., Riquelme, R., and Martinod, J. (2013). Grain size-dependent 10Be concentrations in alluvial stream sediment of the Huasco Valley, a semi-arid Andes region. *Quaternary Geochronology*.

Andermann, C., Crave, A., Gloaguen, R., Davy, P., and Bonnet, S. (2012). Connecting source and transport: Suspended sediments in the Nepal Himalayas. *Earth and Planetary Science Letters* **351,** 158-170.

Attal, M., and Lave, J. (2006). Changes of bedload characteristics along the Marsyandi River (central Nepal): Implications for understanding hillslope sediment supply, sediment load evolution along fluvial networks, and denudation in active orogenic belts. *In* "Tectonics, Climate, and Landscape Evolution." pp. 143-171. Geological Society of America Special Papers.

Balco, G., Briner, J., Finkel, R. C., Rayburn, J. A., Ridge, J. C., and Schaefer, J. M. (2009). Regional beryllium-10 production rate calibration for late-glacial northeastern North America. *Quaternary Geochronology* **4,** 93-107.

Belmont, P., Pazzaglia, F. J., and Gosse, J. C. (2007). Cosmogenic Be-10 as a tracer for hillslope and channel sediment dynamics in the Clearwater River, western Washington State. *Earth and Planetary Science Letters* **264,** 123-135.

Binnie, S. A., Phillips, W. M., Summerfield, M. A., and Fifield, L. K. (2006). Sediment mixing rapidly and basin-wide cosmogenic nuclide analysis in eroding mountainous environments. *Quaternary Geochronology* **1,** 4-14.

Blythe, A. E., Burbank, D. W., Carter, A., Schmidt, K., and Putkonen, J. (2007). Plio-Quaternary exhumation history of the central Nepalese Himalaya: 1. Apatite and zircon fission track and apatite [U-Th]/He analyses. *Tectonics* **26**.

Braucher, R., Brown, E. T., Bourlès, D. L., and Colin, F. (2003). In situ produced ^{10}Be measurements at great depths: implications for production rates by fast muons. *Earth and Planetary Science Letters* **211,** 251-258.

Braucher, R., Merchel, S., Borgomano, J., and Bourl√®s, D. L. (2011). Production of cosmogenic radionuclides at great depth: A multi element approach. *Earth and Planetary Science Letters* **309,** 1-9.

Brown, E. T., Edmond, J. M., Raisbeck, G. M., Yiou, F., Kurz, M. D., and Brook, E. J. (1991). Examination of surface exposure ages of Antarctic moraines using in situ produced ^{10}Be And ^{26}Al. *Geochimica et Cosmochimica Acta* **55,** 2269-2283.

Brown, E. T., Stallard, R. F., Larsen, M. C., Bourles, D. L., Raisbeck, G. M., and Yiou, F. (1998). Determination of predevelopment denudation rates of an agricultural watershed (Cayaguas River, Puerto Rico) using in-situ-produced Be-10 in river-borne quartz. *Earth and Planetary Science Letters* **160,** 723-728.

Brown, E. T., Stallard, R. F., Larsen, M. C., Raisbeck, G. M., and Yiou, F. (1995). Denudation rates determined from the accumulation of in situ produced ^{10}Be in the Luquillo experimental forest, Puerto-Rico. *Earth and Planetary Science Letters* **129,** 193-202.

Burbank, D. W., Blythe, A. E., Putkonen, J., Pratt-Sitaula, B., Gabet, E., Oskin, M., Barros, A., and Ojha, T. P. (2003). Decoupling of erosion and precipitation in the Himalayas. *Nature* **426,** 652-655.

Carretier, S., and Regard, V. (2011). Is it possible to quantify pebble abrasion and velocity in rivers using terrestrial cosmogenic nuclides? *Journal of Geophysical Research-Earth Surface* **116,** 17.

Carretier, S., Regard, V., and Soual, C. (2009). Theoretical cosmogenic nuclide concentration in river bed load clasts: Does it depend on clast size? *Quaternary Geochronology* **4,** 108-123.

Chmeleff, J. r. m., von Blanckenburg, F., Kossert, K., and Jakob, D. (2010). Determination of the 10Be half-life by multicollector ICP-MS and liquid scintillation counting. *Nuclear Instruments and Methods in Physics Research Section B: Beam Interactions with Materials and Atoms* **268,** 192-199.

Clapp, E. M., Bierman, P. R., and Caffee, M. (2002). Using Be-10 and Al-26 to determine sediment generation rates and identify sediment source areas in an arid region drainage basin. *Geomorphology* **45,** 89-104.

Codilean, A. T., Fenton, C. R., Fabel, D., Bishop, P., and Xu, S. (2012). Discordance between cosmogenic nuclide concentrations in amalgamated sands and individual fluvial pebbles in an arid zone catchment. *Quaternary Geochronology*.

Colchen M., L. P. a. P., A. (1986). Annapurna Manaslu Ganesh Himal Geological Map. *Edition du CNRS*, 136.

Dunne, J., Elmore, D., and Muzikar, P. (1999). Scaling factors for the rates of production of cosmogenic nuclides for geometric shielding and attenuation at depth on sloped surfaces. *Geomorphology* **27** 3-11.

France-Lanord C, Galy V, Gajurel A, Lavé J, Lupker M & Morin G (2013) Balancing Chemical and Physical Erosion in the Ganga Basin. *Mineralogical Magazine*, **77(5)** 1103

Gabet, E. J., Burbank, D. W., Putkonen, J. K., Pratt-Sitaula, B. A., and Ojha, T. (2004). Rainfall thresholds for landsliding in the Himalayas of Nepal. *Geomorphology* **63,** 131-143.

Godard, V., Burbank, D. W., Bourles, D. L., Bookhagen, B., Braucher, R., and Fisher, G. B. (2012). Impact of glacial erosion on Be-10 concentrations in fluvial sediments of the Marsyandi catchment, central Nepal. *Journal of Geophysical Research-Earth Surface* **117**.

Granger, D. E., Kirchner, J. W., and Finkel, R. (1996). Spatially averaged long-term erosion rates measured from in situ-produced cosmogenic nuclides in alluvial sediment. *Journal of Geology* **104,** 249-257.

Hovius, N., Stark, C. P., and Allen, P. A. (1997). Sediment flux from a mountain belt derived by landslide mapping. *Geology* **25,** 231-234.

Kober, F., Hippe, K., Salcher, B., Ivy-Ochs, S., Kubik, P. W., Wacker, L., and Hahlen, N. (2012). Debris-flow-dependent variation of cosmogenically derived catchment-wide denudation rates. *Geology* **40,** 935-938.

Korschinek, G., Bergmaier, A., Faestermann, T., Gerstmann, U. C., Knie, K., Rugel, G., Wallner, A., Dillmann, I., Dollinger, G., von Gostomski, C. L., Kossert, K., Maiti, M., Poutivtsev, M., and Remmert, A. (2010). A new value for the half-life of 10Be by Heavy-Ion Elastic Recoil Detection and liquid scintillation counting. *Nuclear Instruments and Methods in Physics Research Section B: Beam Interactions with Materials and Atoms* **268,** 187-191.

Lal, D. (1991). Cosmic ray labeling of erosion surfaces: *in situ* nuclide production rates and erosion models. *Earth and Planetary Science Letters* **104,** 424-439.

Lave, J., and Avouac, J. P. (2000). Active folding of fluvial terraces across the Siwaliks Hills, Himalayas of central Nepal. *Journal of Geophysical Research-Solid Earth* **105,** 5735-5770.

Lave, J., and Avouac, J. P. (2001). Fluvial incision and tectonic uplift across the Himalayas of central Nepal. *Journal of Geophysical Research-Solid Earth* **106,** 26561-26591.

Lave, J., Yule, D., Sapkota, S., Basant, K., Madden, C., Attal, M., and Pandey, R. (2005). Evidence for a great medieval earthquake (approximate to 1100 AD) in the Central Himalayas, Nepal. *Science* **307,** 1302-1305.

Lupker, M., Blard, P.-H., Lave, J., France-Lanord, C., Leanni, L., Puchol, N., Charreau, J., and Bourles, D. (2012). Be-10-derived Himalayan denudation rates and sediment budgets in the Ganga basin. *Earth and Planetary Science Letters* **333,** 146-156.

McSaveney, M. J. (2002), Recent rockfalls and rock avalanches in Mount Cook National Park, New Zealand, in Catastrophic Landslides: Effects, Occurrence, and Mechanisms: Reviews in Engineering Geology, edited by S. G. Evans and J. V. DeGraff, Geol. Soc. Am. Rev. Eng. Geol., XV, 35– 70.

Merchel, S., Arnold, M., Aumaitre, G., Benedetti, L., Bourles, D. L., Braucher, R., Alfimov, V., Freeman, S., Steier, P., and Wallner, A. (2008). Towards more precise (10)Be and (36)Cl

data from measurements at the 10(-14) level: Influence of sample preparation. *Nuclear Instruments & Methods in Physics Research Section B-Beam Interactions with Materials and Atoms* **266,** 4921-4926.

Ni, J., and Barazangi, M. (1984). Seismotectonics of the Himalayan Collision Zone - Geometry of the Underthrusting Indian Plate beneath the Himalaya. *Journal of Geophysical Research* **89,** 1147-1163.

Niemi, N. A., Oskin, M., Burbank, D. W., Heimsath, A. M., and Gabet, E. J. (2005). Effects of bedrock landslides on cosmogenically determined erosion rates. *Earth and Planetary Science Letters* **237,** 480-498.

Nishiizumi, K., Imamura, M., Caffee, M. W., Southon, J. R., Finkel, R. C., and McAninch, J. (2007). Absolute calibration of Be-10 AMS standards. *Nuclear Instruments & Methods in Physics Research Section B-Beam Interactions with Materials and Atoms* **258,** 403-413.

Norton, K. P., and Vanacker, V. (2009). Effects of terrain smoothing on topographic shielding correction factors for cosmogenic nuclide-derived estimates of basin-averaged denudation rates. *Earth Surface Processes and Landforms* **34,** 145-154.

Pandey, M. R., Tandukar, R. P., Avouac, J. P., Lave, J., and Massot, J. P. (1995). Interseismic Strain Accumulation on the Himalayan Crustal Ramp (Nepal). *Geophysical Research Letters* **22,** 751-754.

Pratt-Sitaula, B., Burbank, D. W., Heimsath, A. M., Humphrey, N. F., Oskin, M., and Putkonen, J. (2011). Topographic control of asynchronous glacial advances: A case study from Annapurna, Nepal. *Geophysical Research Letters* **38,** L24502.

Putkonen, J. K. (2004). Continuous snow and rain data at 500 to 4400 m altitude near Annapurna, Nepal, 1999-2001. *Arctic Antarctic and Alpine Research* **36,** 244-248.

Reinhardt, L. J., Hoey, T. B., Barrows, T. T., Dempster, T. J., Bishop, P., and Fifield, L. K. (2007). Interpreting erosion rates from cosmogenic radionuclide concentrations measured in rapidly eroding terrain. *Earth Surface Processes and Landforms* **32,** 390-406.

Riebe, C. S., Kirchner, J. W., and Granger, D. E. (2001). Quantifying quartz enrichment and its consequences for cosmogenic measurements of erosion rates from alluvial sediment and regolith. *Geomorphology* **40,** 15-19.

Safran, E. B., Bierman, P. R., Aalto, R., Dunne, T., Whipple, K. X., and Caffee, M. (2005). Erosion rates driven by channel network incision in the Bolivian Andes. *Earth Surface Processes and Landforms* **30,** 1007-1024.

Schaller, M., and Ehlers, T. A. (2006). Limits to quantifying climate driven changes in denudation rates with cosmogenic radionuclides. *Earth and Planetary Science Letters* **248,** 153-167.

Stone, J. O. (2000). Air pressure and cosmogenic isotope production. *Journal of Geophysical Research - Solid Earth* **105,** 23753-23759.

Strom, A. L., and L. M. Pernik (2006), Utilisation of the data on rockslide dams formation and structure for blast-fill dams design, *Ital. J. Eng. Geol. Environ.*, 1, 133– 135.

von Blanckenburg, F. (2005). The control mechanisms of erosion and weathering at basin scale from cosmogenic nuclides in river sediment. *Earth and Planetary Science Letters* **237,** 462-479.

Weibull, W. (1951), A statistical distribution function of wide applicability, *J. Appl. Mech.*, 18, 837– 843.

Whipp, D. M., Ehlers, T. A., Blythe, A. E., Huntington, K. W., Hodges, K. V., and Burbank, D. W. (2007). Plio-Quaternary exhumation history of the central Nepalese Himalaya: 2. Thermokinematic and thermochronometer age prediction model. *Tectonics* **26**.

Yanites, B. J., Tucker, G. E., and Anderson, R. S. (2009). Numerical and analytical models of cosmogenic radionuclide dynamics in landslide-dominated drainage basins. *Journal of Geophysical Research-Earth Surface* **114**.

^{3}He variability in Ethiopian river sands and implications for basin-scale denudation rates determinations

(Second draft, to be re-submitted to Chemical Geology)

Nicolas Puchol[1], Raphaël Pik[1], Pierre-Henri Blard[1], Bouchaïb Tibari[1], Jérôme Lavé[1]

[1]CRPG, CNRS - Université de Lorraine, UPR 2300, 15 rue Notre Dame des Pauvres, Vandoeuvre-lès-Nancy, 54500, France

Contents of this paper

Abstract

In-situ cosmogenic ^{3}He is a robust tool for determining denudation rates or exposure ages of lavas bearing mafic phenocrysts. However, analyses are often complicated by the presence of several helium sources. In particular, in old magmatic rocks with high radiogenic ^{4}He contents, discriminating cosmogenic ^{3}He from magmatic ^{3}He is not straighforward since both these quantities may largely vary from one aliquot to another.

We sampled sands from the Tekeze and Mile rivers, both draining the Ethiopian highlands, an area where erosion patterns are intimately linked to the tectonics of the East-African rift and to heterogeneous monsoon precipitation. From each river we analysed ~15 pyroxene aliquots of various grain sizes (0.3 mm up to >1 mm). We observed that the total ^{3}He is both higher and more scattered in the bigger grains. Crushing of these biggest grains and subsequent melting of the powder tends to cluster the ^{3}He value, suggesting that magmatic ^{3}He is responsible for most of the inter-aliquot variability. We also performed a Monte Carlo simulation based on a numerical denudation model of the two watersheds. The simulation confirms that cosmogenic ^{3}He variability cannot be responsible for the observed scatter. A compilation of previously published data also indicates that magmatic helium can be significantly variable even between pre-crushed aliquots. Hence, magmatic helium, unlike cosmogenic ^{3}He, is highly variable, even in the case of aliquots of >300 grains. We suggest this is due to their higher probability to bear large melt-inclusion.

Besides, the fact that small and big grains have comparable radiogenic ^{4}He concentrations suggests that grain attrition during the river transport is responsible for the lower magmatic helium content in the smallest grains.

Therefore, one should preferably use small grains (<0.5mm) and homogenous granulometry for in-situ cosmogenic ^{3}He analysis in mafic phenocrysts.

Using the measured cosmogenic ^{3}He, we calculate basin-average denudation rates of 73±18 mm.kyr^{-1} and 57±5 mm.kyr^{-1}, for the Mile and for the Tekeze river, respectively. These values are coherent with long term denudation rates previously proposed from low-temperature thermochronology.

1 Introduction

In-situ cosmogenic nuclides are produced by the flux of secondary cosmic particles in the top few meters of the Earth surface. They represent a useful tool with which to quantify many key Earth-surface processes (see Gosse and Phillips, 2001, for history and review). Along with other cosmogenic isotopes (e.g. ^{10}Be, ^{2}6Al, ^{36}Cl, ^{21}Ne), 3He has been widely used for the past 25 years to date lava flows (Kurz *et al.*, 1990; Ammon *et al.*, 2009), to reconstruct continental paleoclimates (e.g. Licciardi *et al.*, 2001; Blard *et al.*, 2007) or to measure in-situ (Sarda *et al.*, 1993) or basin-averaged (Gayer *et al.*, 2008) denudation rates. ^{3}He presents several advantages compared to more commonly used isotopes like ^{10}Be or ^{26}Al. It does not require a complex chemical preparation, nor the use of an Accelerator Mass Spectrometer (AMS). Besides, many rocks - especially basalts - do not contain significant amounts of quartz, the mineral in which ^{10}Be and ^{26}Al are preferentially analyzed.

However, ^{3}He is not retained in many minerals (Trull *et al.*, 1995). Most studies using ^{3}He have hence been carried out on mafic phenocrysts such as olivine and pyroxene (e.g. Kurz, 1986a), which are known to have a high helium retentivity (Trull *et al.*, 1991; Shuster *et al.*, 2004; Blard and Pik, 2008); In these minerals, the helium budget is a four-component system (Farley *et al.*, 2006; Blard and Farley, 2008) consisting of:

- Cosmogenic ^{3}He ($^{3}He_c$), matrix-sited
- Magmatic inherited ^{3}He and ^{4}He (He_{mag}), fluid inclusion-sited
- Radiogenic ^{4}He ($^{4}He_r$), produced by the decay of ^{238}U, ^{235}U and ^{232}Th, matrix-sited
- Nucleogenic ^{3}He ($^{3}He_{nuc}$), produced by neutron capture on Li nuclei and subsequent disintegration, matrix-sited.

For most young mafic rocks with low U-Th and Li content the radiogenic and nucleogenic components can be neglected or corrected (Blard and Farley, 2008). In this case, the cosmogenic component can be determined by a standard two-step procedure (Kurz, 1986b):

1 – In vacuo mineral crushing to preferentially release and analyse inclusion-sited magmatic helium, allowing the magmatic $^{3}He/^{4}He$ ratio to be measured and also reduces the He_{mag} concentration.

2 - Fusion of the same aliquot as for the crush analysis or a different aliquot of the same sample, in order to measure the bulk ($^{3}He/^{4}He$) melt ratio and the total ^{4}He.

Then, assuming ^{4}Her ~0 at.g^{-1} we can write:

$$^{3}He_c = {}^{4}He_{melt} \cdot [(^{3}He/^{4}He)_{melt} - (^{3}He/^{4}He)_{mag}] \quad (1)$$

Under certain conditions, one can also construct isochrons in the $^{3}He/^{4}He$ *vs* $1/[^{4}He]$ space (Cerling and Craig, 1994b; Blard and Pik, 2008), thereby avoiding the first crushing step, which can trigger possible loss of matrix sited helium (Hilton *et al.*, 1993; Scarsi, 2000; Yokochi *et al.*, 2005; Blard *et al.*, 2006).

However, given the concentrations of U and Th in olivine and pyroxene, the radiogenic ^{4}He component can rarely be neglected (Blard and Farley, 2008). Consequently, in many situations, the amount of magmatic ^{3}He cannot be corrected by measuring the bulk ^{3}He /^{4}He ratio. $^{3}He_c$ determinations thus require a crushing step which needs to be sufficiently long and intense to release most of the trapped magmatic helium, but not too intense in order to avoid releasing the matrix sited cosmogenic ^{3}He (Scarsi, 2000; Yokochi *et al.*, 2005; Blard *et al.*, 2006; Blard *et al.*, 2008). Alternatively, a previous study (Williams *et al.*, 2005) conducted on pyroxene microphenocrysts of Pliocene basalts of Gran Canaria (Canary Islands) has shown that the magmatic component may be negligible in the smallest grains (i.e. 125-250 ⌈m). In the case of moderate to high (> 0.5 $mm.yr^{-1}$) erosion rates, the cosmogenic ^{3}He concentration in river sands is low ($<10^{-17}$ $mol.g^{-1}$), implying that the resulting magmatic ^{3}He correction could represent a significant source of uncertainty. Consequently, it is particularly important to overcome this methodological limitation for old phenocrysts having significant amounts of radiogenic ^{4}He.

In the present study, we test the possibility to yield reliable cosmogenic ^{3}He-based denudation rates in basins dominated by old lavas. We observed that coarse-grained aliquots display very variable ^{3}He concentrations. However, fine-grained aliquots exhibit ^{3}He concentrations homogeneous enough to allow correction of the magmatic component with a reasonable precision and confidence. We then looked for the main source of this variability of the coarse aliquots.

Our experiments were carried on river-borne pyroxenes from two Ethiopian rivers draining two different watersheds of the Ethiopian plateau. This work represents an important step for the study of the geomorphologic processes involved in this region, and, more generally, for estimating erosion rates in old volcanic provinces.

2 Geomorphological setting of the Ethiopian plateau and sampling

The Northwestern Ethiopian plateau is a major feature of the Ethiopian traps, a 1.5 km-thick continental flood basalts (CFB) sequence (Fig. 1) (Mohr, 1983). This imposing volcanic pile was erupted 30 Ma ago, and the entire volume of basalt was emplaced in less than 2 Myr (Hofmann *et al.*, 1997; Rochette *et al.*, 1998). On its eastern margin, along the major Afar escarpment, most of this volcanic sequence consists of ankaramitic porphyritic basalts, with local presence of ignimbrites at the top of the eruptive sequence (Pik *et al.*, 1998; Pik *et al.*, 1999; Ayalew *et al.*, 2002). These geological characteristics are particularly well suited for ^{3}He analyses because rivers draining the Ethiopian plateau bear large amounts of pyroxene and olivine phenocrysts.

Determining patterns in the denudation rate in this region is of great interest for understanding climate-tectonic-erosion interactions. First, erosion has a major long term influence on the global atmospheric CO_2 budget (Berner et al., 1983; Galy et al., 2007), even in the case of spatially and temporally discrete large volcanic provinces emplaced on continents (Dessert et al., 2001). Second, the development of the centrifuge drainage network in this region is key to understanding the uplift and tectonic evolution of the plateau and its margins (McDougall *et al.*, 1975; Cox, 1989; Pik *et al.*, 2003; Pik, 2011). In this study, we focused on the comparison of two river catchments, located on both sides of the main plateau drainage divide (Fig. 1).

On the eastern side of the divide, the topographic scarp undergoes both an active morphological evolution linked to the development of its marginal graben system and moderate monsoon precipitations (700-1000 $mm.yr^{-1}$) (Conway, 2000). The Mile river, whose watershed covers <1600 km^2 with a mean slope of 13°, flows toward the Afar depression through this major topographic feature (Fig. 1). A ~2 kg sample of Mile river sand was collected on the 25th of February, 2009, at the outlet of the basin catchment (11.62696 °N ; 39.97236 °E) where it enters the Afar plain.

By contrast, the northern part of the plateau is generally lower in elevation because most of the original highland morphology has already been eroded by propagation of the Tekeze river. (Fig. 1b). The upper part of the actively propagating Tekeze river catchment has a total surface of <750 km^2 and a mean slope of 16°. As for the Mile river sand sample, a ~2 kg sample of Tekeze river sand was collected at 11.91338 °N ; 38.97681 °E) in February 2009. In each river, the sampled stream-bed sands are mainly composed of lava gravels (essentially basaltic with minor

occurrence of rhyoltic clasts) up to <2 cm in size, single mineral grains (pyroxene, olivine and quartz), and organic debris.

It must be noted that despite their similar mean slopes, these two watersheds display very different morphologies. While the upper part of the Tekeze river is mainly a high plateau incised by deep valleys, the Mile river hillslopes range from steep at its headwater to gentle slopes along several large North-South oriented valleys (Fig 1b).

Cosmogenic nuclide measurement in river sands has proven to be a particularly robust method to constrain basin-averaged denudation rate at timescales of several hundred to thousand years (e.g. (Brown *et al.*, 1995) (von Blanckenburg, 2005), while thermochronology methods quantify denudation over million year timescales (e.g. (Pik *et al.*, 2003). The two watersheds presented here are theoretically particularly suited to this method because they are characterized by an homogenous lithology, sparse vegetal cover, no ice or snow cover, limited influence of catastrophic erosive events such as landslides and no significant storage of sediments.

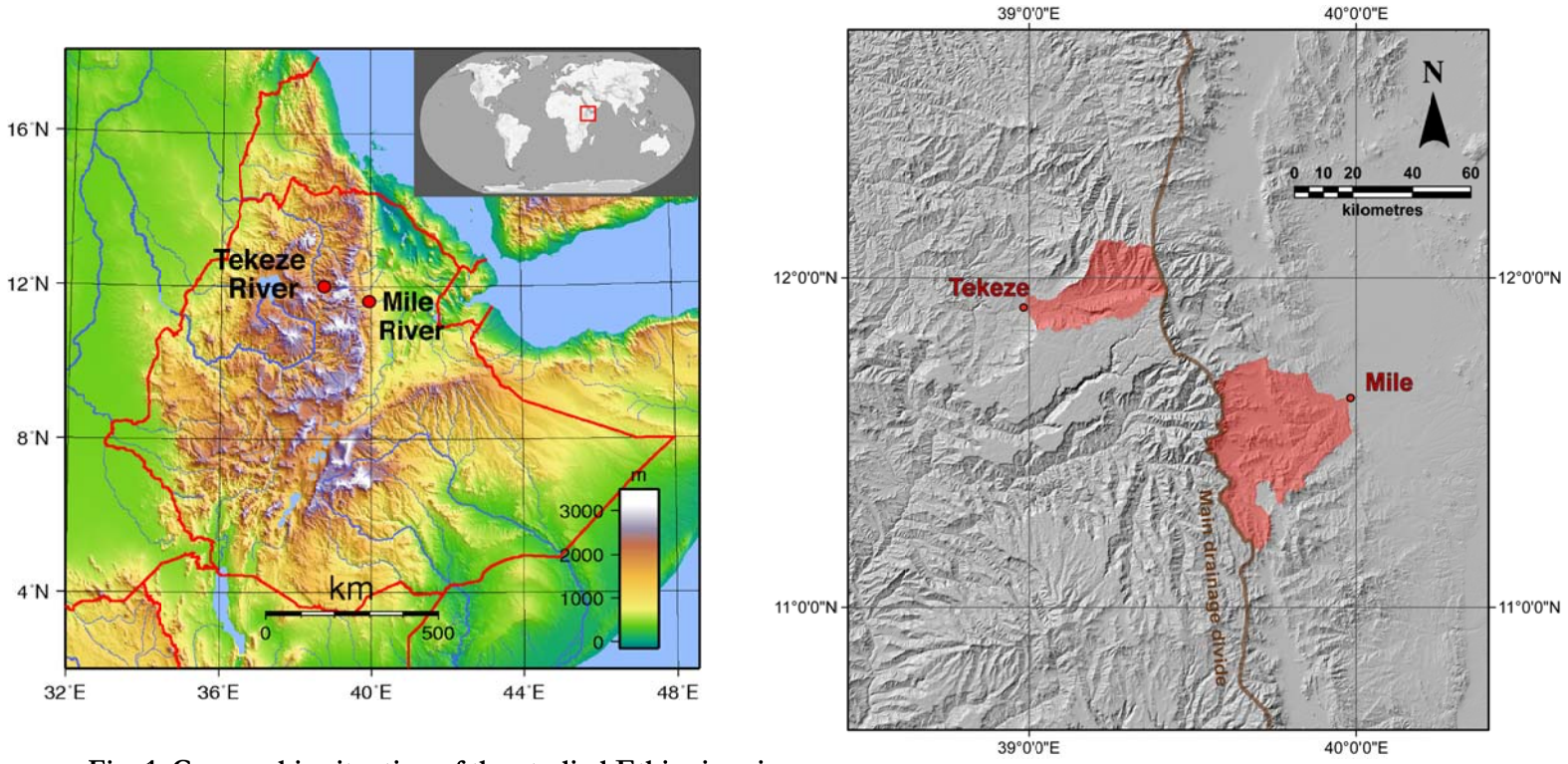

Fig. 1: Geographic situation of the studied Ethiopian rivers.

a) : Relief map of Ethiopia with localization of the two rivers. The WGS 84 coordinates for the sampling spots are: Tekeze River: 11.91338N ; 38,97681E. Mile River: 11.62696N; 39.97236E.

b): Shaded SRTM Digital Elevation Model of the study area (90m resolution) with the two watersheds (red shadow) and their outlets (i.e. the two sampling spots, in red). The main drainage divide of the Ethiopian plateaus (brown line) follows the tectonic scarp, with rivers running toward the Blue Nile and Tekeze River at the west, and toward the Afar at the east.

3 Methods

3.1 Mineral separation

Bulk sands were sieved under flowing water into two granulometric fractions: 0.3-0.5 mm and >0.5 mm.

Concerning the 0.3-0.5 mm fraction, pyroxene grains were first concentrated from the bulk sand using two magnetic separations using a Frantz device. Almost pure pyroxene and olivine grains were then obtained by gravimetric separation in di-iodomethane (density ~3.3 $g.cm^{-3}$). After washing in diethyl ether and drying, the grains were cleaned from any dust impurity in an ultrasonic bath of deionized water and acetone for 15 minutes.

After drying, all grains with attached lava fragments were removed and discarded by handpicking under a binocular microscope. Olivine grains (<5 % of the phenocrysts) were also separated and set aside. We chose to work on pyroxenes because they were more abundant in our samples and thus easier to separate. We interpret these higher modal pyroxene abundances with respect to the basaltic source rocks as due to more rapid abrasion and weathering of the olivines on the slopes and the river stream.

For the >0.5 mm fraction, pyroxene phenocrysts were directly hand picked under a binocular microscope from the bulk sieved sand. They were then cleaned in a deionized water and acetone bath for 15 minutes.

For the Tekeze River, the >0.5 mm bulk sand remaining after the first handpicking was finally sieved again at 1 mm, and phenocrysts from this >1 mm bulk sand were handpicked and cleaned following the same procedure.

3.2 Analytical procedures

In-vacuo crushing extractions were performed with a soft iron slug activated by external solenoids, for 5 minutes at 100 strokes/minute, except for one sample (Tekeze 15 ; 10 minutes). Aliquot weights range between 130 and 360 mg, representing < 100-300 grains for the >0.5 mm fraction and < 800-2200 grains for the 0.3-0.5 mm fraction. Typical ^{4}He and ^{3}He blanks for the crushing experiments were $3.1 \pm 0.4 \cdot 10^{-16}$ mol and $6.0 \pm 1.4 \cdot 10^{-20}$ mol respectively.

The resulting powders were then sieved to remove the <70 ⌈m fraction, and hence minimized any loss of matrix-sited helium that could have occurred during the crushing procedure (Blard *et al.*, 2008). The remaining powders and uncrushed pyroxene aliquots were subsequently wrapped in copper foils and fused at high temperature.

High temperature extractions were performed in a new high temperature furnace designed at CRPG (Nancy, France) (Zimmermann *et al.*, 2012). After a 20-minute temperature ramp, samples were maintained at 1350°C for 20 minutes. Typical ^{4}He and ^{3}He blanks for this procedure were 3.0 ± 0.5 ·10-18 mol and 1.1 ± 0.8 ·10-20 mol respectively. Re-extractions were always in the blank range, indicating that the extraction was complete after the first heating step. After extraction, the gas was purified using activated charcoal at -196°C and with hot (400°C and 600°C) and ambient temperature (21°C) Titanium sponge getters. A complete description of the furnace and the purification line can be found in (Zimmermann *et al.*, 2012).

Helium was analyzed on the GV HELIX Split Flight Tube dual collection mass spectrometer. The instrument sensitivity was determined using the HESJ standard (Matsuda *et al.*, 2002) whose certified $^{3}He/^{4}He$ ratio is 20.63 ± 0.10 Ra (Ra = 1.384×10^{-6} being the atmospheric $^{3}He/^{4}He$ ratio). Most of the Mile river samples were analyzed first. During a 2 months period, external reproducibility was 2.7% and 3.9% (1 ⌠) for ^{4}He and ^{3}He, respectively.

The remaining Mile samples (the crushed Mile 5, 11, 12 and 14) and the Tekeze samples were analyzed with different ionization source settings. Over this one-month period, external reproducibility was always less than 0.4% for 4He and 0.5% for ^{3}He.

4 Results

All helium results are reported in Table 1 and ^{3}He results plotted on Fig 2.

4.1 Crushing analyzes

For the Mile river, crushing of the >0.5 mm grains yielded 3He concentrations ranging between 2.08 ± 0.27 x10-18 mol.g-1 and 5.25 ± 0.63 x10-18 mol.g-1. 3He/4He ratios ranged between 2.67 ± 0.45 and 5.20 ± 0.83 Ra.

For the Tekeze river, crushing of the coarser grains (>0.5 mm and >1 mm) yielded 3He concentrations between 4.20 ± 0.12 x10-18 mol.g-1 and 1.92 ± 0.04 x10-17mol.g-1, which is significantly higher than the Mile river. This discrepancy is probably due to differences in the petrography of the outcropping basalts in the two basins and to a longer sediment transport in the Mile river (see discussion in section 5.2 and 5.3). One 0.3-0.5 mm sample was also crushed and gave a ^{3}He concentration ($2.97 \pm 0.17 \times 10^{-18}$ mol.g^{-1}), lower than the range of the larger grains. ^{3}He /^{4}He ratios ranged between 3.39±0.19 - 13.6±0.7 Ra.

For both rivers 3He/4He ratios are in good agreement with the high ^{3}He mantle plume values reported by Marty *et al.* (1996) from crushing similar high-Ti lava phenocrysts (Pik *et al.,* 1999). It must be noted that the sample crushed for 1000 strokes instead of only 500 is within the range of the other samples, for both ^{3}He concentrations and ^{3}He /^{4}He ratios. A five minute crushing in our apparatus seems therefore sufficient to release at least 90% of the trapped magmatic helium, as shown by Scarsi (2000) with a similar apparatus.

4.2 Heating analyzes

For the Mile river (Fig. 2a), either direct melting of intact >0.5 mm pyroxenes, or addition of the concentrations from crushing and melting steps when applied, yielded high and variable values ($7.35 \pm 0.31 \times 10^{-18}$ to $15.4 \pm 2.2 \times 10^{-18}$ mol.g^{-1}). Conversely, fusion of the bulk 0.3-0.5 mm grains and fusion of the powder obtained from the >0.5 mm crushed grains, yielded homogenous and lower ^{3}He concentrations ($4.62 \pm 0.39 \times 10^{-18}$ to $6.83 \pm 1.41 \times 10^{-18}$ mol.g^{-1}).

The Tekeze river samples display comparable results (Fig. 2b): small and crushed phenocrysts have lower and clustered ^{3}He concentrations ($10.5 \pm 0.2 \times 10^{-18}$ mol.g^{-1} to $14.0 \pm 0.3 \times 10^{-18}$ mol.g^{-1}), while the bigger phenocrysts contain higher and more variable ^{3}He (7.18 ±

0.18 ×10^{-18} mol.g^{-1} to 24.7 ± 0.8 ×10^{-18} mol.g^{-1}). However, 4 out of the 12 aliquots for the >0.5 mm fraction contained less ^{3}He than the 0.3-0.5 mm ones. Additionally, for 6 aliquots, melting of the crushed grains of the > 0.5 and > 1 mm fraction yielded less 3He than the direct melting of 0.3-0.5 mm grains, unlike the Mile River.

For all heating experiments, the 3He/4He ratios were low (between 0.29 ± 0.04. and 1.57 ± 0.08 Ra) for both the bulk samples and for the powders (between 0.36 ± 0.02 and 0.76 ± 0.04 Ra). These very radiogenic values were expected, given the age of the Oligocene traps and their U-Th concentrations (Marty *et al.*, 1996): ^{4}He concentrations were always >6.69 · 10^{-12} mol.g^{-1} in the powders.

For both river sands, crushing and heating experiments hence show that:

- The total ^{3}He content is on average higher in the >0.5 mm fraction (10.2 ± 2.6 × 10^{-18} mol.g^{-1} for Mile and 15.5 ± 6.3 × 10^{-18} mol.g^{-1} for the Tekeze) than in the 0.3-0.5 mm fraction (5.48 ± 0.4 × 10^{-18} mol.g^{-1} for the Mile and 11.5 ± 1.5 × 10^{-18} mol.g^{-1} for Tekeze).
- The coarse grains (> 0.5 mm) have more variable helium contents. While crushing of the bigger grains released variable amounts of ^{3}He, melting of the resulting powders yield similar and low ^{3}He concentrations (Fig 2).
- The similar concentrations obtained by melting the powdered grains indicate that the crushing was able to release a significant proportion of the total fluid-inclusion-sited ^{3}He content.

In the following section we discuss these results taking into account the various helium sources and propose several hypotheses to explain such a grain size-dependent behavior.

Sample provenance and grain size	n¡	Treatment	Sample mass (mg)	^{3}He (10^{-18} mol.g^{-1})	±	^{4}He (10^{-12} mol.g^{-1})	±	^{3}He/^{4}He (R_a)	±
Mile River									
0.3-0.5 mm	1	direct melt.	239	5.55	0.36	11.769	0.005	0.34	0.02
	2	d. m.	250.6	5.20	0.73	12.817	0.001	0.29	0.04
	3	d. m.	251.5	5.40	0.23	12.108	0.004	0.32	0.01
	4	d. m.	242.9	5.79	0.69	13.20	1.38	0.32	0.05
	5	crushing	181.2	2.08	0.27	0.56	0.06	2.67	0.45
		melting	120.8	4.15	0.32	8.261	0.003	0.36	0.03
> 0.5 mm	6	d. m.	302	12.41	0.38	-	-	-	-
	7	d. m.	141.8	8.03	0.93	9.16	0.96	0.63	0.10
	8	d. m.	158.9	9.5	1.1	8.69	0.91	0.79	0.13
	9	d. m.	171.2	15.4	2.2	9.77	1.02	1.1	0.20
	10	d. m.	260	7.35	0.31	8.670	0.001	0.61	0.17
	11	cr.	266.4	2.51	0.33	0.665	0.070	2.7	0.5
		m.		6.21	0.40	6.930	0.002	0.65	0.04
	12	cr.	237.6	5.00	0.59	0.828	0.087	4.4	0.7
		m.	101.5	4.62	0.39	6.694	0.003	0.50	0.04
	13	cr.	268.5	5.25	0.63	0.729	0.076	5.2	0.8
		m.	166.4	6.83	1.41	6.784	0.711	0.7	0.2
	14	cr.	162.2	4.07	0.54	0.600	0.063	4.9	0.8
		m.	113.9	4.03	0.22	8.046	0.002	0.36	0.02
Tekeze River									
0.3-0.5 mm	1	d. m.	267.1	11.58	0.17	10.767	0.042	0.78	0.04
	2	d. m.	232.5	10.51	0.18	12.916	0.051	0.59	0.03
	3	d. m.	186.6	10.77	0.26	10.962	0.044	0.71	0.04
	4	d. m.	189.5	14.02	0.28	11.173	0.044	0.91	0.05
	5	d. m.	174.9	10.48	0.25	10.634	0.043	0.71	0.04
	6	cr.	129	2.97	0.17	0.540	0.004	4.0	0.3
		m.	95.1	-	-	-	-	-	-
> 0.5 mm	7	d. m.	185.5	9.73	0.21	10.047	0.040	0.70	0.04
	8	d. m.	185.2	7.18	0.18	9.00	0.37	0.58	0.04
	9	d. m.	214	10.62	0.20	9.760	0.039	0.78	0.04
	10	d. m.	167.9	8.20	0.21	10.768	0.043	0.55	0.03
	11	d. m.	213.1	24.14	0.33	11.106	0.077	1.57	0.08
	12	cr.	330	5.61	0.10	0.378	0.002	10.71	0.58
		m.	256.5	8.69	0.17	8.303	0.033	0.76	0.04
	13	cr.	302.8	5.29	0.11	1.127	0.005	3.39	0.19
		m.	213.4	17.20	0.30	17.207	0.068	0.72	0.04
	14	cr.	380	6.54	0.14	0.853	0.004	5.5	0.3
		m.	306.8	8.98	0.19	11.556	0.046	0.56	0.03
	15	cr.*	317.1	4.20	0.12	0.494	0.006	6.1	0.2
		m.	108.8	7.62	0.29	8.439	0.085	0.65	0.03
	16	cr.	212.4	16.26	0.24	0.861	0.004	13.6	0.7
	17	m.	248.7	7.82	0.18	8.839	0.035	0.64	0.04
>1 mm	18	cr.	358.5	8.60	0.20	0.695	0.008	8.9	0.2
		m.	65.1	6.13	0.23	9.106	0.091	0.49	0.02
	19	cr.	306.2	19.20	0.41	1.206	0.013	11.5	0.3
		m.	65.1	5.54	0.34	7.292	0.083	0.55	0.03

Table 1 : Helium data

Treatments: d. m. stands for direct melting of the phenocrysts, cr. for crushing and m. for the melting of the powder obtained by crushing.

** Tekeze 15 was crushed with ~1000 strokes, instead of ~500.*

^{3}He/^{4}He ratios are normalized to the atmospheric ratio $R_a = 1.384 \times 10^{-6}$. Errors are $\pm 1\sigma$

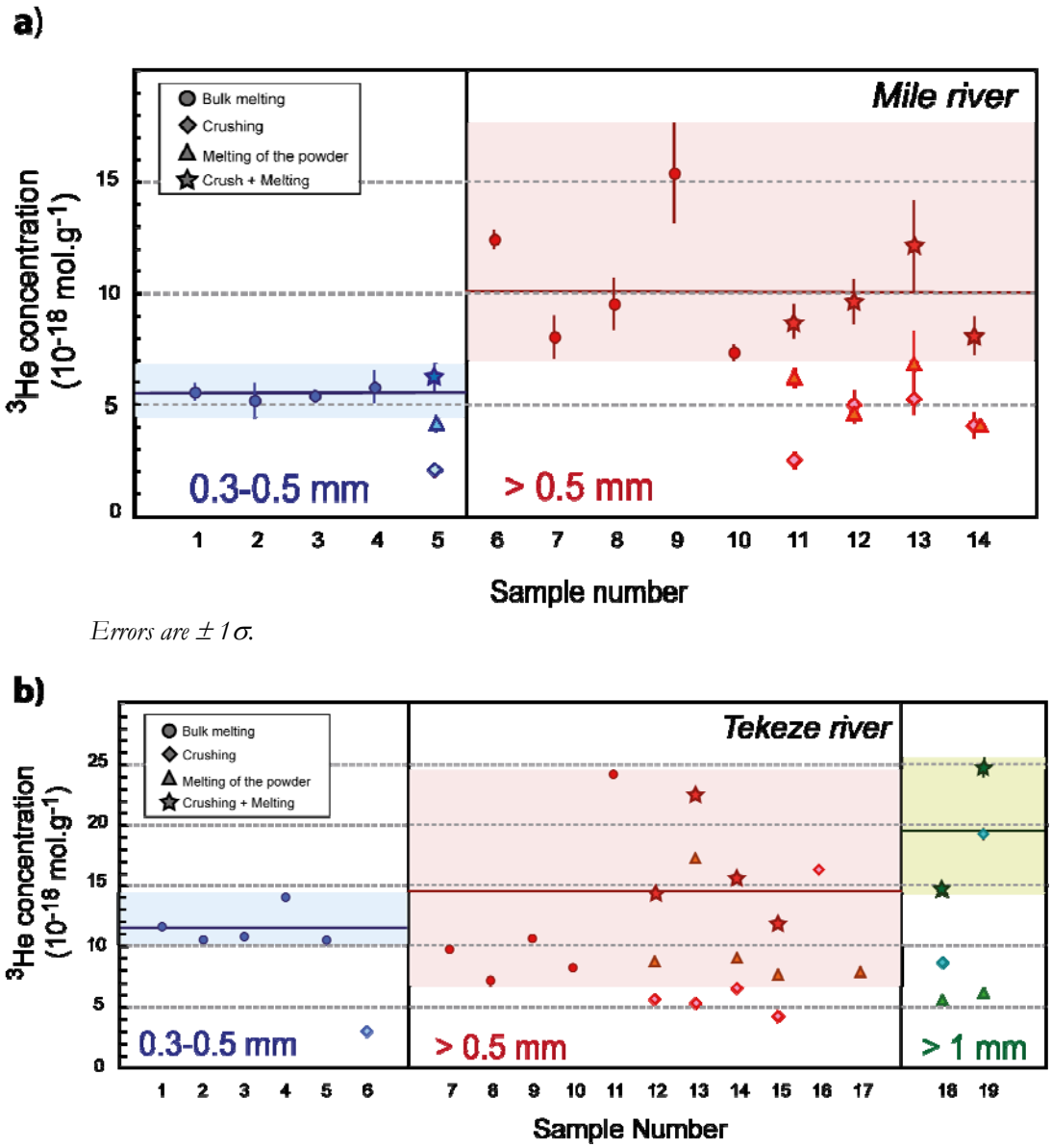

Errors are ± 1σ.

Fig 2 - Compilation of the measured ^{3}He concentrations.

a) results for the Mile River b) results for the Tekeze River.

Concentrations are plotted in 10^{-18} mol.g^{-1} . The sample numbers correspond to the ones used in the result table. The 0.3-0.5mm aliquots are plotted on a blue background, the >0.5mm ones on a red background and the >1mm ones on a green background. For some samples the 1σ error bars are smaller than the size of the dots. Due to analytical problems, we do not have measurements for the melting of the Tekeze aliquots n°6 and 16, and for the crushing of aliquot n°17

5 Discussion

5.1 Influence of nucleogenic ^{3}He

The theoretical long-term nucleogenic ^{3}He production (see section 1) in the studied samples was calculated following Andrews and Kay (1982). We used the chemical contents reported by Pik *et al.* (1998, 1999), and a Li concentration of 2 ppm in olivine and pyroxene, as measured by the Service d'Analyse des Roches et des Minéraux (S.A.R.M.) of CRPG (Nancy, France). The implantation and ejection correction (Farley *et al.*, 2006) was negligible because the phenocryst-lava partition coefficient for Li is very close to 1 for these basalts. The so-calculated ^{3}Hen production rate is $1.1 \cdot 10^{-26}$ mol.g^{-1}.yr^{-1}, which yields a theoretical concentration of $3.3 \cdot 10^{-19}$ mol.g^{-1} on average over 30 Myr. This value represents <6% of the total ^{3}He measured in the sample bearing the lowest amount of matrix-sited ^{3}He. Thus, nucleogenic ^{3}He has only a minor influence in the studied samples compared to the large inter-aliquots ^{3}He variability, and it cannot itself explain it, nor the grain size dependency.

5.2 Influence of the spatial variability of denudation rates

Several studies have suggested that heterogeneous denudation rates within a drainage basin could induce a measurable inter-aliquot variability of the cosmogenic nuclides concentration (Codilean *et al.,* 2008; Gayer *et al.*, 2008). Indeed, average denudation rates can vary up to several orders of magnitude within the same drainage basin. Furthermore, steep drainage basins are characterized by quite variable cosmogenic production rates, as a result of their scaling with the altitude (e.g. Lal, 1991; Stone, 2000; Dunai, 2001).

For the two studied watersheds (Mile and Tekeze rivers), we have developed a simplified Monte Carlo model to simulate the stochastic effects associated with the sampling of small aliquots of river sands. We first applied to a Shuttle Radar Topographic Mission (SRTM) Digital Elevation Model (DEM) a simple fluvial shear stress (Lave and Avouac, 2001; Lave and Burbank, 2004) incision law from slopes gradient and runoff to produce a theoretical denudation map of our watershed (Lave, 2005). The goal here was not to produce a precise model of denudation but a realistic and first order estimate of the denudation variability within the basin. From these denudation maps, we then derived the theoretical cosmogenic concentration at each point of the basin.

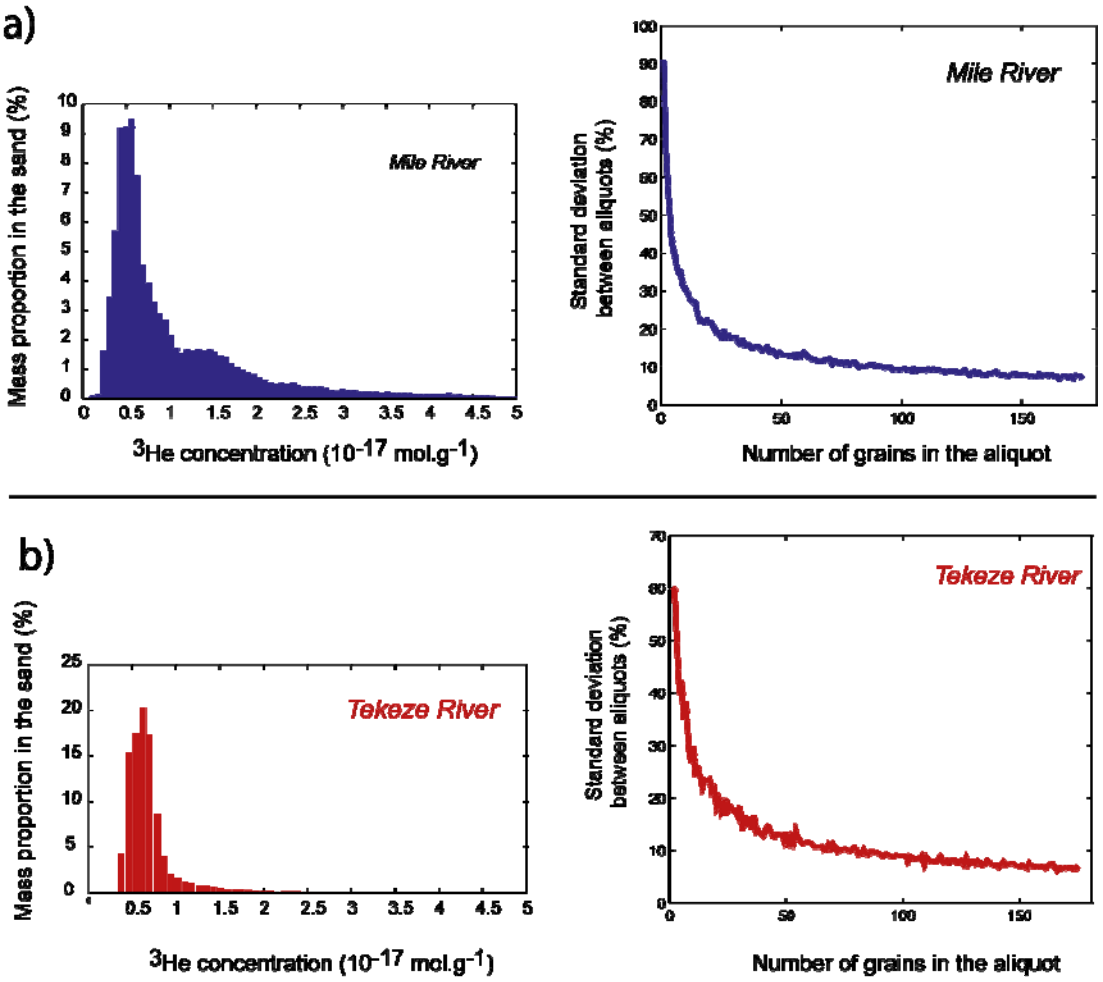

Fig 3 - Modeling of a river sand sampling at the outlet of the Mile (a) and Tekeze (b). *Left: repartition of sediment proportion in each cosmogenic concentration classes, in percent (300 classes were modeled here). Right: Standard deviation between aliquots as a function of the number of grains (500 draws were performed here for each aliquot)*

Production rates were calculated at each point of the DEM grid, using the time-independent scaling of Stone (2000) and the topographic shielding of Dunne *et al.* (1999). We used a Sea Level High Latitude production rate of $1.99 \pm 0.16 \cdot 10^{-22}$ mol.g^{-1}.yr^{-1} (120 ± 9 at.g^{-1}.yr^{-1}) (Goehring *et al.*, 2010). Then we simulated the concentration distribution in a well-mixed sand at the basin outlet. Finally we performed a random picking of aliquots with sizes ranging from 1 to 150 grains (500 draws for each number of grains).

For aliquots of only <80 grains, the standard deviation between aliquots falls below 10%, for both watersheds (Fig 3). Given that the aliquots we analyzed are composed of more than 200 grains (standard deviation <5%), this modeling confirms that the observed ^{3}He inter-aliquots variability cannot be due to a stochastic sampling of grains having recorded variable denudation rates.

In our case, "Nugget effects" (i.e. the case where one or some grains have such an high concentration that they may influence the concentration of the whole aliquot) that would be due to poor sorting in the coarsest samples, could only account for the limited post-crushing variability.

Consequently, the remaining most plausible cause for the observed bulk ^{3}He variability seems to be the heterogeneity of the magmatic ^{3}He amount between the different aliquots. This hypothesis is discussed in the following section.

5.3 Interaliquot variability: impact of the magmatic helium component

As summarized at the end of §4.2, crushing of the coarser aliquots released variable amount of magmatic ^{3}He, while melting of the resulting powders released much more similar quantities of remaining ^{3}He (Fig. 2 and table 1), most probably represented by the sole matrix-sited cosmogenic component. This suggests that most of the variability of the total 3He is due to the fluid inclusion-sited magmatic helium.

As discussed at the end of §5.2, merging hundreds of grains in each aliquot should be enough to homogenize the cosmogenic ^{3}He concentration. Our data prove that it is not necessarily the case for magmatic ^{3}He. Actually, as shown in Fig. 4, numerous published data display a significant variability in magmatic helium. These helium data were obtained in olivine and pyroxene phenocrysts from basalts of different geological settings (Kurz *et al.*, 1990; Licciardi *et al.*, 1999; Dunai and Wijbrans, 2000; Ackert *et al.*, 2003; Blard *et al.*, 2005; Blard *et al.*, 2006; Licciardi *et al.*, 2006; Goehring *et al.*, 2010). In these studies, lavas are usually young (< 200 ka) so that the radiogenic ^{4}He correction does not represent a significant source of uncertainty.

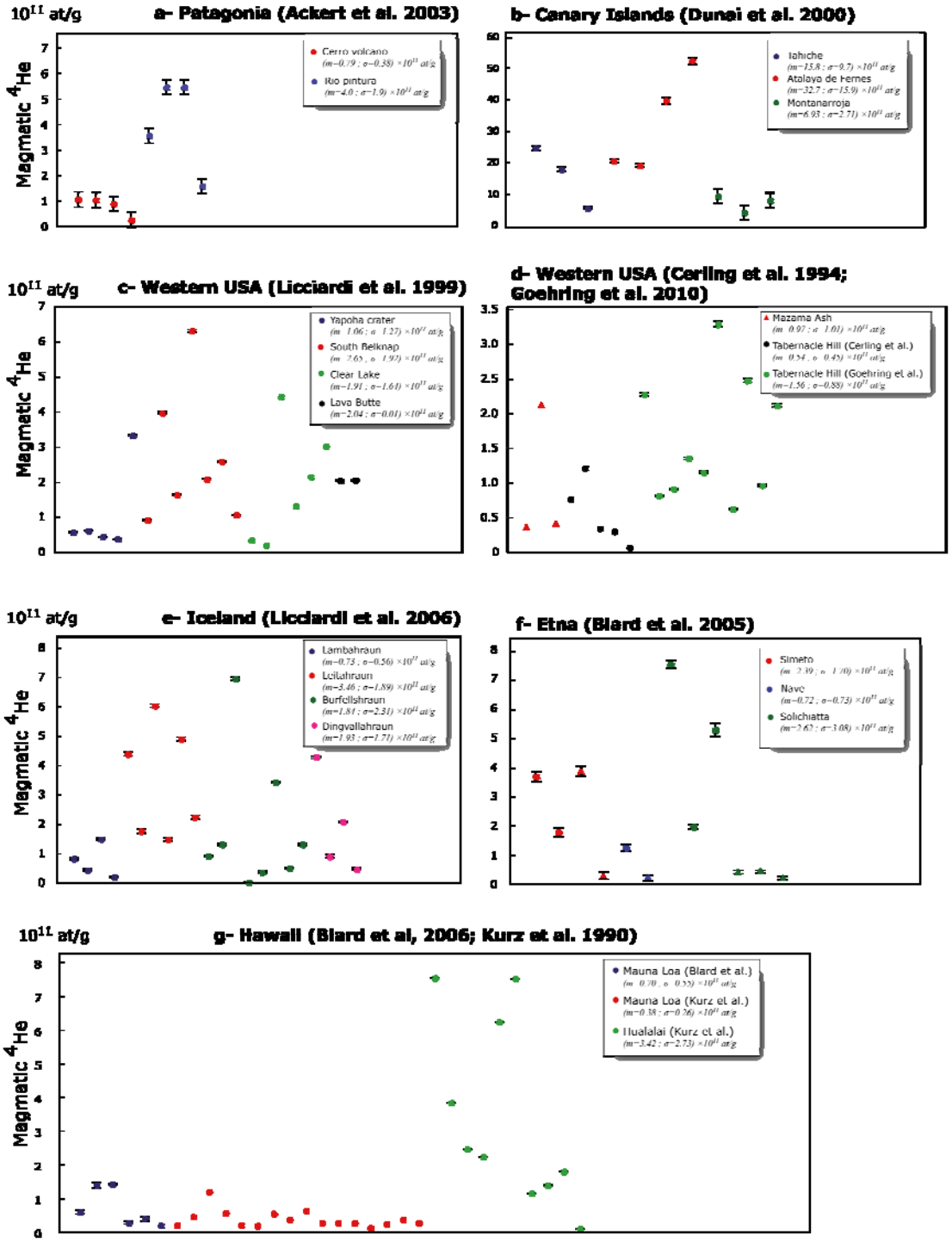

(caption on the next page)

Fig. 4 (previous page) - Magmatic ^{4}He concentrations, compiled from various cosmogenic ^{3}He production rate calibration studies. *All ordinates axes are scaled in (10^{11} at.g^{-1}). Olivine and pyroxene data are represented by circles and triangles, respectively. In all these studies, typical aliquot size was between 100 and 300 mg, ensuring the presence of more than 100 grains. This compilation thus clearly shows that, even between aliquots of several hundreds of grains, the magmatic helium component is commonly higly variable.These concentrations were determined by subtracting the radiogenic ^{4}He from the total ^{4}He concentrations reported in the following references: a- (Ackert et al., 2003) (0.5-1 mm phenocrysts.); b- (Dunai and Wijbrans, 2000); c- (Licciardi et al., 1999); d- (Cerling and Craig, 1994a) and (Goehring et al., 2010)(0.5-1 mm phenocrysts); e- (Licciardi et al., 2006) (0.3-1 mm phenocrysts); f- (Blard et al., 2005) (0.6-1 mm); g- (Kurz et al., 1990) (1-2 mm) and (Blard et al., 2006) (0.6 -1 mm)*

This compilation clearly shows that a large variability in magmatic helium is common between aliquots of hundreds of grains, even when the measured aliquots originate from the same sample of a lava flow surface. Therefore, in the case of aliquots resulting from the mixing of heterogeneous detrital material, such as in our study, it is not surprising to observe a significant variability in magmatic helium concentrations. This effect is larger for aliquots bearing large phenocrysts (> 0.5 mm), as discussed in the following section.

5.4 Magmatic content dependence on the grain size: insights from the radiogenic ^{4}He

Given the age of the basaltic sequence (30 Myr) (Hofmann et al., 1997), the grain's lattice contains large amounts of radiogenic ^{4}He. Most of the ^{3}He/^{4}He variability reported in section 4.1 can be explained by the loss of a small fraction of this radiogenic ^{4}He during the crushing, as discussed by Marty *et al.* (1996). The matrix-sited ^{4}He is furthermore known to be more prone to loss during the crushing procedure than the matrix-sited cosmogenic ^{3}He (Scarsi, 2000).

Assuming: (i) U and Th concentrations in the surrounding lava of 1.5 and 4 ppm, respectively (Pik *et al.,* 1999), (ii) U and Th concentrations in the phenocrysts of 0.060 and 0.100 ppm, respectively, measured by ICP-MS; (iii) an initial grain diameter of 3mm, which is the size of the

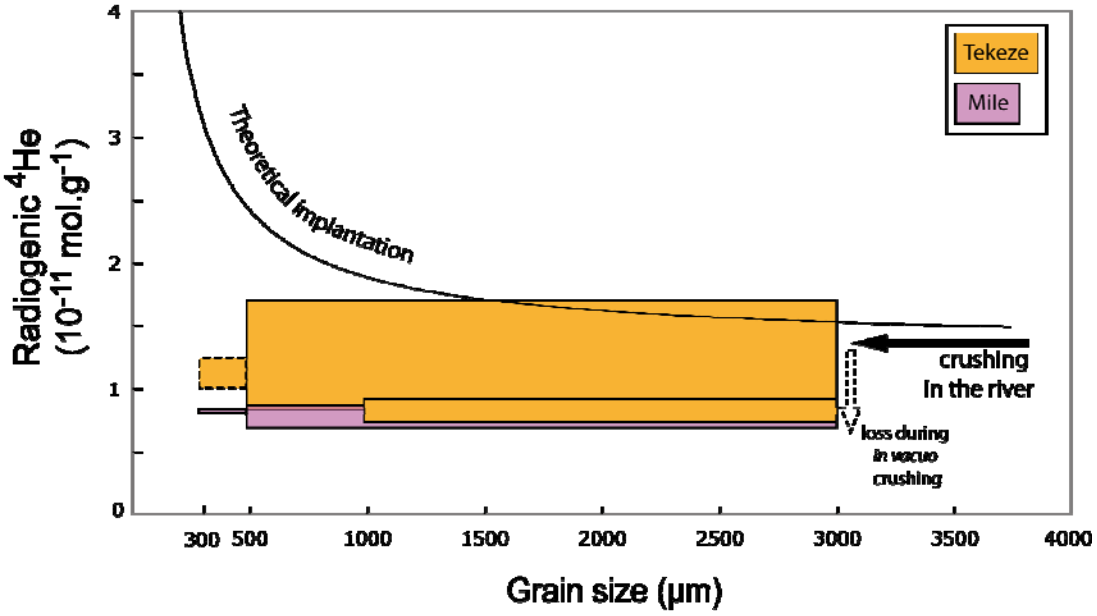

Fig. 5 - Theoretical and measured implantation of radiogenic ^{4}He as a function of grain size. *For the theoretical curve, we used the model of Dunai and Wijbrans (2000). The radiogenic component (^4He_r) is measured by melting powders of grains previously crushed to remove the magmatic ^{4}He (table 1). For the 300-500 µm grains from the Tekeze river, we had no analyze of this type, and thus calculated ^4He_r by subtracting the ^{4}He extracted by crushing of an aliquot from the total ^{4}He in other bulk aliquots. Concentrations are similar in all granulometric fractions and lower than the theoretical value, which suggests a crushing in the river from an originally larger size. Alternatively, a loss of a small fraction of ^4He_r during in-vacuo crushing is possible (see §5.4).*

biggest grains found in the samples, the theoretical 4He radiogenic concentration is 15×10^{-12} mol.g^{-1}, using the calculation of Dunai and Wijbrans (2000) (fig. 5). This theoretical value is close to the analytical values we obtained ($9.4 \pm 1.8 \times 10^{-12}$ mol.g^{-1} for the Mile river and $11 \pm 2 \times 10^{-12}$ mol.g-1 for the Tekeze), and is ~10 times higher than the average magmatic ^{4}He concentrations determined by crushing.

The fact that the radiogenic contents are very similar in the small and big grains strongly suggests that all phenocrysts had similar initial size. This is because the smaller phenocrysts would theoretically have more radiogenic 4He values due to higher 4Her implantation (fig. 5). According to the same calculation, a 0.3 mm grain would for instance contain 2.7×10^{-11} mol.g^{-1} of ^{4}Her, and a 1 mm grain 1.9×10^{-11} mol.g^{-1}, both being significantly higher than what we really measured in the pyroxene grains.

Consequently, grain fragmentation during the sediment transport is probably responsible of the grain size distribution observed today in the river bedload.

Besides, we observe that the crushing of the coarser grains released significantly higher amounts of ^{3}He than the smaller grains. This observation indicates that the bigger minerals tend to contain more magmatic helium than the smaller ones, in line with the conclusions of Williams *et al.* (2005). These authors proposed that the higher magmatic content of the bigger grains is a consequence of magmatic processes. The microphenocrysts would have crystallized later than the bigger ones, in a more degassed magma, and hence would have trapped lower amounts of magmatic helium.

Our results also show a larger variability of the magmatic helium concentration in larger grains (§5.3), which supports a complementary hypothesis in the case of the Ethiopian plateau ankaramitic, high-Ti province: bigger grains have a higher probability to bear several very large melt inclusions. This observation also supports the idea that the smaller river grains result from the crushing of bigger grains during the riverbed transportation and the hillslope processes. This natural crushing of the phenocrysts may have released an important amount of the fluid inclusion-sited helium, explaining the lower magmatic 3He content and the lower variability in smaller grains.

5.5 Denudation rates and geographic repartition over the margin and the Ethiopian plateau

Because it is not possible to simply use the magmatic ^{3}He /^{4}He ratio to correct such radiogenic ^{4}He polluted old Oligocene pyroxenes (equation 1), the only way to calculate and derive a reasonable value for the cosmogenic concentration is to use the most precise estimation of the magmatic concentration in order to subtract it from the total 3He. The complete investigation of the He budget we have done in this study has shown that the magmatic concentration of a sample can be significantly scattered for coarse grain size, whereas it is lower and more homogeneous for the the smallest granulometric fraction (0.3-0.5 mm) (Table 1). Therefore, in such a complex system, we propose to measure by crushing the magmatic concentration on an aliquot of this granulometric fraction and subtract it to any other melted aliquots of the same granulometric fraction. We stress that this can only be done in the case of these smaller grains because in that case the inter-aliquot variability is minimum (Fig. 2) and does not induce a prohibitive error on the estimated magmatic ^{3}He value.

Following this approach, we derived mass-weighted average 3Hec concentrations of $3.5 \pm 0.6 \times 10^{-18}$ mol.g^{-1} ($2.1 \pm 0.4 \times 10^{6}$ at.g^{-1}) for the Mile river and $8.5 \pm 1.5 \times 10^{-18}$ mol.g^{-1} ($5.1 \pm 0.8 \times 10^{6}$ at.g-1) for the Tekeze river. In both cases, this magmatic ^{3}He correction represents about 30% of the total ^{3}He extracted by fusing the 0.3-0.5 mm aliquots.

The basin-averaged denudation can thus be calculated applying (Lal, 1991; Brown *et al.*, 1995):

$$\Sigma = P \cdot \Lambda / (\rho \cdot {}^{3}He_c) \qquad (2)$$

Where P is the basin-averaged surface $^{3}He_c$ production rate (see §5.2), Λ the typical attenuation length (160 g.cm^{-2}, Lal, 1991), and ρ the density of the rock (2.7 g.cm^{-3}).

The calculated average denudation rate for the Mile river is 73 ± 18 mm.kyr^{-1} and 57 ± 11 mm.kyr^{-1} for the Tekeze basin. These similar values are consistent with the fact that both watersheds have comparable geology, steepness and pluviometry (Conway, 2000; Pik *et al.*, 2003). Such denudation rates are also consistent with long term (the last 5-10 Myr) denudation rates (90-180 mm.kyr^{-1}) proposed for a similar geomorphologic and climatic setting in this region by Pik et al. (2003), based on low temperature (U-Th)/^{4}He thermochronology. The very long term (last 25-29 Myr) denudation rate of the central plateau is however significantly lower (30 mm.kyr-1) than our values (Pik *et al.*, 2003). However in this area, the denudation is concentrated in the upper parts of the drainage system were the headwaters are quickly retreating into the plateau (Pik *et al.*, 2003). Hence, small and upstream catchments such as those of the Tekeze and Mile rivers are expected to display such higher modern denudation rate.

6 Conclusions

Crushing and heating experiments conducted on the detrital sands of two Ethiopian rivers indicate that the coarser phenocrysts (>0.5 mm) have higher and more variable concentrations in ^{3}He than the smaller ones (0.3-0.5 mm). In the case of the coarse grains, preliminary crushing reduces most of the discrepancies in bulk ^{3}He concentrations obtained by subsequent melting. This suggests that the magmatic ^{3}He, located in fluid inclusions, is responsible for most of this variability. Also, crushing experiments show that smaller phenocrysts tend to be less concentrated in magmatic ^{3}He. Moreover, Monte-Carlo simulations of a sand sampling in these basins showed that, for an homogenous granulometry and a well-mixed sand, spatial variation of erosion should induce only negligible variations in cosmogenic

^{3}He for aliquots of several hundreds of grains. Our interpretation is that large phenocrysts would be more likely to contain large fluid inclusions. Even several hundreds of grains are not enough to homogenize these heterogeneities and avoid "nugget effects". This may challenge accurate determination of cosmogenic ^{3}He.

Consequently, the more suited small fraction (0.3-0.5 mm) should be used to measure the magmatic concentration by crushing, and then to derive accurate cosmogenic ^{3}He concentrations.

In our case, these smaller grains are probably former bigger grains that have been broken during the transport in the rivers and consequently lost a significant proportion of their magmatic helium. This hypothesis is supported by the homogenous radiogenic ^{4}He implantation found in all grain sizes.

Average cosmogenic ^{3}He concentrations measured in the 0.3-0.5 mm aliquots allows calculation of average denudation rates of 73 ± 18 mm.kyr^{-1} for the Mile river basin and 57 ± 11 mm.kyr^{-1} for the Tekeze river basin. These rates are in good agreement with long-term denudation rates of the Ethiopian plateau as estimated by low temperature thermochronology (Pik *et al.*, 2003).

Acknowledgements

We thank Dereje Ayalew (Adis Abeba University), and Yohannes Haile-Selassie (Cleveland Museum) for their precious help on the field

We thank Pete Burnard, Laurent Zimmermann and Manuel Davy for their assistance in the analyses and mineral separation. Pete Burnard and Jennifer Mabry proofread several sections of a previous draft. Three anonymous reviews have improved greatly this manuscript since its first version.

References for this paper

Ackert, R. P., Singer, B. S., Guillou, H., Kaplan, M. R., and Kurz, M. D. (2003). Long-term cosmogenic ^{3}He production rates from ^{40}Ar/^{39}Ar and K-Ar dated Patagonian lava flows at 47°S. *Earth and Planetary Science Letters* **210,** 119-136.

Ammon, K., Dunai, T. J., Stuart, F. M., Meriaux, A. S., and Gayer, E. (2009). Cosmogenic (3)He exposure ages and geochemistry of basalts from Ascension Island, Atlantic Ocean. *Quaternary Geochronology* **4,** 525-532.

Andrews, J. N., and Kay, R. L. F. (1982). Natural production of tritium in permeable rocks. *Nature* **298,** 361-363.

Ayalew, D., Barbey, P., Marty, B., Reisberg, L., Yirgu, G., and Pik, R. (2002). Source, genesis, and timing of giant ignimbrite deposits associated with Ethiopian continental flood basalts. *Geochimica Et Cosmochimica Acta* **66,** 1429-1448.

Berner, R. A., Lasaga, A. C., and Garrels, R. M. (1983). The Carbonate-Silicate Geochemical Cycle and Its Effect on Atmospheric Carbon-Dioxide over the Past 100 Million Years. *American Journal of Science* **283,** 641-683.

Blard, P.-H., Lave, J., Pik, R., Quidelleur, X., Bourles, D., and Kieffer, G. (2005). Fossil cosmogenic ^{3}He record from K-Ar dated basaltic flows of Mount Etna volcano (Sicily, 38°N): Evaluation of a new paleoaltimeter. *Earth and Planetary Science Letters* **236,** 613-631.

Blard, P.-H., Pik, R., Lavé, J., Bourlès, D., Burnard, P. G., Yokochi, R., Marty, B., and Trusdell, F. (2006). Cosmogenic ^{3}He production rates revisited from evidences of grain size dependent release of matrix sited helium. *Earth and Planetary Science Letters* **247,** 222-234.

Blard, P. H., Lave, J., Pik, R., Wagnon, P., and Bourles, D. (2007). Persistence of full glacial conditions in the central Pacific until 15,000 years ago. *Nature* **449,** 591-U10.

Blard, P. H., and Farley, K. A. (2008). The influence of radiogenic (4)He on cosmogenic (3)He determinations in volcanic olivine and pyroxene. *Earth and Planetary Science Letters* **276,** 20-29.

Blard, P. H., and Pik, R. (2008). An alternative isochron method for measuring cosmogenic He-3 in lava flows. *Chemical Geology* **251,** 20-32.

Blard, P. H., Puchol, N., and Farley, K. A. (2008). Constraints on the loss of matrix-sited helium during vacuum crushing of mafic phenocrysts. *Geochimica Et Cosmochimica Acta* **72,** 3788-3803.

Brown, E. T., Stallard, R. F., Larsen, M. C., Raisbeck, G. M., and Yiou, F. (1995). Denudation rates determined from the accumulation of in situ produced ^{10}Be in the Luquillo experimental forest, Puerto-Rico. *Earth and Planetary Science Letters* **129,** 193-202.

Cerling, T. E., and Craig, H. (1994a). Cosmogenic ^{3}He production rates from 39°N to 46°N latitude, Western Usa and France. *Geochimica et Cosmochimica Acta* **58,** 249-255.

Cerling, T. E., and Craig, H. (1994b). Geomorphology and in-situ cosmogenic isotopes. *Annual Review of Earth and Planetary Sciences* **22,** 273-317.

Codilean, A. T., Bishop, P., Stuart, F. M., Hoey, T. B., Fabel, D., and Freeman, S. (2008). Single-grain cosmogenic Ne-21 concentrations in fluvial sediments reveal spatially variable erosion rates. *Geology* **36,** 159-162.

Conway, D. (2000). The climate and hydrology of the Upper Blue Nile river. *Geographical Journal* **166,** 49-62.

Cox, K. G. (1989). The Role of Mantle Plumes in the Development of Continental Drainage Patterns. *Nature* **342,** 873-877.

Dessert, C., Dupre, B., Francois, L. M., Schott, J., Gaillardet, J., Chakrapani, G., and Bajpai, S. (2001). Erosion of Deccan Traps determined by river geochemistry: impact on the global climate and the Sr-87/Sr-86 ratio of seawater. *Earth and Planetary Science Letters* **188,** 459-474.

Dunai, T. J., and Wijbrans, J. R. (2000). Long-term cosmogenic ^{3}He production rates (152 ka-1.35 Ma) from ^{40}Ar/^{39}Ar dated basalt flows at 29°N latitude. *Earth and Planetary Science Letters* **176,** 147-156.

Dunai, T. J. (2001). Influence of secular variation of the geomagnetic field on production rates of in situ produced cosmogenic nuclides. *Earth and Planetary Science Letters* **193,** 197-212.

Dunne, J., Elmore, D., and Muzikar, P. (1999). Scaling factors for the rates of production of cosmogenic nuclides for geometric shielding and attenuation at depth on sloped surfaces. *Geomorphology* **27** 3-11.

Farley, K. A., Libarkin, J., Mukhopadhyay, S., and Amidon, W. (2006). Cosmogenic and nucleogenic ^{3}He in apatite, titanite, and zircon. *Earth and Planetary Science Letters* **248,** 451-461.

Galy, V., France-Lanord, C., Beyssac, O., Faure, P., Kudrass, H., and Palhol, F. (2007). Efficient organic carbon burial in the Bengal fan sustained by the Himalayan erosional system. *Nature* **450,** 407-U6.

Gayer, E., Mukhopadhyay, S., and Meade, B. J. (2008). Spatial variability of erosion rates inferred from the frequency distribution of cosmogenic 3He in olivines from Hawaiian river sediments. *Earth and Planetary Science Letters* **266,** 303-315.

Goehring, B. M., Kurz, M. D., Balco, G., Schaefer, J. M., Licciardi, J., and Lifton, N. A. (2010). A reevaluation of in situ cosmogenic ^{3}He production rates. *Quaternary Geochronology* **5,** 410-418.

Gosse, J. C., and Phillips, F. M. (2001). Terrestrial in situ cosmogenic nuclides: theory and application. *Quaternary Science Reviews* **20,** 1475-1560.

Hilton, D. R., Hammerschmidt, K., Teufel, S., and Friedrichsen, H. (1993). Helium isotope characteristics of Andean geothermal fluids and lavas. *Earth and Planetary Science Letters* **120,** 265-282.

Hofmann, C., Courtillot, V., Feraud, G., Rochette, P., Yirgu, G., Ketefo, E., and Pik, R. (1997). Timing of the Ethiopian flood basalt event and implications for plume birth and global change. *Nature* **389,** 838-841.

Kurz, M. D. (1986a). In situ production of terrestrial cosmogenic helium and some applications to geochronology. *Geochimica et Cosmochimica Acta* **50,** 2855-2862.

Kurz, M. D. (1986b). Cosmogenic helium in a terrestrial igneous rock. *Nature* **320,** 435-439.

Kurz, M. D., Colodner, D., Trull, T. W., Moore, R. B., and Obrien, K. (1990). Cosmic-ray exposure dating with in situ produced cosmogenic ^{3}He - Results from young Hawaiian lava flows. *Earth and Planetary Science Letters* **97,** 177-189.

Lal, D. (1991). Cosmic ray labeling of erosion surfaces: *in situ* nuclide production rates and erosion models. *Earth and Planetary Science Letters* **104,** 424-439.

Lave, J., and Avouac, J. P. (2001). Fluvial incision and tectonic uplift across the Himalayas of central Nepal. *Journal of Geophysical Research-Solid Earth* **106,** 26561-26591.

Lave, J., and Burbank, D. (2004). Denudation processes and rates in the Transverse Ranges, southern California: Erosional response of a transitional landscape to external and anthropogenic forcing. *Journal of Geophysical Research-Earth Surface* **109,** 31.

Lave, J. (2005). Analytic solution of the mean elevation of a watershed dominated by fluvial incision and hillslope landslides. *Geophysical Research Letters* **32**.

Licciardi, J. M., Kurz, M. D., Clark, P. U., and Brook, E. J. (1999). Calibration of cosmogenic 3He production rates from Holocene lava flows in Oregon, USA, and effects of the Earth's magnetic field. *Earth and Planetary Science Letters* **172,** 261-271.

Licciardi, J. M., Clark, P. U., Brook, E. J., Pierce, K. L., Kurz, M. D., Elmore, D., and Sharma, P. (2001). Cosmogenic ^{3}He and ^{10}Be chronologies of the late Pinedale northern Yellowstone ice cap, Montana, USA. *Geology* **29,** 1095-1098.

Licciardi, J. M., Kurz, M. D., and Curtice, J. M. (2006). Cosmogenic ^{3}He production rates from Holocene lava flows in Iceland. *Earth and Planetary Science Letters* **246,** 251-264.

Marty, B., Pik, R., and Gezahegn, Y. (1996). Helium isotopic variations in Ethiopian plume lavas: Nature of magmatic sources and limit on lower mantle contribution. *Earth and Planetary Science Letters* **144,** 223-237.

Matsuda, J., Matsumoto, T., Sumino, H., Nagao, K., Yammaoto, J., Miura, Y., Kaneoka, I., Takahata, N., and Sano, Y. (2002). The ^{3}He/^{4}He ratio of the new internal He Standard of Japan (HESJ). *Geochemical Journal* **36,** 191-195.

McDougall, I., Morton, W. H., and Williams, M. A. J. (1975). Age and Rates of Denudation of Trap Series Basalts at Blue Nile Gorge, Ethiopia. *Nature* **254,** 207-209.

Mohr, P. (1983). Ethiopian Flood-Basalt Province. *Nature* **303,** 577-584.

Pik, R., Deniel, C., Coulon, C., Yirgu, G., Hofmann, C., and Ayalew, D. (1998). The northwestern Ethiopian Plateau flood basalts. Classification and spatial distribution of magma types. *Journal of Volcanology and Geothermal Research* **81,** 91-111.

Pik, R., Deniel, C., Coulon, C., Yirgu, G., and Marty, B. (1999). Isotopic and trace element signatures of Ethiopian flood basalts: Evidence for plume-lithosphere interactions. *Geochimica et Cosmochimica Acta* **63,** 2263-2279.

Pik, R., Marty, B., Carignan, J., and LavÈ, J. (2003). Stability of the Upper Nile drainage network (Ethiopia) deduced from (U-Th)/He thermochronometry: implications for uplift and erosion of the Afar plume dome. *Earth and Planetary Science Letters* **215,** 73-88.

Pik, R. (2011). Geodynamics: East Africa on the rise. *Nature Geoscience* **4,** 660-661.

Rochette, P., Tamrat, E., Feraud, G., Pik, R., Courtillot, V., Ketefo, E., Coulon, C., Hoffmann, C., Vandamme, D., and Yirgu, G. (1998). Magnetostratigraphy and timing of the Oligocene Ethiopian traps. *Earth and Planetary Science Letters* **164,** 497-510.

Sarda, P., Staudacher, T., Allègre, C. J., and Lecomte, A. (1993). Cosmogenic neon and helium at Réunion: measurement of erosion rate. *Earth and Planetary Science Letters* **119,** 405-417.

Scarsi, P. (2000). Fractional extraction of helium by crushing of olivine and clinopyroxene phenocrysts: Effects on the He-3/He-4 measured ratio. *Geochimica Et Cosmochimica Acta* **64,** 3751-3762.

Shuster, D. L., Farley, K. A., Sisterson, J. M., and Burnett, D. S. (2004). Quantifying the diffusion kinetics and spatial distributions of radiogenic He-4 in minerals containing proton-induced He-3. *Earth and Planetary Science Letters* **217,** 19-32.

Stone, J. O. (2000). Air pressure and cosmogenic isotope production. *Journal of Geophysical Research - Solid Earth* **105,** 23753-23759.

Trull, T. W., Kurz, M. D., and Jenkins, W. J. (1991). Diffusion of cosmogenic ^{3}He in olivine and quartz - Implications for surface exposure dating. *Earth and Planetary Science Letters* **103,** 241-256.

Trull, T. W., Brown, E. T., Marty, B., Raisbeck, G. M., and Yiou, F. (1995). Cosmogenic ^{10}Be and ^{3}He accumulation in Pleistocene beach terraces in Death-Valley, California, Usa - Implications for cosmic-ray exposure dating of young surfaces in hot climates. *Chemical Geology* **119,** 191-207.

von Blanckenburg, F. (2005). The control mechanisms of erosion and weathering at basin scale from cosmogenic nuclides in river sediment. *Earth and Planetary Science Letters* **237,** 462-479.

Williams, A. J., Stuart, F. M., Day, S. J., and Phillips, W. M. (2005). Using pyroxene microphenocrysts to determine cosmogenic ^{3}He concentrations in old volcanic rocks: an example of landscape development in central Gran Canaria. *Quaternary Science Reviews* **24,** 211-222.

Yokochi, R., Marty, B., Pik, R., and Burnard, P. (2005). High ^{3}He/^{4}He ratios in peridotite xenoliths from SW Japan revisited: Evidence for cosmogenic ^{3}He released by vacuum crushing. *Geochemistry Geophysics Geosystems* **6,** doi:10.1029/2004GC000836.

Zimmermann, L., Blard, P. H., Burnard, P. G., Medynski, S., Pik, R., and Puchol, N. (2012). A new single vacuum furnace design for cosmogenic ^{3}He dating. *Geostandard Geoanalytical Research***,** doi: 10.1111/j.1751-908X.2011.00145.x.

Dans la recherche de la connaissance, ce n'est encore que la joie de la volonté, la joie d'engendrer et de devenir que je sens en moi ; et s'il y a de l'innocence dans ma connaissance, c'est parce qu'il y a en elle de la volonté d'engendrer.
Cette volonté m'a attiré loin de Dieu et des Dieux; qu'y aurait-il donc à créer, s'il y avait des Dieux ?

Mais mon ardente volonté de créer me pousse sans cesse vers les hommes ; ainsi le marteau est poussé vers la pierre.
Hélas ! Ô hommes, une statue sommeille pour moi dans la pierre, la statue de mes statues ! Hélas ! Pourquoi faut-il qu'elle dorme dans la pierre la plus affreuse et la plus dure !

Maintenant mon marteau frappe cruellement contre cette prison. La pierre se morcelle : que m'importe ?

F. Nietzsche,
Ainsi parlait Zarathoustra.

Chapitre 4
Paléo-taux de dénudation en Asie Centrale.

Comme on l'a vu dans le chapitre introductif (§1.2.2), l'Asie centrale est une zone clef pour la compréhension des interactions climat-érosion-tectonique de ces 10 derniers millions d'années. Le Tian-Shan siège comme la plus grande chaîne de montagne au coeur de cette zone. Cependant, notre étude de cette région n'a débutée que courant 2010, lorsque nous prîmes conscience de son très bon potentiel pour l'application des isotopes cosmogéniques.

De fait, depuis 2010, c'est dans cette zone que nous avons pu accumuler le plus de données, avec notamment un premier article publié en 2011 dans Earth and Planetary Science Letters, et présenté en annexe de ce manuscrit. Ce premier article, focalisé sur une seule coupe sédimentaire, soulevait toutefois beaucoup de questions. Notamment, si le même signal serait observé régionalement sur toute la chaîne, et si les larges variations de taux de dénudation constatées pouvaient être simplement dues à des processus stochastiques de dépôts sédimentaires. Afin de compléter cette étude préliminaire, cette même coupe et deux nouvelles sédimentaires furent rééchantillonnées à l'automne 2010, ainsi qu'une carotte sédimentaire fournie gracieusement par l'Institut des Sciences de la Terre d'Orléans. Un échantillonnage à très haute résolution fut également effectué dans une séquence sédimentaire afin de tester l'influence des processus de dépôts sur le signal cosmogénique.

Les résultats de ces travaux sont présentés dans ce chapitre, sous la forme d'un article soumis prochainement à Nature Geoscience. Le format des articles de cette revue étant très court, des informations détaillées sur le contexte géologique et les méthodes employées sont fournies à sa suite.

Limited impact of Quaternary glaciations on denudation rates in central Asia.

(to be submitted to Nature Geoscience)

Nicolas Puchol[1], Julien Charreau[1], Pierre-Henri Blard[1], Jérôme Lavé[1], Stéphane Dominguez[2], Raphaël Pik[1], ASTER Team[3,+]

[1]Centre de Recherche Pétrographique et Géochimique, 15 rue Notre Dame des Pauvres, B.P. 20, 54501 Vandoeuvre lès Nancy, France, phone : (33)383594227 Fax: (33)383511798, charreau@crpg.cnrs-nancy.fr, blard@crpg.cnrs-nancy.fr, puchol@crpg.cnrs-nancy.fr,

[2.] Laboratoire Dynamique de la Lithosphère; UMR CNRS/UMII 5573, Bâtiment 22 [cc. 60] Place Bataillon, 34095 Montpellier Cedex, France; Phone: (33)0467144589, Fax: (33)467523908; dominguez@dstu.univ-montp2.fr

[3.] Centre Européen de Recherche et d'Enseignement des Géosciences de l'Environnement, Europole Méditerranéen de l'Arbois BP 80 13545 Aix-en-Provence cedex 4; aster@cerege.fr
[+]Maurice Arnold, Georges Aumaître, Didier L Bourlès, Karim Keddadouche.

Contents for this paper

Main Body

Because of its essential role coupling climate and tectonics, denudation (i.e. the sum of chemical weathering and physical erosion) is a key parameter to constrain all throughout the Earth's surface History. In particular, the impact of both the global climate cooling and the onset of Quaternary glacial cycles since ~5 Ma on worldwide denudation rates is a matter of intense debate (*1-5*).

However, means to derive direct, high resolution denudation rates on time scales >1 Ma are still lacking. Traditional erosion rates estimations from sediment budgets have indeed proved to suffer from severe flaws and potential drawbacks (*4, 6*). On the other hand, the analyze of in situ cosmogenic nuclides, in present-day river sands, has proved to provide, quite straightforwardly, reliable estimations of recent denudation rates from whole drainage basins (*7-9*).

Here, we extend this method to continuous sections of ancient sediments, independently dated by magnetostratigraphy. We focused this study on four sedimentary basins of the northern and southern Tian-Shan range (central Asia). This area is both particularly suited for this method (*10*) and of primary interest as regards climate/erosion interactions during the late Neogene (*2*). The four records, although likely influenced by local particularities, strikingly display a common trend of increasing denudation since at least ~8 Ma, and a period of relatively high and variable denudation since ~4 Ma. We thus do not observe a dramatic increase in denudation rates that would be linked to a Quaternary increased climatic variability.

Important global climate changes occurred during the late Neogene, notably the onset of Quaternary glaciations characterized by a significant global cooling since 2.5 Ma and the appearance of 40 and 100 kyrs, large amplitude climatic cycles(*11*). Those changes are suspected to have strongly impacted the continental denudation, which by feedback mechanisms would have impacted tectonics, high range uplift, as well as climate. In particular, denudation has been held responsible for inducing, or over-amplifying (*12*), a global cooling throughout the Cenozoic, influencing atmospheric CO_2 budget via silicate weathering (*13*), and mechanical burial of organic carbon (*14*). Such complex feedback loops are still largely debated, and solving this question partly necessitate reliable and detailed records of past denudation rates.

Worldwide accumulation rates in both continental and marine basin records have displayed an apparent dramatic increase for the last 3-4 Myrs (*1, 2*). Since this increase is observed in various tectonic settings, and both in glaciated and non-glaciated region, these authors proposed that erosion was enhanced by the Plio-Quaternary increased climate variability. However, interpretation of these records has since been challenged, on the ground of new and more accurate sedimentary volume budget in other basins, flaws inherent to sediment volume reconstruction derived from 1D accumulation rates records (*4-6*) and the demonstration of erroneous sediment dating in Central Asia (*3*). This region holds several large and active mountain ranges, among which the Tian-Shan, where the glacial extent on the reliefs has been limited (*15*). The large, endorheic basins of central Asia store sediments shed from these uplifting reliefs and are insensitive to eustatic variations. Therefore, they are the field of among the most crucial records for the hypothesis of a Quaternary increase in erosion rates.

In-situ cosmogenic nuclides represent a robust quantitative method for measuring denudation rates at the scale of a watershed from small aliquots of river sands (*7, 8, 16*). Although this method has nowadays been extensively used in modern rivers (*17*), only a limited number of studies has extended it to ancient river sediments (i.e. > 1Ma) (*18, 19*). Only one of them being from a continuous high resolution record from 9 to 0 Ma, in the northern Tian-Shan piedmont, in Central Asia (Kuitun river)(*10*). This study showed a transient increase in denudation rates around 2 Ma, possibly linked to the onset of glaciations in this region. However, this study remained limited to a single watershed, and generalization of its conclusion to the whole region remained questionable.

To pursue this work, we present here 3 new records of paleo-denudation rates of the Tianshan mountains over the last 9 Myr: two new sections (Yaha and Jingu-He) and one core drill into sediments of Ebi Lake (see Fig. 2 for localization and Supplementary Info §1 for detailed description of each sampling zone).

Applying cosmogenic nuclides to ancient river sediments is not straightforward. One needs to apply specific corrections, such as nuclide build up during sediment deposition (see Fig. 1 for a concise description of these corrections and supp info §3 for the complete method and calculation).

First, independent dating by magnetostratigraphy is of primary importance. Beside providing a robust, precise, and high-resolution dating, it enables estimation of sediment accumulation rates and correction for the post-deposition ^{10}Be accumulation (Fig. 1 and supp info §3.3). Also, comparison of magnetostratigraphic ages with $^{26}Al/^{10}Be$ burial ages offers a robust criteria to

discard the samples either having been significantly re-exposed since their deposition or presenting a component of recycled older sediments (Supp. Info §3.6).

Second, target sediments must have only suffered a negligible reexposure since their deposition. Well-dated and rapidly exhumed sedimentary section, or drilled cores, are hence well suited for such approach.

In this perspective, the Tianshan piedmonts are not only a key region regarding the debate about the long term variability of denudation rates, but moreover are particularly suited to apply this method. They hold successive parallel fold-and-thrust belts of an ongoing active tectonic wedge into Mesozoic to Quaternary sediments (*20*). Many of these sections have been successfully dated by magnetostratigraphy (*3, 21-23*) up to 10 Ma. Besides, independent terrace datings (*24*) show that Holocene incisions by rivers in these folding sediments are particularly rapid (up to >1 $cm.yr^{-1}$). This ensures negligible modern exposure since the Holocene (see sup. info for calculation).

A total of 33 samples were collected along two magnetostratgraphically dated sections (*21, 23*) located in both sides of the range (Fig. 2) and 16 samples in a magnetostratigraphically dated core drilled in the Ebi Nor lake sediments, located in the southwestern part of the Junggar basin. At last, we collected 10 new samples from the Kuitun section (*22*)

Along with samples from these sedimentary sections, we also included samples from the present day river beds (triangles in fig. 3) and samples from Holocene to Upper Pleistocene terraces (diamonds in fig. 3).

Results are displayed in fig 3 and in supp info table 1.

At the first order, 3 records (Kuitun, Jingou and Yaha) show comparable long-term denudation rates, with averages ranging from ~200 to 550 $m.Myr^{-1}$. The Ebi Nor lake core yielded lower values, with an average around ~90 $m.Myr^{-1}$. The lower denudation rates displayed by the Ebi core, are coherent with its drainage basin integrating a flatter and less active relief in its northern part (fig 2). The Kuitun section, conversely, displays denudation rates slightly higher than the nearby Jingu. Its main striking feature is the large pike between 1.7-1.8 Ma. In 2011(*10*), we interpreted this pike in term of a transient increase due to the onset of Quaternary glaciations. The fact that we do not observe this feature in the other sections, especially in the nearby Jingu section (barely distant from 50km), forces us to reevaluate this interpretation and suggests that a very local geologic or tectonic feature may have play a significant role.

Despite strong climatic differences between the north and south Tianshan, the southern Yaha paleo-denudation records share similar characteristics with the northern records.

One critical uncertainty here is the fact that production rate was estimated using the present hypsometry of the watershed. The paleo-draining basin hypsometry at the time of deposition remains difficult to constrain. Stable isotopes-based paleoaltimetry suggests that the hypsometry of the draining basins (Kuitun and Jingu) remained stable over the 10-5 Ma period(*25*). Since 5 Ma, a significant change in paleo-hypsometry would be inconsistent with the apparently stable long term averages on this period. In any case, we propagated an uncertainty of 150 m to the altitude of the basin, derived from the stable-isotope records (Supplementary info §3.2).

A second important source of uncertainty is the correction for post depositional cosmogenic accumulation. This later was done using the average sedimentary accumulation rates above each sample. Nevertheless, fluvial sediment deposition are likely to be episodic, with period of quick deposition followed by periods of exposure or re-erosion.

To test the influence of such potential high frequency sedimentary processes, we sampled in ~5.3 Myr old Kuitun sediments a high resolution section (6 samples in 3 m) containing various fluvial facies. Given the average accumulation rate at this stratigraphic position, the 3 meters between the two extreme samples represent a ~13 kyr time span.

^{10}Be concentrations fall all in the same range at 1.5σ, except for one sample that falls ~40% above the median, value. Importantly, we do not see any link between the deposition facies and the concentration. We conclude that sediment deposition dynamics did not have a significant impact on the calculated denudation rates at a broader scale, and cannot explain all of the observed fluctuations.

It is fair to wonder whether the observed noisiness of these records could be due to random sampling of sediments produced either during interglacial or glacial periods. Given the observed denudation rates, the cosmogenic nuclides record denudation rates on time scales ranging from ~0.6 (1000 m/Myr) to 6 kyr (100 km/Myr). This is insufficient to totally damper a possible glacial/interglacial variability (*26*). However, several arguments suggest that denudation variations due to orbital cycles are not sufficient to explain either all of the observed variability, or the global augmentation since 8 Ma:

First, comparison between present day river and terraces material dated between 20 kyr and 100 kyr (hence at the core of the last glacial period) show very similar concentrations. Second, to our knowledge, no published paper have reported significant variations in cosmogenic denudation rates signals tighten to orbital cycles (*18, 27, 28*), except (*29*), with much smaller amplitudes, in a more humid and less continental setting, and only since the onset of 100 kyr cycles 0.9 Ma.

To disregard local variation potentially due to local particularity (lithology, altitude of the drainage basin, tectonics), we normalized the paleo-denudation records to their respective present day values in order to compare their relative evolutions (Fig. 4a)

Although the different records exhibit some large discrepancies and short term fluctuations, after smoothing over 1 Myr bins, they together show a long term common trend (Fig. 4): First, a continuous increase (~ ×5) in denudation rate between 9-4 Ma. Second, despite large shorter-term fluctuations, a relatively high, sustained denudation average since ~4 Ma.

Sedimentation records (*21, 22*) and extrapolation of modern GPS speeds (*30*) suggest a major activation of the Tian-Shan convergence and uplift since 11 Ma. The progressive increase in denudation rates displayed by our records could be interpreted as the response to a transient uplift associated with the range re-activation. In this case, however, the drainage basin altimetry, and hence the cosmogenic production rates, would have progressively increased since the beginning of the records. We would consequently overestimate denudation rates, and the records, especially for oldest samples, would have to be seen as maxima. The pace of the progressive increase in denudation of the region would thus be all the more quick. However, as aforementioned, paleo-altimetry proxies suggest a stable hypsometry, at least until 5 Ma (*25*). The potential increase in topography, in this scenario, would have therefore been limited and partially accounted in the large uncertainties of our records.

Importantly and whatever the underlying mechanism of the progressive increase since 9 Ma, we do not observe a major increase in denudation that would be related with the intensification of northern hemisphere glaciations, or increased climate variability since 3-4 Ma. Strikingly, the long-term-averaged regional denudation seems to have increased the most as the global climate remained stable, and to have remained more stable as the global climate shifted significantly (albeit, again, large fluctuations around this average). Our records suggest that the onset of northern hemisphere glaciations, since ~3-4 Ma, had a limited impact on denudation rates, at least in this type of continental, relatively arid setting. This result, if valid in other regions, would be in partial agreement with studies suggesting that the global chemical weathering rates have remained constant over the last 10 Ma (*5*), although a partial decoupling between weathering and bulk denudation is possible.

At last, we show that generalization of cosmogenic nuclides analyses to ancient, independently dated sediments is a powerful method to derive high-resolution denudation rates records. It is a simple and direct mean, that avoids to rely on difficult and imprecise

reconstructions of 3D accumulation rates that, moreover, cannot include chemical weathering. As intuited in other studies (*9, 18, 29*), they represent a unique tool to record tectonic/climate/erosion interplay at the scale of the last ~10Myr, and potentially even further in the past if using stable cosmogenic nuclides such as ^{3}He and ^{21}Ne

Acknowledgements

We warmly thank Shengli Wang (Nanjin University) for its precious assistance on the field, Dimitri Saint-Carlier (CRPG) for assistance on the field and kindly sharing preliminary terrace dating, Yan Chen (ISTO Orléans) for providing the Ebi samples, Laetitia Leanni, Frédéric Chauvet and Régis Braucher (CEREGE, Aix-en-Provence) for their assistance and patience in the lab. Marie-Soraya Cheradame, Lucie Lamourette and Maxime Sorbier (former students at ENSG, Nancy) carried out the sample preparations of the Ebi core.

This work was financed by the Institut National des Sciences de l'Univers (INSU) and the Agence Nationale pour la Recherche (ANR)'s project CALIMERO.

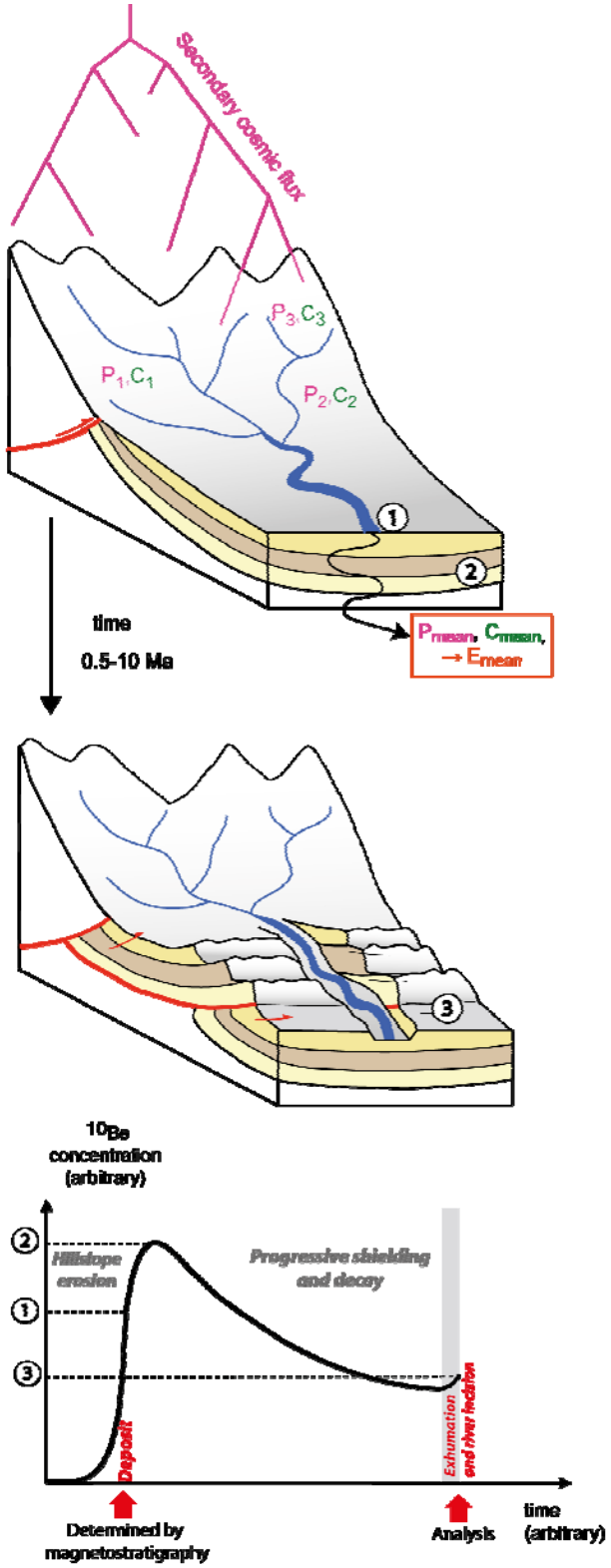

Fig. 1 - Theoretical evolution of the ^{10}Be signal before and after sediment deposition.

1- In each point of the basin, the secondary cosmic flux produce a ^{10}Be concentration C_i, via several different mechanisms, typically in the uppermost ~4m of the surface, with a production rates P_i depending mainly on the altitude. A river sand at the outlet of the basin, composed of thousand of grains from all over the basin, will have an average concentration C_{mean} proportional to the average production rate P_{mean} and inversely proportional to the average denudation rate E_{mean}

2- after deposition, the burial of the sediment is not instantaneous. During this short burial period, it will accumulate a little more ^{10}Be. During this period and afterwards until exhumation by folding, thrusting and river incision, ^{10}Be will decay with a half life $t_{1/2}$= 1.4 Myr. It is possible to test the occurrence of potential re-exposure episodes, or cannibalism of older sediments, by comparing theoretical burial ages from cosmogenic isotopes couples (e.g. ^{26}Al/^{10}Be) and from independent dating (e.g. magnetostratigraphy)

3- at last, if the river incision is not sufficiently rapid, modern exposure of the sediment may induce a re-accumulation of ^{10}Be. In our case this modern accumulation was estimated and is negligible.

The detailed complete method, parameters and corrections calculations are provided as supplementary material.

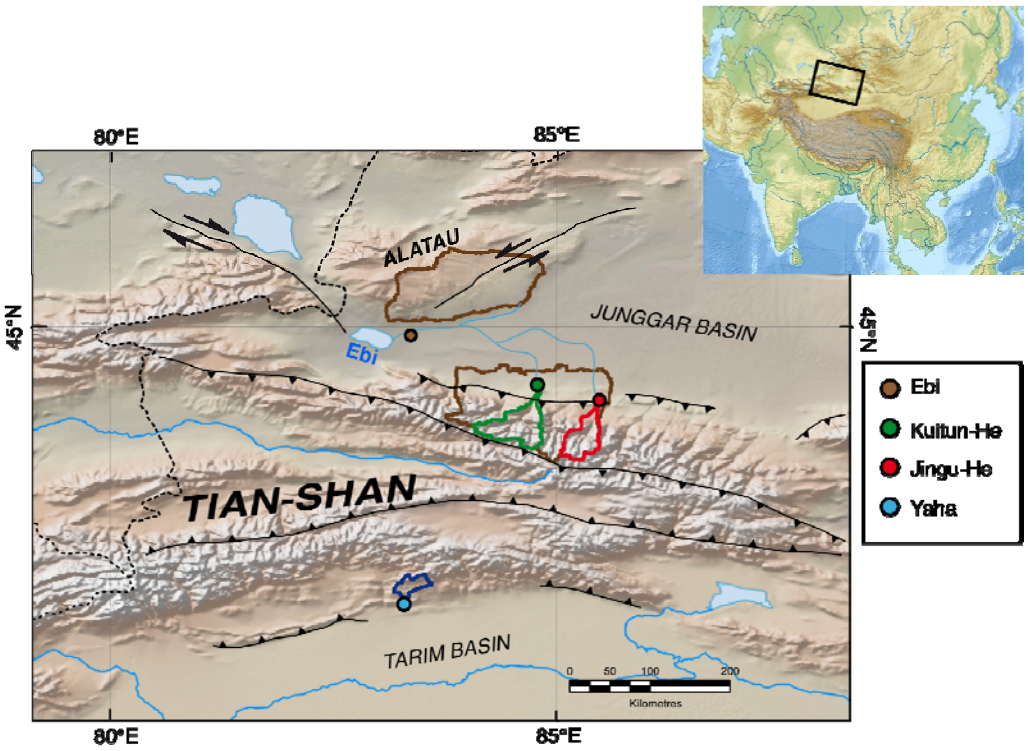

Fig. 2 - Setting

The Tian-Shan range is one of the major relief in central Asia, with a 2500km length and summits reaching up to 7000m. This range had a double history: The main substratum, mostly Island-Arc magmatic rocks and meta-sediment, created throughout a long and complex subduction, accretion and collisions during the Paleozoic. Then, the range was reactivated ~16Ma under the influence of the Indo-Asia collision. The range is active and accommodates at the present ~40% of the Indo-Asia convergence. Successive parallels fold-and-thrust belts constitute a ongoing tectonic wedge into Mesozoic to Quaternary sediments. These systems are currently rapidly incised by rivers, exposing spectacular continuous sections.

The three basins (Yaha, Kuitun, and Jingu rivers) were chosen based on structural simplicity, good exposure conditions, accessibility, and existence of independent magnetostratigraphy dating. We also analyzed samples from a core drilled a few kilometers from the present) day Ebi Lake. The basin both drain the Tian Shan range and a northern part with a lesser relief. For denudation calculations, we excluded the flattest part of the watershed within the Junggar Basin (i.e. <300m in altitude), because this area is not eroding but is in subsidence.

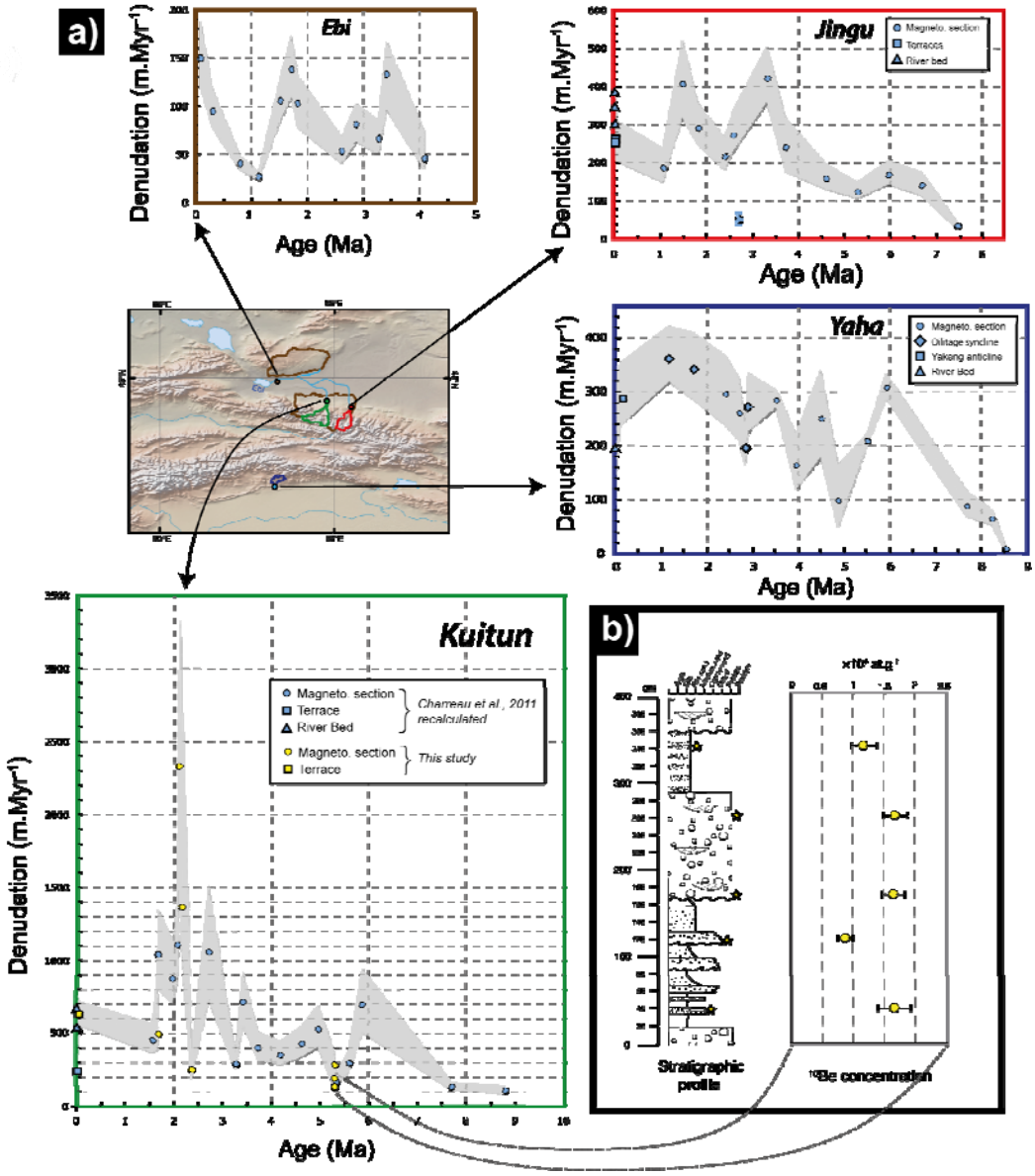

Fig. 3 - Basin-average denudation rates and high resolution sequence.

a) Calculated denudations rates (i.e. physical erosion + chemical weathering), in m.Myr⁻¹ (i.e. 10³ mm.yr⁻¹). The 1σ envelop is represented in shaded grey. Sediment from the magnetostratigraphic section and Ebi Lake drill are represented by circles, terraces samples by squares, modern rivers by triangles. For Yaha sections, we also analyzed sample from the Qilitage anticlines, dated from $^{26}Al/^{10}Be$ burial ages, represented by diamonds (see supp info.)

b) ^{10}Be Concentrations (10^4 at.g⁻¹) measured in a high-resolution fluvial stratigraphic sequence from the Kuitun section, in order to test the influence of fluvial deposition processes on the paleo-cosmogenic signal. Error bars are 1σ. Given the average accumulation rate at this point of the sequence, the 3 meters between the two extreme samples represent a ~13kyr time span.

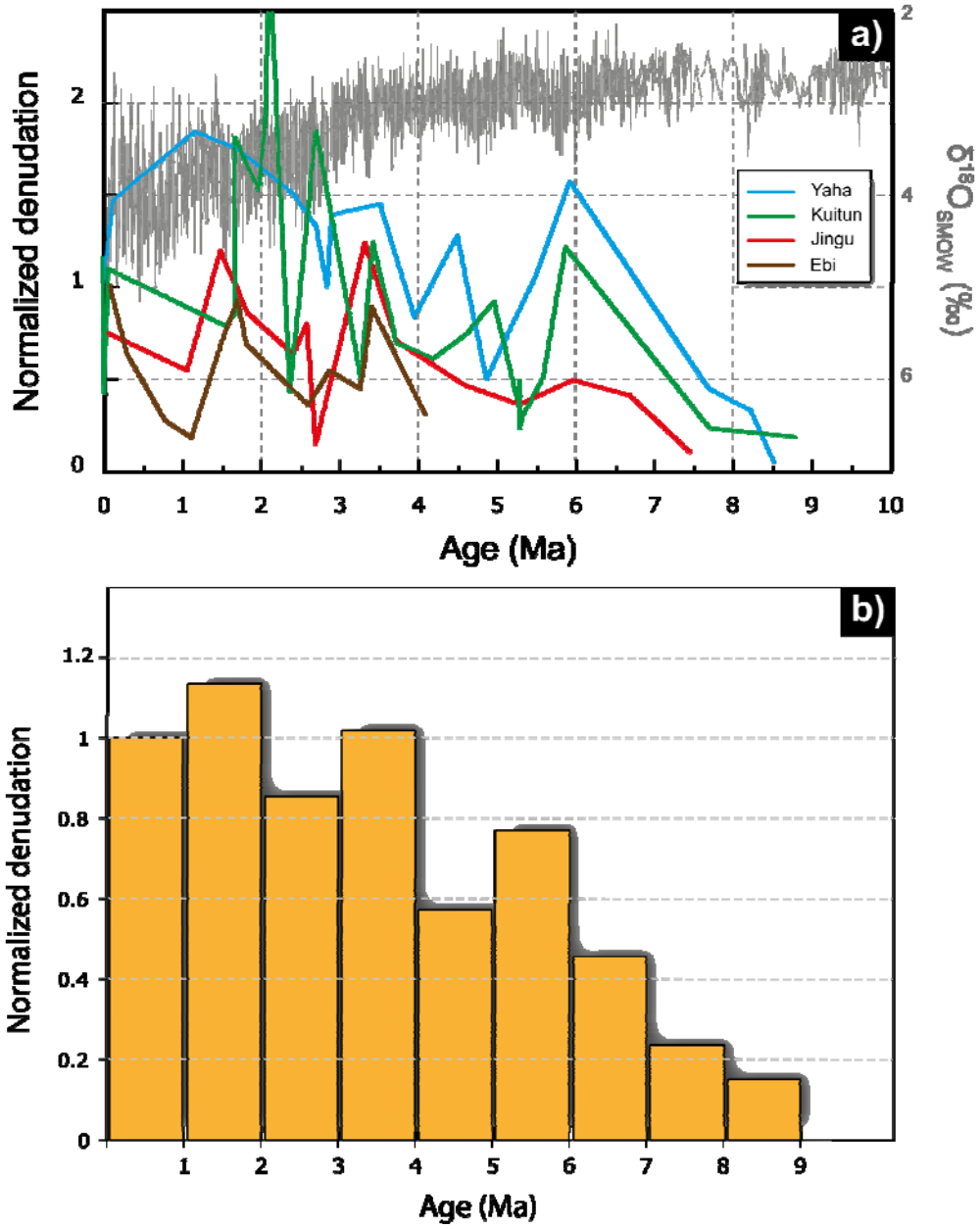

Fig. 4 - Compilation of denudation rates, normalized to the modern values. *a) Denudation records, each one normalized to their respective modern denudation value (present day rivers), or average modern denudation if several value available. For Ebi we used the youngest sample. For the sake of comparison, we also plot the global benthic $\delta^{18}O$ record as a proxy for global temperatures (gray curve) (Zacchos 2001) b) Mean normalized denudations of the 4 basins, averaged over 1 Myr bins.*

References for the main body

1. Zhang, P. Z., Molnar, P., Downs, W. R. (2001), Increased sedimentation rates and grain sizes 2-4 Myr ago due to the influence of climate change on erosion rates, *Nature* **410**.
2. Molnar, P. (2004), Late cenozoic increase in accumulation rates of terrestrial sediment: How might climate change have affected erosion rates?, *Annual Review of Earth and Planetary Sciences* **32**.
3. Charreau, J., Gumiaux, C., Avouac, J.-P., Augier, R., Chen, Y. *et al.* (2009), The Neogene Xiyu Formation, a diachronous prograding gravel wedge at front of the Tianshan: Climatic and tectonic implications, *Earth and Planetary Science Letters* **287**.
4. Schumer, R., Jerolmack, D. J. (2009), Real and apparent changes in sediment deposition rates through time, *Journal of Geophysical Research-Earth Surface* **114**.
5. Willenbring, J. K., von Blanckenburg, F. (2010), Long-term stability of global erosion rates and weathering during late-Cenozoic cooling, *Nature* **465**.
6. Métivier, F. (2002), On the use of sedimentation rates in deciphering global change, *Geophysical Research Letters* **29**.
7. Brown, E. T., Stallard, R. F., Larsen, M. C., Raisbeck, G. M., Yiou, F. (1995), Denudation rates determined from the accumulation of in situ produced ^{10}Be in the Luquillo experimental forest, Puerto-Rico, *Earth and Planetary Science Letters* **129**.
8. Granger, D. E., Kirchner, J. W., Finkel, R. (1996), Spatially averaged long-term erosion rates measured from in situ-produced cosmogenic nuclides in alluvial sediment, *Journal of Geology* **104**.
9. von Blanckenburg, F. (2005), The control mechanisms of erosion and weathering at basin scale from cosmogenic nuclides in river sediment, *Earth and Planetary Science Letters* **237**.
10. Charreau, J., Blard, P. H., Puchol, N., Avouac, J. P., Lallier-Verges, E. *et al.* (2011), Paleo-erosion rates in Central Asia since 9 Ma: A transient increase at the onset of Quaternary glaciations?, *Earth and Planetary Science Letters* **304**.
11. Zachos, J., Pagani, M., Sloan, L., Thomas, E., Billups, K. (2001), Trends, rhythms, and aberrations in global climate 65 Ma to present, *Science* **292**.
12. Molnar, P., England, P. (1990), Late Cenozoic uplift of mountain ranges and global climate change - Chicken or egg ?, *Nature* **346**.

13. Berner, R. A., Lasaga, A. C., Garrels, R. M. (1983), The Carbonate-Silicate Geochemical Cycle and Its Effect on Atmospheric Carbon-Dioxide over the Past 100 Million Years, *American Journal of Science* **283**.
14. Galy, V., France-Lanord, C., Beyssac, O., Faure, P., Kudrass, H. *et al.* (2007), Efficient organic carbon burial in the Bengal fan sustained by the Himalayan erosional system, *Nature* **450**.
15. Kong, P., Fink, D., Na, C., Huang, F. (2009), Late Quaternary glaciation of the Tianshan, Central Asia, using cosmogenic Be-10 surface exposure dating, *Quaternary Research* **72**.
16. Lal, D. (1991), Cosmic ray labeling of erosion surfaces: *in situ* nuclide production rates and erosion models, *Earth and Planetary Science Letters* **104**.
17. Portenga, E., W., Bierman, P. R. (2011), Understanding Earth's eroding surface with 10Be, *GSA Today* **21**.
18. Schaller, M., von Blanckenburg, F., Hovius, N., Veldkamp, A., van den Berg, M. W. *et al.* (2004), Paleoerosion rates from cosmogenic Be-10 in a 1.3 Ma terrace sequence: Response of the river meuse to changes in climate and rock uplift, *Journal of Geology* **112**.
19. Refsnider, K. A. (2011), Dramatic increase in late Cenozoic alpine erosion rates recorded by cave sediment in the southern Rocky Mountains, *Earth and Planetary Science Letters* **297**.
20. Avouac, J. P., Tapponnier, P., Bai, M., You, H., Wang, G. (1993), Active Thrusting and Folding Along the Northern Tien-Shan and Late Cenozoic Rotation of the Tarim Relative to Dzungaria and Kazakhstan, *Journal of Geophysical Research-Solid Earth* **98**.
21. Charreau, J., Chen, Y., Gilder, S., Barrier, L., Dominguez, S. *et al.* (2009), Neogene uplift of the Tian Shan Mountains observed in the magnetic record of the Jingou River section (northwest China), *Tectonics* **28**.
22. Charreau, J., Chen, Y., Gilder, S., Dominguez, S., Avouac, J. P. *et al.* (2005), Magnetostratigraphy and rock magnetism of the Neogene Kuitun He section (northwest China): implications for Late Cenozoic uplift of the Tianshan mountains, *Earth and Planetary Science Letters* **230**.
23. Charreau, J., Gilder, S., Chen, Y., Dominguez, S., Avouac, J. P. *et al.* (2006), Magnetostratigraphy of the Yaha section, Tarim Basin (China): 11 Ma acceleration in erosion and uplift of the Tian Shan mountains, *Geology* **34**.
24. Poisson, B., Avouac, J. P. (2004), Holocene hydrological changes inferred from alluvial stream entrenchment in North Tian Shan (Northwestern China), *Journal of Geology* **112**.

25. Charreau, J., Kent-Corson, M. L., Barrier, L., Augier, R., Ritts, B. D. *et al.* (2012), A high-resolution stable isotopic record from the Junggar Basin (NW China): Implications for the paleotopographic evolution of the Tianshan Mountains, *Earth and Planetary Science Letters* **341**.

26. Schaller, M., Ehlers, T. A. (2006), Limits to quantifying climate driven changes in denudation rates with cosmogenic radionuclides, *Earth and Planetary Science Letters* **248**.

27. Balco, G., Stone, J. O. H. (2005), Measuring middle Pleistocene erosion rates with cosmic-ray-produced nuclides in buried alluvial sediment, Fisher Valley, southeastern Utah, *Earth Surface Processes and Landforms* **30**.

28. Wittmann, H., von Blanckenburg, F., Kruesmann, T., Norton, K. P., Kubik, P. W. (2007), Relation between rock uplift and denudation from cosmogenic nuclides in river sediment in the Central Alps of Switzerland, *Journal of Geophysical Research-Earth Surface* **112**.

29. Schaller, M., von Blanckenburg, F., Veldkamp, A., Tebbens, L. A., Hovius, N. *et al.* (2002), A 30 000 yr record of erosion rates from cosmogenic ^{10}Be in Middle European river terraces, *Earth and Planetary Science Letters* **204**.

30. Abdrakhmatov, K. Y., Aldazhanov, S. A., Hager, B. H., Hamburger, M. W., Herring, T. A. *et al.* (1996), Relatively recent construction of the Tien Shan inferred from GPS measurements of present-day crustal deformation rates, *Nature* **384**.

Supplementary information

1 Setting

1.1 General setting

General Tian-Shan history

The Tian-Shan ("the celestial mountains" in Chinese) stretch over 2500 km in length 200-400 km in width and dominate the topography of Central Asia with summits higher than 7000 m. It is bounded by two major endorheic sedimentary basins, the Tarim, to the South, and the Junggar, to the North.

The geology of the range inherits from a complex series of subduction/collision during the Paleozoic. The range was originally built up throughout the Ordovician to the Silurian from the convergence along two zones of subduction of three main continental blocs that collided later probably during the Silurian to the Devonian. Although different models of timing and geometry of these events have been proposed (Windley *et al.*, 1990; Gao *et al.*, 1998; Charvet *et al.*, 2007), all agree that the accretion of the southern and northern blocs were completed by the beginning of Permian.

After these first tectonics phases, during the end of Paleozoic the Tarim, the Junggar, and other intra-mountainous basins underwent a massive sediment filling, together with episodes of arc magmatism,. During the Mesozoic, as evidenced by recent thermochronogical studies (Dumitru *et al.*, 2001; Jolivet *et al.*, 2010) carried out in the high range, the Tian-Shan underwent several episodes of relatively rapid uplift. These episodes were interpreted as far-field effects of either the accretion of blocks such as the Kohistan-Dras arc to the southwest, or of the extensional processes that affected the lithosphere in the Siberia-Mongolia-North China zone. As a consequence, the Tarim and Junggar basins underwent a new major accumulation of sediment. At this point the geology of the Tianshan range is mainly composed of granite, Paleozoic and Mesozoic detrital sediments and arc magmatism rocks.

Latter, during the Cenozoic, the India-Asia collision reactivated the pre-existent Paleozoic and Mesozoic structures of the range. This second main tectonic phase probably started between 25Ma and 10Ma though the exact timing remains unknown (Tapponnier and Molnar, 1979; Avouac *et al.*, 1993; Hendrix *et al.*, 1994; Abdrakhmatov *et al.*, 1996; Bullen *et al.*, 2001; Dumitru

et al., 2001; Charreau *et al.*, 2005; Charreau *et al.*, 2006; Heermance *et al.*, 2007; Charreau *et al.*, 2009a). Associated to this tectonic reactivation, the sediment accumulation has seemingly undergone a major increase in the basins surrounding the range. But, though many magnetostratigraphic studies were carried out in some remarkable section of the Junggar and Tarim basin, the overall sediment dating remain loose and avoid a good and accurate reconstruction of the basins dynamic that is critical to better constrain the timing of the reactivation.

During this time, the deformation also progressively propagated toward the basins and several tectonic wedges developed in both side of the range. Today, the Tian-Shan is actively deformed as attested by an intense seismicity. The shortening rates derived from GPS measurement can reach 20 $mm.yr^{-1}$ in the western part of the range which represents, in this particular region, up to ~40% of the total India-Asia collision (Abdrakhmatov *et al.*, 1996; Reigber *et al.*, 2001). If the total shortening progressively decrease from West to East, the detailed repartition of this deformation within the range remains poorly constrained (Burchfiel *et al.*, 1999).

The Eastern Tian-Shan piedmonts

In the eastern part of the Tian-Shan range, the northern and southern piedmonts are relatively similar and display series of parallel fold-and-thrust belts that progressively encroach the foreland basins (FIG. A). If the timing of deformation of each individual structure is often unknown, except for some well documented structures (e.g Daeron *et al.*, 2007; Hubert-Ferrari *et al.*, 2007; Charreau *et al.*, 2008), the oldest folds were likely formed closer to the Paleozoic basement where Mesozoic sediments are exhumed. The youngest structures are probably sited more distally into the basins, where folding and thrusting exhume mainly Pliocene to Pleistocene sediments (Avouac *et al.*, 1993; Molnar *et al.*, 1994; Brown *et al.*, 1998; Burchfiel *et al.*, 1999).

In both piedmonts, several large rivers flow perpendicularly to these foreland structures and have deeply and quickly entrenched the uplifting folds and faults since the Holocene (Poisson *et al.*, 2004), yielding to deep gorges (sometimes >200 m), exposing continuous sections of tilted sediments. The incision by the rivers have left numerous strath terraces, that may represent passive morphological markers of the tectonic deformation (Molnar *et al.*, 1994; Brown *et al.*, 1998; Poisson and Avouac, 2004), and more importantly that enable the quantification of the incisions rates, which is critical to estimate the potential contribution of recent exposure to cosmic ray (§3.4).

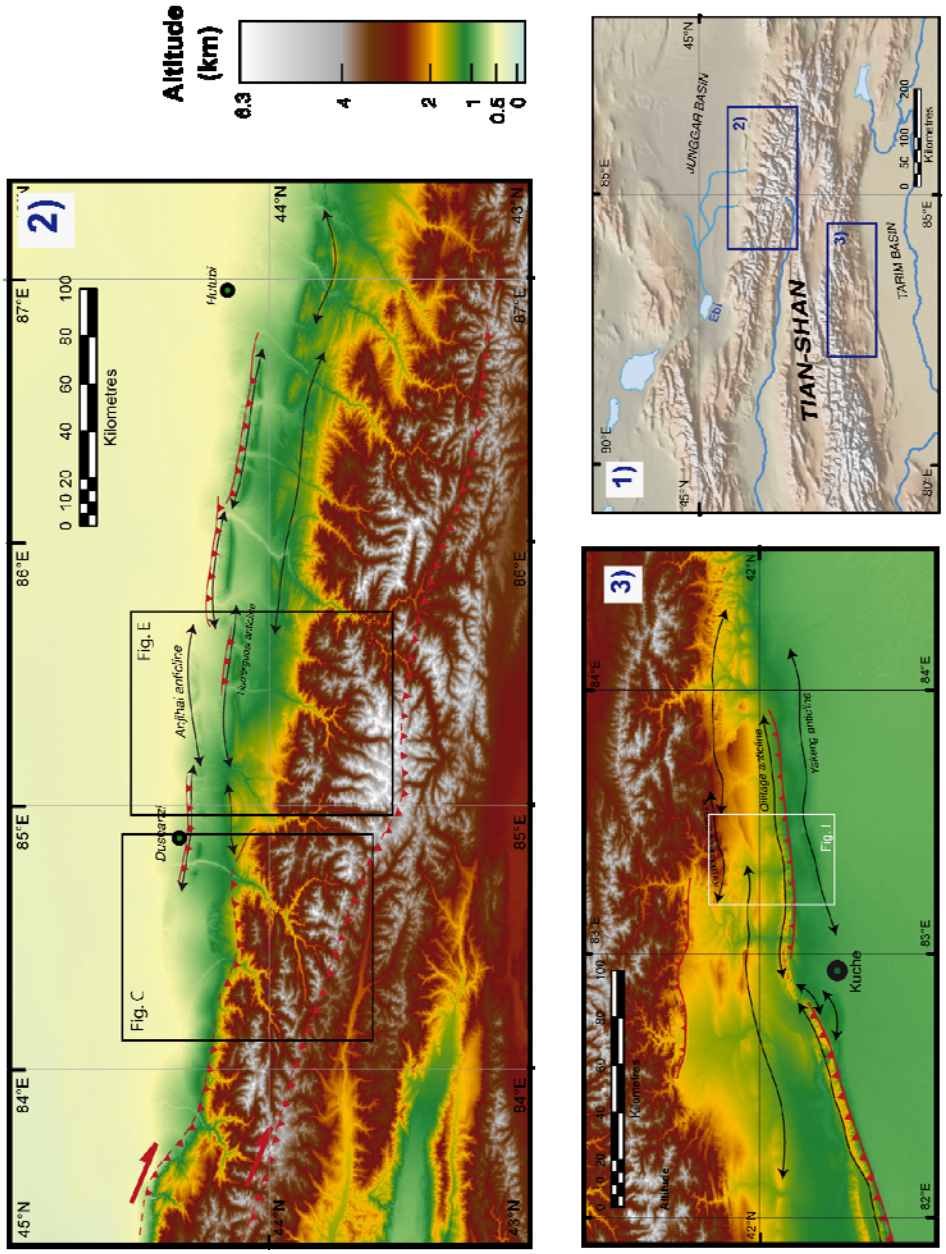

FIG. A - *General setting and location of the Eastern Tian-Shan piedmonts. 1) Composite relief map of the region; 2) Shuttle Radar Topographic Mission (SRTM) Digital Elevation Model (DEM) of the, northern piedmont. Black double arrows indicate major anticlines folds in the piedmonts. Red lines indicate major thrusting. Boxes indicate the position of the Kuitun section (FIG. C) and Jingu section (FIG. E); 3) Same as 2) for the southern piedmont, with the position of Yaha section (FIG. I). Major cities are located by the black and green dots*

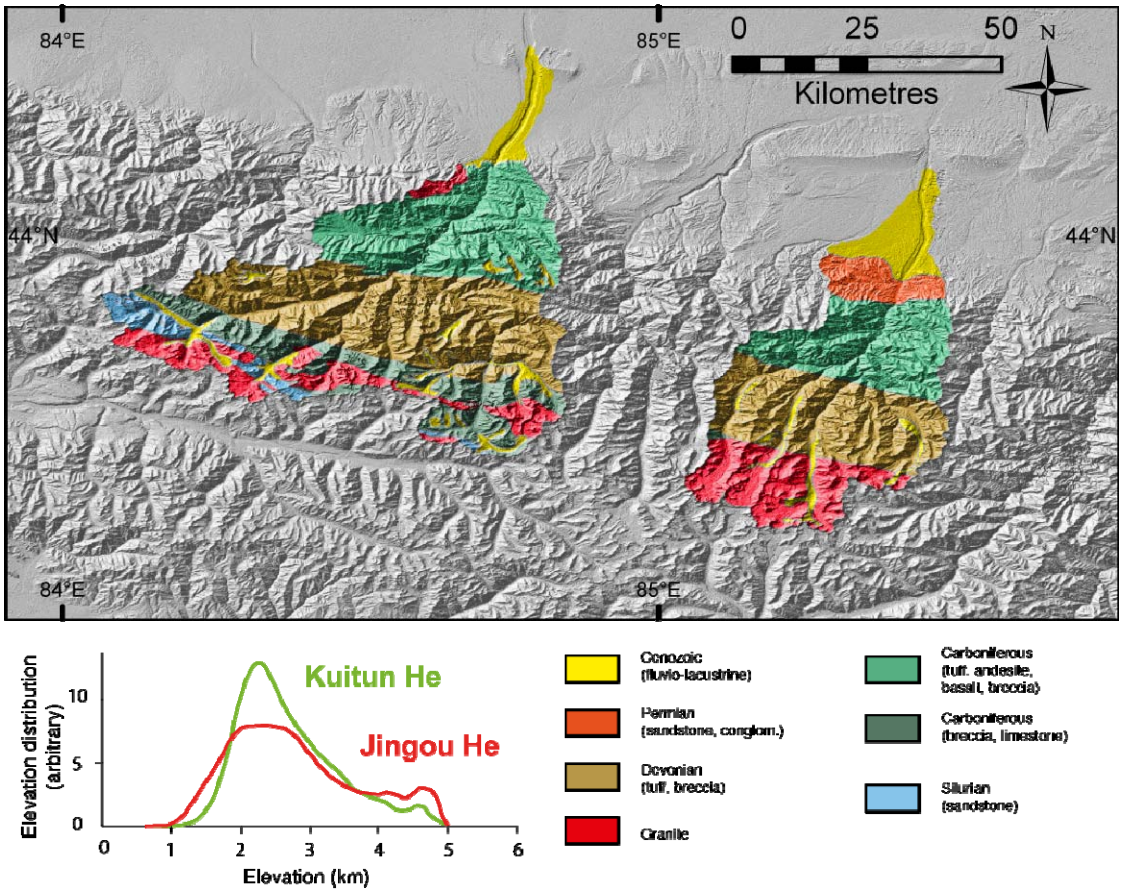

FIG. B - *Simplified lithology map and shaded DEM of the Kuitun (west) and Jingou (east) watersheds (from translation of the Xinjiang BGMRX geological map, 1993). Left Bottom: hypsometric curves of the two watersheds.*

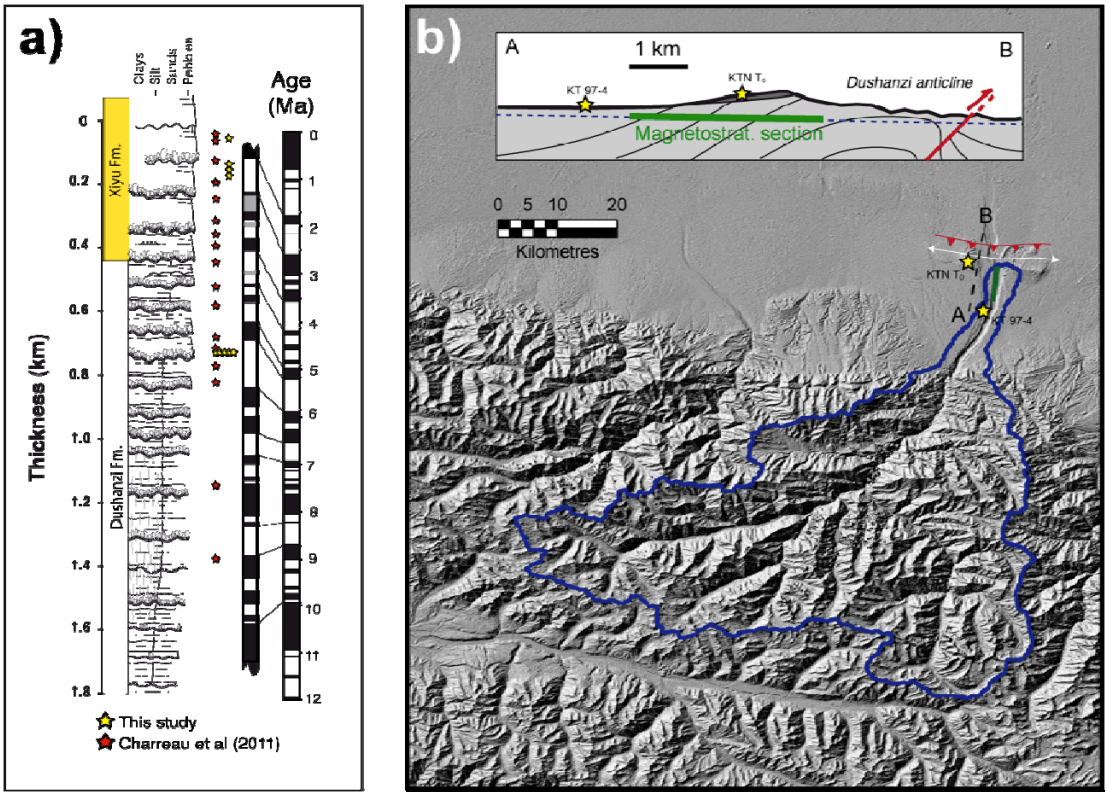

FIG. C - ***a)*** *Stratigraphic profile of the Kuitun section, with Paleomagnetism data from Charreau et al. (2005), and their correlation to the reference scale of Lourens et al. 2004. Stars indicate the position of the samples.* ***b)*** *Shaded SRTM (spatial resolution: 90m) Digital Elevation Model (D.E.M.) and cross section of the Kuitun section (top box), with locations of terrace samples. Blue line: limits of the watershed; White double arrow: Dushanzi anticline. In the cross section sketch, the blue dashed line represents the current level of the river.*

1.2 The Kuitun section

The Kuitun section is located in the Northern Tianshan piedmont where the Kuitun river ("Kuitun-He") has entrenched the active Dushanzi anticline (as named by Burchfiel *et al.*, 1999), exposing a continuous section of the south Junggar foreland sediments. The upper part of the section is composed of a thick conglomeratic unit named the Xiyu formation and coresponds to a fan-shaped braided fluvial system (Charreau *et al.*, 2009b).

The series becomes progressively fine grained toward the base, being composed predominantly of dark red to yellow sandstone and siltstone which correspond to the underlying Dushanzi formation which has been interpreted as a fluvial system with a coarse-grained flood plain (Charreau *et al.*, 2009b). In the Kuitun section these two formations were described in the Chinese literature as Quaternary and Neogene in age, respectively. However, these age assignments were loose as only based on litho-facies correlations. Hence, the section has since been dated by magnetostratigraphy between 10.5 and 1.5 Ma (Charreau *et al.*, 2005).
17 samples of sediment from this well dated section were collected for in situ cosmogenic analyses. We also analyzed sand samples from the modern river bed in three locations, and a 15 kyr old terrace. These data have been published in a previous study (Charreau *et al.*, 2011) but were recalculated here (see §3). We additionally refined the sediment sampling between 1.7-2.4 Ma (4 samples), a high resolution profile in a fluvial sequence (5 samples), and sampled the highest and likely oldest alluvial terraces enveloping the main fold. This terrace was dated at ~60 kyr by other studies (Molnar *et al.*, 1994; Poisson, 2002) and preliminary O.S.L. analyses.

The present drainage basin was extracted from the SRTM (Shuttle Radar Topographic Mission) D.E.M using a GIS treatment. It has a mean, minimum and maximum elevation of 3030, 756, and 4920 m, respectively. The geology of the basin is dominated by Devonian to Carboniferous arc-volcanism rocks (tuff, andesite, basalt and breccia), and granite in its extreme south-west part (FIG. B) (Bureau of Geological and Mineral Ressources of the Xinjiang Uygur 1993).

FIG. D - *Pictures from the Kuitun section. Top: The core of the Dushanzi anticline, incised by the Kuitun river. Bottom: the top terrace covering the envelop surface of the Dushanzi anticline, with sampling point of KTN-T$_0$ (see also FIG. C)*

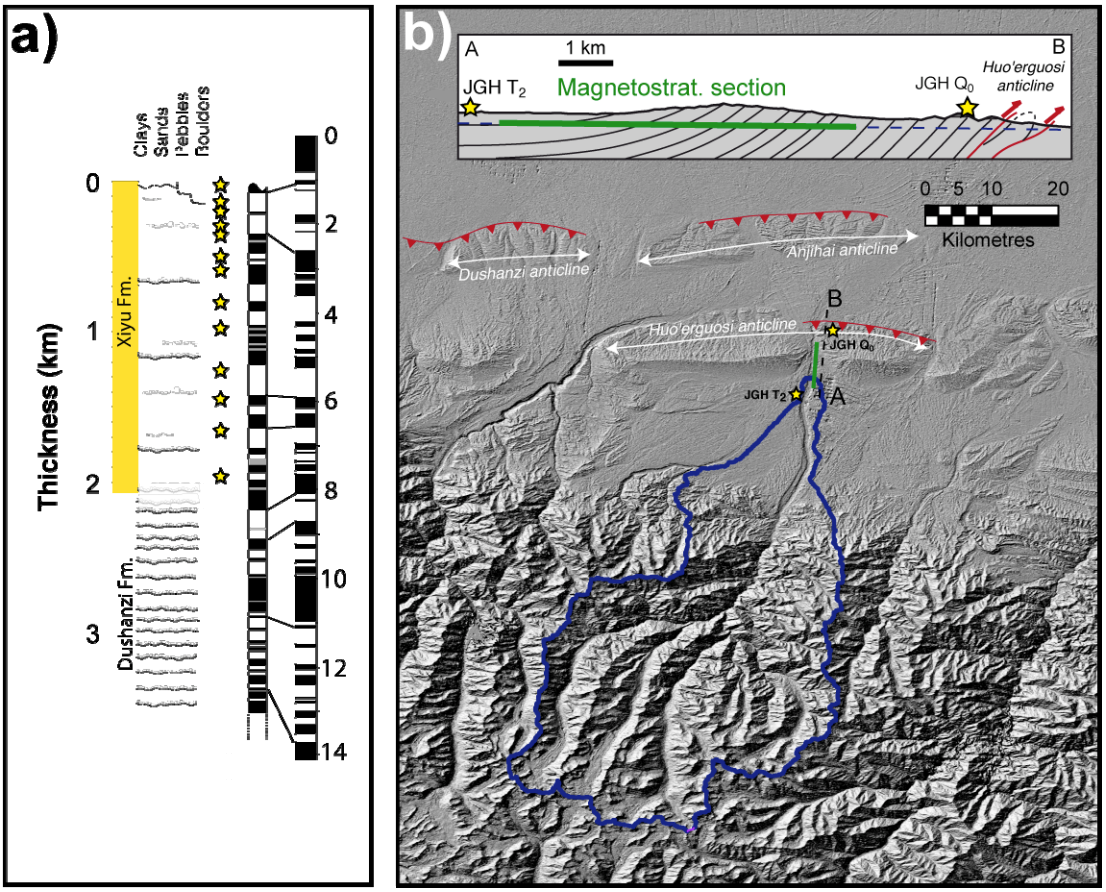

FIG. E - *a) Stratigraphic profile of the Jingou section, with Paleomagnetism data from Charreau et al. (2009a), and their correlation to the reference scale of Lourens et al. (2004). Stars indicate the position of the samples. b) Shaded SRTM (spatial resolution: 90m) Digital Elevation Model (D.E.M.) and cross section of the Jingu section (top box), with locations of terrace samples. Blue line: limits of the watershed; White double arrows: anticlines. In the cross section sketch, the blue dashed line represents the current level of the river.*

1.3 Jingou section

The Jingou section (named after the Jingou-He river which means "the river of gold") is located ~50 km to the east of the Kuitun section. In this remarkable section, Oligocene to Quaternary Junggar foreland sediments are folded by the Huo'erguosi anticline (FIG. E and F) and outcrops in the southern limb of the fold where a spectacular and continuous section is accessible (FIG. F). This section exhibits five lithostratigrahic formations described in the Chinese literature (e.g. BGMRX, 1993) as, from bottom to top, the Anjihaihe, Shawan, Taxihe, Dushanzi and Xiyu formations. Based on analysis of lithology and sedimentary structures these formations were interpreted in term of depostional environments (Charreau *et al.*, 2009b) which evolve from lacustrine to fluvial and, later, alluvial fan system (i.e the Xiyu formation). The section has also been dated by a magnetostratigraphic analyze (Charreau *et al.*, 2009a), which constrains the depositional ages from 1 to 25 Ma. Because of analytical limitation induced by the ^{10}Be decay (see §2), we limited our sampling to the last 7.5 Myr. 13 samples were therefore collected in the Jingou section plus three samples of the modern river bed. We also carried out one depth profile in one of the numerous strath terraces present in the Jingou valley. The analyses of this depth profile using the method described in Braucher *et al.*. (2009) yielded an abandon age of the terrace of ~12 kyr (Dimitri Saint-Carlier, Personal Communication). From this profile we also derived the inherited concentration of in-situ cosmogenic nuclides that will be used to constrain the denudation rates at the time of deposition of the terrace. Furthermore, we also sampled the highest terrace that dominates the Jingou river (Fig. F). This terrace was uplifted in the southern limb of the Hu'erguosi anticline and lies now at ~100 m above the present river. From uplift rates across the fold (Charreau *et al.*, 2008) together with the extrapolation of the incision rates derived from the 12 kyr old terrace we estimate the age of this higher terrace to a ~66 kyr age.,

The drainage basin topography was also extracted from SRTM DEM and is roughly similar to the Kuitun river watershed (Charreau *et al.*, 2012). Its main, minimum and maximum elevations are 3092, 880 and 5250 m respectively, and the geology similarly exhibits arc-volcanic and granite lithologies plus the presence, here, of Permian sandstone and conglomerates located between the foreland basin and the Carboniferous volcanic units aforementioned (FIG. B)

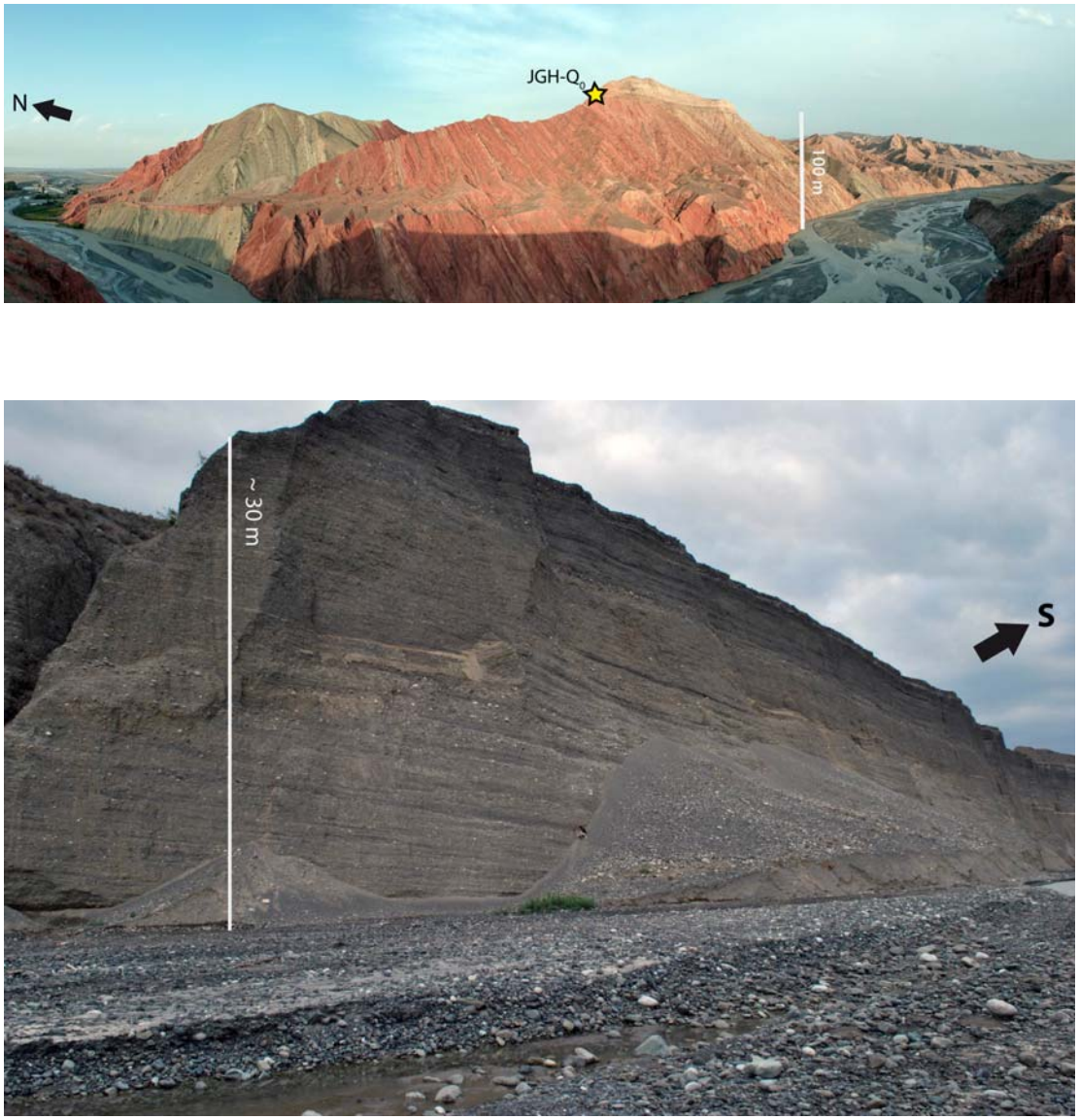

FIG. F - *Pictures from the Jingou section. Top: The Huo'erguosi anticline, with the sampling location of JGH-Q0. Bottom: sediments of the so called Xiyu formation, exposed by the river incision (spot located between samples JGH-13 and JGH-14)*

1.4 Ebi Lake

The Ebi Lake ("Ebi Nor"), is located in the extreme western part of the Junggar basin. It represents the main outlet of several large rivers draining the northern Tian-Shan (Bohoro-Shan), the southern Dzungarskiy Alatau, and the Western Alatau (FIG. G). The most eastern rivers of the Northern Tian-Shan and Alatau drains towards the Manas lake.

The present lake is very shallow (~1 m) and hypersaline (100 $g.L^{-1}$), but has lost about half of its volume because of intense irrigation since the 50's. As revealed by paleo-shoreline ridges, the lake level has however fluctuated during the Holocene, with a maximum elevation about 50 m above the present day lake elevation (a study of the recent level evolutions of the Ebi lake can be found, in English language, in B. Poisson, 2002, chapter IV, available at http://tel.archives-ouvertes.fr/).

In 2004, a core was drilled by the Xinjiang Geological Survey in the northwestern part of the Ebi Lake. The drilled sediments mainly comprise fluvial and lacustrine deposits that were dated by magnetostratigraphy from 5 to 0 Ma (see chapter V, in English, in A. Gallaud, 2008, for detailed description of the paleo-environmental reconstruction and the magnetostratigraphic analyses, available at: http://tel.archives-ouvertes.fr)

At the drilling site location, the flowing water, and hence the transported sediments, are presently drained from a large area which comprise the southern Alatau, but more importantly the northern Tian-Shan (FIG. G). From these uplifting reliefs to their final destination in the Ebi lake, the rivers wander on a large floodplain where deposition probably dominates. Yet, to calculate denudation rates from in situ cosmogenic nuclids in river sediments only the eroding part must be considered (Wittmann and von Blanckenburg, 2009; Wittmann *et al.*, 2009; Lupker *et al.*, 2012). Therefore, for later computations of cosmogenic production rate and hence denudation rates(see §3), were considered only the areas of the watershed located above the altitude of 390 m which represents a clear rupture in the hypsometry of the drainage basins and probably corresponds to the limit between the depositional zone in the subsiding Junggar foreland basin and the eroding, uplifting parts of the Tian-Shan and Alatau.

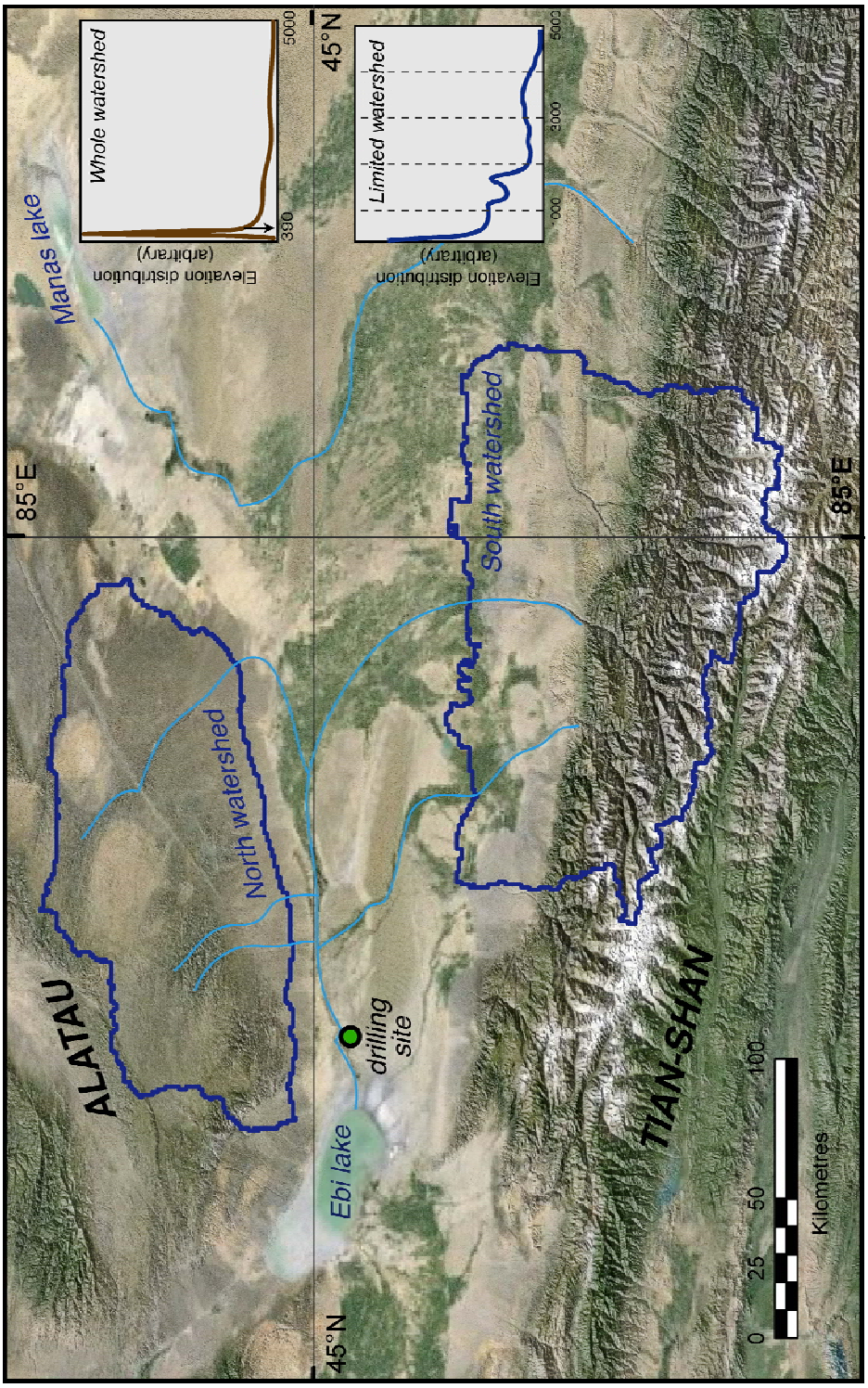

FIG. G - *Blend of shaded D.E.M. and of Google Earth image of the Ebi lake and western Junggar basin, with drilling site location. The corresponding watershed considered for computation is delimited by a deep blue line. Right: hypsometric curves of the theoretical whole watershed and the watershed excluding the alluvial plain.*

Therefore, the drainage basin is subdivided into two distinct areas: the southern one, bringing most of the water discharge (including the Kuitun-He and Jingu-He), draining higher relief, and the dryer, northern one, marked by a smoother relief (FIG. G). It is not straightforward to evaluate how the sediment provenance have evolved throughout the ~5 Myr of the studied record. Nevertheless, paleo-environmental proxies suggest that the water depth and hydrodynamics have, in average, not varied significantly at the core location during this period (Gallaud, 2008). Furthermore, given the geometry of the considered drainage basin and their very large area, potential changes in river network and sediment sources probably did not significantly affect the overall cosmogenic production rates (see §3.2)

31 samples were collected in the drilled core and consist mainly of fine to coarse sandstone. Given the small size of each samples, and to ensure enough material after the sample treatment and Quartz enrichment, only coarser samples were selected and several stratigraphically contiguous samples were often amalgamated.

1.5 Yaha section

The Yaha section is located in the southern piedmont of the Eastern Tian-Shan, ~30 km from the Kuche (or "Kuqa") city (FIG. A) where the south-flowing Yaha River entrench the impressive Qilitage anticline (Fig. I and J) defined by Hubert Ferrari *et al.* (2007) as a 225-km-long active ramp anticline. In the northern limb of this fold a remarkable continuous section can be observed. In this section, as in many others around the Tian-Shan, the sediments progressively coarsened up starting from dark red, muddy sandstone intercalated with siltstone and green-gray sandstone at the base of the section, which corresponds to the Kuche formation, toward a thick gray conglomerate unit, described as the Xiyu Formation.

The depositional ages were also constrained by a magnetostratigraphic analyses which date the section between 12.5 and 1.7 Ma. The corresponding watershed was also derived from the SRTM DEM and has a mean, maximum and minimum elevations of 2050, 3900 and 1390 m, respectively. The geology of the drainage basin includes Cretaceous to Triassic detrital sediments, folded into the Kaiyileiaikeng anticline (Fig. H) (Burchfiel *et al.*, 1999), and Permian/Carboniferous silicic shale, sandstones and conglomerates. It must be noted that, unlike the sections studied in the Northern Tian-Shan, the current watershed mainly drains a limited part of the high range.

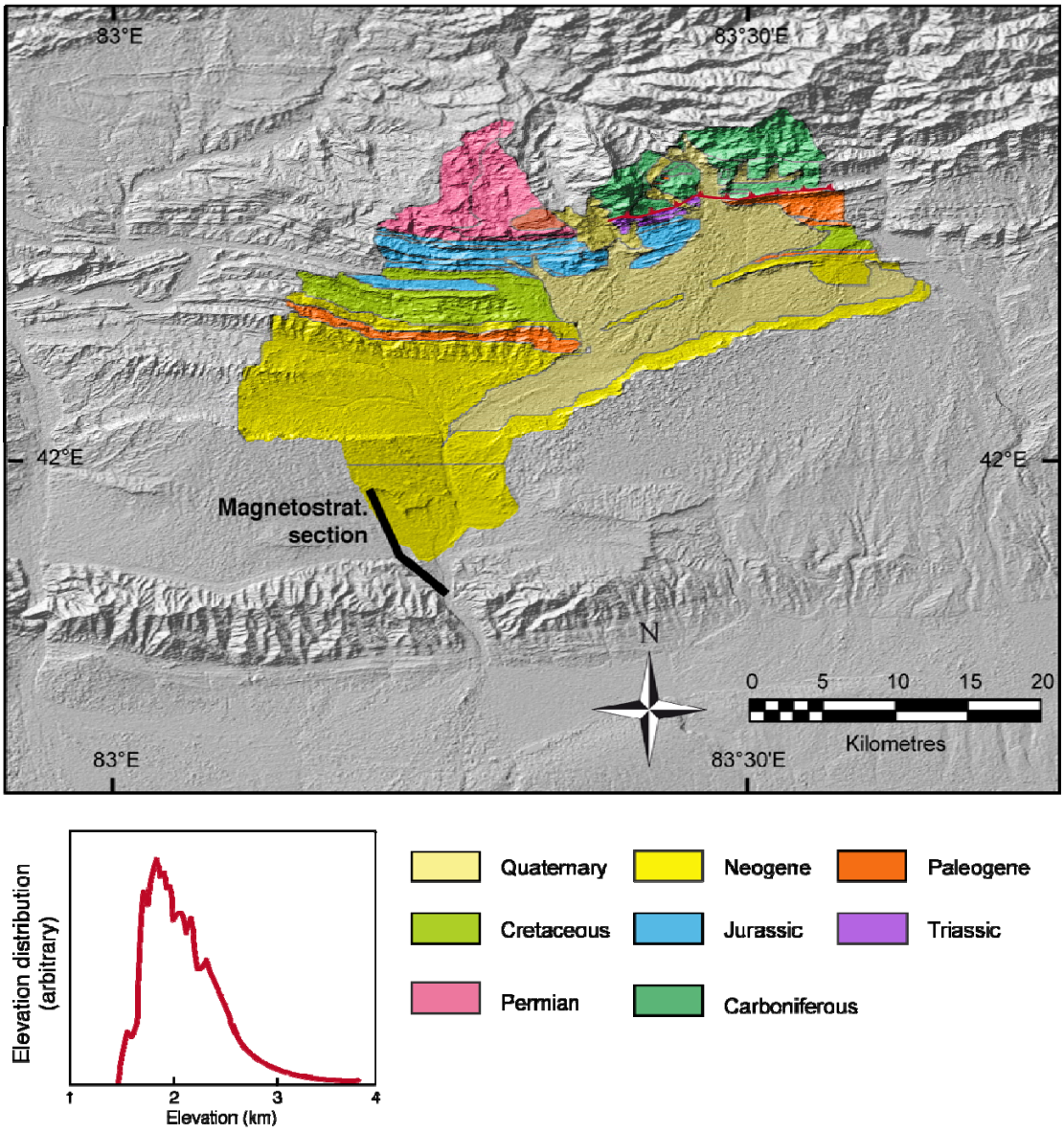

FIG. H - *Simplified geologic map of the Yaha watershed. All units are composed of detrital shales, sandstones and conglomerates. The Carboniferous also contains levels of volcanic breccias (BGMRX, 1993). Left Bottom: hypsometric curve of the present-day watershed*

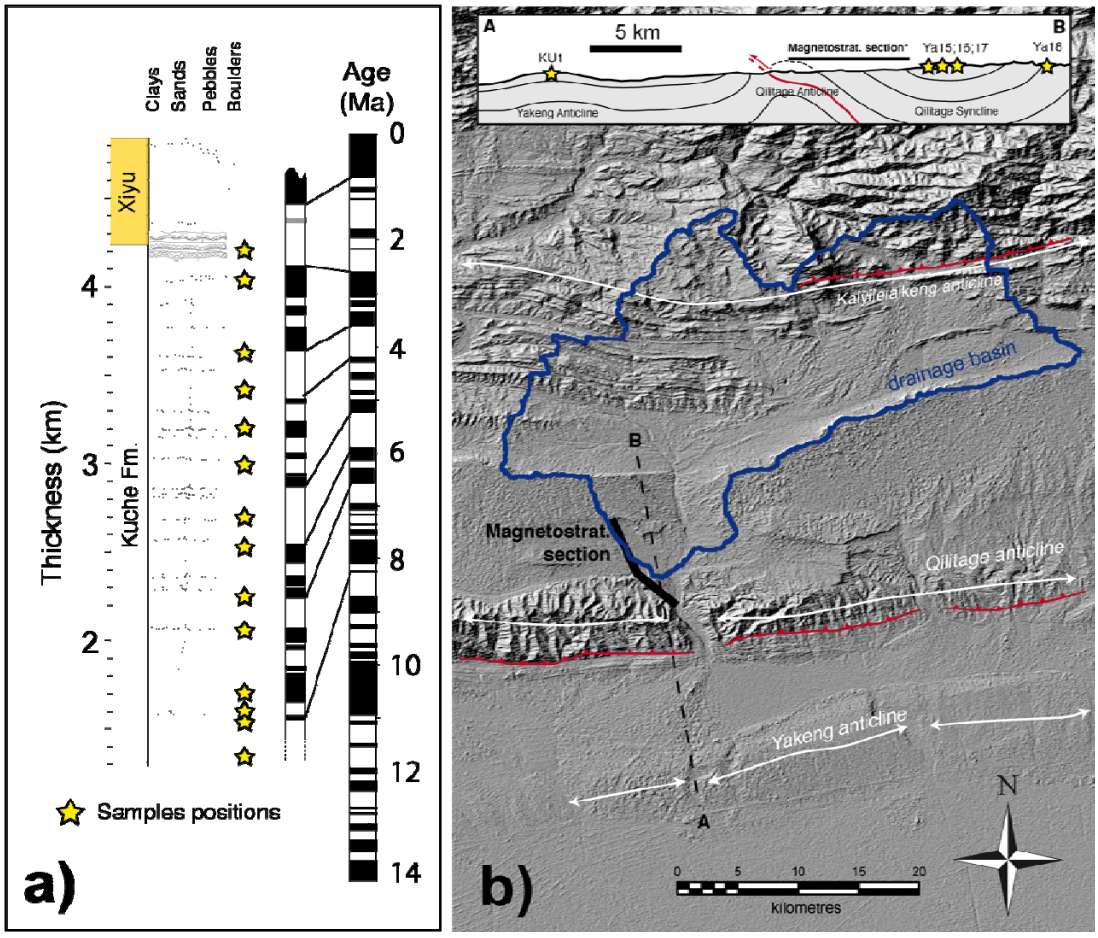

FIG. I - a) *Stratigraphic profile of the Yaha section, with Paleomagnetism data from Charreau et al. (2006, 2009b), and their correlation to the reference scale of Lourens et al. (2004). Stars indicate the position of the paleo-denudation samples.* ***b)*** *Shaded SRTM (spatial resolution: 90m) Digital Elevation Model (D.E.M.) and cross section (top box) of the Yaha section. Blue line: limits of the watershed; White double arrows: major anticlines; Red lines: major thrusts.*

This is mainly because the Kaiyileiaikeng anticline, in the north-western part of the watershed, has uplifted Mesozoic sediments that isolated the streams from the higher Paleozoic relief (unlike, for instance, the nearby Kuche river) (Burchfiel *et al.*, 1999; Hubert-Ferrari *et al.*, 2007). So, one may wonder when the folding and uplift of the Kaiyileiaikeng anticline started and whether or not it has changed the drainage basins especially during the time which corresponds to our sediments samples (i.e 0-8 Ma). The onset of deformation across the Quilitage and Yakeng folds probably started at least 5 Ma (Hubert-Ferrari *et al.*, 2007). Because the

Kaiyileiaikeng anticline is located further to the North in the inner part of the Kuche foreland piedmont, the onset of deformation across this structure likely predates the deformation across the Quilitage and Yakeng anticlines.

In the northern limb of the Quilitage anticline, we collected 14 samples of medium to coarse sandstone. To reach younger sediments we also picked up 4 samples in the core of the Qilitage syncline (FIG. I). Since a magnetostratigraphic analysis was not amenable in this conglomeratic formation, the depositional ages are constrained from $^{26}Al/^{10}Be$ burial dating (see §3.6 and e.g. Granger and Muzikar, 2001, for a description of this method).

At last, 20 km to the south, across the Yakeng anticline, the rivers have left several well preserved strath terraces. In one of them we also carried out a depth profile for cosmogenic analyses, which constrain both the age of the surface abandon to ~120 kyr, and the inherited concentration at the time of the terrace deposition.

FIG. J - *Left : Picture of the oldest part of the Yaha section, at the north of the Qilitage anticline core with sampling location of YA-1 and YA-2. Right: Picture at the bottom of the "Xiyu" formation, at the south flank of the Qilitage syncline (near the sampling point of YA-15).*

2 ^{10}Be and ^{26}Al analysis

2.1 Sampling

In the river sections, the sampling site were carefully selected to ensure low exposure to recent cosmic ray,. To limit to the minimum recent muonic production, we systematically favored samples located at the bottom of the highest available cliffs, in small caves when possible. We also took care to refresh the first ~50 cm of the surfaces to avoid contamination by sands washed from above.

The ^{10}Be and ^{26}Al decays are one of the main challenging limitations to extend the use of cosmogenic nuclides to ancient sediments. In rapidly eroding region, the initial concentration might be low and, therefore, the final concentrations measured after radioactive decay might be close to the detection limits of modern Accelerator Mass Spectrometers (AMS), yielding to large analytical uncertainties in old sediment.

Thus, to lower those uncertainties the total mass of material analyzed on the AMS must be relatively high. The mass of sediments collected and processed to enrich the quartz is therefore much larger than the one usually used, for instance, in modern rivers. Typically, for the oldest samples, between ~2 and 5 kg of sandstone were sampled and processed, yielding ~150 g of purified 200-800 μm quartz grains (see §2.2 bellow).

In the Ebi lake core, because the processing of silty and clay samples is tricky and leads to a lesser yield, we focused our sampling to the most sandy part. However, the available material remained often low, and we amalgamated several tens of centimeters (which corresponds, given the accumulation rates in this case, to an average on 2 up to 6 kyr periods) to obtain the minimum sample mass required to and ensure low analytical uncertainties.

2.2 Sediment processing

All samples were crushed and sieved to isolate the 200-800 μm fraction. Ebi samples, usually finer, were sieved into 60-500 μm fractions in order to keep as much material as possible. Quartz was first enriched through successive magnetic separations, and flotation.

To eliminate all mineral phases but quartz the enriched fraction underwent successive leachings in pure 4/5 H_2SiF_6 + 1/5 HCl, in order. This method, unlike the most commonly used of (Kohl and Nishiizumi, 1992) has the triple advantage to (i) not involve the very hazardous HF, (ii) use the most cheaper hexafluorosilicic acid, (iii) be adequate for the large sample masses required in this study (see above). Typically, the processing of 300 g quartz-enriched sand to obtain pure

quartz requires ~6 leaching steps in 700 mL of H_2SiF6 + HCl, while leaching in a diluate HF+HNO3 (Brown *et al.*, 1991) would involve ~40 liters.

The pure quartz underwent 3 leachings in concentrated HF in order to eliminate atmospheric ^{10}Be (Nishiizumi *et al.*, 2007)

In all of these steps, the Ebi samples were filtered through 60 μm nylon filters to avoid loss of the suspended particles and maximize the yield.

2.3 ^{10}Be and ^{26}Al chemical extraction and analysis

The purified quartz was then completely dissolved in HF. We added 100 μL of a 3.025 10^{-3} g/g ^{9}Be carrier solution, and 150 μL of another 2.020 10^{-3} g/g ^{9}Be carrier for the Ebi samples. These carriers were made in-house from phenakite minerals and have extremely low $^{10}Be/^{9}Be$ ratios (< 4×10^{-16}), which is particularly important to accurately analyze old samples with very low ^{10}Be concentrations.

In the samples where insufficient natural ^{27}Al was presumed, we added adapted amounts of a commercial ^{27}Al 1mg/mL standard (typically between 700 and 1000 μL).

Following subsequent purification on chromatography columns by anion exchange, cation exchange, alkaline precipitations and oxidation, purified beryllium and aluminum oxides were analyzed at the French national AMS (Accelerator Mass Spectrometer) facility ASTER (Accelerator for Earth Sciences, Environment and Risks) located at the CEREGE laboratory (Aix en Provence, France).

^{10}Be concentrations measured at ASTER are normalized to $^{10}Be/^{9}Be$ SRM 4325 NIST reference material with an assigned value of $(2.79\pm0.03)\times10^{-11}$. This standardization is equivalent to 07KNSTD within rounding error. Two samples of the present Kuitun river bed were collected in 1997 (KT97-1 and KT97-4) were actually normalized to KNSTD3770 when measured in 1997. Therefore we re-normalized those two samples to 07KNSTD to take account of the KNSTD renormalization (Nishiizumi *et al.*, 2007). Analytical $^{10}Be/^{9}Be$ blank ratios have been in average $1.5\pm0.8\times10^{-15}$ for these series.

^{26}Al concentrations were normalized to ASTER's in-house standard SM-Al-11, with a $^{26}Al/^{27}Al$ value of $(7.40\pm0.06)\times10^{-12}$. Analytical $^{26}Al/^{27}Al$ blank ratios have been in average $3.0\pm4.3\times10^{-15}$ for these series.

Natural ^{27}Al concentration were measured by ICP-OES spectrometry in the dissolved samples, after evaporation and substitution of fluorides by HNO_3, at the Service National d'Analyse des Roches et Minéraux (SARM, CRPG, Vandoeuvres, France). In the Ebi and some of the Yaha

samples, we also tested the presence of natural ^{9}Be in the quartz. The measured amounts were always equal within uncertainties to the amounts introduce by spiking.

3 From analysis to paleo-denudation rates

3.1 Theoretical background

At a single location i, in surficial rocks undergoing continuous thin-layers removal by erosion, the concentration (atom.g^{-1}) of cosmogenic isotopes N_i (e.g. ^{10}Be), is expressed by the following equation (Lal, 1991):

$$\varepsilon_i = \frac{\Lambda}{\rho_r}\left(\frac{P_i}{N_i} - \lambda\right) \quad (1)$$

where P_i (atom g^{-1} a^{-1}) is the surface production rate, Λ (g.cm^{-2}) the attenuation length, λ (a^{-1}) the radioactive decay constant of the nuclide, ε (cm.yr^{-1}) the erosion rate and ρ_r (g.cm^{-3}) the density of the bedrock. It must be noted that this equation is valid only if the surface exposure time is sufficiently long (i.e. $t >> 1/(\lambda+\varepsilon\rho/\Lambda)$) to have reached steady state and if the inherited cosmogenic concentration can be neglected. Importantly, but under certain conditions discussed bellow, the cosmogenic nuclide concentration measured in river sands has the remarkable property of averaging the concentration of all surficial rocks outcropping in the drainage basin (Brown *et al.*, 1995; Granger *et al.*, 1996). It is thus possible to determine the average erosion rate $\overline{\varepsilon}$ for a whole drainage basin by measuring the mean cosmogenic nuclide concentration $\overline{N_i}$ in river bed sand (circle ℵ in FIG. K).

However, as soon the sediment is deposited in the basin the concentration will evolve significantly. Two simultaneous processes will change the original concentration. First, during its bruial the sediment is partly exposed to the cosmic flux. This process may last for thousand of years since fast and slow muons can penetrate deeply in the sediments up up to several tens of meters depth continuing to produce some cosmogenic nuclides (circle ℑ in FIG. K). Second,

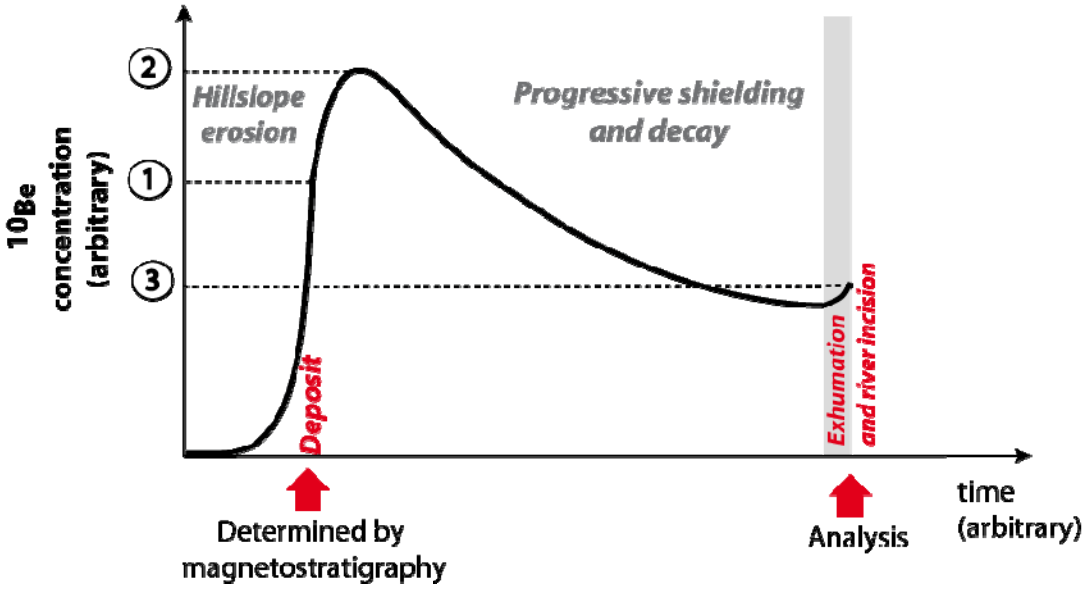

FIG. K - *Theoretical evolution of the ^{10}Be concentration from the hillslopes until sampling.*

^{10}Be as a radioactive isotopes will decay through time with a half-life $t_{1/2}$ of 1.39 ± 0.01 x 10^6 years (Chmeleff *et al.*, 2010; Korschinek *et al.*, 2010)

During this post-depositional period, the overall produced concentration N_{shield} which include both burial processes and radiaoctive decay can be estimated as follow:

$$N_{shield} = \sum_j \left[\frac{P_j}{\lambda - \frac{A\,\rho_s}{\Lambda_j}} \left(e^{-t\frac{A\,\rho_s}{\Lambda_j}} - e^{-\lambda t} \right) \right] \qquad (2)$$

with $\mathbf{P_j}$ the surface production rates by spallation, by fast muons and by slow muon captures (in at.g^{-1}.yr^{-1}), $\boldsymbol{\lambda}$ the radioactive decay constant, $\boldsymbol{\rho_s}$ the overlying sediment density, **A** the sediment accumulation rate (cm.yr^{-1}) , Λ_j the typical attenuation lengths of the different production mechanisms (g.cm^{-2}) and **t** (yr) the time during which the sediment is getting buried.

At last, the sediment may be again exposed during modern times, prior to the sampling, and can accumulate a supplementary N_{recent} signal (circle ℜ in FIG. K)

Thus, combining all of this history, the total concentration in a sample will be described as

$$N_{total} = N_{denud} + N_{shield} + N_{recent}$$

$$N_{total} = \sum_j \left[\frac{\overline{P}_j}{\frac{\overline{\varepsilon}\rho_r}{\Lambda_j}} e^{-\lambda t} + \frac{P_j}{\lambda - \frac{A\rho_s}{\Lambda_j}} \left(e^{-t\frac{A\rho_s}{\Lambda_j}} - e^{-\lambda t} \right) \right] + N_{recent} \quad (3)$$

With $\overline{P_j}$ the overall paleo-production rates averaged over the basin at the time of erosion which account for all cosmogenic production mechanism (spallation, slow and fast muons).
Iin the following section, we discuss the different parameters requested to solve this equation and their respective uncertainties on the final result.

3.2 Basin averaged production rate

Present-day average cosmogenic production rate calculation

A scaling factor, multiplying the fictive Sea Level High Latitude (SLHL) production rate, is associated to each basin. We used the scaling scheme of Lal/Stone (Lal, 1991; Stone, 2000) for spallation processes, and the parameters recommended in Braucher *et al.*, (2003) and Braucher *et al.* (2011) for muons. This scaling factor depends on the altitude and the latitude of each point in the basin. We used to this purpose the Shuttle Radar Topographic Mission (SRTM) Digital Elevation Model (DEM), with a spatial resolution of 90m.
The topographic shielding induce by the hillslopes was also considered using the S.R.T.M D.E.M and following Dunne et al. (Dunne *et al.*, 1999). All scaling factors, basin averaged, and at the deposition location, are reported in table 1.

Paleo-elevation of the basin

To estimate past denudation rates from in situ cosmogenic concentration in sediment, the cosmogenic production rate must be known at the time of deposition. Yet, cosmogenic production rate strongly relies on the elevation of the drainage basin and therefore, this later should be known throughout time.. In the Northern Tianshan recent analyses of pedogenetic carbonate in the same Kuitun and Jingou-He section yielded relatively constant values of $\delta^{18}O$ for the last 10 Ma, which suggests that the hypsometry of the drainage basins was relatively

steady during this time (Charreau *et al.*, 2012). We do not have similar data for the Yaha section but we will assume a similar history. To take into account the weight of these assumptions, we propagated to the calculated erosion rates an uncertainty of 150 m attached to the catchment average elevation. This elevation uncertainty results from the standard deviation of the $\delta^{18}O$ record (Charreau *et al.*, 2012) considering that the $\delta^{18}O$-altitude dependence is -2.8 ‰/km (Chamberlain and Poage, 2000).

Basin lithology

If the cosmogenic nuclide concentration measured in a given river sand has the remarkable property of averaging the concentration of all surficial rocks outcropping in the drainage basin, it relies on the assumption that the quartz content of all eroded rocks is similar. The geology of the drainage basin is therefore critical. However, it is almost impossible to constraint the quartz content of all rocks for such large watershed, especially in the Tianshan range, where roads are scarce and because the Chinese authorities restrain the access to several areas. Nevertheless, a good knowledge of the drainage basin geology may enable to, at least, disregard possible zones without quartz. 1:100000 Chinese geological (BGMRX, 1993) maps corresponding to all three studied drainage basins suggest that quartz is fully present over the entire watershed area (FIG. B and H). Although the ignorance of the Quartz content could induce a bias in the absolute denudation values, it does not have an influence on the relative variations throughout or records.

Magnetic field variability

Given the relatively high latitude of the Kuitun watershed (45°N), time variations of the geomagnetic field (Biggin *et al.*, 2009) induced cosmogenic production variations of less than 5% over the considered time period (i.e. the last 10 Myr) (Dunai, 2001).

3.3 Post depositional accumulation

Sediment accumulation rate (A) is a critical parameter in equations (2) and (3) to calculate the contribution of post depositional cosmogenic accumulation in the measured signal and to correct accordingly. Thanks to the detailed magnetostratigraphic analyses (Charreau *et al.*, 2005; Charreau *et al.*, 2006; Gallaud, 2008; Charreau *et al.*, 2009a), the accumulation rate was calculated for each polarity chrons of the correlation and then the overall sediment accumulation above each sample was estimated. These accumulation rates were also corrected for compaction following (Métivier *et al.*, 1999).

However, the cosmogenic accumulation during burial is relatively limited by the fact that it occurs at much lower altitude that the sediment production in the basin even for low accumulation rates (see table 1). Thus, the cosmogenic production rate at this point is much lower than in average in the whole watershed (see table 1).

Moreover, as discussed in the main body of the paper, since accumulation may be episodic one may question the grounds of this correction. As described therein, we tested the potential bias of this correction (see also fig 3b), due to episodic sediment burial, by sampling a high resolution fluvial sedimentary sequence, in which we did not observed significant variations in ^{10}Be concentrations or correlation with sedimentary facies. We also propagated a conservative error of 50 % for the accumulation rates.

3.4 Correction for recent exposure

Except for the Ebi drill, the samples have been exposed during the Holocene incision in the sediment section. In the Kuitun and Jingu-He sections, Holocene terraces have been dated by Optically Stimulated Luminescence (OSL) and cosmogenic profiles (Molnar *et al.*, 1994; Poisson and Avouac, 2004). It is thus possible to evaluate the vertical incision of the river during this period at ~1 cm.yr^{-1}.

From this erosion rate, it is then possible to calculate N_{recent} from equation (1) and shielding correction from (Dunne *et al.*, 1999).

Due to this rapid incision, the topographic shielding of the cliff, the low latitude of the sampling point, and the sampling strategy described above designed to ensure minimal exposure, the contribution of the recent component can be considered as negligible, i.e. 15 at.g^{-1} for the Kuitun and Yaha section, 7 at.g^{-1} for the Jingu section. These values account for in any case < 0.5 % of the total measured signal.

3.5 Numerical solving and error propagation

Equation (3) is not solvable analytically. Hence, we instead used a numerical regression approach (we used the software Matlab). This is the most accurate way to proceed since it avoids having to neglect terms like the muonic production or the λ parameter in denominators, which are not taken into many studies.

Given the number of different parameters in equation (3), errors were not propagated numerically but with a Monte Carlo simulation (10 000 draws for each samples). First, this is the more handy approach since partial derivation of such an equation would be outstandingly

laborious. Second, this is also the more realistic one in this case where uncertainties on some of the parameters can attain several tens of percents.

All the constant and parameter used are reported in table 2 .

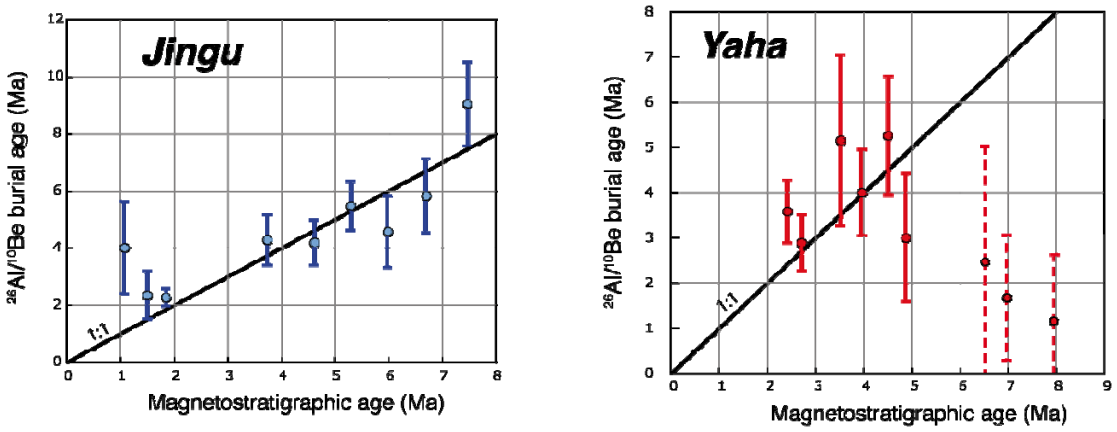

FIG. L - *Comparison of ages determined from magnetostratigraphy and from $^{26}Al/^{10}Be$ burial dating. On the Yaha section, the three samples older than 6 Ma were discarded because they most probably underwent a recent episode of exposure.*

3.6 Comparison between $^{26}Al/^{10}Be$ ages and magnetostratigraphy

It is possible to date the theoretical burial age of a given sediment by using its $^{26}Al/^{10}Be$ ratio. In surficial rocks these two cosmogenic isotopes are produced at a fixed ratio which for the $^{26}Al/^{10}Be$ couple equals to 6.75. However, each individual cosmogenic nuclide have different decay constants : 4.997×10^{-7} yr^{-1} for ^{10}Be and 9.79×10^{-7} yr^{-1} for ^{26}Al (Nishiizumi, 2004). So, as soon the sediment is buried at sufficient depth to ensure a complete shielding from the cosmic rays, the concentration of each cosmogenic isotopes will decay at different rate and the $^{26}Al/^{10}Be$ ratio will change accordingly.

A comparison of the cosmogenic burial ages to the depositional ages derived from magnetostratigraphy can be quite useful:

- if the $^{26}Al/^{10}Be$ burial age is significantly younger than the magnetostratigraphic age, it means that the sediment has probably been significantly reexposed between the first deposition and today (not necessarily at the surface, but for example for a long time at low depth).
- if the $^{26}Al/^{10}Be$ burial age is significantly older, it might suggest that part of the analyzed sediment has been reworked from older sediments.

We performed these analysis in the Jingu, and Yaha sections and in Ebi lake drilled core. Results are reported in table 1 and FIG. L. For some of the samples (see table 1), it was not possible to analyze the ^{26}Al because it fell under the detection limits of the AMS. For the older samples, this is actually reassuring: if the sediment had not been reexposed, we would expect extremely low concentrations in aluminum (as it radioactive decay is faster than ^{10}Be). Unfortunately, all ^{26}Al concentrations measured in the Ebi samples, albeit not being very old, fell under blank levels and were therefore not relevant. This is likely due to the very small size and poor chemical yield of the Ebi lake samples.

In the Jingou section, all "cosmogenic" and magnetostratigraphic ages are in very good agreement. This suggests these sediments did not underwent complex re-exposure histories since their first deposition. This is also reassuring for the Kuitun section: we did not analyze ^{26}Al in this section, but its sedimentary setting, river dynamics and tectonic context are quite similar to the nearby Jingou section.

In the Yaha section, some of the samples display $^{26}Al/^{10}Be$ much higher than their theoretical depositional ages, which suggests important episodes of re-exposure. It is almost impossible to constrain the duration and number of these possible re-exposures. These samples were therefore not considered to calculate paleo-denudation rates at the time of deposition. In both sections, any sample displayed "cosmogenic" ages older than their theoretical depositional age, suggesting that sediment reworking of ancient terraces or older sediments are limited in these basins.

Tables

Table 1a - Yaha section data

Sample	Age (Ma)	Accum. rate (mm.yr-1)	10Be (10^3 at.g-1)	1σ	26Al (10^3 at.g-1)	1σ	26Al/10Be theoretical age (Ma)	1σ	Paleo Denudation rate (m.Myr-1)	+1σ	-1σ
Magnetostratigraphic section											
Ya 1	8.54	0.75	21.0	13.9	-	-	-	-	9	4	3
Ya 2	8.24	0.82	4.4	0.8	-	-	-	-	64	16	12
Ya 3	7.96	0.68	3.1	0.5	12.1	8.4	1.1*	1.5	-	-	-
Ya 4	7.70	0.37	4.5	1.2	-		-	-	87	27	21
Ya 5	6.97	0.65	9.6	1.6	29.0	18.6	1.7*	1.4	-	-	-
Ya 6	6.52	0.65	3.3	0.6	6.7	8.0	2.5*	2.5	-	-	-
Ya 7	5.94	0.60	3.6	0.8	-		-	-	307	91	72
Ya 8	5.51	0.60	6.2	1.1	-		-	-	207	57	44
Ya 9	4.88	0.91	15.7	1.2	25.2	16.9	3.0	1.4	97	18	14
Ya 10	4.51	0.58	8.9	1.0	4.8	2.9	5.3	1.3	249	61	47
Ya 11	3.96	0.57	16.5	3.2	16.4	6.5	4.0	0.9	163	45	34
Ya 12	3.53	0.57	13.2	1.1	7.6	6.8	5.2	1.9	283	68	50
Ya 13	2.71	0.57	21.3	1.4	35.6	10.0	2.9	0.6	259	60	43
Ya 14	2.42	0.64	21.8	1.5	26.4	8.3	3.6	0.7	294	67	49
Quilitage syncline (age from 26Al/10Be burial dating)											
Ya 15	-	0.57	20.1	2.2	59.4	19.3	1.7	0.6	342	104	87
Ya 16	-	0.57	24.8	3.9	94.9	25.1	1.2	0.6	360	116	98
Ya 17	-	0.57	19.5	2.9	33.2	14.4	2.9	0.7	195	67	57
Ya 18	-	0.57	13.9	0.8	23.0	5.5	2.9	0.4	272	71	58
Yakeng Anticline (age from depth profile)	**Age (ka)**	**1σ**	**initial Be**	**1σ**							
KU1	0.136	0.048	30.4	58.5	-	-	-	-	286	234	122
River Bed											
TS10-10	-	-	81.5	2.8	-	-	-	-	196	26	23

SCALING FACTORS	**Neutrons**	**Muons**
Basin average	5.54	2.18
Deposit location	3.09	1.82

* Ya 3, Ya 5 and Ya 6 were not considered in the discussion because their $^{26}Al/^{10}Be$ burial dating indicates an important re-exposure episodes (see supplementary info 3.6)

Table 1b - Jingu section data

Sample	Age (Ma)	Accum. rate (mm.yr-1)	10Be (10^3 at.g-1)	1σ	26Al (10^3 at.g-1)	1σ	26Al/10Be theoretical age (Ma)	1σ	Paleo Denudation rate (m.Myr-1)	+1σ	-1σ
Section											
JGH 01	7.47	0.599	18.7	1.1	1.6	1.1	9.0	1.5	33	5	4
JGH 02	6.70	0.392	7.4	1.3	3.0	1.7	5.8	1.3	139	35	27
JGH 03	5.98	0.354	9.1	1.0	6.7	3.9	4.6	1.3	167	37	28
JGH 04	5.30	0.345	16.8	1.5	8.1	3.1	5.5	0.9	122	25	18
JGH 05	4.62	0.502	18.4	2.8	16.5	5.5	4.2	0.8	157	38	29
JGH 06	3.74	0.089	26.3	6.0	22.5	7.7	4.3	0.9	239	79	65
JGH 07	3.33	0.833	13.6	1.0	-	-	-	-	420	84	63
JGH 08	3.10		-	-	24.6	16.0	-	-			
JGH 10	2.59	0.292	33.1	3.2	-	-	-	-	271	62	47
JGH 11.5	2.42	0.225	45.9	3.8	-	-	-	-	215	49	37
JGH 12	1.85	0.24	47.4	2.2	107.5	13.7	2.3	0.3	290	64	47
JGH 13	1.50	0.227	43.5	7.1	94.8	34.8	2.3	0.8	406	115	90
JGH 14	1.07	0.221	101.8	18.2	99.5	74.1	4.0	1.6	185	50	39
Terraces											
	Age (ka)	**1σ**									
JGH-Q0	100*	20	100.2	3.1	-	-	-	-	257	33	29
JGH T2	11.9**	7.2	105.3	18.5	-	-	-	-	251	60	45
River Bed											
TS-10-20	-	-	89.0	12.5	-	-	-	-	297	63	48
JTS09_jin1	-	-	76.2	5.8	-	-	-	-	343	53	44
JTS09_jin2	-	-	68.3	4.5	-	-	-	-	382	55	48

SCALING FACTORS	Neutrons	Muons
Basin average	9.04	3.91
Deposit location	2.02	1.5

Magnetostratigraphic ages from Charreau *et al.*, (2009)

*Age estimated from the Huo'erguosi anticlineuplifting speed and terrace altitude (Poisson and Avouac, 2004)

**Age determined from cosmogenic depth-profile in terraces (D. Saint-Carlier, personal communication)

Table 1c - Kuitun section data

Sample	Age	Accum. rate	10Be	1σ	Paleo Denudation rate	+1σ	-1σ
	(Ma)	(mm.yr-1)	(10^3 at.g-1)		(m.Myr-1)		
Mag. Section							
TF500	8.8	0.27	3.5	0.9	105	32	25
TF400	7.7	0.30	4.8	0.8	132	32	26
KBe1	5.9	0.23	3.2	0.8	695	255	196
TF200	5.6	0.23	7.3	1.2	292	84	62
KBe3	5.3	0.23	13.2	1.8	169	43	32
KBe4	5.0	0.15	7.2	0.8	526	164	123
KBe5	4.6	0.20	9.2	1.3	426	120	96
KBe6	4.2	0.19	13.4	1.8	349	95	74
KBe7	3.7	0.19	15.4	1.6	397	109	79
KBe8	3.4	0.21	11.6	1.3	712	216	161
KBe9	3.3	0.42	21.5	1.8	287	65	47
KBe11	2.7	0.11	18.2	1.8	1056	464	330
KTN 01	2.4	0.10	46.6	14.6	249	92	71
KTN 02	2.2	0.54	10.3	1.3	1365	382	294
KTN 03	2.1	0.53	6.9	2.6	2328	1061	786
KBe12	2.1	0.53	12.5	1.9	1104	312	248
KBe13	2.0	0.53	15.8	2.0	873	238	180
KBe14	1.7	0.23	20.9	1.8	1038	312	243
KTN 04	1.7	0.23	33.7	6.4	495	156	115
KBe15	1.6	0.23	39.5	4.6	449	114	91
High definition sequence							
P1	5.3	0.22	16.53	3.16	132	37	28
P2	5.3	0.22	8.72	1.77	281	85	66
P3	5.3	0.22	16.45	2.23	134	32	24
P4	5.3	0.22	16.75	2.56	132	34	25
P5	5.3	0.22	11.68	3.97	190	65	51
Terraces	**(kya)**						
KTN T0	60*		40.9	2.8	629	89	78
KT97-4	15**	3	110.0	6.2	240	32	29
River Bed							
KT97-1	-	-	48.4	21.4	532	195	148
RBKTN1	-	-	51.5	11.5	531	150	106
KUITUNDAM	-	-	41.2	6.1	661	137	109

SCALING FACTORS	Neutrons	Muons
Basin average	9.47	2.94
Deposit location	1.94	1.46

Magnetostratigraphic ages fromCharreau *et al.* (2005). All raw ^{10}Be data, except for samples beginning with "KTN" and "P", have been previously published in Charreau *et al.* (2011), but paleo-denudation rates have been re-calculated.

* Age determined from OSL dating (Molnar *et al.*, 1994; Poisson and Avouac, 2004)

**Age determined from cosmogenic depth profile dating.

Table 1d - Ebi Lake core data

Sample	Age (Ma)	Accum. rate (mm.yr-1)	10Be (10^3 at.g-1)	1σ	Paleo Denudation rate (m.Myr-1)	+1σ	-1σ
Sample reference							
7	0.09	0.09	129.2	7.6	149	40	31
37	0.31	0.09	167.5	7.4	94	23	18
122	0.79	0.18	245.6	7.9	40	8	7
270	1.13	0.28	294.8	9.8	27	5	4
382	1.52	0.12	79.5	5.9	105	25	20
439	1.72	0.12	57.8	5.9	138	36	29
466	1.82	0.10	71.0	13.4	102	29	25
543	2.62	0.08	85.7	18.6	53	15	13
588	2.88	0.08	54.3	7.4	81	22	18
665	3.27	0.11	47.9	10.9	66	19	16
678	3.42	0.01	59.9	6.0	132	34	36
756	4.10	0.07	52.2	7.8	45	28	11

SCALING FACTORS	Neutrons	Muons
Basin average	4.68	1.17
Deposit location	2.23	1.11

All the ^{26}Al analysis were under the analytical blank.

Ages published in A. Gallaud PhD Thesis (2008)

Table 2 - Parameters used for paleo-denudation calculations

Parameter and unit	symbol	value	1σ	Reference / comments
10Be decay constant (yr^{-1})	λ	4.997×10^{-7}	0.043×10^{-7}	(Chmeleff *et al.*, 2010; Korschinek *et al.*, 2010)
Sea Level High Latitude 10Be production rate - neutrons ($at.g^{-1}.yr^{-1}$)	-	3.9	0.3	(Balco *et al.*, 2009; Balco *et al.*, 2008) recalculated to include the new STD-ICN values (Nishiizumi *et al.*, 2007)
Sea Level High Latitude 10Be production rates - fast muons ($at.g^{-1}.yr^{-1}$)	-	0.026	0.006	(Braucher *et al.*, 2011), corrected from (Braucher *et al.*, 2003)
Sea Level High Latitude 10Be production rates - slow muons ($at.g^{-1}.yr^{-1}$)	-	0.029	0.012	(Braucher *et al.*, 2011), corrected from (Braucher *et al.*, 2003)
Attenuation length - neutrons ($g.cm^{2}$)	Λ_s	160	10	(Lal, 1991)
Attenuation length - fast muons ($g.cm^{2}$)	Λ_{fmuons}	4320	950	(Braucher *et al.*, 2003; Braucher *et al.*, 2011; Heisinger *et al.*, 2002b)
Attenuation length - slow muons ($g.cm^{2}$)	Λ_{smuons}	1510	100	(Braucher *et al.*, 2003; Braucher *et al.*, 2011; Heisinger *et al.*, 2002a)
sediment volumic mass ($g.cm^{3}$)	ρ_s	2.4	0.13	From seismic speeds (Yan Chen; personal communication)
bedrock volumic mass ($g.cm^{3}$)	ρ_r	2.4	0.13	From seismic speeds (Yan Chen; personal communication)

References for the supplementary information

Abdrakhmatov, K. Y., Aldazhanov, S. A., Hager, B. H., Hamburger, M. W., Herring, T. A., Kalabaev, K. B., Makarov, V. I., Molnar, P., Panasyuk, S. V., Prilepin, M. T., Reilinger, R. E., Sadybakasov, I. S., Souter, B. J., Trapeznikov, Y. A., Tsurkov, V. Y., and Zubovich, A. V. (1996). Relatively recent construction of the Tien Shan inferred from GPS measurements of present-day crustal deformation rates. *Nature* **384,** 450-453.

Avouac, J. P., Tapponnier, P., Bai, M., You, H., and Wang, G. (1993). Active Thrusting and Folding Along the Northern Tien-Shan and Late Cenozoic Rotation of the Tarim Relative to Dzungaria and Kazakhstan. *Journal of Geophysical Research-Solid Earth* **98,** 6755-6804.

Balco, G., Stone, J. O., Lifton, N. A., and Dunai, T. J. (2008). A complete and easily accessible means of calculating surface exposure ages or erosion rates from (10)Be and (26)Al measurements. *Quaternary Geochronology* **3,** 174-195.

Balco, G., Briner, J., Finkel, R. C., Rayburn, J. A., Ridge, J. C., and Schaefer, J. M. (2009). Regional beryllium-10 production rate calibration for late-glacial northeastern North America. *Quaternary Geochronology* **4,** 93-107.

Biggin, A. J., Strik, G. H. M. A., and Langereis, C. G. (2009). The intensity of the geomagnetic field in the late-Archaean: new measurements and an analysis of the updated IAGA palaeointensity database. *Earth Planets and Space* **61,** 9-22.

Braucher, R., Brown, E. T., Bourlès, D. L., and Colin, F. (2003). In situ produced ^{10}Be measurements at great depths: implications for production rates by fast muons. *Earth and Planetary Science Letters* **211,** 251-258.

Braucher, R., Del Castillo, P., Siame, L., Hidy, A. J., and Bourles, D. L. (2009). Determination of both exposure time and denudation rate from an in situ-produced Be-10 depth profile: A mathematical proof of uniqueness. Model sensitivity and applications to natural cases. *Quaternary Geochronology* **4,** 56-67.

Braucher, R., Merchel, S., Borgomano, J., and Bourl√®s, D. L. (2011). Production of cosmogenic radionuclides at great depth: A multi element approach. *Earth and Planetary Science Letters* **309,** 1-9.

Brown, E. T., Edmond, J. M., Raisbeck, G. M., Yiou, F., Kurz, M. D., and Brook, E. J. (1991). Examination of surface exposure ages of Antarctic moraines using in situ produced ^{10}Be And ^{26}Al. *Geochimica et Cosmochimica Acta* **55,** 2269-2283.

Brown, E. T., Stallard, R. F., Larsen, M. C., Raisbeck, G. M., and Yiou, F. (1995). Denudation Rates Determined from the Accumulation of in Situ-Produced Be-10 in the Luquillo Experimental Forest, Puerto-Rico. *Earth and Planetary Science Letters* **129,** 193-202.

Brown, E. T., Bourles, D. L., Burchfiel, B. C., Deng, Q. D., Li, J., Molnar, P., Raisbeck, G. M., and Yiou, F. (1998). Estimation of slip rates in the southern Tien Shan using cosmic ray exposure dates of abandoned alluvial fans. *Geological Society of America Bulletin* **110,** 377-386.

Bullen, M. E., Burbank, D. W., Garver, J. I., and Abdrakhmatov, K. Y. (2001). Late Cenozoic tectonic evolution of the northwestern Tien Shan: New age estimates for the initiation of mountain building. *Geological Society of America Bulletin* **113,** 1544-1559.

Burchfiel, B. C., Brown, E. T., Deng, Q. D., Feng, X. Y., Li, J., Molnar, P., Shi, J. B., Wu, Z. M., and You, H. C. (1999). Crustal shortening on the margins of the Tien Shan, Xinjiang, China. *International Geology Review* **41,** 665-700.

Bureau of Geological and Mineral Ressources of the Xinjiang Uygur , A. R. (1993). "Regional geology of the Xinjiang Uygur Autonomous region." Geological memoirs.

Chamberlain, C. P., and Poage, M. A. (2000). Reconstructing the paleotopography of mountain belts from the isotopic composition of authigenic minerals. *Geology* **28,** 115-118.

Charreau, J., Chen, Y., Gilder, S., Dominguez, S., Avouac, J. P., Sen, S., Sun, D. J., Li, Y. G., and Wang, W. M. (2005). Magnetostratigraphy and rock magnetism of the Neogene Kuitun He section (northwest China): implications for Late Cenozoic uplift of the Tianshan mountains. *Earth and Planetary Science Letters* **230,** 177-192.

Charreau, J., Gilder, S., Chen, Y., Dominguez, S., Avouac, J. P., Sen, S., Jolivet, M., Li, Y. G., and Wang, W. M. (2006). Magnetostratigraphy of the Yaha section, Tarim Basin (China): 11 Ma acceleration in erosion and uplift of the Tian Shan mountains. *Geology* **34,** 181-184.

Charreau, J., Avouac, J.-P., Chen, Y., Dominguez, S., and Gilder, S. (2008). Miocene to present kinematics of fault-bend folding across the Huerguosi anticline, northern Tianshan (China), derived from structural, seismic, and magnetostratigraphic data. *Geology* **36,** 871-874.

Charreau, J., Chen, Y., Gilder, S., Barrier, L., Dominguez, S., Augier, R., Sen, S., Avouac, J.-P., Gallaud, A., Graveleau, F., and Wang, Q. (2009a). Neogene uplift of the Tian Shan

Mountains observed in the magnetic record of the Jingou River section (northwest China). *Tectonics* **28**.

Charreau, J., Gumiaux, C., Avouac, J.-P., Augier, R., Chen, Y., Barrier, L., Gilder, S., Dominguez, S., Charles, N., and Wang, Q. (2009b). The Neogene Xiyu Formation, a diachronous prograding gravel wedge at front of the Tianshan: Climatic and tectonic implications. *Earth and Planetary Science Letters* **287,** 298-310.

Charreau, J., Blard, P. H., Puchol, N., Avouac, J. P., Lallier-Verges, E., Bourles, D., Braucher, R., Gallaud, A., Finkel, R., Jolivet, M., Chen, Y., and Roy, P. (2011). Paleo-erosion rates in Central Asia since 9 Ma: A transient increase at the onset of Quaternary glaciations? *Earth and Planetary Science Letters* **304,** 85-92.

Charreau, J., Kent-Corson, M. L., Barrier, L., Augier, R., Ritts, B. D., Chen, Y., France-Lannord, C., and Guilmette, C. (2012). A high-resolution stable isotopic record from the Junggar Basin (NW China): Implications for the paleotopographic evolution of the Tianshan Mountains. *Earth and Planetary Science Letters* **341,Äì344,** 158-169.

Charvet, J., Shu, L., and Laurent-Charvet, S. (2007). Paleozoic structural and geodynamic evolution of eastern Tianshan (NW China): welding of the Tarim and Junggar plates. *Episodes* **30,** 162-186.

Chmeleff, J. r. m., von Blanckenburg, F., Kossert, K., and Jakob, D. (2010). Determination of the 10Be half-life by multicollector ICP-MS and liquid scintillation counting. *Nuclear Instruments and Methods in Physics Research Section B: Beam Interactions with Materials and Atoms* **268,** 192-199.

Daeron, M., Avouac, J.-P., and Charreau, J. (2007). Modeling the shortening history of a fault tip fold using structural and geomorphic records of deformation. *Journal of Geophysical Research-Solid Earth* **112**.

Dumitru, T. A., Zhou, D., Chang, E. Z., Graham, S. A., Hendrix, M. S., Sobel, E. R., and Carroll, A. R. (2001). Uplift, exhumation, and deformation in the Chinese Tian Shan. *Paleozoic and Mesozoic Tectonic Evolution of Central Asia: from Continental Assembly to Intracontinental Deformation* **194,** 71-99.

Dunai, T. J. (2001). Influence of secular variation of the geomagnetic field on production rates of in situ produced cosmogenic nuclides. *Earth and Planetary Science Letters* **193,** 197-212.

Dunne, J., Elmore, D., and Muzikar, P. (1999). Scaling factors for the rates of production of cosmogenic nuclides for geometric shielding and attenuation at depth on sloped surfaces. *Geomorphology* **27** 3-11.

Gallaud, A. (2008). "Interaction Orogenèse – Climat – Erosion en Asie Centrale durant le Cénozoïque : L'impact de la surrection de la chaîne du Tianshan sur le climat dans le bassin du Junggar." Université d'Orléans.

Gao, J., Li, M. S., Xiao, X. C., Tang, Y. Q., and He, G. Q. (1998). Paleozoic tectonic evolution of the Tianshan Orogen, northwestern China. *Tectonophysics* **287,** 213-231.

Granger, D. E., Kirchner, J. W., and Finkel, R. (1996). Spatially averaged long-term erosion rates measured from in situ-produced cosmogenic nuclides in alluvial sediment. *Journal of Geology* **104,** 249-257.

Granger, D. E., and Muzikar, P. F. (2001). Dating sediment burial with in situ-produced cosmogenic nuclides: theory, techniques, and limitations. *Earth and Planetary Science Letters* **188,** 269-281.

Heermance, R. V., Chen, J., Burbank, D. W., and Wang, C. (2007). Chronology and tectonic controls of Late Tertiary deposition in the southwestern Tian Shan foreland, NW china. *Basin Research* **19,** 599-632.

Heisinger, B., Lal, D., Jull, A. J. T., Kubik, P., Ivy-Ochs, S., Knie, K., and Nolte, E. (2002a). Production of selected cosmogenic radionuclides by muons; 2. Capture of negative muons. *Earth and Planetary Science Letters* **200** 357-369.

Heisinger, B., Lal, D., Jull, A. J. T., Kubik, P., Ivy-Ochs, S., Neumaier, S., Knie, K., Lazarev, V., and Nolte, E. (2002b). Production of selected cosmogenic radionuclides by muons; 1. Fast muons. *Earth and Planetary Science Letters* **200,** 345-355.

Hendrix, M. S., Dumitru, T. A., and Graham, S. A. (1994). Late Oligocene Early Miocene Unroofing in the Chinese Tien-Shan - an Early Effect of the India-Asia Collision. *Geology* **22,** 487-490.

Hubert-Ferrari, A., Suppe, J., Gonzalez-Mieres, R., and Wang, X. (2007). Mechanisms of active folding of the landscape (southern Tian Shan, China). *Journal of Geophysical Research-Solid Earth* **112**.

Jolivet, M., Dominguez, S., Charreau, J., Chen, Y., Li, Y., and Wang, Q. (2010). Mesozoic and Cenozoic tectonic history of the central Chinese Tian Shan: Reactivated tectonic structures and active deformation. *Tectonics* **29**.

Kohl, C. P., and Nishiizumi, K. (1992). Chemical Isolation of Quartz for Measurement of Insitu-Produced Cosmogenic Nuclides. *Geochimica Et Cosmochimica Acta* **56,** 3583-3587.

Korschinek, G., Bergmaier, A., Faestermann, T., Gerstmann, U. C., Knie, K., Rugel, G., Wallner, A., Dillmann, I., Dollinger, G., von Gostomski, C. L., Kossert, K., Maiti, M., Poutivtsev, M., and Remmert, A. (2010). A new value for the half-life of 10Be by Heavy-Ion Elastic Recoil Detection and liquid scintillation counting. *Nuclear Instruments*

and Methods in Physics Research Section B: Beam Interactions with Materials and Atoms **268,** 187-191.

Lal, D. (1991). Cosmic ray labeling of erosion surfaces: *in situ* nuclide production rates and erosion models. *Earth and Planetary Science Letters* **104,** 424-439.

Lupker, M., Blard, P.-H., Lave, J., France-Lanord, C., Leanni, L., Puchol, N., Charreau, J., and Bourles, D. (2012). Be-10-derived Himalayan denudation rates and sediment budgets in the Ganga basin. *Earth and Planetary Science Letters* **333,** 146-156.

Métivier, F., Gaudemer, Y., Tapponnier, P., and Klein, M. (1999). Mass accumulation rates in Asia during the Cenozoic. *Geophysical Journal International* **137,** 280-318.

Molnar, P., Brown, E. T., Burchfiel, B. C., Qidong, D., Xianyue, F., Jun, L., Raisbeck, G. M., Jianbang, S., Zhangming, W., Yiou, F., and Huichuan, Y. (1994). Quaternary Climate-Change and the Formation of River Terraces across Growing Anticlines on the North Flank of the Tien-Shan, China. *Journal of Geology* **102,** 583-602.

Nishiizumi, K., Imamura, M., Caffee, M. W., Southon, J. R., Finkel, R. C., and McAninch, J. (2007). Absolute calibration of Be-10 AMS standards. *Nuclear Instruments & Methods in Physics Research Section B-Beam Interactions with Materials and Atoms* **258,** 403-413.

Poisson, B. (2002). "Impact du climat et de la tectonique sur l'évolution géomorphologique d'un piémont. Exemple du piémont Nord du TIan Shan depuis la fin du Pleistocène." Université Paris XI.

Poisson, B., and Avouac, J. P. (2004). Holocene hydrological changes inferred from alluvial stream entrenchment in North Tian Shan (Northwestern China). *Journal of Geology* **112,** 231-249.

Reigber, C., Michel, G. W., Galas, R., Angermann, D., Klotz, J., Chen, J. Y., Papschev, A., Arslanov, R., Tzurkov, V. E., and Ishanov, M. C. (2001). New space geodetic constraints on the distribution of deformation in Central Asia. *Earth and Planetary Science Letters* **191,** 157-165.

Stone, J. O. (2000). Air pressure and cosmogenic isotope production. *Journal of Geophysical Research - Solid Earth* **105,** 23753-23759.

Tapponnier, P., and Molnar, P. (1979). Active Faulting and Cenozoic Tectonics of the Tien Shan, Mongolia, and Baykal Regions. *Journal of Geophysical Research* **84,** 3425-&.

Windley, B. F., Allen, M. B., Zhang, C., Zhao, Z. Y., and Wang, G. R. (1990). Paleozoic Accretion and Cenozoic Redeformation of the Chinese Tien-Shan-Range, Central-Asia. *Geology* **18,** 128-131.

Wittmann, H., and von Blanckenburg, F. (2009). Cosmogenic nuclide budgeting of floodplain sediment transfer. *Geomorphology* **109,** 246-256.

Wittmann, H., von Blanckenburg, F., Guyot, J. L., Maurice, L., and Kubik, P. W. (2009). From source to sink: Preserving the cosmogenic Be-10-derived denudation rate signal of the Bolivian Andes in sediment of the Beni and Mamore foreland basins. *Earth and Planetary Science Letters* **288,** 463-474.

Xinjiang, B. o. G. a. M. R. o. t. (1993). "Regional geology of the Xinjiang Uygur Autonomous region." Geological memoirs.

Dorénavant, si j'avais encore la manie de faire parler de moi, je ne sais où je pourrais courir, afin d'attirer l'attention du public : peut-être reprendrais-je mon ancien projet de la découverte du passage au pôle nord ; peut-être remonterais-je le Gange. Là, je verrais la longue ligne noire et droite des bois qui défendent l'accès de l'Himalaya.

François-René de Chateaubriand,
Mémoires d'outre-tombe.

Chapitre 5
Paléo-taux de dénudation en Himalaya.

Chaîne des extrêmes par son relief (passage de 0 à plus de 8000 m d'altitude en à peine 150 km de largeur), l'Himalaya est aussi, depuis le début de son orogenèse, il y a ~50 millions d'années, le plus gros pourvoyeur de sédiments du globe. Capable d'affecter, suite à l'uplift du plateau tibétain, tout le système climatique de l'hémisphère Nord (e.g. Ruddiman & Kutzbach, 1989), l'orogenèse Himalayenne a également affecté le climat global au cour du Cénozoïque, de par son action sur le cycle du carbone atmosphérique (voir §1.1).

Marquées par d'intenses précipitations lors des mois de mousson, des sommets englacés, et une érosion extrême (voir Chapitre 3), les relations entre climat et tectonique Himalayenne sont au coeur d'actifs débats. D'une part, quand à la corrélation des taux d'exhumation avec les taux de précipitation (e.g. Burbank *et al.*, 2003; Wobus *et al.*, 2003; Thiede *et al.*, 2004; Vannay *et al.*, 2004; Blythe *et al.*, 2007), et d'autre part quand à une hypothétique accélération de cette dénudation lors du développement des glaciations quaternaires à partir de ~2.5 Ma (Huntington *et al.*, 2006; Blythe *et al.*, 2007; Thiede *et al.*, 2009). Ces études reposent cependant, pour la plupart, sur des thermochronomètres basse température in-situ, qui enregistrent une exhumation localisée et non intégrée sur des bassins versant. Peu d'études avaient été jusqu'à présent menées sur des minéraux détritiques (Bernet *et al.*, 2006; van der Beek *et al.*, 2006), plus intégrateurs.

Forts de nos premiers résultats encourageants au Tian-Shan, nous débutâmes fin 2010 l'étude de sections des monts Siwaliks, avant garde de l'Himalaya bâtie dans ses propres sédiments. En particulier, la priorité fut donnée à la section "Surai" qui, comme on le verra dans ce chapitre, réunissait de nombreux atouts pour l'emploi des isotopes cosmogéniques.

J'ai décidé de présenter ce chapitre en anglais. Toutefois, il ne s'agit pas encore véritablement d'un article, car plusieurs points nécessiteront certainement, d'ici soumission, de plus amples analyses et une maturation de ma réflexion.

A high resolution, 6 Myr record of paleo-denudation rates in Central Himalayas, as inferred from cosmogenic nuclides

(In preparation)

Nicolas Puchol[1], Julien Charreau[1], Jérôme Lavé[1], Pierre-Henri Blard[1], Raphaël Pik[1], ASTER Team[2,+]

[1]Université de Lorraine - CNRS, CRPG, 15 rue Notre-Dame des pauvres, 54500 Vandoeuvre-lès-Nancy, France

[2]Université Aix-Marseille, CNRS-IRD-Collège de France, UM 34 CEREGE, Technopôle de l'Environnement Arbois-Méditerranée, BP80, 13545 Aix-en-Provence, France

[+]Maurice Arnold, Georges Aumaître, Didier L Bourlès, Karim Keddadouche.

Contents of this paper

1 Introduction

Like Central Asia, the Himalayas stands out as a key area to address the general question of how the Quaternary glaciations may have impacted denudation rates. This mountain range is by far the highest producer of detrital sediments in the world. The range indeed stretches on ~2500 km in length, associated to extreme reliefs and intense climatic conditions due to heavy monsoon precipitations focused on its southern flank. This setting implies high erosion and, hence, high sediment flux to the surrounding basins. Since the onset of the India-Asia collision, this material transfer has been suspected to have impacted the world's global climate through its control on the atmospheric CO_2 by silicate weathering and organic carbon burial (e.g. Raymo and Ruddiman, 1992; FranceLanord and Derry, 1997).

While the recent and modern denudation rates of the range have been extensively documented by various techniques for the last decades (e.g. Bernet *et al.*, 2001; Thiede *et al.*, 2004; Gabet *et al.*, 2008; Andermann *et al.*, 2012; Godard *et al.*, 2012; Lupker *et al.*, 2012), few is known about the past, large-scale integrated, denudation rates, and their evolution in space and time. In the Himalayas, sediment budgets reconstructions in surrounding basins are very difficult because the depositional areas which store these sediments shed are very large, including the Ganga basin, the Indus fan, and the Bengal fan. It is moreover not straightforward to accurately assess both the complex geometry of the sediment infilling and its chronology. Consequently, the compilation of the Cenozoic Himalayan sedimentary budgets published in the literature yielded contradictory results (e.g. Burbank *et al.*, 1993; Metivier *et al.*, 1999; Clift, 2006).

More recently, several authors carried out low-temperature thermochronometers in molasses deposits in the Himalayan piedmonts (Bernet *et al.*, 2006; Szulc *et al.*, 2006b; van der Beek *et al.*, 2006), surprisingly displaying quite stable basin-averaged denudation rates over the last few million years. If these methods do not share the flaws of sediment budgets reconstructions (see Chapter 1), they average denudation rates on scales of few million-years and could possibly buffer rapid changes related to the onset of the Quaternary glaciations. Cosmogenic nuclides and the approach we have developed in the Tianshan piedmonts could better reveal the shorter time scale denudation evolutions of the range and are, therefore, probably more relevant to study the potential impact of glaciations in the Himalayas. The characteristic time window recorded by Terrestrial Cosmogenic Nuclides (TCN) is indeed <5 kyr for erosion rates larger than 0.1 $mm.yr^{-1}$.

On the other hand, because of intense tectonics and climate, the averaged denudation rates in this range are usually extremely high(> 1 mm.yr^{-1}), which implies very low initial cosmogenic isotopes concentrations in shed sediments. One could therefore fear potential technical limitation to measure several Myr old, low concentrated sediments. Moreover, it is also necessary to ensure that the correction for recent exposure remains negligible compared to the fossil ^{10}Be signal.

To develop this approach in such framework, we therefore focused on a very well documented, dated, continuous and freshly exposed section of the Himalayas piedmont: the Surai Khola section. We show that, not only our approach was feasible at least until the oldest sample we picked (6.5 Myr old), but, importantly, that it might bring new insights on the recent tectonic evolutions of central Himalayas, as well as on the response of erosion to Cenozoic climatic changes.

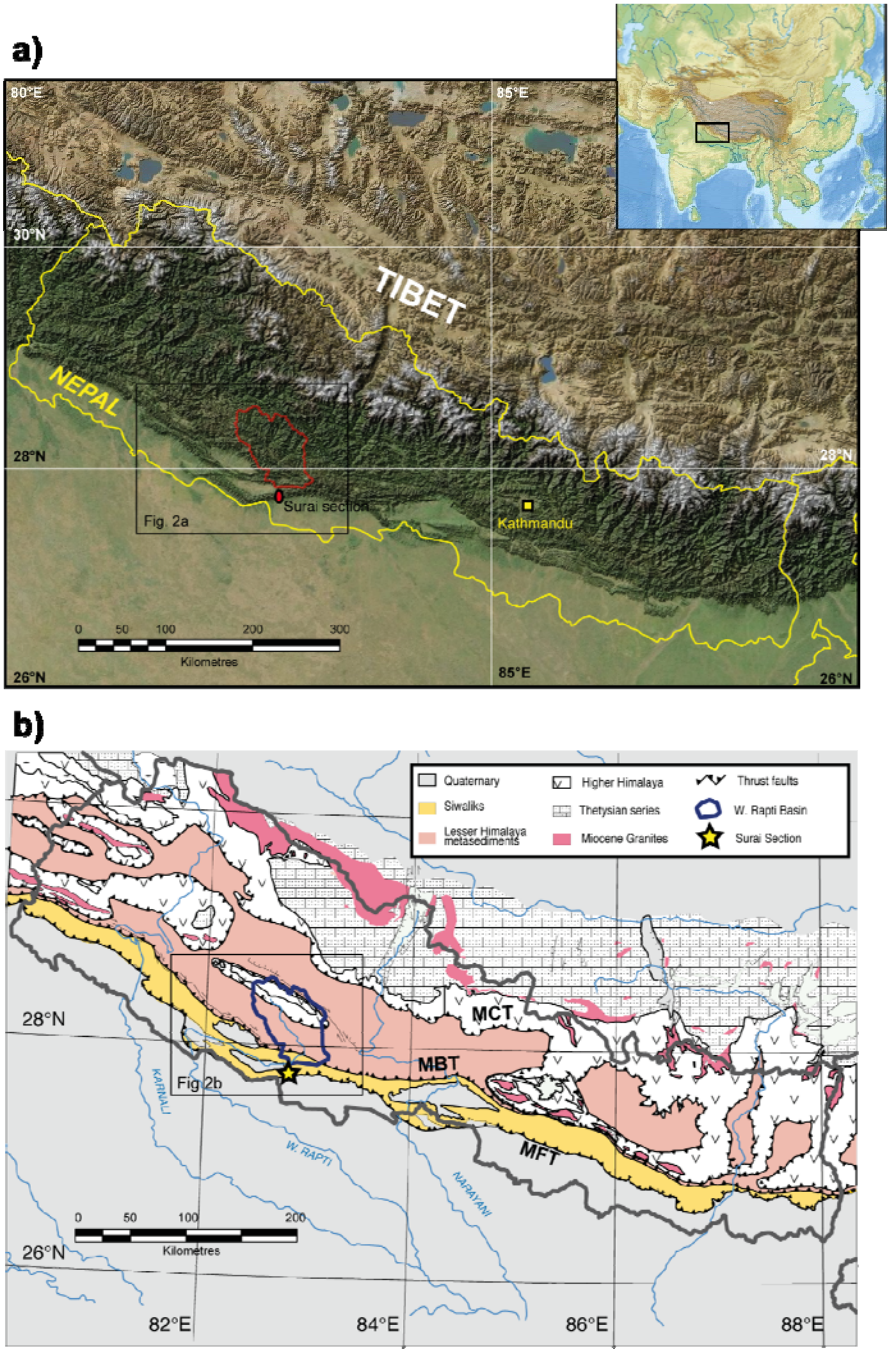

FIG. 1 - General setting.

a) Blended satelite image and shaded digital elevation model of Nepal (yellow frontier), with localisation of the Surai section and the Rapti river basin (red line).

b) Simplified geologic map of Nepal (thick grey bounday). MFT = Main Frontal Thrust, MBT = Main Boundary Thrust; MCT = Main Central Thrust

2 Setting

2.1 Structural background

The Himalayan arc in Nepal can be traditionally divided in four main units (FIG. 1b) including from North to South the Thethysian sediments, the Higher Himalaya, the Lesser Himalaya and the Siwaliks. These units are bounded by thrust faults that propagated southward since the Early Miocene. To the South of the Tibetan plateau, the Thethysian series are composed of Mesozoic and Paleozoic marine sediments and low-grade metamorphic rocks. They are separated from the Higher Himalaya (HH) series by the Southern Tibetan Detachment (STD). The HH is constituted by high-grade crystalline metamorphic units. Both series are intruded by Miocene leucogranites, and form the highest relief of the Nepalese Himalaya.

To the South, on the Main Central Thrust (MCT) the HH overthrusts the Lesser Himalaya series which are composed of low-grade Precambrian detrital continental meta-sediments and Cretaceous to Eocene marine sediments. Topographically, the LH form most of the Midland, which represent an intermediate relief between the higher relief of the HH to the north and the Siwaliks Hills to the south. In the western Midland, LH series are still thrusted by two major klippes of HH. The south of the Midland is bonded by the Mahabharat, which form the first important relief of the range. Southward, the LH overthrusts the Neogene foreland molasses by the Main Boundary Thrust (MBT). These foreland molasses result from several million years of Himalayas erosion. They represent the Sub-Himalayan group, also named the Siwaliks series.

2.2 The Siwaliks Hills

North of the Ganga basin the Siwaliks Hills represent the first significant relief at the front of the Himalayas (FIG 1a and 2a). This range is bounded, to the South, by the Main Frontal Thrust (MFT) (FIG 1b and 2b), which, according to deformed fluvial terraces, is currently accommodating almost all of the Himalayan convergence, with a slip rate of about 20 $mm.yr^{-1}$ (Lave and Avouac, 2000). The Siwaliks range is organized in successive fold and thrust belts oriented WNW-ESE along the Himalayas. According to deformed fluvial terraces, the Siwaliks frontal fold are currently uplifted very rapidly (~10 $mm.yr^{-1}$) (Lave and Avouac, 2001).

While the maximum altitudes do not exceed 1000 meters above sea level, the relief in the range can be quite abrupt. Large Himalayan rivers, as well as small tributaries, incise deeply in the rapidly uplifting folds, exposing continuous sections.

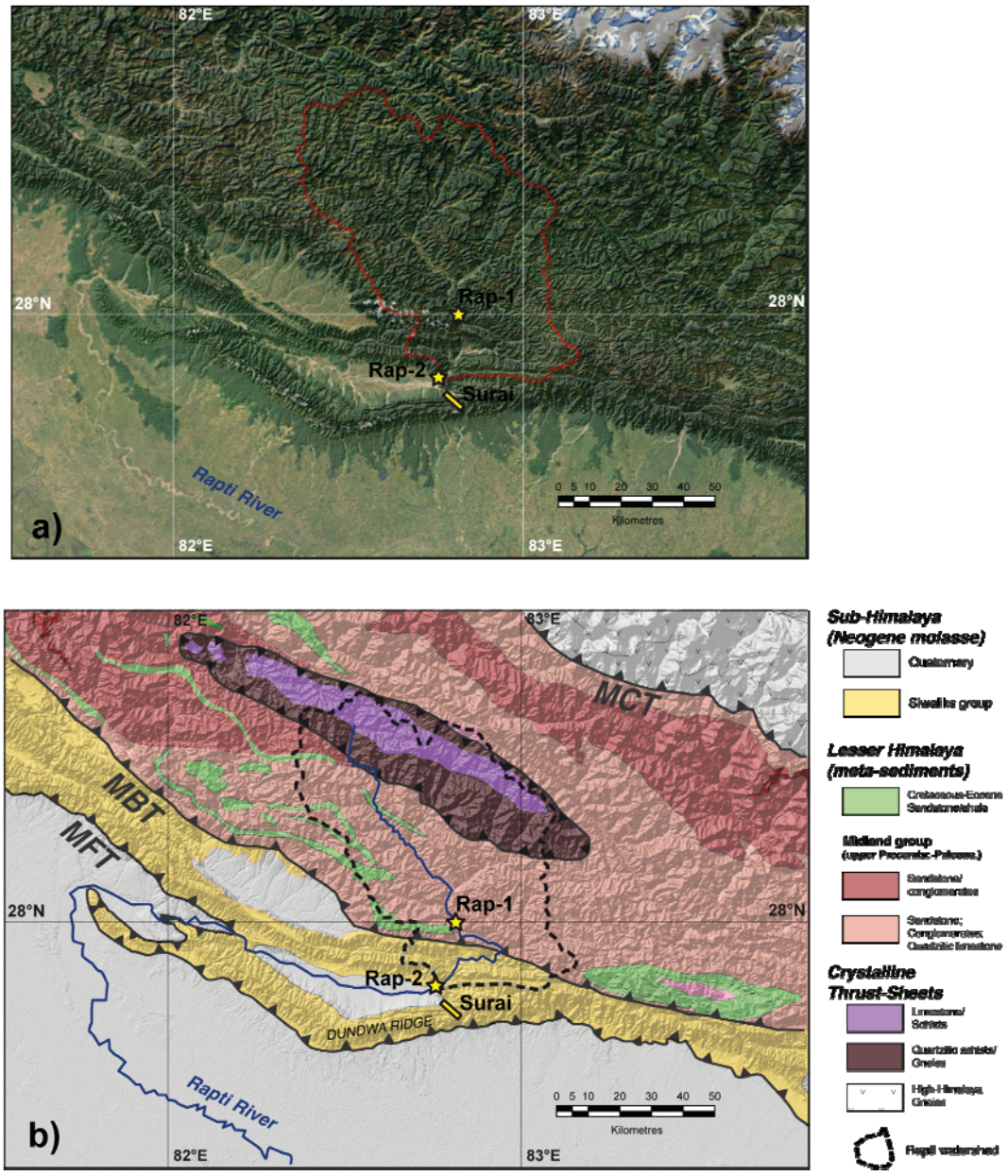

FIG. 2 - Setting of the study area.

a) *Blended satellite image and shaded digital elevation model of the midland and Siwaliks hills in western-central Nepal, with localisation of the two modern river samples (yellow stars), the Surai section (yellow bar), and modern Rapti river drainage catchment (red line).*

b) Simplified geologic map and description of the main lithologies outcropping in the present and potential past Rapti river catchment.

As aforementioned, the Siwaliks are constituted by a thick (> 6 km) pile of Neogene molasses, produced by the intense erosion of the Himalayas for several million years. While facies may vary considerably along the >2000 km-long Siwaliks range, molasses are usually divided in three main sedimentary formations (DeCelles *et al.*, 1998): The Lower Siwaliks (fine-grained sandstone, mudstone and clays), Middle Siwaliks (medium to coarse sandstone alternating with occasional clay and mudstone layers) and Upper Siwaliks (conglomeratic alluvial fans and gravely braided rivers deposits). However, these sedimentary distinctions remain rough, as only based on the overall lithology and should not be considered as chronostratigraphic unit but rather traduce lithostratigraphical variations related to the propagation front of the Himalayan thrust wedge (e.g. Tokuoka *et al.*, 1986; DeCelles *et al.*, 1998; Corvinus and Rimal, 2001).

2.3 The Surai section

The Surai section is located in the southern part of the western-central Nepal, ~5 km to the south-east of the Bhalubang town. In this region, Siwaliks sediments are folded into a ~750 m high, >100 km ridge developed on the hanging wall of the Main Frontal Thrust (MFT): the so-called Dundwa ridge, which is progressively propagating to the west (Champel *et al.*, 2002). On the north of the relief, a piggy-back basin has developed, in which the "West" Rapti River (not to be confused with the "East" Rapti river, which is a tributary of the Narayani river) is deviated to the West (FIG. 1 and 2). The Surai Khola (*khola* means river in Nepalese), which drains the most southern segment of the Siwaliks (Dundwa ridge, FIG. 2) into the Ganga plain, has deeply incised this uplifting relief. Thanks to the construction of the RH01 road (between Butwal and Lamahi) between 1983 and 1986 in this valley, continuous and fresh outcrops of the Siwaliks sediments are now available. Because the outcrops are continuous, and since the depositional ages of the sediments were constrained by magnetostratigraphy (Appel *et al.*, 1991; Rosler and Appel, 1998; Gautam and Rosler, 1999; Ojha *et al.*, 2009), this section has probably been the most extensively studied in the Nepalese Siwaliks. For example biostratigraphical (Corvinus and Rimal, 2001), geochemical (Huyghe *et al.*, 2001; Huyghe *et al.*, 2005; Szulc *et al.*, 2006b), mineralogical (Sanyal *et al.*, 2005; Szulc *et al.*, 2006b) or thermochronological surveys (DeCelles *et al.*, 1998; Bernet *et al.*, 2006; Szulc *et al.*, 2006b; van der Beek *et al.*, 2006) have been carried out during the last decades. Most importantly, the fresh exposure of these old sediments should avoid "contamination" of the paleo-cosmogenic signal by recently produced cosmogenic isotopes (see Chapter 2 and Chapter 4 Supp. Info).

3 Sampling strategy and methods

3.1 Magnetostratigraphy

In Nepal, in the absence of volcanic tuffs in the sub-Himalayan groups, unlike for instance in India or Pakistan, dating of Siwalik sediments have been mainly based on magnetostratigraphy since the 1980's (e.g. Tokuoka *et al.*, 1986). The Surai section, in particular, has been targeted by several surveys since the 1990's. The first published study was from Appel *et al.* (1991) which was later revised bv Gautam and Rosler (1999), using the new reference polarity-time scale of Cande and Kent (1995). Then, the section were completed by co-workers Rosler and Appel (1998) and Corvinus and Rimal (2001), who refined the correlation adding biostratigraphical markers. Recently, arguing that previous studies had focused their sampling on sandstone and cemented paleo-soils believed to produce inconsistent paleomagnetic results, Ojha *et al.* (2009) resampled the whole section but finally proposed an overall similar dating, at least for the middle and lower Siwaliks groups (ranging respectively in age from ~4 Ma up to 10 Ma and 10 up to 14 Ma). Despite these several studies, the dating of the upper part of the section remained poorly constrained, the age of this upper group being bracketed between 4 and 1.5 Ma. Indeed, this part almost exclusively contains very coarse conglomerates, and classic drilled sampling of adequate sediments is quite difficult. In order to better constrain the dating of the upper sequence, we sampled soft silty beds inserting by hand quartz cylinders. A total of 38 new hand oriented samples were collected from the finer horizons in the upper part of the Surai section, where drilling was not amenable. Bedding attitude was measured at each sampling layer and sampling location was determined using GPS, and stratigraphically replaced according to the previous stratigraphic studies carried out along this section.

To isolate the characteristic and primary magnetic remanence directions, the 38 samples were demagnetized using alternating field and 10 to 12 steps, in the paleomagnetism laboratory of the Ludwig-Maximilians University of Munich. The remanences at each steps were measured using a three-axis DC Squid in the same laboratory. For 18 samples this treatment was successful to isolate a relatively stable direction with declination and inclination coherent to the previously published data. For 11 samples the remanence trajectories are spread out about a great circle while never reaching a stable endpoint. In these cases the polarity was estimated using the great circle approach. At last, 9 samples show unstable or intermediate directions useless to establish the polarity column

FIG 3 - Pictures from the Surai section.

Up: In the middle Siwaliks group (between samples SU-COS 6 and 7). Bottom, in the upper Siwaliks group, north to Dobbata village, between samples SU-COS 21 and 22.

3.2 Cosmogenic samples for paleo-denudation rates

17 samples were collected for paleo-denudation rates analyses along the road-cut. Sampling locations were selected in order to minimize possible recent exposure. According to our new magnetostratigraphic correlation (see below), the sampled section covers a time range between 6.5 and ~0.4 Ma. We thus aimed for an age span of ~300 kyr. Samples were typically medium to coarse grained sands. Since we expected high denudation rates (> 1 $mm.yr^{-1}$) in the paleo-draining area, we also expected low ^{10}Be concentrations (< 10^4 $at.g^{-1}$), especially in the oldest samples. Therefore, we sampled unusually large masses of sands (sometimes > 5 kg) in order to ensure sufficient extraction of pure quartz and then measurable amounts of ^{10}Be.

At last, we also sampled sands from two river bank deposits in the present-day West Rapti river: First, upstream from the Siwaliks group ~5 km north to the MBT (sample RAP-1), and second, in the piggy back basin at the north of the Surai section (Bahlubang bridge, sample RAP-2) where the river is deviated to the west (FIG. 2). The purpose of this sampling was, first, to compare the present day denudation of this drainage area to the paleo-denudation record, and, second, to test the potential influence of the Siwaliks sediments reworking into the river on the cosmogenic signal (RAP-2 being located in the middle of the Siwaliks group).

3.3 $^{26}Al/^{10}Be$ dating samples

In the upper part of the section, we also sampled at several points quartzite pebbles to analyze their $^{26}Al/^{10}Be$ content. These two cosmogenic isotopes are produced at the Earth surface by cosmogenic particles at a given ratio (6.75, Nishiizumi *et al.*, 2007; Balco and Rovey, 2008). As ^{26}Al and ^{10}Be have different radioactive decay (0.71 and 1.39 Ma, respectively), this ratio will change as soon as the sediments are buried at a sufficient depth (> 10 m) to be shielded from the cosmogenic production flux. The measured ratio in a given sediment may therefore record the theoretical time of sediment deposition (Granger and Muzikar, 2001) (see also Chapter 2). We analyzed the $^{26}Al/^{10}Be$ ratio in 3 sand samples, in 2 quartzite pebbles and in 2 modern river sands (cf Table x). This experiment had two goals : first, in the upper part of the section, additional dating may provide useful constraints to better correlate the magnetostratigraphic section to the reference scale. Second, $^{26}Al/^{10}Be$ ages incoherent with their supposed magnetostratigraphic ages can provide valuable insights on the sedimentary dynamics before or after the actual depositing time (see Chapter 2). A $^{26}Al/^{10}Be$ age significantly older might indicate sediment recycling within the foreland basin, whereas a much younger age might indicate a recent re-exposure to the cosmic flux.

The analytical, computation, and correction methods we used are the same as described in Chapters 2 and 4 (supplementary information), we invite the reader to refer to these sections.

4 Results

4.1 Magnetostratigraphy

From the new measured directions, together with already published data, we established an updated magnetostratigraphic column of the Surai section (Fig. 4b). However, despite our new sampling in the upper section, we must notice that the magnetostratigraphic column in this part, hence its correlation to the reference scale, remain loose. To better address the possible related ambiguities we correlated the Surai column using a numerical method based on the Dynamic Time Warping algorithm (Lallier *et al.*, 2013). This new method automatically provides a large number of likely correlations which can be scrutinized for further interpretation. Figure 4b show a density plot made from the compilation of 10,000 possible correlations calculated using this numerical approach. In the lower part of the section, the results show a good consistency with previous proposed correlations in the literature. In the upper part, albeit some loose sampling, the correlation remains relatively well constrained with few different solutions. Our results yield accumulation rates ranging from 0.07 up to 1 mm.yr^{-1}.

FIG. 4 - (next page)

a) *Lithologic log of the Surai section, with the position of analyzed paleo-denudation samples, and position of small rivers tributaries (Khola means river in Nepalese). After Corvinus & Rimal PALAEO 2001)*

b) (Figure by Julien Charreau) Compilation of paleomagnetic data from Appel et al (1991) (blue dots) and our new analyses (red dots). Correlation to the reference time scale has been computed by Julien Charreau with the Cupidon software (Lallier et al. 2013). The color white represent the most likely correlation, and blue the least likely.

(caption on previous page)

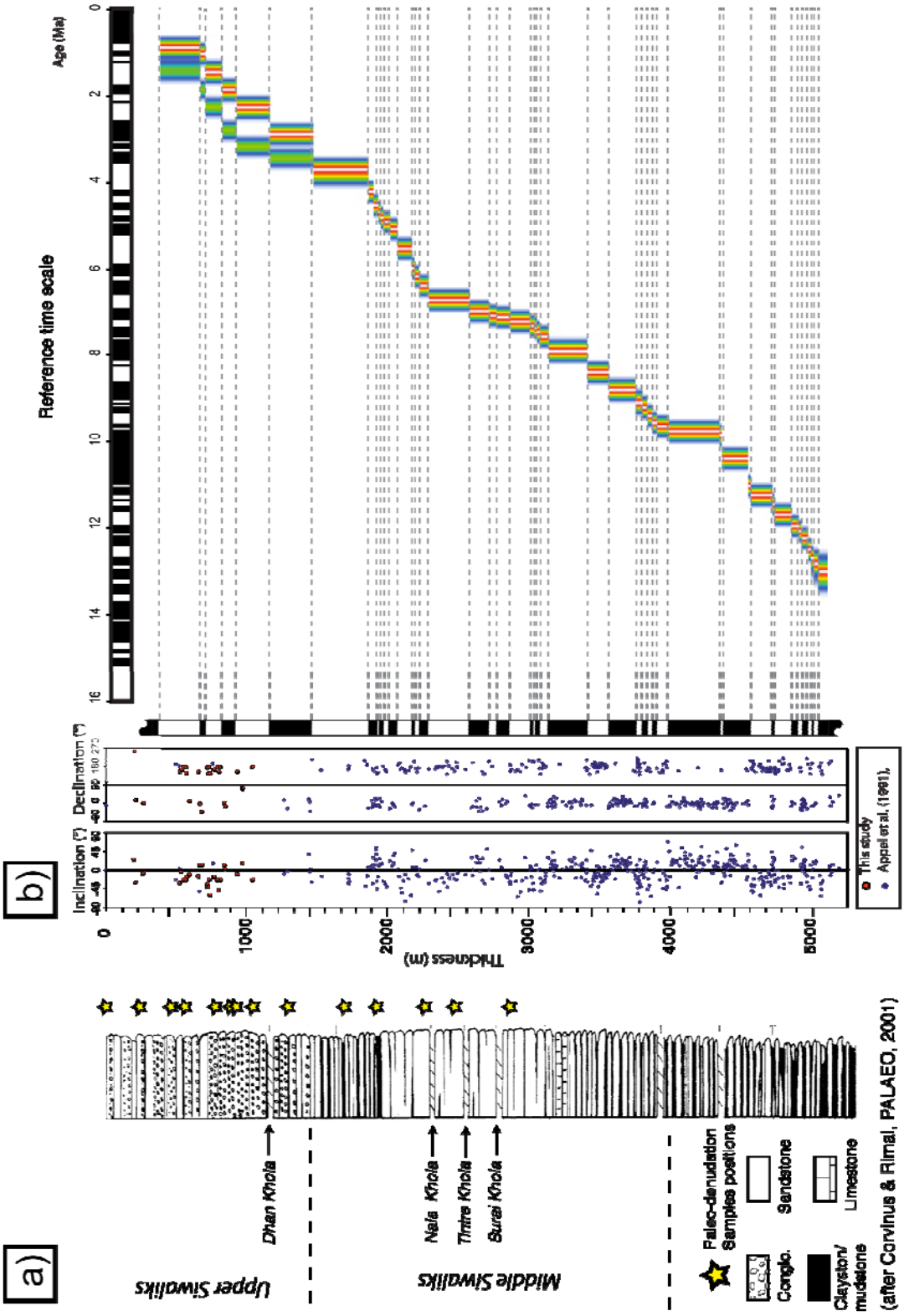

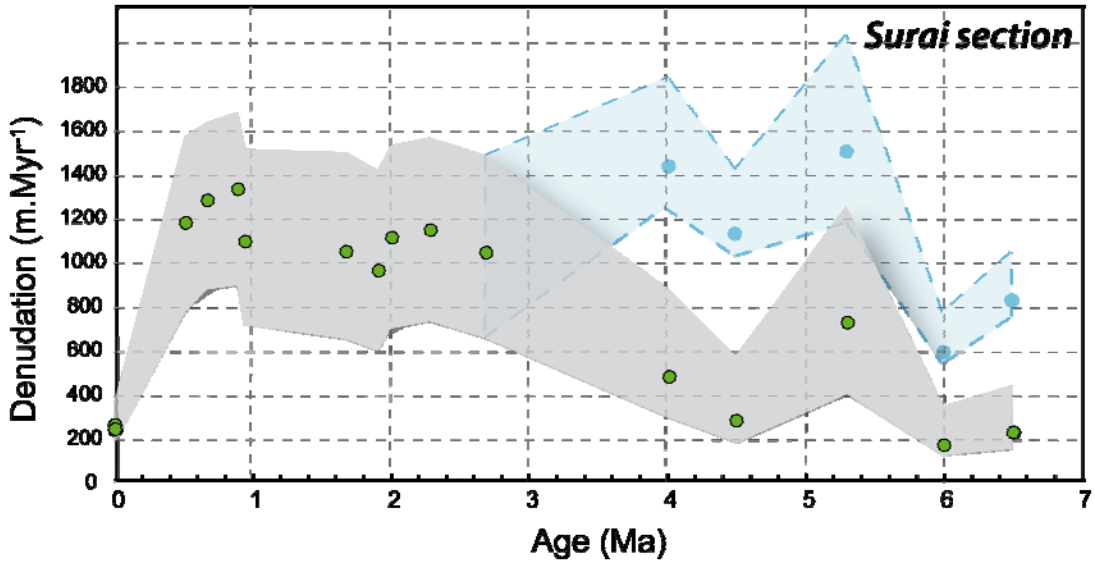

FIG. 5 - Paleo-denudation rates derived from ^{10}Be.

Green dots: using the present day Rapti river catchment for computation; blue dots: using the Karnali river catchment, for samples >4Ma. Grey and blue envelops are the 1σ envelops.

4.2 Paleo-denudation rates

Results are presented in table 5.1 and derived paleo-denudation rates are presented on FIG. 5.

Two gaps in the sampling interval must be noted between 1 and 1.6 Ma, and then between 2.8-4 Ma. Both gaps are due to the absence of suitable outcrops along the road and unexpected sediment accumulation rates variations that degraded the temporal regularity of our sampling. While we initially performed a spatially regular sampling, our new dating of the upper section revealed deposition rates sometimes quite different from what we expected based on previous dating and stratigraphic logs.

In term of absolute denudation values, the record displays three main periods. First, a relatively low-denudation period between 6.5 and 4 Ma, with paleo-denudation rates around ~0.4 mm.yr^{-1}. Second, between 3 and 0.5 Ma, a period of stable and high denudation from 1 up to 1.2 mm.yr^{-1}. Third, the two present-day rivers samples are characterized by a quite low denudation rate of ~0.25 mm.yr^{-1}. Importantly, all of these denudation rates have been calculated taking into account the present production rates derived from the present day river basin, which may be disputable, as discussed later in §5.1.

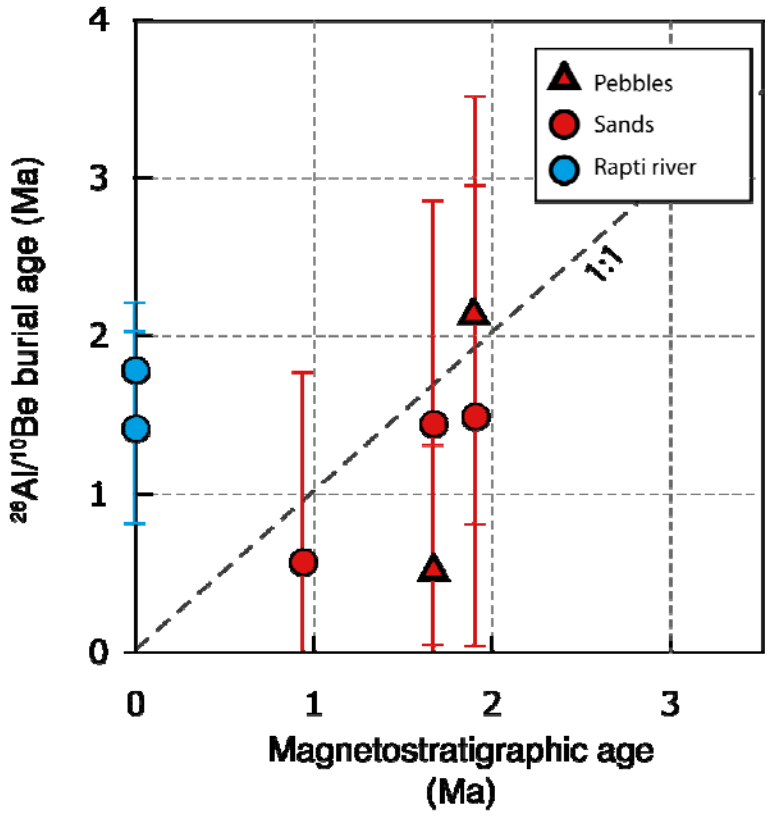

FIG. 6 - Theoretical $^{26}Al/^{10}Be$ burial ages as a function of paleomagnetic ages

It must also be noted that relative uncertainties are higher than those of the Tian-Shan records. This is mainly due to very low ^{10}Be concentrations in the samples ($< 5.10^3$ at.g^{-1}), and therefore lower counting statistics during Accelerator Mass Spectrometry analysis.

4.3 $^{26}Al/^{10}Be$ dating

Results are reported in table 5.1, and theoretical burial ages are plotted in FIG. 6. ^{26}Al analyses were successful on only 5 samples out of 10 analyzed. Four out of the five unsuccessful samples in which the ^{26}Al was not measurable were actually the oldest of the record. This is reassuring, because if we presume high denudation rates in the drainage basin as expected for the Himalayas, the ^{26}Al concentrations in these old sands was probably low before burial, even lower after million years of shielding and radioactive decay, and therefore barely measurable. High measured concentrations in those samples would have been suspect, as probably due to a re-exposure episode (see §5.2).

Because of both high analytical uncertainties on ^{10}Be and ^{26}Al measurements, derived theoretical burial ages are burdened by large error bars that can reach 100%. Nevertheless, they are all in agreement with the proposed magnetostratigraphic ages, except for a one-pebble sample (SU-COS 20). However, burial ages determined from unique or agglomerated pebbles are usually to be taken with caution because of the risk of agglomerating one outlier affecting the whole isotopic ratio (Balco and Rovey, 2008). Given these large uncertainties, and possible complexities in the sediment history (see §5.2), these burial ages cannot, by themselves, constrain potential magnetostratigraphy ambiguities.

The Rapti River samples both display similar burial ages (~1.5 Ma). These ages are very surprisingly old, especially in the case of RAP-1 samples, wich was collected upstream from the Siwaliks group (§5.2).

Table 5.1 - Analytical results and paleo-denudation rates calculation for the Surai section

Sample	Age (Ma)	Accum. rate (mm.yr-1)	10Be (10^3 at.g-1)	1σ	26Al (10^3 at.g-1)	1σ	26Al/10Be theoretical age (Ma)	1σ	Paleo Denudation rate (mm.yr-1)					
									Using Rapti basin			Using Karnali basin		
										+1σ	-1σ		+1σ	-1σ
Magnetostratigraphic section SU-COS...														
[Sand/sandstone]														
1	6.50	2.95	1.14	0.36	-	-	-	-	0.2	0.2	0.1	0.8	0.4	0.03
2	6.00	0.92	2.29	0.64	-	-	-	-	0.2	0.2	0.1	0.6	0.4	0.2
4	5.30	0.2	1.00	0.49	-	-	-	-	0.7	0.5	0.3	1.5	0.2	0.3
8	4.50	0.32	3.27	0.43	-	-	-	-	0.3	0.3	0.1	1.1	0.4	0.3
10	4.02	0.62	2.32	0.59	-	-	-	-	0.5	0.4	0.2	1.4	0.3	0.3
13	2.69	1.05	1.60	0.64	-	-	-	-	1.0	0.4	0.4			
16	2.28	0.26	3.01	0.45	-	-	-	-	1.2	0.4	0.4			
14	2.01	0.26	3.44	0.75	-	-	-	-	1.1	0.4	0.4			
19	1.91	0.26	4.80	0.64	15.9	10.9	1.5	1.5	1.0	0.5	0.4			
21	1.67	0.18	4.83	0.87	16.3	10.6	1.4	1.4	1.1	0.4	0.4			
26	0.94	0.63	4.62	1.01	23.8	12.6	0.6	1.2	1.1	0.4	0.4			
27	0.89	0.63	3.06	0.56	-	-	-	-	1.3	0.3	0.4			
29	0.67	0.63	4.26	0.56	-	-	-	-	1.3	0.4	0.4			
32	0.51	0.63	5.22	0.98	-	-	-	-	1.2	0.4	0.4			
[Quartzite Pebbles]														
18	1.91	0.26	9.0	0.8	21.6	13.9	2.2	1.4	-	-	-			
20	1.67	0.18	3.9	0.7	20.6	6.6	0.5	0.8	-	-	-			
25	0.94	0.63	3.4	0.8	-	-	-	-						
River Bed														
RAP-COS 1	-	-	20.2	1.5	69.1	19.4	1.4	0.6	0.3	0.1	0.1			
RAP-COS 2	-	-	21.9	1.6	63.0	11.7	1.8	0.4	0.2	0.1	0.1			

SCALING FACTORS	Neutrons	Muons
Basin average	1.97	1.32
Deposit location*	0.745*	0.728*

*Altitude of the Ganga plain level

5 Discussion

5.1 Comparison with previously published denudation data.

Before discussing further interpretations of our record, and to make sure it is not based on a totally erroneous data set, let us take a brief look to previously proposed denudation or erosion rates, past or present, in this area.

Van der Beek *et al.* (2006) and Bernet *et al.* (2006) published in two companion papers low-temperature tehrmochronology data of fission tracks in detrital zircon (ZFT) and apatite (AFT) from the Surai section. They report, for the whole section, consistent exhumation rates of 1.5 ± 0.4 mm.yr^{-1} (ZFT, averaged on ~5 Myr) and 3.5 ± 2.1 mm.yr^{-1} (AFT, averaged on ~1 Myr). Since their computation was always based on the youngest peak of the mineral population, the derived exhumation rates must be considered as a "maximum" and not a *stricto sensu* "basin-averaged" rate. However, these values are very coherent with our own paleo-denudation rates ranging from 1 up to 1.2 mm.yr^{-1} between 3 and 0.7 Ma. Szulc *et al.*, (2006), based on ^{39}Ar-^{40}Ar dating in micas also reports similar exhumation rate of ~ 1.5 mm.yr^{-1} but associated to longer time scales (~10 Myr). We must keep in mind, however, that all of these low-temperature thermochronoly data represent exhumation rates averaged on much longer time scales than our cosmogenic data (~0.3-1 kyr), and that they are blind to some episodic or recent denudation changes. Modern and recent denudation rates in the lesser Himalayas remain relatively coherent withreported erosion rates based from sediment discharge/runoff models (therefore not taking into account the chemical denudation) between $0.2^{+0.4}/_{-0.1}$ and $1.9\ ^{5.9}/_{-0.6}$ mm.yr^{-1} (Andermann *et al.*, 2012). Thus, at least, our data seem coherent with previously reported denudation rates in the same area.

5.2 Siwaliks recycling

One limitation of cosmogenic nuclides to determine past denudation rates is the potential impact of sediment reworking. Before erosion, the bedrock within the drainage basin must be initially free of cosmogenic nuclides. This is true if the geology of the basin is constituted by old metamorphic and/or igenous rocks as for example those of the LH and HH. It is however disputable if part of the basin includes relatively young (<6 Ma) sediments that may have undergone a previous cycle of erosion and exposure. If so, denudation rates will be under-estimated, because of artificially higher cosmogenic ^{10}Be concentrations. This concern is particularly true in the case of the Siwaliks deposits.

Indeed, since denudation rates of the small-order drainage basins within the Siwaliks are relatively high (Lave and Avouac, 2001), their associated sediment flux delivered to the main trans-himalayan rivers is probably important and may contaminate the overall signal shed from the Higher Himalayas, especially for the reworking of the youngest upper-Siwaliks sediment that potentially still contained significant amounts of ^{10}Be and ^{26}Al.

The Surai section is located on the north flank of the Dundwa ridge (FIG. 2). Paleo-current direction measurements nevertheless indicate a consistent southward drainage all along the Surai section (DeCelles *et al.*, 1998; Szulc *et al.*, 2006b). Therefore, all of the sediments of the Surai section should derive primarily from rivers draining from the North, and not from local reworking driven by the Dundwa ridge uplift. This probably began concomitantly to the MFT activation ~2 Ma (van der Beek *et al.*, 2006).
However, the Surai section is located ~30 km south of the MBT (FIG. 2b). Trans-Himalayan rivers sediment could have been "contaminated" by some inputs of the Siwaliks sediments uplifted between the sampling location and the MBT. Van der Beek *et al.* (2006) found surprisingly old detritic Apatite Fission Tracks (AFT) ages in one single sample of the upper Surai section with an average AFT mean ages ~7 Myr older than the stratigraphical age (1 Myr), whereas in the rest of the section this lag-time remained around ~1 Myr. These authors explain this large lag time by Siwalik sediment reworking. However, this potential important recycling has not been observed by other thermochronometers such as Zircon Fission Tracks (SFT) (Bernet *et al.*, 2006) or ^{39}Ar-^{40}Ar in micas (Szulc *et al.*, 2006a).
Our ^{26}Al/^{10}Be burial dating neither support any major Siwaliks reworking since 2 Ma (FIG. 6). Even with large uncertainties, the cosmogenic burial ages are never significantly older than their magnetostratigraphic ages (FIG. 6). This suggests that either the sediment input from Himalayan areas has always largely dominated the Sub-Himalayan (Siwaliks) input and/or that most of the Siwaliks recycled sediments were old enough to have lost all of their original cosmogenic radionuclides, by simple decay since their deposition.

To better address the potential impact of Siwaliks reworking, the 2 modern sand samples can bring useful information. Indeed, RAP-1 is located in the modern Rapti river bed upstream from the Siwaliks group, while RAP-2 is north of the Dundwa ridge, in the piggy-back basin. On one hand, they both display equal ^{10}Be and ^{26}Al concentrations within uncertainties (table 5.1), confirming limited influence of the Siwaliks input on the cosmogenic signal of the river at this point. On the other hand, their ^{26}Al/^{10}Be ratios are ~3, much lower than the theoretical steady-state exposure production rates ratio (6.75, Nishiizumi *et al.*, 2007; Balco and Rovey,

2008) These ratios should theoretically corresponds to burial duration of ~1.4-1.8 Myr. While these value could be explained by recycling of old sediments in the case of RAP-2, it is very puzzling in the case of RAP-1, because there is no long-term sediment storage in the Rapti basin upstream to this point and the sand transfer time should be extremely short given the basin relief and water discharges.

To conclude, and to our current state of knowledge, paleo-current directions, most of low temperature thermochronology data and $^{26}Al/^{10}Be$ ratios suggest that the recycling of the Siwaliks has been limited in the upper Surai section (and *a fortiori* before the activation of the MFT <1 Ma).

5.3 Paleo-denudation rates and morpho-tectonic evolutions of the central Nepal.

As mentioned above, we distinguish three distinct periods of paleo-denudation rates (present day: e ~ 0.2 mm.yr^{-1}; 0.5-2.8 Ma: e = 1 up to 1.3 mm.yr^{-1}; 4-6.5 Ma e = 0.2 up to 0.6 mm.yr^{-1}). Several scenarii may explain these changes and below we will present and discuss the different hypotheses that can be proposed.

5.3.1 Has the catchment topography remained the same for the last 6.5 Myr?

As mentioned in Chapter 2, §2.3 and Chapter 4 (supp. info.), the calculation of the denudation rates from cosmogenic concentrations in river sediments requests the knowledge of the average cosmogenic production rates, which relies primarily on the drainage basin topography. In the absence of available paleo-elevation data, we here assumed that the topography of the drainage basin had remained unchanged and is similar to present. This hypothesis may be considered quite crude, especially in such active and dynamic morpho-tectonic settings. Indeed, temporal variations of the in situ cosmogenic concentrations may result from unrecognized changes in the paleotopography of the drainage basin rather than variations of the denudation rates.

At the very front of the Himalaya, in the Ganga plain, the sediments are deposited through series of very large alluvial fans. These deposits represent sediments coming from the whole Himalayas and alternate with smaller interfans that originate only from the midlands. Nowadays, the Rapti river, which represents the main source of sediments in the studied area, drains only up to the Lesser Himalayas. But, because of the Himalayan tectonic wedge

progradation, the depositional environment in the Surai area may have evolved during the past from large alluvial fan to interfan deposits (Fig. 7). The present relief and topography in Rapti river drainage basin has a maximum elevation of ~3000 m a.s.l., which remains low in comparison with the highest Himalayan zones. Hence, the basin-averaged cosmogenic production rate of the present Rapti river is much lower (~7.7 $at.g^{-1}.yr^{-1}$ for the spallogenic production) than basin draining the whole Himalayan sequence (e.g. ~32.8 $at.g^{-1}.yr^{-1}$ for the Karnali River basin). Such scenario of a tectonic wedge propagation with a change from large fans to small inter-fans would therefore have a strong impact on the derived denudation rates. In particular, it may explain the lower calculated denudation rates between 4 and 6.5 Ma and their increase above 1 $mm.yr^{-1}$ around 4 Ma.

Let us assume higher average cosmogenic production rate linked to a higher average topography of the drainage basin for the 4 to 6.5 Ma period (i.e. related to large fan). This would increase the derived apparent denudation rate. With an average production rate of ~33 $at.g^{-1}.yr^{-1}$, this would imply denudation rates around ~1.7 $mm.yr^{-1}$ (blue curve in FIG. 5). While remaining a crude estimate, this value is coherent with detrital low-temperature thermochrology such as AFT and ZFT (Bernet *et al.*, 2006; van der Beek *et al.*, 2006). Furthermore, based on zircon ages, (DeCelles *et al.*, 1998) suggested a wide uplift and unroofing of the northern Lesser-Himalaya zone after ~5 Ma. Thus, the apparent increase in denudation rates observed between 3 and 4 Ma could actually be an artifact due to the isolation of the catchment from the higher-Himalaya areas and its limitation to the midland (FIG. 5), as proposed in the tectonic wedge scenario. In this case, our record would actually display a slight decrease in denudation rate after 4 Ma (blue curve in FIG. 5), which would be also coherent with a fluvial system draining, in average, lower relief (§5.4). If this scenario is true, it would imply that denudation rates in west-central Nepal have remained quite stable between 6.5 and 0.5 Ma with an average value of ~1.4 $mm.yr^{-1}$,despite possible major morpho-tectonic evolutions and global climate changes throughout this period.

Unfortunately, we lack paleo-elevation data, and only potential modifications in rocks sources may be deciphered from the sediment record through mineralogical, isotopical data and geochemical data. If such data may enable to distinguish between the Lesser and Higher Himalayan sequences, in the studied area the geology is complicated by the presence an overthrusting crystalline klippe of HH over the midland (FIG. 2b). This may compromise reliable reconstruction of the paleo drainage basin in the sedimentary records. Reassuringly, based on sedimentological paleo-environment studies, DeCelles *et al.* (1998) suggested that the rivers that deposited the upper and middle Surai sections were similar to the present day major

trans-Himalayan rivers (DeCelles *et al.*, 1998), and has followed the same monsoon hydrologic regime for the last ~7 Ma (Quade *et al.*, 1995).

We can apply a similar reasoning for the 0-2.8 Ma period, which is characterized by denudation rates higher than 1 $mm.yr^{-1}$. In the Surai section, mineralogical and geochemical tracers do not shown any systematic source change since 5 Ma (Huyghe *et al.*, 2001; Szulc *et al.*, 2006) and suggest that the exhumation of Lesser-Himalaya has rather begun ~11 Ma ago. Hence, for this period, and since we can rule out a pure Siwaliks reworking (§5.2), the paleo-Rapti has continuously eroded a proportion of rocks from the higher-Himalaya group. Therefore, the paleo-drainage basin has always, at least, reached the higher-Himalaya klippe thrusting over the mid-land (Fig. 2b). Thus, the relatively low initial ^{10}Be concentrations, and so-derived high denudation rates, observed between 0.5 and 2.8 Ma, cannot be due to a change of the catchment to lower elevation. Conversely, it is very unlikely that these sediments were derived from catchment reaching altitudes much higher than nowadays. This would not be coherent with the general propagation of the Himalayas tectonic wedge and, moreover, if we supposed a drainage basin comparable to the one of the present-day Karnali river, so-calculated denudation rates would reach ~5 $mm.yr^{-1}$, a value unreasonably higher than any denudation rate reported in this area (e.g. Lupker 2012).

5.3.2 Insights on the tectonic evolution of central Nepal

In the scenario assuming a constant basin topography for the last 6.5 Myr, our denudation record can also be interpreted has a marker of the tectonic evolution of the Himalayan thrusting wedge. The increase in denudation rates at 3-4 Ma may, in this case, indicates enhanced uplift of the lesser Himalayan, due for example to an acceleration of the MBT.

The denudation rates recorded in the present day Rapti river are particularly low in comparison with the rest of the record. These values are nonetheless similar to other found in midland-draining basins of central Nepal (Andermann, 2011; Andermann *et al.*, 2012), but smaller than averaged rates on longer time scale from detrital ZFT and AFT (Bernet *et al.*, 2006; van der Beek *et al.*, 2006). Such a drop in denudation could be explained by the activation of the MFT to the south of the Dundwa ridge, and a transfer of most of the Himalayan convergence, and active uplift in this area, downstream to the present position of the Surai section. We therefore suggest that the onset of the uplift of the Dundwa ridge and slip transfer to the present-day MFT occurred between 0.5 Ma (age of our younger Surai sample) and today.

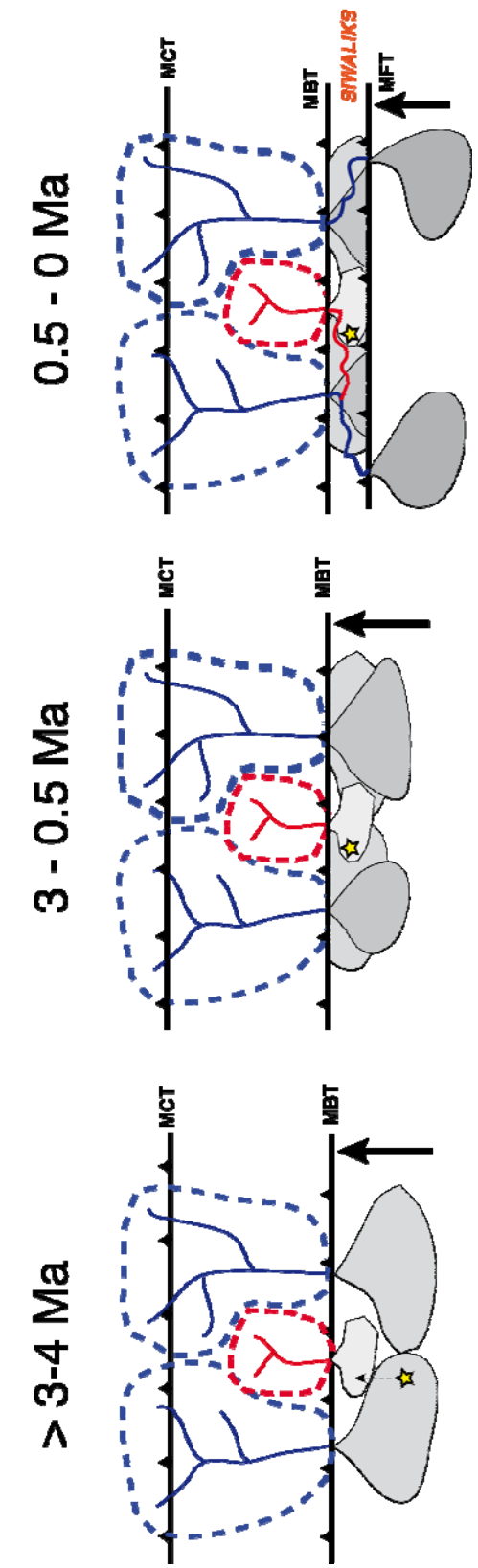

FIG. 7 - Scenario of a propagating depocenter due to the Himalayan thrust wedge progression.

Before 3-4 Ma, the current location of the Surai section is located in the depositing zone of a major transhimalayan river, such as the present day Karnali River. After 3-0.5 Ma, this position has converged toward a position more proximal to the front, in the inter flune zone, where accumulate only sediments from lower-order catchment (such as the present day Rapti river)

Between 0.5 Ma and present day, the Dundwa ridge is uplifted along the MFT. The Rapti river is deviated to the west, and transfer of most of the active convergence downstream this point lead to a neat decrease in average denudation rates upstream from the MBT.

5.4 Influence of the global climate?

The apparent increase in denudation 3-4 Ma is synchronous to the major intensification of northern hemisphere glaciations, and global climate cooling. However, it remains limited to a factor of ~2, and is real only if we consider that the elevation of the basin has never changed. In that case, the drainage basin drained only the midlands and has never been glaciated. Thus, the potential onset of glaciers on the Himalayan summits, by themselves, cannot explain the apparent 3-4 Ma increase. In the other scenario discussed above, this apparent increase may be a simple artifact. The denudation rates before 4 Ma could have been higher (between 1-1.7 $mm.yr^{1}$) if the basin included the higher reliefs of the HH. Therefore, if this scenario is true, the onset of large glaciers in the drainage area would have had a negligible effect, or even would have decreased the average denudation rates. However, the evolution of the global climate that occurred about 3 Ma was not limited to the onset of glaciers (Zhang *et al.*, 2001). For example, changes in both precipitations rates and climate cyclicity may have significantly disturbed the overall equilibrium between denudation and rock uplift. This may yield to important repercussions on denudation dynamics in such extreme mountainous environment, favoring for example stochastic event as landslide. However, stable isotopes in paleo-soils, along with paleo-botanical studies, have not reported major changes in the local climate since at least 7 Ma (Quade *et al.*, 1995).

Moreover, if the acceleration between 3 and 4 Ma is real, we must therefore consider that the denudation rates has remained stable between 3 and 0.5 Ma. Yet, paradoxically, during this period, the global climate underwent an intensified cooling and the onset of the 100 kyr glacial cycles since ~1 Ma (Zachos et al., 2001).

Therefore, even if denudation rates had increased between 3-4 Ma, and if this is not only an effect of a catchment area shift, such increase remained very limited. This suggests that the intense Quaternary cooling only had a limited impact on the paleo-denudation of the Himalayas. Finally, the spectacular decrease in denudation, observed between 0.5 Ma and nowadays, is not synchronous with any global climatic event of our knowledge.

5.5 Comparison with the Tianshan paleo-denudation rates.

If some discrepancies exist between the denudation rates calculated in the Surai and the Tianshan sections, none of these records exhibit any dramatic acceleration of denudation rates at the Plio-Pleistocene transition.

Moreover, if the decrease in initial ^{10}Be concentrations observed between 3-4 Ma is really an indicator of enhanced denudation rates, this enhancement can also result from the tectonic

evolutions of the Himalayan thrust wedge. Furthermore, this increase in denudation has different magnitude and timing than the one observed in Tian-Shan. Interestingly, for the densely sampled 0.5-2.7 Ma period, we do not observe the large variations displayed, during the same period of time, in the Tian-Shan denudation rates records. The very different climatic settings of both studied regions may explain this difference. First, the Tian-Shan is located at a higher latitude, in a very continental setting where the climate since the beginning of the Pliocene has probably been more variable than in the warm and wet Himalayas (Quade *et al.*, 1995; Sun *et al.*, 2007; Gallaud, 2008). Second, the Tian-Shan basins have been, although in a limited extent, more glaciated than the Surai basin. Glaciers could have amplified denudation rates variations between glacial and interglacial periods. Third, the climate in both south and north Tian-Shan has been consistently much arid than in the Himalayas during this period (Quade *et al.*, 1995; Sun *et al.*, 2007; Gallaud, 2008). We can therefore expect some sediment transport dynamics marked by important millennial cyclicity in Tian-Shan, which can let imprints in cosmogenic nuclides record, while in Nepal the yearly transport cyclicity, induce by the monsoon, would have been averaged by cosmogenic nuclides on large scale basins.

6 Conclusion

The Surai section in the central Siwaliks is well suited for a cosmogenic-based paleo-denudation study. It exposes fresh, continuous outcrops of medium-grained sandstone and conglomerates where we picked up 20 paleo-denudation samples and analyzed 14 so far. We also refined the magneto-stratigraphic dating of the upper section, and tried to analyzed $^{26}Al/^{10}Be$ ratio in order to constrain burial ages and test potential sediment recycling. At last, we sampled the present larger nearby river, the Rapti, in two locations, upstream and in the middle of the Siwaliks to also better address a potential reworking issue.

The record displays three distinct periods: one period of relatively high pre-depositional ^{10}Be concentrations 6.5-4 Ma, a period of lower and stable initial concentrations 2.7-0.5 Ma, and again higher concentrations in the modern river. To derive basin-average denudation rates, if we consider the present-day Rapti river catchment at this point, these concentrations correspond to average denudation rates of ~0.4, ~1.1 and 0.2 $mm.yr^{-1}$ respectively. Despite large uncertainties due to low cosmogenic concentrations, $^{26}Al/^{10}Be$ ages do not suggest any dominant Siwaliks reworking since 2 Ma. This is also supported by detrital thermochronology (Bernet *et al.*, 2006; Szulc *et al.*, 2006) and paleo-currents directions (DeCelles *et al.*, 1998; Szulc *et al.*, 2006b).

Provenance studies (Szulc *et al.*, 2006), and the very low concentrations between 2.7-0.5 Ma, suggest that the catchment topography has remained relatively stable for this period and equivalent to the present day Rapti system, draining only the mid-land (essentially Lesser Himalaya but also a Klipp of High-Himalaya thrust sheet). However the higher cosmogenic concentrations for the 6.5-4 Ma period may traduce a river catchment reaching higher reliefs, potentially north to the MCT, which is consistent with previously proposed tectonic history of central/western Nepal (DeCelles *et al.* 1998, Huyghe *et al.,* 2001, Szulc *et al.,* 2006). In such case, we propose two scenarios to explain this drainage system change: First, an accelerated uplift and unroofing of the northern Lesser-Himalaya, as proposed by DeCelles *et al.* (1998); Second, and more simply, a progradation of a shift from large fan to interfan depositional environment related to the general progradation of the Himalayan thrust-wedge system. We suggest that the decrease in denudation rate observed between 0.5 Ma and present is due to a transfer of almost all of the Himalayan convergence and hence uplift and deformation to the most southern frontal MFT, which is located downstream from the Rapti samples and the Surai section.

These denudation rates variations can hardly be linked to global climate evolutions. If there was an increase in denudation rates about 4 Ma, the mechanism by which it would have been caused by the concomitant global climate cooling would be unclear, since this basin has never been glaciated, and its hydrologic regime seems to have remained stable since at least ~7 Ma in this region (Quade *et al.*, 1995). Furthermore, and contrarily to the Tian-Shan paleo-denudation records, erosion seems to have remained stable within uncertainties for the 2.7-0.5 Ma period, confirming that the onset of northern hemisphere glaciations and then glacial/interglacial cycle seems to have had a limited impact on this wet, warm-latitude relief.

In any case, cosmogenic isotopes, thanks to their shorter time resolution, have here proved their ability to enlighten denudation rates variations or absence of variation, that were otherwise invisible to low-temperature thermochronology or sediment budget (e.g. Burbank *et al.*, 1993; Metivier *et al.*, 1999).

References for this paper

Andermann, C. (2011). "Climate, topography and erosion in the Nepal Himalayas." Rennes 1.

Andermann, C., Crave, A., Gloaguen, R., Davy, P., and Bonnet, S. (2012). Connecting source and transport: Suspended sediments in the Nepal Himalayas. *Earth and Planetary Science Letters* **351,** 158-170.

Appel, E., Rosler, W., and Corvinus, G. (1991). Magnetostratigraphy of the Miocene Pleistocene Surai-Khola Siwaliks in West Nepal. *Geophysical Journal International* **105,** 191-198.

Balco, G., and Rovey, C. W., II. (2008). An Isochron Method for Cosmogenic-Nuclide Dating of Buried Soils and Sediments. *American Journal of Science* **308,** 1083-1114.

Bernet, M., Zattin, M., Garver, J. I., Brandon, M. T., and Vance, J. A. (2001). Steady-stale exhumation of the European Alps. *Geology* **29,** 35-38.

Bernet, M., van der Beek, P., Pik, R., Huyghe, P., Mugnier, J.-L., Labrin, E., and Szulc, A. (2006). Miocene to Recent exhumation of the central Himalaya determined from combined detrital zircon fission-track and U/Pb analysis of Siwalik sediments, western Nepal. *Basin Research* **18,** 393-412.

Burbank, D. W., Derry, L. A., and Francelanord, C. (1993). Reduced Himalayan Sediment Production 8 Myr Ago Despite an Intensified Monsoon. *Nature* **364,** 48-50.

Cande, S. C., and Kent, D. V. (1995). Revised Calibration of the Geomagnetic Polarity Timescale for the Late Cretaceous and Cenozoic. *Journal of Geophysical Research-Solid Earth* **100,** 6093-6095.

Champel, B., van der Beek, P., Mugnier, J.-L., and Leturmy, P. (2002). Growth and lateral propagation of fault-related folds in the Siwaliks of western Nepal: Rates, mechanisms, and geomorphic signature. *Journal of Geophysical Research: Solid Earth* **107,** ETG 2-1-ETG 2-18.

Clift, P. D. (2006). Controls on the erosion of Cenozoic Asia and the flux of clastic sediment to the ocean. *Earth and Planetary Science Letters* **241,** 571-580.

Corvinus, G., and Rimal, L. N. (2001). Biostratigraphy and geology of the neogene siwalik group of the Surai Khola and Rato Khola areas in Nepal. *Palaeogeography Palaeoclimatology Palaeoecology* **165,** 251-279.

DeCelles, P. G., Gehrels, G. E., Quade, J., Ojha, T. P., Kapp, P. A., and Upreti, B. N. (1998). Neogene foreland basin deposits, erosional unroofing, and the kinematic history of the Himalayan fold-thrust belt, western Nepal. *Geological Society of America Bulletin* **110,** 2-21.

FranceLanord, C., and Derry, L. A. (1997). Organic carbon burial forcing of the carbon cycle from Himalayan erosion. *Nature* **390,** 65-67.

Gabet, E. J., Burbank, D. W., Pratt-Sitaula, B., Putkonen, J., and Bookhagen, B. (2008). Modem erosion rates in the High Himalayas of Nepal. *Earth and Planetary Science Letters* **267,** 482-494.

Gallaud, A. (2008). "Interaction Orogenèse – Climat – Erosion en Asie Centrale durant le Cénozoïque : L'impact de la surrection de la chaîne du Tianshan sur le climat dans le bassin du Junggar." Université d'Orléans.

Gautam, P., and Rosler, W. (1999). Depositional chronology and fabric of Siwalik group sediments in Central Nepal from magnetostratigraphy and magnetic anisotropy. *Journal of Asian Earth Sciences* **17,** 659-682.

Godard, V., Burbank, D. W., Bourles, D. L., Bookhagen, B., Braucher, R., and Fisher, G. B. (2012). Impact of glacial erosion on Be-10 concentrations in fluvial sediments of the Marsyandi catchment, central Nepal. *Journal of Geophysical Research-Earth Surface* **117**.

Granger, D. E., and Muzikar, P. F. (2001). Dating sediment burial with in situ-produced cosmogenic nuclides: theory, techniques, and limitations. *Earth and Planetary Science Letters* **188,** 269-281.

Huyghe, P., Galy, A., Mugnier, J. L., and France-Lanord, C. (2001). Propagation of the thrust system and erosion in the Lesser Himalaya: Geochemical and sedimentological evidence. *Geology* **29,** 1007-1010.

Huyghe, P., Mugnier, J. L., Gajurel, A. P., and Delcaillau, B. (2005). Tectonic and climatic control of the changes in the sedimentary record of the Karnali River section (Siwaliks of western Nepal). *Island Arc* **14,** 311-327.

Lallier, F., Antoine, C., Charreau, J., Caumon, G., and Ruiu, J. (2013). Management of ambiguities in magnetostratigraphic correlation. *Earth and Planetary Science Letters* **371,** 26-36.

Lave, J., and Avouac, J. P. (2000). Active folding of fluvial terraces across the Siwaliks Hills, Himalayas of central Nepal. *Journal of Geophysical Research-Solid Earth* **105,** 5735-5770.

Lave, J., and Avouac, J. P. (2001). Fluvial incision and tectonic uplift across the Himalayas of central Nepal. *Journal of Geophysical Research-Solid Earth* **106,** 26561-26591.

Lupker, M., Blard, P.-H., Lave, J., France-Lanord, C., Leanni, L., Puchol, N., Charreau, J., and Bourles, D. (2012). Be-10-derived Himalayan denudation rates and sediment budgets in the Ganga basin. *Earth and Planetary Science Letters* **333,** 146-156.

Metivier, F., Gaudemer, Y., Tapponnier, P., and Klein, M. (1999). Mass accumulation rates in Asia during the Cenozoic. *Geophysical Journal International* **137,** 280-318.

Nishiizumi, K., Imamura, M., Caffee, M. W., Southon, J. R., Finkel, R. C., and McAninch, J. (2007). Absolute calibration of Be-10 AMS standards. *Nuclear Instruments & Methods in Physics Research Section B-Beam Interactions with Materials and Atoms* **258,** 403-413.

Ojha, T. P., Butler, R. F., Decelles, P. G., and Quade, J. (2009). Magnetic polarity stratigraphy of the Neogene foreland basin deposits of Nepal. *Basin Research* **21,** 61-90.

Quade, J., Cater, J. M. L., Ojha, T. P., Adam, J., and Harrison, T. M. (1995). Late Miocene Environmental-Change in Nepal and the Northern Indian Subcontinent - Stable Isotopic Evidence from Paleosols. *Geological Society of America Bulletin* **107,** 1381-1397.

Raymo, M. E., and Ruddiman, W. F. (1992). Tectonic forcing of Late Cenozoic climate. *Nature* **359,** 117-122.

Rosler, W., and Appel, E. (1998). Fidelity and time resolution of the magnetostratigraphic record in Siwalik sediments: high-resolution study of a complete polarity transition and evidence for cryptochrons in a Miocene fluviatile section. *Geophysical Journal International* **135,** 861-875.

Sanyal, P., Bhattacharya, S. K., and Prasad, M. (2005). Chemical diagenesis of Siwalik sandstone: Isotopic and mineralogical proxies from Surai Khola section, Nepal. *Sedimentary Geology* **180,** 57-74.

Sun, J., Xu, Q., and Huang, B. (2007). Late Cenozoic magnetochronology and paleoenvironmental changes in the northern foreland basin of the Tian Shan Mountains. *Journal of Geophysical Research: Solid Earth* **112,** B04107.

Szulc, A. G., Najman, Y., Sinclair, H. D., Pringle, M., Bickle, M., Chapman, H., Garzanti, E., Ando, S., Huyghe, P., Mugnier, J. L., Ojha, T., and DeCelles, P. (2006a). Tectonic evolution of the Himalaya constrained by detrital Ar-40-Ar-39, Sm-Nd and petrographic data from the Siwalik foreland basin succession, SW Nepal. *Basin Research* **18,** 375-391.

Thiede, R. C., Bookhagen, B., Arrowsmith, J. R., Sobel, E. R., and Strecker, M. R. (2004). Climatic control on rapid exhumation along the Southern Himalayan Front. *Earth and Planetary Science Letters* **222,** 791-806.

Tokuoka, T., Takayasu, K., Yoshida, M., and Hisatomi, K. (1986). The Churia (Siwalik) group of the Arung Khola area, west central Nepal. *Mem. Fac. Sci. Shimane Univ* **20,** 135-210.

van der Beek, P., Robert, X., Mugnier, J.-L., Bernet, M., Huyghe, P., and Labrin, E. (2006). Late Miocene – Recent exhumation of the central Himalaya and recycling in the foreland basin assessed by apatite fission-track thermochronology of Siwalik sediments, Nepal. *Basin Research* **18,** 413-434.

Il me faudra peut-être lire dans ces milliers de volumes, pour y voir que les hommes se sont tourmentés sur tout, et que çà et là un heureux s'est montré sur la terre ! — Ô toi, pauvre crâne vide, pourquoi sembles-tu m'adresser ton ricanement ? Est-ce pour me dire qu'il a été un temps où ton cerveau fut, comme le mien, rempli d'idées confuses ? qu'il chercha le grand jour, et qu'au milieu d'un triste crépuscule, il erra misérablement dans la recherche de la vérité ? Instruments que je vois ici, vous semblez me narguer avec toutes vos roues, vos dents, vos anses et vos cylindres ! J'étais à la porte, et vous deviez me servir de clef. Vous êtes, il est vrai, plus hérissés qu'une clef ; mais vous ne levez pas les verrous. Mystérieuse au grand jour, la nature ne se laisse point dévoiler, et il n'est ni levier ni machine qui puisse la contraindre à faire voir à mon esprit ce qu'elle a résolu de lui cacher.

Goethe,

Faust

Conclusion et perspectives

Une meilleur compréhension des interactions complexes entre climat, tectonique, altération et érosion requiert une quantification de ces facteurs au cours de l'histoire de la Terre. En particulier, la fin du Cénozoïque (depuis ~10 Ma) fut indubitablement une période de bouleversements climatiques majeurs (e.g. Zachos *et al.* 2001). En revanche, un intense débat sur les interactions réciproques entre ces changements climatiques et les taux d'érosion et d'altération à l'échelle globale anime la communauté scientifique, en grande partie à cause de l'équivocité des méthodes employées pour remonter à ces grandeurs.

Durant cette thèse, nous avons exploré le potentiel des isotopes cosmogéniques *in-situ* à remonter à des enregistrements continus de paléo-taux de dénudation, cette méthode ayant déjà fait ses preuves dans la quantification de taux de dénudation actuels. Nous avons tout d'abord exploré des points méthodologiques spécifiques de certaines des zones ciblées, au Tianshan, en Himalaya et en Ethiopie, en testant l'influence de plusieurs facteurs géologiques et géochimiques sur le signal cosmogénique contenu dans des sédiments actuels. Ensuite, nous avons appliqué cette méthode dans des sédiments datés par magnétostratigraphie entre 0 et ~10 Ma, au Tianshan et en Himalaya. Nous nous sommes attachés à circonscrire les limites théoriques et pratiques de cette méthode. Les zones d'études cibles furent choisies pour leur importance vis à vis des débats susmentionnés, et pour leur compatibilité *a priori* avec l'utilisation des isotopes cosmogéniques.

Nos études dans l'actuel confirment la relative fiabilité des isotopes cosmogénique, y compris dans des contextes défavorables :

- En Himalaya, nous avons travaillé sur un petit bassin versant (rivière Khudi, ~100 km2) où l'érosion est dominée par les glissements de terrain. Nous avons montré que les glissements influencent tant le signal cosmogénique moyen que la distribution granulométrique des sables de rivière. Cependant, les taux de dénudation dérivés de l'analyse du ^{10}Be dans la fraction sableuse (0.5-1 mm) sont dans les mêmes ordres de grandeur que ceux reportés par d'autres études et avec d'autres méthodes(1-2.5 mm.yr-1)

- En Ethiopie, nous avons testé l'analyse de l'^{3}He cosmogénique dans des olivines et pyroxènes détritiques. La difficulté de cette analyse réside dans la correction de la composante magmatique de ^{3}He. Etant donné l'âge des trapps éthiopiens (30 Ma), l'écrasante majorité du

^{4}He est d'origine radiogénique, ce qui empêche d'utiliser cet isotope comme un traceur fiable du ^{3}He magmatique. Cependant, nos tests ont montré qu'il était possible de surmonter ce problème en sélectionnant les tailles de grains adéquats (<500 μm dans ce cas), permetant de s'affranchir de la composante magmatique de l'hélium.

Cinq séries sédimentaires anciennes (jusqu'à ~10 Ma) ont été analysées : quatre des piedmonts de la chaîne du Tianshan, et une de l'Himalaya.

- Au Tianshan, les cinq enregistrements montrent des paléo taux de dénudation variés (moyennes entre ~80 et 500 m.Ma^{-1}), y compris entre bassins géographiquement proches (<50 km), et marqués par des fluctuations à haute fréquence (typiquement facteurs 1.5 à 2 sur quelques centaines de milliers d'années). Ces fluctuations peuvent trouver leur sourc dans les nombreux facteurs d'incertitudes pesant sur cette méthode, une variabilité climatique marquée dans ce contexte aride et très continental (Sun *et al.*, 2007; Gallaud, 2008), ou des particularités tectoniques locales. En revanche, un profil sédimentaire haute résolution (deux échantillons/m) semble montrer que l'influence du caractère épisodique des processus de dépôt reste limitée.

La moyenne de ces quatre enregistrements normalisés, intégrée sur des périodes de 1 Ma afin de lisser ces fluctuations, montre une augmentation progressive (facteur 3) des taux de dénudation entre 9 Ma, début de l'enregistrement, et 4 Ma. Entre 4 Ma et l'actuel, cette moyenne semble se stabiliser autour de 4-5 fois la valeur déterminée vers 9 Ma. Ces enregistrements montrent donc que :

- S'il y a bien une augmentation régionale de la dénudation, celle-ci a débuté depuis au moins 9 Ma, c'est à dire largement avant le développement des glaciations quaternaires.
- S'il y a bien une légère accélération à ~4 Ma, qui serait concomitante avec l'accélération du refroidissement du climat global, celle ci est très limitée par rapport à celle proposée par des études précédemment basées sur les taux d'accumulation sédimentaires (Metivier & Gaudemer, 1997; Metivier *et al.*, 1999; Zhang *et al.*, 2001).

- En Himalaya, l'unique section sédimentaire analysée révèle un tableau assez différent. Trois périodes distinctes se dégagent dans cet enregistrement : des hautes concentrations en 10Be initial entre 6.5-4 Ma, des basses concentrations entre 2.7-0.5 Ma, et à nouveau une haute concentration dans les sédiments de la rivière actuelle. Contrairement au Tianshan, sur chacune de ces périodes, les palo-taux de dénudations restent stables, et non caractérisés par la même variabilité haute fréquence que les données du Tianshan. Par ailleurs, les changements apparents de taux de dénudation entre ces trois périodes (~0.4, ~1.1 et ~0.2 mm.a-1 respectivement) sont probablement explicables par des réorganisations du système de drainage et, donc, des

changements de taux de production cosmogéniques. Ces changements seraient liés à la progradation tectonique du front Himalayen, soit par le transfert successif de la convergence himalayenne sur ses grandes failles structurales (MCT, MBT, MFT), soit par le passage de la zone de dépôt sédimentaire d'un cône alluvial à un autre. Ainsi, il est probable que les taux de dénudation moyen des bassins versant approvisionneurs soient restés stables entre 0.5 et 5.5 Ma, autours de 1.2 mm.a-1.

Nous n'observons aucune variation de taux de dénudation explicable par des changements climatiques globaux. Cependant, cette zone tropicale très humide fut vraisemblablement peu affectée par ces changements (Quade et al., 1995).

Ces études confirment le potentiel des isotopes cosmogéniques, mais aussi leurs limites :

- Nos résultats confirment en effet la nécessité de travailler sur des séries indépendamment datées, afin de pourvoir corriger de la production cosmogénique syn-dépôt et des éventuels réexpositions post-dépôt.
- Il serait idéal de pouvoir estimer les évolutions passées du bassin versant (hypsométrie et provenances des sédiments). Les progrès méthodologiques en paléo-altimétrie seraient déterminant pour améliorer ces aspects.
- Le cas échéant, nous avons montré qu'il était possible de repousser les limites analytiques imposées par la décroissance radioactive du ^{10}Be, en combinant l'analyse de grandes quantités de quartz (>100 g) avec des blancs particulièrement bas ($^{10}Be/^{9}Be < 10^{-15}$).

Malgré ces limites, et les incertitudes associées, les isotopes cosmogéniques s'avèrent capables d'apporter des informations uniques sur les paléo-dénudations, notamment sur des échelles de temps inaccessibles à d'autres méthodes, et avec une relative facilité d'échantillonnage et d'analyse.

Sur l'ensemble des deux zones étudiées, les changement climatiques du Plio-Pleistocène ne semblent pas avoir eu un impact important sur les taux de dénudation. Ces résultats participent donc à une sérieuse remise en cause du paradigme d'une augmentation majeur (x 5 à 10) des taux de dénudation mondiaux, liée à la variabilité climatique du Quaternaire (Zhang *et al.*, 2001; Molnar, 2004). Cependant, nos résultats ne concernent que deux chaînes de montagnes (Himalaya et Tianshan) qui sont particulièrement actives sur le plan tectonique..Il est ainsi possible, et même probable, que d'autres chaînes (Alpes par exemple) marquées par des contextes tectoniques et des géométries orogéniques différentes, aient répondu de manière plus marqué à ces changements climatiques (Whipple and Meade, 2006; Whipple, 2009).

Suite à ces résultats prometteurs, on peut envisager deux pistes dans le développement de cette méthode :

- D'une part, son application à plusieurs régions, dominées par des contextes climatiques et tectoniques très divers. Cependant, il faut noter que les bassins versants englacés sur une forte proportion de leur surface (>30%) ne seront pas à même de fournir des taux de dénudation fiables par les isotopes cosmogéniques, à cause de l'écrantage par la glace et les granulométries particulières des sédiments glaciaires (Wittmann et al., 2007; Godard et al., 2013).
- D'autre part, le développement des isotopes cosmogéniques stables, dans des zones faborables ou sur de nouvelles phases minérales, qui permettrait de remonter à de très anciens paléo-taux de dénudation (plusieurs dizaines de Ma).

Cette méthode permettra alors, sans doute, d'apporter des informations importantes et de raffiner encore nos connaissances des interactions de surface à l'échelle du millier à plusieurs millions d'années.

Références bibliographiques

(Les articles inclus aux Chapitres 3, 4 et 5 disposent de leurs propres bibliographies)

Amidon, W. H., Farley, K. A., Burbank, D. W., and Pratt-Sitaula, B. (2008). Anomalous cosmogenic (3)He production and elevation scaling in the high Himalaya. *Earth and Planetary Science Letters* **265,** 287-301.

Amidon, W. H., Rood, D. H., and Farley, K. A. (2009). Cosmogenic He-3 and Ne-21 production rates calibrated against Be-10 in minerals from the Coso volcanic field. *Earth and Planetary Science Letters* **280,** 194-204.

Amidon, W. H., and Farley, K. A. (2010). Cosmogenic He-3 production rates in apatite, zircon and pyroxene inferred from Bonneville flood erosional surfaces. *Quaternary Geochronology* **6,** 10-21.

Amidon, W. H., and Farley, K. A. (2012). Cosmogenic He-3 and Ne-21 dating of biotite and hornblende. *Earth and Planetary Science Letters* **313,** 86-94.

Balco, G., and Stone, J. O. H. (2005). Measuring middle Pleistocene erosion rates with cosmic-ray-produced nuclides in buried alluvial sediment, Fisher Valley, southeastern Utah. *Earth Surface Processes and Landforms* **30,** 1051-1067.

Balco, G., and Rovey, C. W., II. (2008). An Isochron Method for Cosmogenic-Nuclide Dating of Buried Soils and Sediments. *American Journal of Science* **308,** 1083-1114.

Belmont, P., Pazzaglia, F. J., and Gosse, J. C. (2007). Cosmogenic Be-10 as a tracer for hillslope and channel sediment dynamics in the Clearwater River, western Washington State. *Earth and Planetary Science Letters* **264,** 123-135.

Berger, A. L., Gulick, S. P. S., Spotila, J. A., Upton, P., Jaeger, J. M., Chapman, J. B., Worthington, L. A., Pavlis, T. L., Ridgway, K. D., Willems, B. A., and McAleer, R. J. (2008). Quaternary tectonic response to intensified glacial erosion in an orogenic wedge. *Nature Geoscience* **1,** 793-799.

Berner, R. A., Lasaga, A. C., and Garrels, R. M. (1983). The Carbonate-Silicate Geochemical Cycle and Its Effect on Atmospheric Carbon-Dioxide over the Past 100 Million Years. *American Journal of Science* **283,** 641-683.

Bernet, M., van der Beek, P., Pik, R., Huyghe, P., Mugnier, J.-L., Labrin, E., and Szulc, A. (2006). Miocene to Recent exhumation of the central Himalaya determined from combined detrital zircon fission-track and U/Pb analysis of Siwalik sediments, western Nepal. *Basin Research* **18,** 393-412.

Binnie, S. A., Phillips, W. M., Summerfield, M. A., Fifield, L. K., and Spotila, J. A. (2010). Tectonic and climatic controls of denudation rates in active orogens: The San Bernardino Mountains, California. *Geomorphology* **118,** 249-261.

Blard, P.-H., Bourlès, D., Lavé, J., and Pik, R. (2006). Applications of ancient cosmic-ray exposures: Theory, techniques and limitations. *Quaternary Geochronology* **1,** 59-73.

Blard, P. H., Bourles, D., Pik, R., and Lave, J. (2008). In situ cosmogenic Be-10 in olivines and pyroxenes. *Quaternary Geochronology* **3,** 196-205.

Blard, P. H., and Farley, K. A. (2008). The influence of radiogenic (4)He on cosmogenic (3)He determinations in volcanic olivine and pyroxene. *Earth and Planetary Science Letters* **276,** 20-29.

Blythe, A. E., Burbank, D. W., Carter, A., Schmidt, K., and Putkonen, J. (2007). Plio-Quaternary exhumation history of the central Nepalese Himalaya: 1. Apatite and zircon fission track and apatite [U-Th]/He analyses. *Tectonics* **26**.

Braucher, R., Bourles, D. L., Brown, E. T., Colin, F., Muller, J. P., Braun, J. J., Delaune, M., Minko, A. E., Lescouet, C., Raisbeck, G. M., and Yiou, F. (2000). Application of in situ-produced cosmogenic Be-10 and Al-26 to the study of lateritic soil development in tropical forest: theory and examples from Cameroon and Gabon. *Chemical Geology* **170,** 95-111.

Braun, J. (2002). Estimating exhumation rate and relief evolution by spectral analysis of age-elevation datasets. *Terra Nova* **14,** 210-214.

Brown, E. T., Edmond, J. M., Raisbeck, G. M., Yiou, F., Kurz, M. D., and Brook, E. J. (1991). Examination of surface exposure ages of Antarctic moraines using in situ produced ^{10}Be And ^{26}Al. *Geochimica et Cosmochimica Acta* **55,** 2269-2283.

Brown, E. T., Stallard, R. F., Larsen, M. C., Raisbeck, G. M., and Yiou, F. (1995). Denudation rates determined from the accumulation of in situ produced ^{10}Be in the Luquillo experimental forest, Puerto-Rico. *Earth and Planetary Science Letters* **129,** 193-202.

Burbank, D. W., Blythe, A. E., Putkonen, J., Pratt-Sitaula, B., Gabet, E., Oskin, M., Barros, A., and Ojha, T. P. (2003). Decoupling of erosion and precipitation in the Himalayas. *Nature* **426,** 652-655.

Cerling, T. E., and Craig, H. (1994). Cosmogenic ^{3}He production rates from 39°N to 46°N latitude, Western Usa and France. *Geochimica et Cosmochimica Acta* **58,** 249-255.

Champagnac, J.-D., Molnar, P., Sue, C., and Herman, F. (2012). Tectonics, climate, and mountain topography. *Journal of Geophysical Research-Solid Earth* **117**.

Champagnac, J. D., Molnar, P., Anderson, R. S., Sue, C., and Delacou, B. (2007). Quaternary erosion-induced isostatic rebound in the western Alps. *Geology* **35,** 195-198.

Charreau, J., Chen, Y., Gilder, S., Dominguez, S., Avouac, J. P., Sen, S., Sun, D. J., Li, Y. G., and Wang, W. M. (2005). Magnetostratigraphy and rock magnetism of the Neogene Kuitun He section (northwest China): implications for Late Cenozoic uplift of the Tianshan mountains. *Earth and Planetary Science Letters* **230,** 177-192.

Charreau, J., Gilder, S., Chen, Y., Dominguez, S., Avouac, J. P., Sen, S., Jolivet, M., Li, Y. G., and Wang, W. M. (2006). Magnetostratigraphy of the Yaha section, Tarim Basin (China): 11 Ma acceleration in erosion and uplift of the Tian Shan mountains. *Geology* **34,** 181-184.

Charreau, J., Chen, Y., Gilder, S., Barrier, L., Dominguez, S., Augier, R., Sen, S., Avouac, J.-P., Gallaud, A., Graveleau, F., and Wang, Q. (2009a). Neogene uplift of the Tian Shan Mountains observed in the magnetic record of the Jingou River section (northwest China). *Tectonics* **28**.

Charreau, J., Gumiaux, C., Avouac, J.-P., Augier, R., Chen, Y., Barrier, L., Gilder, S., Dominguez, S., Charles, N., and Wang, Q. (2009b). The Neogene Xiyu Formation, a diachronous prograding gravel wedge at front of the Tianshan: Climatic and tectonic implications. *Earth and Planetary Science Letters* **287,** 298-310.

Charreau, J., Kent-Corson, M. L., Barrier, L., Augier, R., Ritts, B. D., Chen, Y., France-Lannord, C., and Guilmette, C. (2012). A high-resolution stable isotopic record from the Junggar Basin (NW China): Implications for the paleotopographic evolution of the Tianshan Mountains. *Earth and Planetary Science Letters* **341,Äì344,** 158-169.

Chmeleff, J. r. m., von Blanckenburg, F., Kossert, K., and Jakob, D. (2010). Determination of the 10Be half-life by multicollector ICP-MS and liquid scintillation counting. *Nuclear Instruments and Methods in Physics Research Section B: Beam Interactions with Materials and Atoms* **268,** 192-199.

Clark, M. K. (2007). The significance of paleotopography. *In* "Paleoaltimetry: Geochemical and Thermodynamic Approaches." pp. 1-21. Reviews in Mineralogy & Geochemistry.

Clift, P. D. (2006). Controls on the erosion of Cenozoic Asia and the flux of clastic sediment to the ocean. *Earth and Planetary Science Letters* **241,** 571-580.

Codilean, A. T., Fenton, C. R., Fabel, D., Bishop, P., and Xu, S. (2012). Discordance between cosmogenic nuclide concentrations in amalgamated sands and individual fluvial pebbles in an arid zone catchment. *Quaternary Geochronology*.

Desilets, D., and Zreda, M. (2003). Spatial and temporal distribution of secondary cosmic-ray nucleon intensities and applications to in situ cosmogenic dating. *Earth and Planetary Science Letters* **206,** 21-42.

Dixon, J. L., Heimsath, A. M., and Amundson, R. (2009). The critical role of climate and saprolite weathering in landscape evolution. *Earth Surface Processes and Landforms* **34,** 1507-1521.

Dunai, T. J. (2001). Influence of secular variation of the geomagnetic field on production rates of in situ produced cosmogenic nuclides. *Earth and Planetary Science Letters* **193,** 197-212.

Dunai, T. J. (2010). "Cosmogenic Nuclides, Principle, Conceptes and Applications in the Earth Surface Sciences." Cambridge University Press.

Ebelmen, J. J. (1845). Sur les produits de la décomposition des espèces minérales de la famille des silicates. *Annales des Mines* **7,** 3-66.

Egholm, D. L., Nielsen, S. B., Pedersen, V. K., and Lesemann, J. E. (2009). Glacial effects limiting mountain height. *Nature* **460,** 884-U120.

Ehlers, T. A., and Farley, K. A. (2003). Apatite (U-Th)/He thermochronometry: methods and applications to problems in tectonic and surface processes. *Earth and Planetary Science Letters* **206,** 1-14.

Farley, K. A., Libarkin, J., Mukhopadhyay, S., and Amidon, W. (2006). Cosmogenic and nucleogenic ^{3}He in apatite, titanite, and zircon. *Earth and Planetary Science Letters* **248,** 451-461.

Finnegan, N. J., Hallet, B., Montgomery, D. R., Zeitler, P. K., Stone, J. O., Anders, A. M., and Yuping, L. (2008). Coupling of rock uplift and river incision in the Namche Barwa-Gyala Peri massif, Tibet. *Geological Society of America Bulletin* **120,** 142-155.

FranceLanord, C., and Derry, L. A. (1997). Organic carbon burial forcing of the carbon cycle from Himalayan erosion. *Nature* **390,** 65-67.

Gabet, E. J. (2007). A theoretical model coupling chemical weathering and physical erosion in landslide-dominated landscapes. *Earth and Planetary Science Letters* **264,** 259-265.

Gabet, E. J., and Mudd, S. M. (2009). A theoretical model coupling chemical weathering rates with denudation rates. *Geology* **37,** 151-154.

Gallaud, A. (2008). "Interaction Orogenèse – Climat – Erosion en Asie Centrale durant le Cénozoïque : L'impact de la surrection de la chaîne du Tianshan sur le climat dans le bassin du Junggar." Université d'Orléans.

Galloway, W. E., Whiteaker, T. L., and Ganey-Curry, P. (2011). History of Cenozoic North American drainage basin evolution, sediment yield, and accumulation in the Gulf of Mexico basin. *Geosphere* **7,** 938-973.

Galy, V., France-Lanord, C., Beyssac, O., Faure, P., Kudrass, H., and Palhol, F. (2007). Efficient organic carbon burial in the Bengal fan sustained by the Himalayan erosional system. *Nature* **450,** 407-U6.

Gayer, E., Pik, R., Lave, J., France-Lanord, C., Bourles, D., and Marty, B. (2004). Cosmogenic ^{3}He in Himalayan garnets indicating an altitude dependence of the ^{3}He/^{10}Be production ratio. *Earth and Planetary Science Letters* **229,** 91-104.

Glotzbach, C., Bernet, M., and van der Beek, P. (2011). Detrital thermochronology records changing source areas and steady exhumation in the Western European Alps. *Geology* **39,** 239-242.

Godard, V., Burbank, D. W., Bourles, D. L., Bookhagen, B., Braucher, R., and Fisher, G. B. (2012). Impact of glacial erosion on Be-10 concentrations in fluvial sediments of the Marsyandi catchment, central Nepal. *Journal of Geophysical Research-Earth Surface* **117**.

Goehring, B. M., Kurz, M. D., Balco, G., Schaefer, J. M., Licciardi, J., and Lifton, N. (2010). A reevaluation of in situ cosmogenic 3He production rates. *Quaternary Geochronology* **5,** 410-418.

Gosse, J. C., and Phillips, F. M. (2001). Terrestrial in situ cosmogenic nuclides: theory and application. *Quaternary Science Reviews* **20,** 1475-1560.

Granger, D. E., Kirchner, J. W., and Finkel, R. (1996). Spatially averaged long-term erosion rates measured from in situ-produced cosmogenic nuclides in alluvial sediment. *Journal of Geology* **104,** 249-257.

Granger, D. E., Fabel, D., and Palmer, A. N. (2001). Pliocene-Pleistocene incision of the Green River, Kentucky, determined from radioactive decay of cosmogenic Al-26 and Be-10 in Mammoth Cave sediments. *Geological Society of America Bulletin* **113,** 825-836.

Granger, D. E., and Muzikar, P. F. (2001). Dating sediment burial with in situ-produced cosmogenic nuclides: theory, techniques, and limitations. *Earth and Planetary Science Letters* **188,** 269-281.

Hay, W. W., Sloan, J. L., and Wold, C. N. (1988). Mass age distribution and composition of sediments on the ocean-floor and the global rate of sediment subduction. *Journal of Geophysical Research - Solid Earth And Planets* **93,** 14933-14940.

Hay, W. W., Soeding, E., DeConto, R. M., and Wold, C. N. (2002). The Late Cenozoic uplift - climate change paradox. *International Journal of Earth Sciences* **91,** 746-774.

Henck, A. C., Huntington, K. W., Stone, J. O., Montgomery, D. R., and Hallet, B. (2011). Spatial controls on erosion in the Three Rivers Region, southeastern Tibet and southwestern China. *Earth and Planetary Science Letters* **303,** 71-83.

Herman, F., Rhodes, E. J., Braun, J., and Heiniger, L. (2010). Uniform erosion rates and relief amplitude during glacial cycles in the Southern Alps of New Zealand, as revealed from OSL-thermochronology. *Earth and Planetary Science Letters* **297,** 183-189.

Hu, X., Kirby, E., Pan, B., Granger, D. E., and Su, H. (2011). Cosmogenic burial ages reveal sediment reservoir dynamics along the Yellow River, China. *Geology* **39,** 839-842.

Huntington, K. W., Blythe, A. E., and Hodges, K. V. (2006). Climate change and Late Pliocene acceleration of erosion in the Himalaya. *Earth and Planetary Science Letters* **252,** 107-118.

Ivy-Ochs, S., Kubik, P. W., Masarik, J., Wieler, R., Bruno, L., and Schluchter, C. (1998). Preliminary results on the use of pyroxene for ^{10}Be surface exposure dating. *Schweizerische Mineralogische und Petrographische Mitteilungen* **78,** 375-382.

Kashiwagi, H., Ogawa, Y., and Shikazono, N. (2008). Relationship between weathering, mountain uplift, and climate during the Cenozoic as deduced from the global carbon,Äìstrontium cycle model. *Palaeogeography, Palaeoclimatology, Palaeoecology* **270,** 139-149.

Klein, J., Giegengack, R., Middleton, R., Sharma, P., Underwood, J. R., and Weeks, R. A. (1986). Revealing histories of exposure using in situ produced ^{26}Al and ^{10}Be in Libyan desert glass. *Radiocarbon* **28,** 547-555.

Kober, F., Ivy-Ochs, S., Leya, I., Baur, H., Magna, T., Wieler, R., and Kubik, P. W. (2005). In situ cosmogenic ^{10}Be and ^{21}Ne in sanidine and in situ cosmogenic ^{3}He in Fe-Ti-oxide minerals. *Earth and Planetary Science Letters* **236,** 404-418.

Kohl, C. P., and Nishiizumi, K. (1992). Chemical isolation of quartz for measurement of in situ-produced cosmogenic nuclides. *Geochimica et Cosmochimica Acta* **56,** 3583-3587.

Koppes, M. N., and Montgomery, D. R. (2009). The relative efficacy of fluvial and glacial erosion over modern to orogenic timescales. *Nature Geoscience* **2,** 644-647.

Korschinek, G., Bergmaier, A., Faestermann, T., Gerstmann, U. C., Knie, K., Rugel, G., Wallner, A., Dillmann, I., Dollinger, G., von Gostomski, C. L., Kossert, K., Maiti, M., Poutivtsev, M., and Remmert, A. (2010). A new value for the half-life of 10Be by Heavy-Ion Elastic Recoil Detection and liquid scintillation counting. *Nuclear Instruments and Methods in Physics Research Section B: Beam Interactions with Materials and Atoms* **268,** 187-191.

Kuhlemann, J., Frisch, W., Dunkl, I., and Szekely, B. (2001). Quantifying tectonic versus erosive denudation by the sediment budget: the Miocene core complexes of the Alps. *Tectonophysics* **330,** 1-23.

Kuhlemann, J., Frisch, W., Székely, B., Dunkl, I., and Kazmér, M. (2002). Post-collisional sediment budget history of the Alps: tectonic versus climatic control. *International Journal of Earth Sciences* **91,** 818-837.

Kurz, M. D. (1986). In situ production of terrestrial cosmogenic helium and some applications to geochronology. *Geochimica et Cosmochimica Acta* **50,** 2855-2862.

Kurz, M. D., Colodner, D., Trull, T. W., Moore, R. B., and Obrien, K. (1990). Cosmic-ray exposure dating with in situ produced cosmogenic ^{3}He - Results from young Hawaiian lava flows. *Earth and Planetary Science Letters* **97,** 177-189.

Lal, D. (1991). Cosmic ray labeling of erosion surfaces: *in situ* nuclide production rates and erosion models. *Earth and Planetary Science Letters* **104,** 424-439.

Lauer, J. W., and Willenbring, J. (2010). Steady state reach-scale theory for radioactive tracer concentration in a simple channel/floodplain system. *Journal of Geophysical Research-Earth Surface* **115**.

Lavier, L. L., Steckler, M. S., and Brigaud, F. (2001). Climatic and tectonic control on the Cenozoic evolution of the West African margin. *Marine Geology* **178,** 63-80.

Libarkin, J. C., Quade, J., Chase, C. G., Poths, J., and McIntosh, W. (2002). Measurement of ancient cosmogenic ^{21}Ne in quartz from the 28 Ma Fish Canyon Tuff, Colorado. *Chemical Geology* **186,** 199-213.

Lifton, N., Smart, D. F., and Shea, M. A. (2008). Scaling time-integrated in situ cosmogenic nuclide production rates using a continuous geomagnetic model. *Earth and Planetary Science Letters* **268,** 190-201.

Lupker, M., Blard, P.-H., Lave, J., France-Lanord, C., Leanni, L., Puchol, N., Charreau, J., and Bourles, D. (2012). Be-10-derived Himalayan denudation rates and sediment budgets in the Ganga basin. *Earth and Planetary Science Letters* **333,** 146-156.

Matmon, A., Stock, G. M., Granger, D. E., and Howard, K. A. (2012). Dating of Pliocene Colorado River sediments: Implications for cosmogenic burial dating and the evolution of the lower Colorado River. *Geological Society of America Bulletin* **124,** 626-640.

Metivier, F., and Gaudemer, Y. (1997). Mass transfer between eastern Tien Shan and adjacent basins (central Asia): Constraints on regional tectonics and topography. *Geophysical Journal International* **128,** 1-16.

Metivier, F., and Gaudemer, Y. (1999). Stability of output fluxes of large rivers in South and East Asia during the last 2 million years: implications on floodplain processes. *Basin Research* **11,** 293-303.

Metivier, F., Gaudemer, Y., Tapponnier, P., and Klein, M. (1999). Mass accumulation rates in Asia during the Cenozoic. *Geophysical Journal International* **137,** 280-318.

Métivier, F. (2002). On the use of sedimentation rates in deciphering global change. *Geophysical Research Letters* **29**.

Misra, S., and Froelich, P. N. (2012). Lithium Isotope History of Cenozoic Seawater: Changes in Silicate Weathering and Reverse Weathering. *Science* **335,** 818-823.

Molnar, P., and England, P. (1990). Late Cenozoic uplift of mountain ranges and global climate change - Chicken or egg ? *Nature* **346,** 29-34.

Molnar, P. (2004). Late cenozoic increase in accumulation rates of terrestrial sediment: How might climate change have affected erosion rates? *Annual Review of Earth and Planetary Sciences* **32,** 67-89.

Molnar, P. (2008). Closing of the Central American Seaway and the ice age: A critical review. *Paleoceanography* **23**.

Molnar, P. (2009). The state of interactions among tectonics, erosion, and climate: A polemic. *GSA Today* **19,** 44-45.

Niedermann, S., Graf, T., Kim, J. S., Kohl, C. P., Marti, K., and Nishiizumi, K. (1994). Cosmic-ray produced ^{21}Ne in terrestrial quartz - The neon inventory of Sierra Nevada quartz separates. *Earth and Planetary Science Letters* **125,** 341-355.

Niedermann, S. (2000). The ^{21}Ne production rate in quartz revisited. *Earth and Planetary Science Letters* **183,** 361-364.

Niedermann, S. (2002). Cosmic-Ray-Produced Noble Gases in Terrestrial Rocks: Dating Tools for Surface Processes. *Reviews in Mineralogy and Geochemistry* **47,** 731-784.

Niemi, N. A., Oskin, M., Burbank, D. W., Heimsath, A. M., and Gabet, E. J. (2005). Effects of bedrock landslides on cosmogenically determined erosion rates. *Earth and Planetary Science Letters* **237,** 480-498.

Nishiizumi, K., Klein, J., Middleton, R., and Craig, H. (1990). Cosmogenic ^{10}Be, ^{26}Al, and ^{3}He in olivine from Maui lavas. *Earth and Planetary Science Letters* **98,** 263-266.

Nishiizumi, K. (2004). Preparation of 26Al AMS standards. *Nuclear Instruments and Methods in Physics Research Section B: Beam Interactions with Materials and Atoms* **223,Äì224,** 388-392.

Parsons, B. (1982). Causes and Consequences of the Relation between Area and Age of the Ocean-Floor. *Journal of Geophysical Research* **87,** 289-302.

Pedersen, V. K., and Egholm, D. L. (2013). Glaciations in response to climate variations preconditioned by evolving topography. *Nature* **493,** 206-210.

Portenga, E., W., and Bierman, P. R. (2011). Understanding Earth's eroding surface with 10Be. *GSA Today* **21,** 7.

Quade, J., Cater, J. M. L., Ojha, T. P., Adam, J., and Harrison, T. M. (1995). Late Miocene Environmental-Change in Nepal and the Northern Indian Subcontinent - Stable Isotopic Evidence from Paleosols. *Geological Society of America Bulletin* **107,** 1381-1397.

Raymo, M. E., and Ruddiman, W. F. (1992). Tectonic forcing of Late Cenozoic climate. *Nature* **359,** 117-122.

Refsnider, K. A. (2011). Dramatic increase in late Cenozoic alpine erosion rates recorded by cave sediment in the southern Rocky Mountains. *Earth and Planetary Science Letters* **297,** 505-511.

Reverman, R. L., Fellin, M. G., Herman, F., Willett, S. D., and Fitoussi, C. (2012). Climatically versus tectonically forced erosion in the Alps: Thermochronometric constraints from the Adamello Complex, Southern Alps, Italy. *Earth and Planetary Science Letters* **339,** 127-138.

Riebe, C. S., Kirchner, J. W., and Granger, D. E. (2001a). Quantifying quartz enrichment and its consequences for cosmogenic measurements of erosion rates from alluvial sediment and regolith. *Geomorphology* **40,** 15-19.

Riebe, C. S., Kirchner, J. W., Granger, D. E., and Finkel, R. C. (2001b). Minimal climatic control on erosion rates in the Sierra Nevada, California. *Geology* **29,** 447-450.

Royer, D. L., Berner, R. A., and Park, J. (2007). Climate sensitivity constrained by CO2 concentrations over the past 420 million years. *Nature* **446,** 530-532.

Ruddiman, W. F., and Kutzbach, J. E. (1989). Forcing of Late Cenozoic Northern Hemisphere Climate by Plateau Uplift in Southern Asia and the American West. *Journal of Geophysical Research-Atmospheres* **94,** 18409-18427.

Sadler, P. M. (1981). Sediment accumulation rates and the completeness of stratigraphic sections. *The Journal of Geology***,** 569-584.

Sadler, P. M. (1999). The influence of hiatuses on sediment accumulation rates. *In* "GeoResearch Forum." pp. 15-40.

Schaller, M., von Blanckenburg, F., Veldkamp, A., Tebbens, L. A., Hovius, N., and Kubik, P. W. (2002). A 30 000 yr record of erosion rates from cosmogenic ^{10}Be in Middle European river terraces. *Earth and Planetary Science Letters* **204,** 307-320.

Schaller, M., von Blanckenburg, F., Hovius, N., Veldkamp, A., van den Berg, M. W., and Kubik, P. W. (2004). Paleoerosion rates from cosmogenic Be-10 in a 1.3 Ma terrace sequence: Response of the river meuse to changes in climate and rock uplift. *Journal of Geology* **112,** 127-144.

Schaller, M., and Ehlers, T. A. (2006). Limits to quantifying climate driven changes in denudation rates with cosmogenic radionuclides. *Earth and Planetary Science Letters* **248,** 153-167.

Schumer, R., and Jerolmack, D. J. (2009). Real and apparent changes in sediment deposition rates through time. *Journal of Geophysical Research-Earth Surface* **114**.

Schumer, R., Jerolmack, D., and McElroy, B. (2011). The stratigraphic filter and bias in measurement of geologic rates. *Geophysical Research Letters* **38**.

Seidl, M. A., Finkel, R. C., Caffee, M. W., Hudson, G. B., and Dietrich, W. E. (1997). Cosmogenic isotope analyses applied to river longitudinal profile evolution: Problems and interpretations. *Earth Surface Processes and Landforms* **22,** 195-209.

Seranne, M., and Anka, Z. (2005). South Atlantic continental margins of Africa: A comparison of the tectonic vs climate interplay on the evolution of equatorial west Africa and SW Africa margins. *Journal of African Earth Sciences* **43,** 283-300.

Sternai, P., Herman, F., Champagnac, J.-D., Fox, M., Salcher, B., and Willett, S. D. (2012). Pre-glacial topography of the European Alps. *Geology* **40,** 1067-1070.

Stone, J. O. (2000). Air pressure and cosmogenic isotope production. *Journal of Geophysical Research - Solid Earth* **105,** 23753-23759.

Sun, J., Xu, Q., and Huang, B. (2007). Late Cenozoic magnetochronology and paleoenvironmental changes in the northern foreland basin of the Tian Shan Mountains. *Journal of Geophysical Research: Solid Earth* **112,** B04107.

Thiede, R. C., Bookhagen, B., Arrowsmith, J. R., Sobel, E. R., and Strecker, M. R. (2004). Climatic control on rapid exhumation along the Southern Himalayan Front. *Earth and Planetary Science Letters* **222,** 791-806.

Thiede, R. C., Ehlers, T. A., Bookhagen, B., and Strecker, M. R. (2009). Erosional variability along the northwest Himalaya. *Journal of Geophysical Research-Earth Surface* **114**.

Thomson, S. N., Brandon, M. T., Tomkin, J. H., Reiners, P. W., Vasquez, C., and Wilson, N. J. (2010). Glaciation as a destructive and constructive control on mountain building. *Nature* **467,** 313-317.

Trull, T. W., Kurz, M. D., and Jenkins, W. J. (1991). Diffusion of cosmogenic ^{3}He in olivine and quartz - Implications for surface exposure dating. *Earth and Planetary Science Letters* **103,** 241-256.

Valla, P. G., Shuster, D. L., and van der Beek, P. A. (2010). Significant increase in relief of the European Alps during mid-Pleistocene glaciations. *Nature Geoscience* **4,** 688-692.

van der Beek, P., Robert, X., Mugnier, J.-L., Bernet, M., Huyghe, P., and Labrin, E. (2006). Late Miocene – Recent exhumation of the central Himalaya and recycling in the foreland

basin assessed by apatite fission-track thermochronology of Siwalik sediments, Nepal. *Basin Research* **18,** 413-434.

Vannay, J. C., Grasemann, B., Rahn, M., Frank, W., Carter, A., Baudraz, V., and Cosca, M. (2004). Miocene to Holocene exhumation of metamorphic crustal wedges in the NW Himalaya: Evidence for tectonic extrusion coupled to fluvial erosion. *Tectonics* **23**.

von Blanckenburg, F. (2005). The control mechanisms of erosion and weathering at basin scale from cosmogenic nuclides in river sediment. *Earth and Planetary Science Letters* **237,** 462-479.

Whipple, K. X., and Meade, B. J. (2006). Orogen response to changes in climatic and tectonic forcing. *Earth and Planetary Science Letters* **243,** 218-228.

Whipple, K. X. (2009). The influence of climate on the tectonic evolution of mountain belts. *Nature Geoscience* **2,** 97-104.

Willenbring, J. K., and von Blanckenburg, F. (2010). Long-term stability of global erosion rates and weathering during late-Cenozoic cooling. *Nature* **465,** 211-214.

Willenbring, J. K., Codilean, A. T., and McElroy, B. (2013). Earth is (mostly) flat: Apportionment of the flux of continental sediment over millennial time scales. *Geology* **41,** 343-346.

Willett, S. D. (1999). Orogeny and orography: The effects of erosion on the structure of mountain belts. *Journal of Geophysical Research - Solid Earth* **104,** 28957-28981.

Willett, S. D. (2010). Late Neogene Erosion of the Alps: A Climate Driver? *In* "Annual Review of Earth and Planetary Sciences, Vol 38." pp. 411-437. Annual Review of Earth and Planetary Sciences.

Wittmann, H., Von Blanckenburg, F., Guyot, J. L., and Kubik, P. W. (2007a). Modeling cosmogenic nuclide accumulation during sediment transport in the upper Amazon basin. *Geochimica Et Cosmochimica Acta* **71,** A1122-A1122.

Wittmann, H., von Blanckenburg, F., Kruesmann, T., Norton, K. P., and Kubik, P. W. (2007b). Relation between rock uplift and denudation from cosmogenic nuclides in river sediment in the Central Alps of Switzerland. *Journal of Geophysical Research-Earth Surface* **112**.

Wittmann, H., von Blanckenburg, F., Guyot, J. L., Maurice, L., and Kubik, P. W. (2009a). From source to sink: Preserving the cosmogenic Be-10-derived denudation rate signal of the Bolivian Andes in sediment of the Beni and Mamore foreland basins. *Earth and Planetary Science Letters* **288,** 463-474.

Wittmann, H., von Blanckenburg, F., Maurice, L., Guyot, J. L., and Kubik, P. W. (2009b). Recycling of Amazon floodplain sediment quantified by cosmogenic 26Al and 10Be. *Geology* **39,** 467-470.

Wittmann, H., von Blanckenburg, F., Guyot, J. L., Laraque, A., Bernal, C., and Kubik, P. W. (2011). Sediment production and transport from in situ-produced cosmogenic Be-10 and river loads in the Napo River basin, an upper Amazon tributary of Ecuador and Peru. *Journal of South American Earth Sciences* **31,** 45-53.

Wobus, C. W., Hodges, K. V., and Whipple, K. X. (2003). Has focused denudation sustained active thrusting at the Himalayan topographic front? *Geology* **31,** 861-864.

Yanites, B. J., Tucker, G. E., and Anderson, R. S. (2009). Numerical and analytical models of cosmogenic radionuclide dynamics in landslide-dominated drainage basins. *Journal of Geophysical Research-Earth Surface* **114**.

Zachos, J., Pagani, M., Sloan, L., Thomas, E., and Billups, K. (2001). Trends, rhythms, and aberrations in global climate 65 Ma to present. *Science* **292,** 686-693.

Zhang, P. Z., Molnar, P., and Downs, W. R. (2001). Increased sedimentation rates and grain sizes 2-4 Myr ago due to the influence of climate change on erosion rates. *Nature* **410,** 891-897.

Et ce fut tout.

G. Flaubert,
L'éducation sentimentale.

Annexes

Annexe A

Code Matlab® de calcul des paléo-taux de dénudation

```
%CE PROGRAMME CALCULE UNE PALEOEROSION A PARTIR D'UNE MATRICE DE DONNEES
%(CONCENTRATION EN COSMO, TAUX D'ACCUMULATIONS, AGES) ET D'UNE MATRICE DE
% PARAMETRE FIXES
%(TAUX DE PRODUCTION...), ET ESTIME SON ERREUR ASSOCIEE A PARTIR DES
%ERREURS SUR CHAQUE PARAMETRES PAR SIMULATION DE M.-CARLO.


close all;
clear all;

%Pour plus de détails sur les paramètres et données en input, cf
%solve_paleroero.m

%EntrÈe= matrice x:10 (colonnes:
%Nmes, ls_Mes, Accun, ls.., Accum1, ls..., Accum2, ls.., t, s_t)

Dat=load('Donnees_zonedetude.txt');
[a,b]=size(Dat);

Const=load('Constantes_zonedetude.txt');

Paleoero=zeros(a,3);

% DÈfinition des paramètres fixes et de leurs incertitudes
%/! A rentrer dans cet ordre

fnmean = Const(1,1);
s_fnmean = Const(1,2);

fm1mean = Const(2,1);
s_fm1mean = Const(2,2);

fm2mean = Const(3,1);
s_fm2mean = Const(3,2);

fn = Const(4,1);
s_fn = Const(4,2);

fm1 = Const(5,1);
s_fm1 = Const(5,2);

fm2 = Const(6,1);
s_fm2 = Const(6,2);

ro = Const(7,1);
s_ro = Const(7,2);

rosed = Const(8,1) ;
s_rosed = Const(8,2);

Pn = Const(9,1);
s_Pn = Const(9,2);

Ln = Const(10,1);
s_Ln = Const(10,2);

Pm1 = Const(11,1);
s_Pm1 = Const(11,2);

Lm1 = Const(12,1);
s_Lm1 = Const(12,2);

Pm2 = Const(13,1);
s_Pm2 = Const(13,2);

Lm2 = Const(14,1);
s_Lm2 = Const(14,2);


% Choisir le Lambda adapté:
%10Be 4.997e-7
%26Al 9.6673e-7
%3He ou 21Ne = 0

lamb = 4.997e-7;


for i=1:a

   clear W
   clear ero

% Données entrées en matrice

Nmes = Dat(i,1);
% Concentration isotopes cosmo mesurée :
%/!\ A CORRIGER,EN AMONT,DE L'EXPOSITION MODERNE

s_Nmes = Dat(i,2); % Incertitudes

Accun = Dat(i,3);    %taux d'accu pris pour spalla
s_Accun = Dat(i,4);

Accum1 = Dat(i,5);   %taux d'accu pour fast muons
s_Accum1 = Dat(i,6);

Accum2 = Dat(i,7);   % taux d'accu pour slow muons
s_Accum2 = Dat(i,8);

t = Dat(i,9);
s_t = Dat(i,10);




% Nbre de tirages
n = 10000;
k = 0;

%Initiallisation de la résolution: on utilise ici une equation simplifiée,
%sans les muons

Ini = (Ln/ro)*...
    (fnmean*Pn*exp(-lamb*t)/...
    (Nmes-(fn*Pn/(lamb-Accun*rosed/Ln)*(exp(-t*Accun*rosed/Ln)-exp(-lamb*t))))-↙
lamb);

for j = 1:n

% Tirage aléatoire des paramètres
```

```
%toutes les petites boucles de condition while <0 pour éviter les tirages
%négatifs (absurdes physiquement)

    Nmesx = normrnd(Nmes,s_Nmes);
     while Nmesx < 0 do
        Nmesx= normrnd(Nmes,s_Nmes);
     end_while

    fnmeanx = normrnd(fnmean, s_fnmean);
     while fnmeanx < 0 do
fnmeanx = normrnd(fnmean, s_fnmean);
     end_while

    fm1meanx = normrnd(fm1mean, s_fm1mean);
     while fm1meanx < 0 do
        fm1meanx= normrnd(fm1mean, s_fm1mean);
     end_while

    fm2meanx = normrnd(fm2mean, s_fm2mean);
     while fm2meanx < 0 do
        fm2meanx= normrnd(fm2mean, s_fm2mean);;
    end_while

    fnx = normrnd(fn,s_fn);
     while fnx < 0 do
        fnx= normrnd(fn,s_fn);
     end_while

    fm1x = normrnd(fm1,s_fm1);
     while fm1x < 0 do
        fm1x= normrnd(fm1,s_fm1);
     end_while

    fm2x = normrnd(fm2,s_fm2);
     while fm2x < 0 do
        fm2x= normrnd(fm2,s_fm2);
    end_while

    rox = normrnd(ro,s_ro);
     while rox < 0 do
        rox= normrnd(ro,s_ro);
     end_while

    rosedx = normrnd(rosed,s_rosed);
     while rosedx < 0 do
        rosedx= normrnd(rosed,s_rosed);
    end_while

    Pnx = normrnd(Pn,s_Pn);
     while rosedx < 0 do
        rosedx= normrnd(Pn,s_Pn);
    end_while

    Lnx = normrnd(Ln,s_Ln);
     while rosedx < 0 do
        rosedx= normrnd(Ln,s_Ln);
     end_while

     Pm1x = normrnd(Pm1,s_Pm1);
     while Pm1x < 0 do
        Pm1x= normrnd(Pm1,s_Pm1);
     end_while

    Lm1x = normrnd(Lm1,s_Lm1);
     while Lm1x < 0 do
        Lm1x= normrnd(Lm1,s_Lm1);
    end_while

    Pm2x = normrnd(Pm2,s_Pm2);
     while Pm2x < 0 do
        Pm2x= normrnd(Pm2,s_Pm2);
     end_while

    Lm2x = normrnd(Lm2,s_Lm2);
     while Lm2x < 0 do
        Lm2x= normrnd(Lm2,s_Lm2);
     end_while

    Accunx = normrnd(Accun, s_Accun);
    while Accunx < 0 do
        Accunx= normrnd(Accun, s_Accun);
    end_while

    Accum1x = normrnd(Accum1, s_Accum1);
    while Accum1x < 0 do
        Accum1x= normrnd(Accum1, s_Accum1);
    end_while

    Accum2x = normrnd(Accum2, s_Accum2);
    while Accum2x < 0 do
        Accum2x= normrnd(Accum2, s_Accum2);
    end_while

    tx = normrnd(t, s_t);
     while tx < 0 do
        tx= normrnd(t, s_t);
    end_while

    %Resolution numérique (fontion solve_paleoero)

    option = optimset('MaxFunEvals',10000, 'MaxIter', 10000, 'Display', 'off');

    [X,FVAL] = fzero(@solve_paleoero, Ini, option,...
        Nmesx, Accunx, Accum1x, Accum2x, tx,...
        fnmeanx, fm1meanx,fm2meanx, fnx, fm1x, fm2x,...
        lamb,...
        rox, rosedx, ...
        Pnx, Lnx, Pm1x, Lm1x, Pm2x, Lm2x);

    if X > 0
        k=k+1;
    ero(k,1) =  X;
       end

end

W=exist('ero','var');

% Conversion en m/Ma
% condition de vérification qu'au moins une solution a été trouvée. Sinon, la
```

```
valeur 99999 est retournée
240
241 if W==0
242     ero=99999;
243
244 else
245     ero = 1e4.*ero;
246 end
247
248 e=size(ero);
249 M=mean(ero);
250
251 %Pour séparer les erreurs + et -
252 clear plus
253 clear moins
254
255 p=1;
256 m=1;
257 for l=1:e;
258
259     if W==0
260         plus=0;
261         moins=0;
262     else
263 if ero(l,1)>M
264     plus(p,1)=(ero(l,1)-M)^2;
265     p=p+1;
266 else moins(m,1)=(M-ero(l,1))^2;
267     m=m+1;
268 end
269     end
270 end
271
272 %Creation de la matrice de résultats
273
274 Paleoero(i,1) = M;
275 Paleoero(i,2)=sqrt(mean(plus));
276 Paleoero(i,3)=sqrt(mean(moins));
277
278 %Optionnel : afficher les distributions des solutions pour chaque échantillon
279 figure
280 hist(ero, 100);
281     end
282
283 %Ecriture d'un fichier texte en sortie
284 dlmwrite('Paleo_zonedetude.txt', Paleoero)
285
286
287
```

```
1 function s = solve_paleoero(ero,  Nmes, Accun, Accum1, Accum2, t,...
2         fnmean, fm1mean,fm2mean, fn, fm1, fm2,...
3         lamb,...
4         ro, rosed, ...
5         Pn, Ln, Pm1, Lm1, Pm2,Lm2)
6
7 % Equation de Lal 1991 à l'Èquilibre sÈculaIre +Equation production dans
8 % un sÈdiment en accumulation
9 %
10 % Inputs :
11 %       * Nmes : concentration (at/g)
12 %       * f : Facteur de correction gÈographique incluant altitude, masque,
13 %               végétation...
14 %
15 %           fn : pour spallation à l'endroit du dÈpot,
16 %           fm1 : pour fast muons à l'endroit du dÈpot
17 %           fm2 : pour slow muons à l'endroit du dÈpot
18 %           f...mean : idem, moyenne pour le bassin versant
19 %
20 %       * lamb : constante de dÈsintÈgration radioactive (an-1)
21 %       * ro : densitÈ de la roche mÈre (g.cm-3)
22 %           rosed : densitÈ du sÈdiment (g.cm-3)
23 %       * Pn : taux de production SLHL spallation (at.g-1.an-1)
24 %       * Pm1 : taux de production SLHL muons rapides
25 %       * Pm2 : taux de production SLHL muons lents
26 %       * Lm1 : longueur d'attÈnuation muons rapides (g.cm-2)
27 %       * Lm2 : longueur d'attÈnuation muons lents
28 %       * Accun, Accum1, Accum2: taux d'accumulation du sÈdiment pris en
29 %       compte pour spallation, fats muons, slow muons (cm/an)
30 %       * ero: erosion moyenen du bassin (cm/an)
31 %       * t : age du dÈpot (an)
32 %
33
34 N = (((fnmean*Pn/(ro*ero/Ln))...
35     + (fm1mean*Pm1/(ro*ero/Lm1))...
36     + (fm2mean*Pm2/(ro*ero/Lm2)))*exp(-lamb*t))...
37     + (...
38     (fn*Pn/(lamb-Accun*rosed/Ln)*(exp(-t*Accun*rosed/Ln)-exp(-lamb*t)))...
39     +(fm1*Pm1/(lamb-Accum1*rosed/Lm1)*(exp(-t*Accum1*rosed/Lm1)-exp(-lamb*t)))...
40     +(fm2*Pm2/(lamb-Accum2*rosed/Lm2)*(exp(-t*Accum2*rosed/Lm2)-exp(-lamb*t))));
41
42 s = N - Nmes;
43
44
45
```

Annexe B

Article paru dans la revue Géochronique

(Société géologique de France, 2012)

La thermochronologie comporte des méthodes mises au point depuis une trentaine d'années et en constante évolution. La combinaison de ces méthodes avec des outils de modélisation numérique et le développement de nouvelles méthodes comme le 3He/4He (ou la thermochronologie OSL) permettent maintenant de les utiliser d'une façon beaucoup plus quantitative, de tester des hypothèses et scénarios tectoniques et morphologiques et de tracer l'évolution du relief au cours du temps géologique.

P. VAN DER BEEK et J. BRAUN

Les nucléides cosmogéniques : traceurs à haute résolution des taux d'érosion au cours du temps

La dénudation (somme de l'érosion physique et de l'altération chimique) des reliefs joue un rôle majeur dans l'amplification ou la régulation des interactions entre tectonique et climat. Ainsi, la dénudation contrôle à la fois l'isostasie et la structure thermique d'un orogène, et, de fait, la réponse tectonique associée. De plus, l'érosion physique et l'altération chimique des silicates calciques, sont présentées par plusieurs auteurs comme des acteurs prépondérants du cycle du carbone à l'échelle des temps géologiques, contribuant ainsi à refroidir le climat (France-Lanord et Derry, 1997 ; Raymo et Ruddiman, 1992). À l'inverse, le climat joue aussi un rôle prépondérant sur ces mécanismes de destruction des orogènes. Pour mieux comprendre l'amplitude et le sens des rétroactions reliant tectonique, érosion et climat, il est fondamental d'établir une meilleure quantification des flux de dénudation régionaux et globaux au cours de milliers voire de millions d'année. En effet, ce sont sur ces échelles de

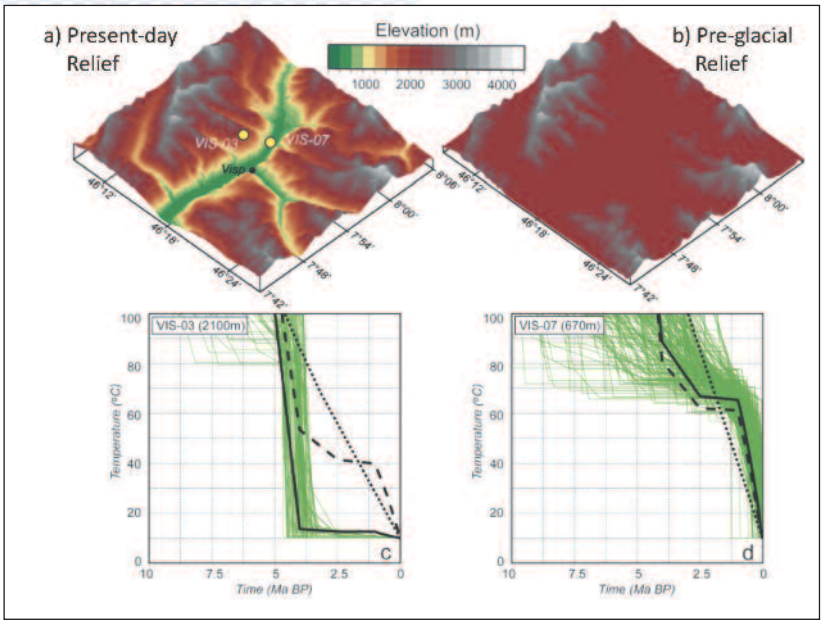

Fig. 1-6. – Évolution de la vallée du Rhône (Valais suisse) contraint par des données 3He/4He sur apatite (fig. modifiée de Valla et al., 2011). En bas, les chemins de refroidissement permis par les données 3He/4He sont indiqués en vert pour un échantillon (VIS-03) provenant d'une altitude élevée et un autre (VIS-07) du fond de vallée (voir la topographie actuelle avec les lieux d'échantillonnage en haut à gauche). En noir, les chemins prédits par des modélisations Pecube : en pointillé pour une vitesse d'exhumation constante sous un relief fixe ; en tirets pour une histoire impliquant deux phases d'exhumation séparées par une période stable sous un relief fixe ; en continu pour une phase d'exhumation rapide entre 4 et 5 Ma suivie par un creusement de la vallée depuis 1 Ma ; seul ce dernier scénario permet d'expliquer à la fois les données de haute altitude et du fond de la vallée. En haut à droite : la topographie pré-glaciaire prédite par le modèle.

temps que se sont produits les changements climatiques majeurs (apparition des glaciations à la transition Plio-Pléistocène il y a environ 2,5 Ma, cycles glaciaire-interglaciaire de Milankovitch, variabilité rapide de la circulation océanique, phénomènes de mousson) ou tectoniques (accélération ou ralentissement d'une collision entre continents, élévation d'une montagne offrant une barrière aux masses d'air). Même si les sédiments, produits de la dénudation, recouvrent une grande partie des surfaces continentales et des fonds marins, il reste paradoxalement très difficile de quantifier les taux de dénudation à l'échelle des temps géologiques.

Plusieurs auteurs ont ainsi essayé de déterminer les taux de dénudation en calculant les volumes de sédiments accumulés dans les bassins. Par cette approche, Zhang *et al.* (2001) sont par exemple arrivés à la conclusion que les taux de dénudation ont significativement augmenté à l'échelle globale depuis 2,5 Ma, au moment de l'apparition des glaciations du Quaternaire.

Cependant, si l'accélération est réelle dans de nombreux bassins, elle peut aussi être expliquée par une simple baisse du niveau marin, qui aurait engendré une re-mobilisation du matériel détritique meuble stocké sur les marges continentales nouvellement émergées. Les enregistrements sédimentaires en domaine continental ne sont pas sensibles à cet artefact. Mais, dans ce cas, du fait de l'absence de marqueurs biostratigraphiques, la chronologie est souvent plus difficile à établir. Ainsi, la compilation des volumes sédimentaires réalisée par Zhang *et al.* (2001) repose en grande partie sur des

séries d'Asie centrale dont les datations ont longtemps été incertaines, et qui ont largement été remises en cause depuis Charreau *et al.* (2009). De plus, il est très difficile d'estimer de façon fiable les volumes de sédiments dans les bassins car la géométrie en trois dimensions des dépôts sédimentaires est souvent difficile à déterminer (Métivier, 2002). Ceci nécessite des forages et des coupes sismiques sériées très coûteux à produire.

Plusieurs chercheurs ont donc essayé de développer des méthodes alternatives plus intégratives. Par exemple, l'analyse du rapport $^{9}Be/^{10}Be$ dans les sédiments océaniques représente d'après (Willenbring et von Blanckenburg, 2010), un traceur géochimique de l'altération continentale. Leurs résultats vont à l'encontre des conclusions de Zhang *et al.* (2001), puisqu'ils suggèrent une stabilité de l'altération au cours du Cénozoïque. Cependant, cette approche se limite à l'altération chimique et ne permet pas de quantifier dans son ensemble la dénudation.

C'est pourquoi une méthode beaucoup plus directe commence à être développée avec des résultats préliminaires très prometteurs. Il s'agit d'appliquer à des séries sédimentaires anciennes un des outils les plus fiables pour quantifier les processus de surface : les nucléides cosmogéniques *in situ* (*cf* Godard *et al.*, dans ce dossier). Ces isotopes créés par l'interaction des rayons cosmiques avec les roches de la surface terrestre permettent en effet de quantifier le taux de dénudation moyen d'un bassin versant. Ainsi, plus une roche est exposée longtemps à la surface, plus sa concentration en isotopes cosmogéniques est élevée. La quantité d'isotopes cosmogéniques présents dans les sédiments est donc fonction du taux d'érosion. Cette méthode est déjà utilisée en routine dans les sédiments modernes de rivière. En étant appliquée à des sédiments anciens, celle-ci permet théoriquement de quantifier les paléo-taux de dénudation au moment du dépôt (fig. 1-7).

Cependant, il n'est pas interdit d'étendre cette méthode à l'étude de sables âgés de plusieurs milliers ou millions d'années. Les deux isotopes les plus couramment utilisés sont le ^{10}Be et le ^{26}Al. En effet, ils ont l'avantage d'être complètement retenus dans le quartz – un minéral résistant à l'altération et ubiquiste à la surface de la Terre – et, d'autre part, leur production étant uniquement d'origine cosmogénique, leur concentration ne dépend pas d'autres sources, comme dans le cas des gaz rares cosmogéniques (^{3}He et ^{21}Ne). En revanche, contrairement à ces deux derniers isotopes, ^{10}Be et ^{26}Al sont radioactifs et décroissent avec des demi-vies de ~1,4 Ma et ~0,72 Ma, respectivement. On ne peut donc pas les utiliser pour des sédiments plus âgés que ~10 Ma, et ce seulement pour des taux d'érosion faible (< 0,5 $mm.a^{-1}$), sans quoi les concentrations sont en dessous des limites de détection instrumentales.

À cette limite purement analytique s'ajoutent d'autres complications d'ordre géologique. Tout d'abord, la concentration en isotopes cosmogéniques d'un sable est fonction du taux de production de ces isotopes sur le bassin versant étudié, taux qui dépend de son altitude. Il faut donc s'assurer que celle-ci n'a pas changé significativement sur la période de temps considérée. Ensuite, contrairement aux sables de rivières actuelles, les sédiments continentaux anciens ont pu avoir été réexposés au rayon-

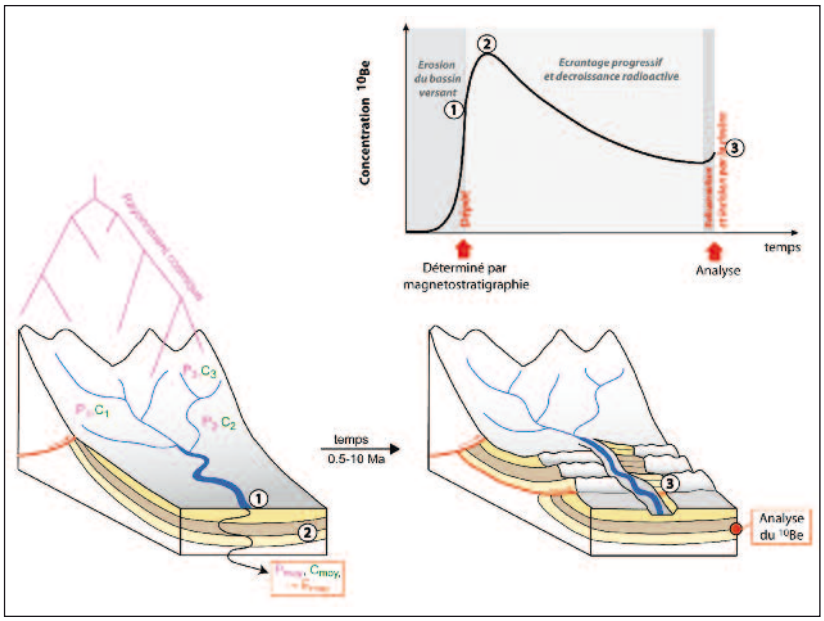

Fig. 1-7. – Schéma de l'évolution de la concentration en isotopes cosmogéniques dans une série sédimentaire.

1) - Érosion des versants. Chaque roche de surface est exposée au rayonnement cosmique et se charge d'une concentration C en isotopes cosmogéniques à un taux P dépendant de l'altitude. Des grains de ces roches provenant de tout le bassin versant sont ensuite mélangés par la rivière puis déposés dans un bassin sédimentaire.

2) - Le sable est enfoui progressivement sous d'autres sédiments, accumulant encore un peu d'isotopes cosmogéniques, et simultanément la concentration décroît avec la désintégration radioactive de ceux-ci.

3) - Les séries sédimentaires sont tectonisées et incisées rapidement par les rivières ou les constructions humaines. On peut ainsi échantillonner un enregistrement continu de paléo-sables, et remonter après corrections à la concentration moyenne au moment du dépôt, et donc au paléo-taux de dénudation.

nement cosmique postérieurement à leur érosion sur le bassin versant, soit au moment de leur dépôt, avant qu'ils ne soient totalement enfouis sous d'autres sédiments, soit lors de l'exhumation à la surface par l'effet combiné de l'incision des rivières et du soulèvement tectonique. Toutes ces complications liées à un "réenrichissement" potentiel en isotopes cosmogéniques sont donc sources d'incertitude. Il faut par conséquent pouvoir les minimiser et dans tous les cas les quantifier.

Pour cela, il faut privilégier les échantillons les plus récemment exposés à l'affleurement ou les mieux "écrantés" (enfouis). Les sédiments marins obtenus à partir des forages océaniques ne souffrent pas de ces inconvénients, l'écrantage total est immédiat et il n'y pas de réexposition postérieure au dépôt. Cependant, il est plus difficile d'obtenir des carottes marines dans des faciès ayant une granulométrie adéquate. Les séries continentales, dont la granulométrie est souvent plus grossière, sont en cela plus adaptées à la mesure des isotopes cosmogéniques. De plus, elles constituent des enregistrements indépendants des variations eustatiques. Les séries à fort taux de sédimentation sont les plus prometteuses, non seulement parce qu'elles permettent un échantillonnage à haute résolution temporelle, mais aussi parce que, dans ce cas, l'exposition syn-dépôt est la plus faible.

Les études pionnières ont porté sur l'évolution des taux de dénudation au cours des derniers cycles glaciaires-interglaciaires. Cependant, ces travaux ont été menés sur des terrasses alluviales, qui représentent des enregistrements discrets au cours du temps (Schaller *et al.*, 2004). La méthode donnera des résultats plus complets si elle est appliquée à des séries plus anciennes, continues dans le temps, qu'il s'agisse de sédiments exhumés à la faveur de la tectonique, ou de carottage dans les bassins sédimentaires et les cônes alluviaux.

Ainsi, nous poursuivons actuellement l'analyse de sédiments provenant des piémonts de la chaîne du Tianshan, en Asie centrale. Ces séries, dont l'âge de dépôt est déterminé par magnétostratigraphie entre 0,5 et 20 Ma (Charreau *et al.*, 2005), sont situées dans une zone intracontinentale clé pour l'étude des couplages entre tectonique, climat et érosion au cours de la fin du Néogène. Si les premiers résultats issus du Tianshan suggéraient une augmentation transitoire de la dénudation au moment de la transition climatique du Plio-Pleistocène (Charreau *et al.*, 2011), l'étude de nouveaux bassins versants de la région ne montre, au contraire, pas d'augmentation synchrone (Puchol *et al.*, in prep). Les isotopes cosmogéniques semblent donc mettre à mal un paradigme vieux de 10 ans, faisant ainsi la preuve qu'ils peuvent apporter beaucoup d'informations de premier ordre à la compréhension des paléo-processus de surface. Reste à les appliquer sur d'autres sites dans le monde, soumis à d'autres conditions climatiques ou tectoniques.

N. PUCHOL, P.-H. BLARD,
J. CHARREAU, R. PIK

Mesure de la dénudation des bassins versants par les nucléides cosmogéniques

Problématique

La surface topographique terrestre est l'interface où se fait la rencontre et l'interaction entre les processus internes (tectonique) et externe (climat) par le biais de la dénudation (érosion). Comprendre les modalités de cette dénudation nécessite des outils permettant d'en quantifier précisément la vitesse dans différents types d'environnements géomorphologiques.

Plusieurs types d'outils sont disponibles pour permettre cette quantification, depuis le très court terme avec, par exemple, les mesures de flux de sédiments charriés par les rivières à l'échelle de quelques années, jusqu'au très long terme avec, par exemple, la thermochronologie qui quantifie les vitesses de refroidissement des roches pendant leur exhumation vers la surface à l'échelle de plusieurs millions d'années. Entre ces gammes de temps se trouve l'intervalle 1 000-100 000 ans qui a une importance particulière, car il correspond à l'échelle de temps de nombreux processus climatiques (oscillations quaternaires,…) et tectoniques (cycle sismique, croissance de la topographie,…). Il est donc crucial de disposer d'outils spécifiques permettant de mesurer les vitesses de dénudation intégrées sur ces échelles de temps.

Méthode

Les nucléides cosmogéniques, tels que le ^{10}Be, sont des isotopes rares, produits en permanence dans la croûte terrestre et l'atmosphère par l'interaction du rayonnement cosmique avec la matière. Au sein des roches cette production, qui est infime (de l'ordre de quelques atomes à quelques centaines d'atomes par an et par gramme de matière), se fait principalement dans les 2-3 premiers mètres sous la surface. Ainsi, plus une roche présentera une concentration élevée en ^{10}Be et plus elle aura résidé longtemps dans cette portion superficielle. La mesure de cette concentration dans un échantillon collecté sur le terrain va donc fournir des informations sur la durée d'exposition de cette roche à la surface ou sur la vitesse des processus de dénudation qui ont permis de l'y amener.

Les taux de dénudation ainsi obtenus n'ont toutefois qu'une valeur loca-

Annexe C

Article sur la section Kuitun

(Earth and Planetary Science Letters, 2011)

Earth and Planetary Science Letters 304 (2011) 85–92

Contents lists available at ScienceDirect

Earth and Planetary Science Letters

journal homepage: www.elsevier.com/locate/epsl

Paleo-erosion rates in Central Asia since 9 Ma: A transient increase at the onset of Quaternary glaciations?

J. Charreau [a,*,1], P.-H. Blard [a,1], N. Puchol [a,1], J.-P. Avouac [b,2], E. Lallier-Vergès [c], D. Bourlès [d], R. Braucher [d], A. Gallaud [c], R. Finkel [d,e], M. Jolivet [f], Y. Chen [c], P. Roy [a]

[a] Centre de Recherche Pétrographique et Géochimique, 15 rue Notre Dame des Pauvres, B.P. 20, 54501 Vandoeuvre lès Nancy, France
[b] Tectonics Observatory, California Institute of Technology; Mail Code 100–23, Pasadena CA 91125, United States
[c] Institut des Sciences de la Terre d'Orléans; Bâtiment Géosciences, rue de Saint Amand, BP 6759, 45067 Orléans Cedex 2, France
[d] Centre Européen de Recherche et d'Enseignement des Géosciences de l'Environnement, Europole Méditerranéen de l'Arbois BP 80 13545 Aix-en-Provence Cedex 4, France
[e] Earth and Planetary Science Department, University of California, Berkeley, Berkeley CA, United States
[f] Géosciences Rennes (UMR CNRS 6118), Université de Rennes1, Bâtiment 15, Campus de Beaulieu, CS 74205, F-35042 Rennes Cedex, France

ARTICLE INFO

Article history:
Received 6 December 2010
Received in revised form 18 January 2011
Accepted 18 January 2011
Available online 20 February 2011

Editor: T.M. Harrison

Keywords:
Quaternary glaciation
erosion rates
Tianshan
cosmogenic nuclide
magnetostratigraphy
^{10}Be

ABSTRACT

Erosion is a fundamental player of the interactions existing between internal geodynamics and climate, in particular through its influence on the carbon dioxide budget. However, long term (>1 Ma) erosion rates, estimated indirectly from sediment budget, remain poorly constrained. While some studies suggest that worldwide erosion rates increased at the Plio-Pleistocene climatic transition (~4–2 Ma), the validity of this observation and its significance is a matter of debate due to potential biases of the sedimentary record and to the influence of sea level fall on the global sedimentary flux to marginal basins. In the present study, we estimate erosion rates over the last ~9 Ma using in situ produced cosmogenic ^{10}Be concentrations measured in magnetostratigraphically dated continental sediments. We focus on an intracontinental endorheic watershed draining the northern Tianshan in Central Asia, a key region regarding the ongoing debate. While erosion rates between 0.1 and 1 mm·yr^{-1} are derived from most of our record, they reach values as high as ~2.5 mm·yr^{-1} from 2.5 to 1.7 Ma. Then, after 1.7 Ma, recent and modern erosion rates fell below 1 mm·yr^{-1}. This temporary increase is correlated with the onset of Quaternary ice ages and suggests that global climate had a significant and transient impact on erosion.

1. Introduction

Erosion is a key factor governing the evolution of the Earth's surface evolution and provides a source of multiple feedback mechanisms linking climate and tectonics (France-Lanord and Derry, 1997; Molnar, 2004; Raymo and Ruddiman, 1992). First, erosion controls mass transfer from uplifting highlands. The ensuing redistribution of mass influences isostatic compensation in a way that induces tectonic deformation (Dahlen and Suppe, 1988; Whipple and Meade, 2006; Willett and Brandon, 2002). The resulting vertical movement of mass affects the thermal structure of the crust and hence its rheology (Avouac and Burov, 1996; Zeitler et al., 2001). Second, erosion is considered as a first order driving mechanism of the Earth's climate at the geological time scales because of its potential impact on atmospheric CO_2 through the creation of new surfaces enabling silicate weathering (Berner et al., 1983) but also because of its influence on the mechanical burial of organic carbon (Galy et al., 2007). Quantitative records of past erosion rates over geological time scales are thus of major importance to untangle the complex interactions between tectonics, climate and surface processes. Importantly, records of erosion rate over the last 10 Ma are crucial for addressing the respective causes and effects of glacial cycles that were initiated at the Cenozoic–Quaternary boundary.

Some authors (Molnar, 2004; Zhang et al., 2001) have reported a worldwide acceleration in accumulation rates at the Plio-Pleistocene transition (2–4 Ma) (Fig. 1) that they link to enhanced erosion. This finding, which suggests a major influence of Quaternary glaciation on global erosion rates, has recently been questioned on the ground of a new global ^{10}Be/^{9}Be record (Willenbring and von Blanckenburg, 2010). Interpreted as a proxy of continental weathering, this ratio has remained nearly constant over the last 12 Ma which led Willenbring and von Blanckenburg (2010) to conclude that the global Quaternary cooling

* Corresponding author. Tel.: +33 383594227; fax: +33 383511798.
E-mail addresses: charreau@crpg.cnrs-nancy.fr (J. Charreau), blard@crpg.cnrs-nancy.fr (P.-H. Blard), puchol@crpg.cnrs-nancy.fr (N. Puchol), avouac@gps.caltech.edu (J.-P. Avouac), elisabeth.verges@univ-orleans.fr (E. Lallier-Vergès), bourles@cerege.fr (D. Bourlès), braucher@cerege.fr (R. Braucher), audrey.gallaud@gmail.com (A. Gallaud), finkel@cerege.fr (R. Finkel), marc.jolivet@univ-rennes1.fr (M. Jolivet), Yan.Chen@univ-orleans.fr (Y. Chen), Pierre.Roy@etudiant.ensg.inpl-nancy.fr (P. Roy).
[1] These authors contributed equally to this work.
[2] Tel.: +1 626 395 4239; fax: +1 626 395 1740.

0012-821X/$ – see front matter © 2011 Elsevier B.V. All rights reserved.
doi:10.1016/j.epsl.2011.01.018

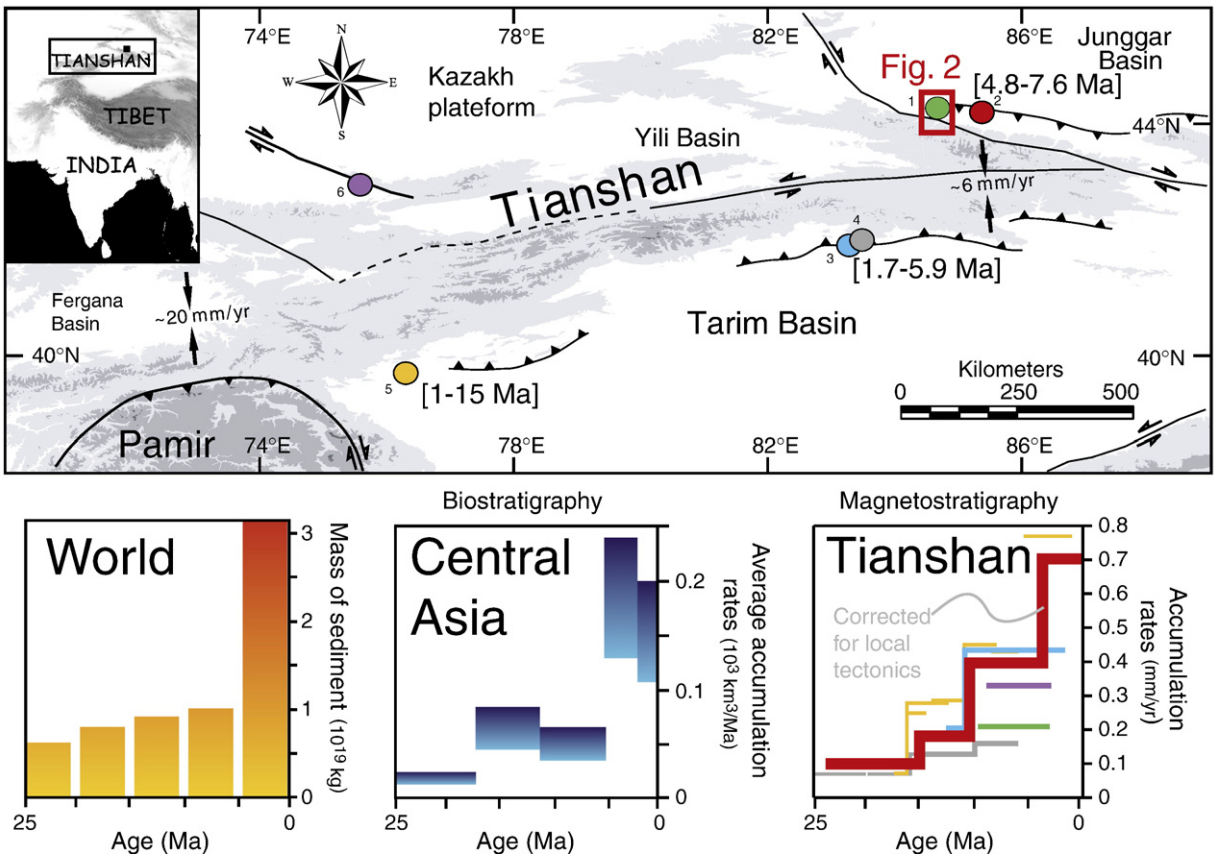

Fig. 1. Sediment flux and accumulation rates in Central Asia basins over the last 25 Myr. Topographic map of Central Asia with locations of all accumulation rate records derived from magnetostratigraphy in this region (see references in Charreau et al., 2009b). The basal age of the conglomeratic 'Xiyu' formation found at each of these locations is indicated in bracket (see references in Charreau et al., 2009b). At the bottom, from left to right, the evolution of sediment flux to basins for the world (Zhang et al., 2001), and Central Asia (Métivier and Gaudemer, 1997) and the accumulation rate records derived from magnetostatigraphy around the Tianshan (see references in Charreau et al., 2009b). The red box shows the location of Figure 2.

had no profound effect on global weathering rates. Moreover, erosion rates derived from sediment budgets suffer from drawbacks and potential flaws due to uncertainties on depositional ages in intracontinental areas (Charreau et al., 2009b), poor constraints on basin geometry (Clift, 2006) and inaccurate volume reconstruction methods (Métivier, 2002). Furthermore, the global sediment budget might actually be biased by the effect of the sea level drop during glacial times that remobilized loose sediments previously stored on the continental margins (Hay et al., 1988). Finally, the Quaternary increase of local accumulation rates could reflect an observational artifact, due to the increasing likelihood that sedimentary deposits will have been lost with the increasing age of the deposit (Sadler, 1999).

Central Asia stands out as a key area with regard to this debate. Indeed, because of its intracontinental endorheic setting, the sediment budget in this region is insensitive to global sea-level variations and can be constrained reasonably well from the closed basins systems (Fig. 1). The large Pleistocene increase of sediment flux to the basins reported in previous studies (Métivier and Gaudemer, 1997; Zhang et al., 2001) is therefore a key observation. However, these observations are also prone to hiatus artifacts and they relied heavily on the assumption that the widely distributed conglomeratic units, often referred to the Xiyu Formation, were regionally synchronous. Several magnetostratigraphic studies (Charreau et al., 2009b; Heermance et al., 2007) have however shown that the onset of formation of the Xiyu conglomerates is, in fact, diachronous, with ages ranging between 1 and 15 Ma (Fig. 1). Moreover, accumulation rates derived from these studies (Fig. 1) yield widely varying results for the 0–5 Ma period, probably because of tectonics modulation on the available space in the piedmont (Charreau et al., 2008).

In situ produced cosmogenic nuclide concentration in river sediments allow the derivation of average erosion rates within a given watershed (Brown et al., 1995, 1998), because at steady state, the nuclide concentration is inversely proportional to the denudation rate and because the river sediments have moreover the remarkable property to provide a spatially averaged erosion rate for the whole drainage basin (von Blanckenburg, 2005). This method has been successfully applied to determine erosion rates in a broad range of modern (von Blanckenburg, 2005) and relatively recent (less than ~1 Ma old) environments (Blard et al., 2006; Schaller et al., 2002). So far, only Refsnider (2010) using cosmogenic analysis of cave sediments has provided an estimate of erosion rate since 5 Ma, in the Rocky Mountains.

Here, we expand the method to longer geological records to infer erosion rates by measuring the fossil in situ produced cosmogenic signal in buried sediments along a magnetostratigraphically dated section (Charreau, 2005) from the North Tianshan Piedmont in Central Asia (Figs. 1 and 2). This record spans from 9 Ma to the present, a time period that is particularly relevant to address the feedbacks between long-term global climate, tectonics and erosion. This study moreover demonstrates the possibility of estimating past erosion rates combining cosmogenic analyses with magnetostratigraphic dating of sediments.

2. Geological settings and sampling

We analyze sediments from the Kuitun river watershed which drains the northern Tianshan shedding sediments to the Junggar foreland basin (Figs. 1 and 2). The Tianshan is a 2500-km-long

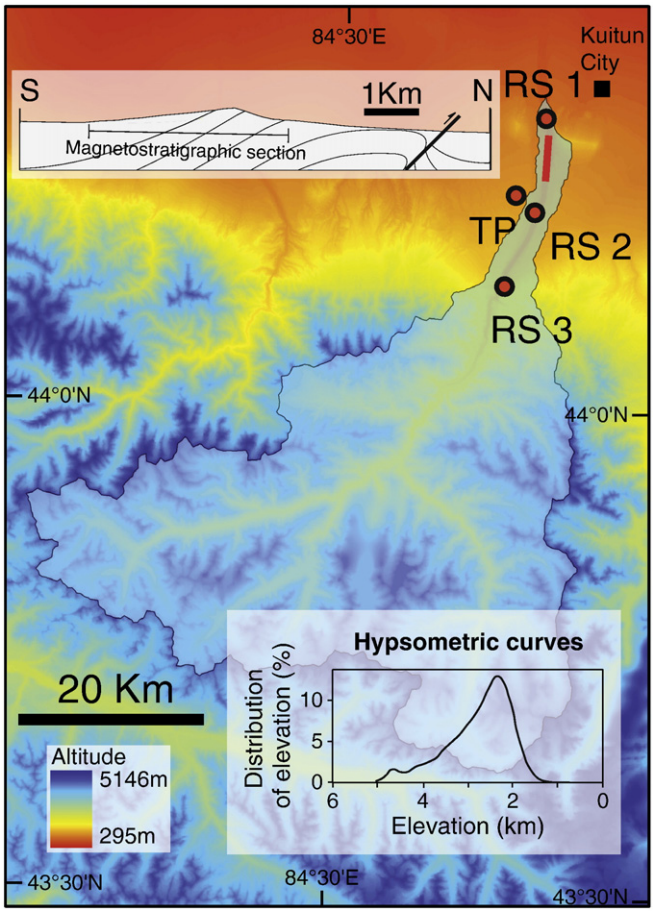

Fig. 2. Geographic and stratigraphic setting of the samples. Map of the Kuitun river's watershed area with location of the river sands (RS) and terrace profile (TP) cosmogenic samples. Red line AA' shows location of the magnetostratigraphic section where samples were also collected for cosmogenic analysis. Top: structural cross section of the Dushanzi anticline and extent of the magnetostratigraphic section. Right: magnetostratigraphic column of the Kuitun section and its correlation to the polarity reference scale with red stars indicating the stratigraphic position of the samples collected for cosmogenic analysis.

tectonically active mountain range that dominates Central Asia with an average altitude of 2500 m and summits reaching up to 7000 m. While its geology consists of mainly island arc rocks linked to a long-lived Paleozoic history of subduction/collision (Burtman, 1975; Charvet et al., 2007; Gao et al., 1998; Lin et al., 2008; Wang et al., 2008; Windley et al., 1990), the present high topography attests to a more recent and intense deformation. This later owes its origin to the Cenozoic reactivation of the range during the Oligocene to early Miocene (>16 Ma) (Avouac et al., 1993; Bullen et al., 2001, 2003; Charreau et al., 2005, 2006, 2009a; Dumitru et al., 2001; Sobel and Dumitru, 1997; Sobel et al., 2006; Windley et al., 1990; Yin et al., 1998), under the influence of the ongoing India–Asia collision. The Tianshan range indeed plays a major role in the India–Asia collision since it presently accommodates up to 40% of the total convergence between those two continents (Abdrakhmatov et al., 1996; Reigber et al., 2001). It is sandwiched between two large intracontinental basins (Fig. 1) filled by the eroded materials shed from the uplifting range. In the piedmonts, tectonic wedges constituted of numerous fold and thrust belts have overthrusted Lower Mesozoic to Quaternary sediments that were initially deposited in the foreland basin. Thanks to strong Holocene river entrenchment (Poisson and Avouac, 2004) into these piedmont fold-and-thrust belts, several exceptional sections are well exposed and now enable high resolution analysis of this thick and continuous sedimentary records.

Our study focuses on the 1.8-km-thick Kuitun section that is located near the Dushanzi city, 300 km west of Urumqi (Fig. 2). This location is very suitable because cosmogenic production due to recent exposure can be accurately quantified (Poisson and Avouac, 2004) and because depositional ages are independently well constrained by a magnetostratigraphic analysis (Charreau et al., 2005) that yielded ages from ~10.5 to ~1.5 Ma (Fig. 3). Magnetostratigraphic dating also permitted these authors to constrain the sediment accumulation rates between 0.12 and 0.46 mm/yr. This constraint is fundamental to estimate the cosmogenic production during sediment burial (see below).

Seventeen sandstone samples were collected along the freshly exposed outcrop of this Cenozoic section(Fig. 2), as well as three modern sands from the Kuitun river bed and a 150-cm-thick profile from a 15 ± 3 ka terrace (Molnar et al., 1994; Poisson and Avouac, 2004) (Fig. 2).

3. Methods and measurements

3.1. Cosmogenic isotopes in modern river sediments

At a single location i, in surficial rocks undergoing continuous thin-layers removal by erosion, the concentration (atom·g^{-1}) of cosmogenic isotopes N_i (e.g. ^{10}Be), is expressed by the following equation (Lal, 1991):

$$\varepsilon_i = \frac{\Lambda}{\rho}\left(\frac{P_i}{N_i} - \lambda\right), \quad (1)$$

where P_i (atom g^{-1} a^{-1}) is the surface production rate, Λ (g·cm^{-2}) the attenuation length, λ (a^{-1}) the radioactive decay constant of the nuclide, ε (cm·yr^{-1}) the erosion rate and ρ (g·cm^{-3}) the density. It must be noted that this equation is valid only if the surface exposure time is sufficiently long (i.e. $t >> 1/(\lambda + \varepsilon\rho/\Lambda)$ to have reached steady state and if the inherited cosmogenic concentration can be neglected.

Importantly, the cosmogenic nuclide concentration measured in river sands has the remarkable property of averaging the concentration of all surficial rocks outcropping in the drainage basin (Brown et al., 1995; von Blanckenburg, 2005). It is thus possible to determine the average erosion rate $\overline{\varepsilon}$ for a whole drainage basin by measuring the mean cosmogenic nuclide concentration $\overline{N}$ in river sand. Eq. (1) requires calculation of the average production rate $\overline{P}$ at the surface in the drainage basin. The modern production rate was calculated here using the present day watershed hypsometry by combining the S.R.T.M. (Shuttle Radar Topography Mission) D.E.M. (Digital Elevation Model) of the Kuitun watershed (Fig. 2) along with the geological map to precisely identify the altitude of quartz rock sources. A scaling factor multiplying the sea level production rate is associated to each altitude. The arithmetic mean of these scaling factors is 9.5 ± 0.7 for the whole drainage. The scaling factor is 1.9 ± 0.2 at the location of the sediment deposition. These values are obtained using the scaling scheme of Lal/Stone (Lal, 1991; Stone, 2000). The topographic shielding was also considered using the S.R.T.M D.E.M and following Dunne et al. (1999).

3.2. Cosmogenic isotopes in buried sediments

Deriving erosion rates from cosmogenic isotopes in an old sedimentary sequence requires knowledge of: i) the age of deposition of the studied sedimentary archive, ii) the cosmogenic paleo-production rate of the whole drainage basin at the time of deposition and iii) the build-up of cosmogenic nuclides between the times of sediment deposition and sample collection (Fig. 4).

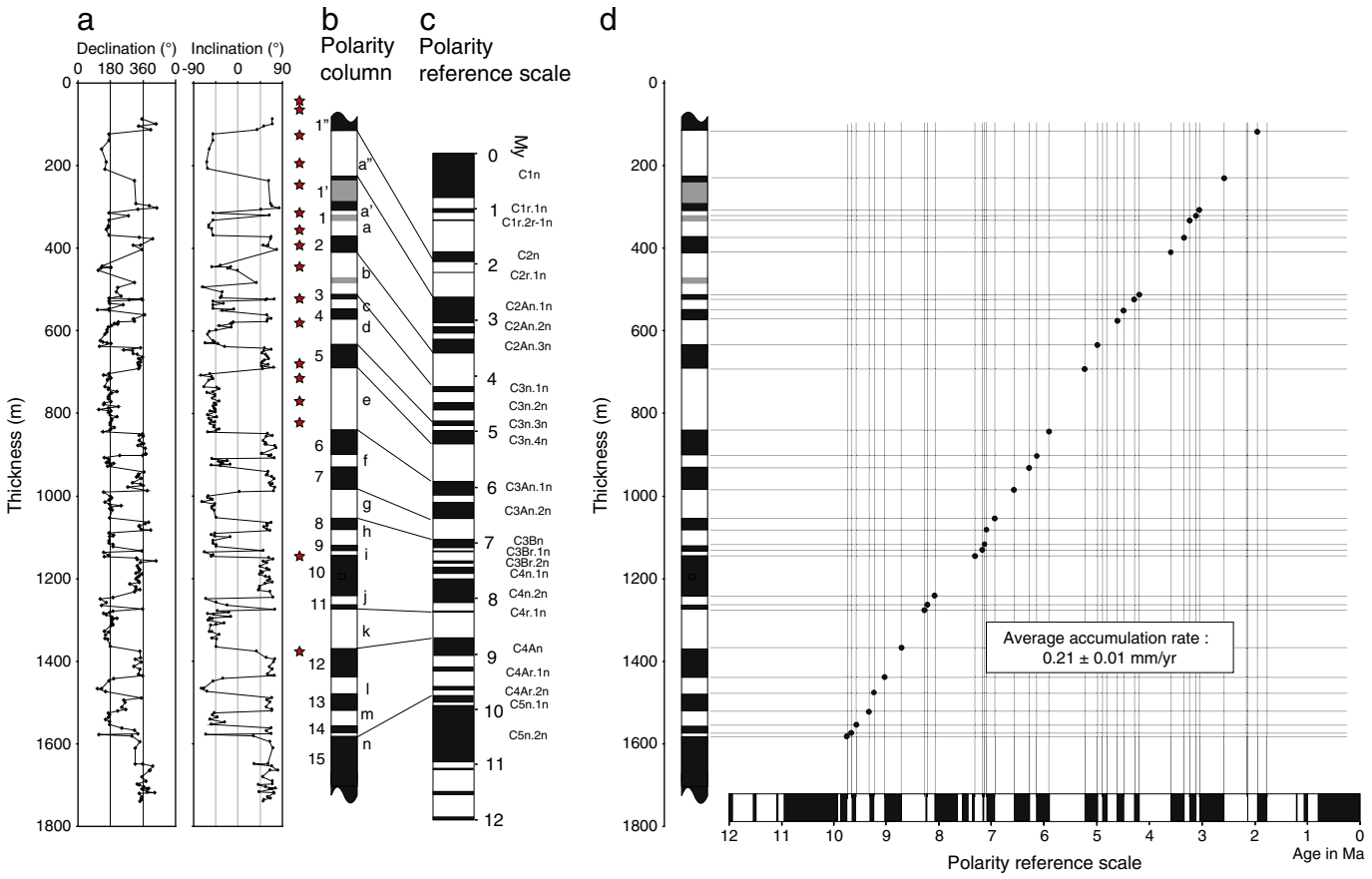

Fig. 3. Magnetostratigraphic analysis of the Kuitun section (after Charreau et al., 2005). (a) Magnetic declination and inclination measured in the Kuitun section. (b) Magnetostratigraphic column of the Kuitun section. Each normal (black) and reverse (white) polarity chron is defined by at least two samples from two different sedimentary horizons. Reversals found in a single bed are shown in gray. (c) Reference polarity time scale after Lourens et al. (2004); (d) age versus depth plot of the Kuitun section, using the data and correlation from 3b and 3c.

3.2.1. Estimation of the cosmogenic paleo-production rate

Recent analyses of pedogenetic carbonate in the same Kuitun section yielded constant $\delta^{18}O$ over the last 10 Ma, which suggests the hypsometry of the Kuitun drainage basin was relatively steady during this time (Kent-Corson et al., 2008). Moreover, given the relatively high latitude of the Kuitun watershed (45°N), time variations of the geomagnetic field (Biggin et al., 2009) induced cosmogenic production variations of less than 5% over the considered time period (last

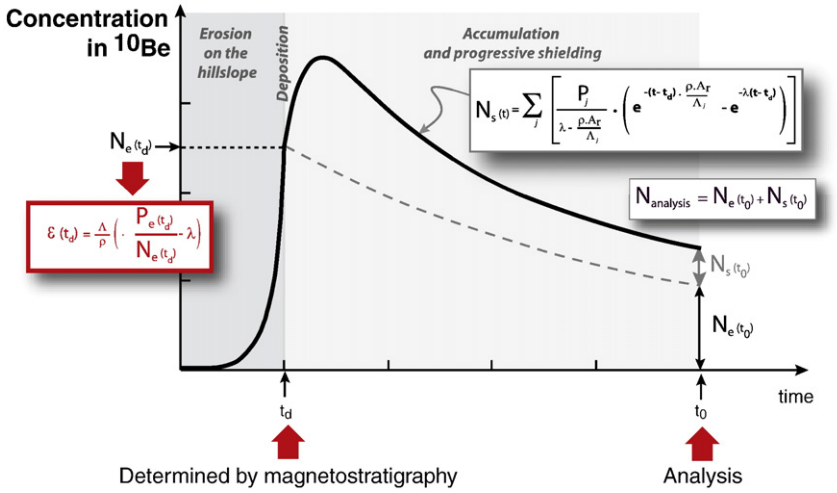

Fig. 4. Theoretical evolution of the ^{10}Be concentration in a quartz grain from its erosion on the hillslope to its deposition and burial in the foreland basin. The possible later phase of accumulation related to exhumation of the sample is not represented here. t_0: time of the analysis; t_d: time of deposition; $N_{analysis}$: concentration measured at a time t_0 in a given sediment sample (in at·g^{-1}·yr^{-1}); $N_s(t_0)$: concentration acquired during sediment burying minus the loss due to radioactive decay (in at·g^{-1}·yr^{-1}); $N_e(t_0)$: concentration acquired during the erosion minus the loss due to radioactive decay (in at·g^{-1}·yr^{-1}); $N_e(t_d)$: concentration acquired during the erosion on the drainage basin (in at·g^{-1}·yr^{-1}); A_r: accumulation rate (in cm·yr^{-1}); P_j: the surface production rates by spallation, fast muons and slow muons captures (in at·g^{-1}·yr^{-1}) at the deposition location; λ: the radioactive decay constant (in yr^{-1}); ρ: the overlying sediment density (in g·cm^{-3}); Λ_j: attenuation lengths (g·cm^{-2}) of spallogenic and muogenic productions; $P_e(t)$: the average spallation production rate for the whole drainage basin (in at·g^{-1}·yr^{-1}); $\varepsilon(t_d)$: the erosion rates on the drainage basin at the time of deposition (in cm·yr^{-1}).

10 Myr) (Dunai, 2001). Therefore, we assume that the paleo-production rate of ^{10}Be was similar to the modern rate. To take into account the weight of this assumption, we also propagated to the calculated erosion rates an uncertainty of 150 m attached to the catchment average elevation. This elevation uncertainty results from the standard deviation of the δ^{18}O record (Kent-Corson et al., 2008) considering that the δ^{18}O-altitude dependence is −2.8‰/km (Chamberlain and Poage, 2000).

3.2.2. Corrections of the post-depositional ^{10}Be accumulation

The ^{10}Be concentration analyzed in a given sample is the sum of the concentration inherited during the erosion on the hillslope plus that due to the post-depositional accumulation during burial and the accumulation during the modern exposure at the surface (Fig. 4). Therefore, to retrieve the true paleo-erosion rates one must correct the measured concentration from both the post-depositional and modern exposure accumulation.

When buried at a sufficient depth (~4 m), sediments are almost totally shielded from cosmic rays and, the radioactive cosmogenic nuclides consequently decay with time. In continental environments, the process of fluvial sediment deposition is in many cases too slow to provide an immediate shielding from cosmic rays. The ^{10}Be build-up during the progressive sediment burial can however be described by the following equation (Braucher et al., 2000):

$$N_{\text{shield}} = \sum_j \left[\frac{P_j}{\lambda - \frac{A_r \rho}{\Lambda_j}} \left(e^{-t\frac{A_r \rho}{\Lambda_j}} - e^{-\lambda t} \right) \right], \quad (2)$$

with P_j the surface production rates by spallation, by fast muons and by slow muon captures (in at.g^{-1}.yr^{-1}, see below), λ the radioactive decay constant (4.997×10^{-7} yr^{-1}) (Chmeleff et al., 2010), ρ the overlying sediment density (2.4 ± 0.13 g·cm^{-3}, determined from seismic speeds), A_r the accumulation rate (cm·yr^{-1}), Λ_j the typical attenuation lengths (g·cm^{-2}, see below) and t (yr) the time during which the sediment is getting buried.

To calculate the ^{10}Be production during the burial accumulation, the crucial parameter A_r was determined by using the high-resolution paleomagnetic record of Charreau et al. (2005). This magnetostratigraphic study constraints the accumulation rate at the time of deposition between 0.115 ± 0.006 and 0.418 ± 0.021 cm·yr^{-1}. The use of an 'instantaneous' accumulation rate (i.e. calculated for each magnetic chron) is justified for the spallation reactions from rapid neutrons because production by spallation is characterized by a short attenuation length (~160 g·cm^{-2}) (Lal, 1991), and becomes negligible below ~3 m. However, accumulation rate derived from magnetostratigraphy represent a long term (>20 Ka) average. Yet, in such continental and fluvial settings, rapid and short time scale variations in accumulation rate probably exist. Their potential impact on the cosmogenic building remains difficult to constrain and will be assumed negligible in this study. In future studies, complementary cosmogenic analysis will be required to test this assumption.

In contrast, the production by slow muon capture and fast muon reactions has a long attenuation length (respectively 5300 ± 950 g·cm^{-2} and 1500 ± 100 g·cm^{-2}) (Braucher et al., 2003) and remains significant for a long period of time even under several tens of meters of sediments. We therefore used an average accumulation rate of the whole sedimentary pile overlying each sample to correct for the post burial muonic production.

We used a sea level, high latitude surface production rate of 4.5 ± 0.3 at·g^{-1}·yr^{-1} (Amidon and Farley (2011) recalculated after Balco et al. (2008)). Both fast and slow muonic production were taken as $0.8 \pm 0.25\%$ (Braucher et al., 2003) of the total production rate at sea level, then scaled with the altitude following Stone (2000). Figure 4 shows the theoretical evolution of the cosmogenic concentration in a sedimentary material that has been successively eroded, transported and deposited. The present-day cosmogenic concentration $N_{\text{analysis}}(t_0)$ measured in a given sediment sample is the sum of $N_e(t_0)$, which represents the concentrations acquired during erosion and $N_s(t_0)$, which represents the concentration acquired during sediment burial (Fig. 4). Given the considered time-scales, both $N_e(t_0)$ and $N_s(t_0)$ may have undergone a significant radioactive decay since the initial ^{10}Be production (Blard et al., 2006). The possible later phase of accumulation during the recent exposure of the sample is not represented on Figure 4. Knowing independently the depositional age t_d and the accumulation rates A_r, Eq. (2) allows calculation of $N_s(t_0)$ and therefore $N_e(t_0)$. Then, knowing t_d, $N_e(t_0)$ can be directly corrected for the radioactive decay to calculate $N_e(t_d)$. Finally, $N_e(t_d)$ is converted into erosion rate $\varepsilon(t_d)$ at the time of deposition using Eq. (1).

It is important to note that the correction for production during sediment deposition is the major source of uncertainty of the paleo-erosion rates determined here. Indeed, when the ratio of erosion/accumulation is high (>>1), then the measured paleo-erosion rate is close to the detection limit of the method.

The sampled sediments were exposed during the Holocene incision of the Kuitun River at a rate constrained to 1 cm·yr^{-1}, by Optically Simulated Luminescence dating of terraces (Poisson and Avouac, 2004). Considering the present geometry of the Kuitun canyon at this location, this rate corresponds to a lateral cliff retreat of 3.5 cm·yr^{-1}. Due to this rapid incision, along with the topographic shielding of the cliff and a sampling strategy designed to ensure a current burial thickness of at least 1 m, the contribution of the modern exposure can be considered as negligible (i.e. 15 at.g^{-1}). It indeed ranges between less than 0.1% and 0.3% of the total present-day cosmogenic signal.

3.3. Samples treatment and measurement of ^{10}Be concentrations

Cosmogenic ^{10}Be concentration measurements were mainly performed at the French national AMS (Accelerator Mass Spectrometer) facility ASTER (Accelerator for Earth Sciences, Environment and Risks) located at the CEREGE laboratory (Aix en Provence, France) except for two samples, RS1 and TP, which were analyzed at the Center for Accelerator Mass Spectrometry at Lawrence Livermore National Laboratory in California (USA). All samples were crushed and the 200–500 μm fraction was treated as follows. Quartz was first enriched through successive magnetic separation, and flotation. Then, the enriched fraction was leached in H_2SiF6, HCl and HF to eliminate all remaining mineral phases but quartz and quartz surfaces were decontaminated from atmospheric ^{10}Be following the chemical procedures developed earlier (Brown et al., 1991). TP and RS1 were treated similarly but did not undergo flotation or H_2SiF_6 treatment. The purified quartz was then completely dissolved in HF after addition of 100 μl of an in-house $3.025\,10^{-3}$ g/g ^{9}Be carrier solution (in the case of TP and RS1 about 0.45 mg of a ^{9}Be carrier with a ^{10}Be blank of ^{10}Be/^{9}Be $= 6.7 \times 10^{-15}$ was used). Following subsequent purification by anion exchange, cation exchange and alkaline precipitations, purified beryllium oxide samples were analyzed on the AMS. ^{10}Be concentrations measured at ASTER are normalized to ^{10}Be/^{9}Be SRM 4325 NIST reference material with an assigned value of $(2.79 \pm 0.03) \times 10^{-11}$. This standardization is equivalent to 07KNSTD within rounding error. TP and RS1 were normalized to KNSTD3770 when they were measured in 1997 and were renormalized to 07KNSTD to take account of the KNSTD renormalization (Nishiizumi et al., 2007). The ^{10}Be half-life of $(1.39 \pm 0.01) \times 10^6$ yr used is that recently recommended by Chmeleff et al. (2010) and Korschinek et al. (2010) according to their two independent measurements. Measured ^{10}Be/^{9}Be blank ratios were $2.5 \pm 0.7 \times 10^{-15}$.

4. Results

All ^{10}Be results are presented in Table 1. In situ produced cosmogenic ^{10}Be concentrations measured in these samples range

between $(3.23\pm0.78)\times10^3$ and $(1.10\pm0.67)\times10^5$ at·g^{-1}. Erosion rates were calculated after correcting for the ^{10}Be radioactive decay and for the build-up of ^{10}Be during sediment accumulation following the methods presented above. Figure 5 shows the erosion rates plotted against the depositional ages along with the global deep-sea oxygen isotope records as a proxy for global climate (Zachos et al., 2001). Between 9 Ma and 3.5 Ma, erosion rates remained within 0.1 and 1 mm·yr^{-1}, with little fluctuations around an average value of 0.4 mm·yr^{-1} over that period of time. A significant sediment pulse characterized by erosion rates larger than 1 mm·yr^{-1} is evidenced between 3.5 Ma and 1.7 Ma, with a peak of 2.5 mm·yr^{-1} at 2 Ma. One additional sample (KBe12) from this time period (with age estimated to 2.1 Ma) is characterized by a low ^{10}Be concentration. Due to the supposed post-depositional correction, this precludes a precise estimation of erosion rates (see larges uncertainties in Table 1) for this sample. This is nevertheless consistent with the occurrence of very high (>2 mm·yr^{-1}) erosion rates over that period of time. After 1.5 Ma, the erosion rates dropped back to ~0.5 mm·yr^{-1}, a value consistent with the modern erosion rates of ~0.6 mm·yr^{-1} derived from the river sands and not significantly different from the value of 0.3 mm·yr^{-1} inferred from the Holocene (~15 ka) terrace material (Table 1).

5. Discussion and conclusion

This record shows a clear erosion pulse (from 3 to 1.7 Ma) that coincides with the onset of Quaternary glaciations as recorded by the global deep-sea oxygen isotope records (Zachos et al., 2001) (Fig. 5). Our data support the hypothesis that Quaternary glaciations were accompanied by a significant (>2 fold) increase of physical erosion rates in Central Asia, thereby confirming previous inferences that global climate influenced erosion rates (Shuster et al., 2005; Zhang et al., 2001). The apparent invariance of global weathering rates over the last 10 Ma (Willenbring and von Blanckenburg, 2010) might then indicate that physical erosion fluctuations during glacial times can be decoupled from weathering changes.

In addition, our record suggests a decrease of erosion rates after 1.7 Ma possibly suggesting that the erosional response to the onset of glaciations in the Quaternary would have been transient. This transient impact of climate on erosion is questionable at this point because there is only a limited number of data over the last 2 Ma. The large amplitude of the 100 ka glacial cycles, which appeared after 1.8 Ma, could in particular have produced a high frequency variability of the erosion signal. Therefore, we cannot exclude that the 3 younger samples of our record (at 1.58 Ma, 15 ka and present-day river sands) might fortuitously coincide with periods of low erosion. If true, this reduction in erosion observed after 1.7 Ma would only reflect a sampling bias. However, the probability of such a systematic observational artifact is low considering that interglacial periods have a short duration (<20 ka). In addition Shuster et al. (2005) have presented a thermochronometric record from the Coast Mountains suggesting a similar transient increase in erosion. Such a transient augmentation of erosion could make sense at a global scale. Indeed, under constant tectonic forcing and climate, the topography of an uplifting range is supposed to reach a steady state in which the sediment flux balances crustal shortening (Whipple and Meade, 2006). If the shortening rate across the orogeny is assumed constant while climate changes, it may cause enhanced physical erosion, leading to a transient disequilibrium until the balance between erosion and tectonic is restored back. Whipple and Meade (2006) provide simulations showing such a transient adjustment within the framework of the critical wedge theory. The time needed for this adjustment is probably scale dependent and must depend on the factors which govern isostatic rebound (i.e., the mechanical properties

Table 1
^{10}Be data. Abbreviations are: t_d, depositional age; Δt_d, the minimum and maximum ages of the reference polarity chron in which the sample falls; A_r, the accumulation rate at the time of deposition; N_a (1σ), the ^{10}Be concentration measured in the sample and its 1σ analytical uncertainty, respectively; N_s(1σ), the post-accumulation correction and its 1σ uncertainty, respectively; ε and Δε, paleo-erosion rate and its uncertainty, respectively.

Sample	t_d (Ma)	Δt_d		Ar	N_a (at.g^{-1})	1σ (N_a)	N_s (at.g^{-1})*	1σ (N_s)		N_a/N_s	ε (m/Myr)	Δε (mm/yr)	
		+	−					+	−			+	−
Kuitun section													
TF500	8.80	0.298	0.03	0.027	3.46E+03	9.1E+02	353	55	53	9.80	112	61	68
TF400	7.72	0.390	0.02	0.030	4.82E+03	7.6E+02	553	116	109	8.72	140	52	27
KBe1	5.88	0.154	0.64	0.023	3.23E+03	7.8E+02	1702	246	238	1.90	985	1059	417
TF200	5.60	0.430	0.37	0.023	7.29E+03	1.2E+03	1955	282	273	3.73	324	113	76
KBe3	5.34	0.696	0.10	0.023	1.32E+04	1.8E+03	2234	353	338	5.93	179	50	34
KBe4	4.97	0.262	0.17	0.015	7.19E+03	8.4E+02	3722	523	508	1.93	682	281	208
KBe5	4.63	0.007	0.13	0.020	9.22E+03	1.3E+03	3579	528	509	2.58	500	173	129
KBe6	4.18	0.01	0.60	0.019	1.34E+04	1.8E+03	4594	674	651	2.91	399	128	96
KBe7	3.73	0.453	0.14	0.019	1.54E+04	1.6E+03	5767	812	788	2.68	455	121	103
KBe8	3.43	0.161	0.10	0.021	1.16E+04	1.3E+03	5682	811	785	2.03	868	309	254
KBe9	3.28	0.051	0.07	0.042	2.15E+04	1.8E+03	6141	879	864	3.5	360	67	67
KBe10	3.09	0.028	0.06	0.023**	1.07E+04	1.1E+03	6755	982	949	1.59	1544	810	612
KBe11	2.72	0.316	0.13	0.023**	1.82E+04	1.8E+03	8135	1218	1198	2.23	729	210	188
KBe12	2.07	0.508	0.13	0.023**	1.25E+04	1.9E+03	11213	1591	1540	1.12	7660	38498	13537
KBe13	1.99	N/A	N/A	0.023**	1.58E+04	2.0E+03	11697	1691	1634	1.35	2535	2836	1483
KBe14	1.68	N/A	N/A	0.023**	2.09E+04	1.8E+03	13655	1940	1878	1.53	1701	896	700
KBe15	1.57	N/A	N/A	0.023**	3.95E+04	4.6E+03	14401	1880	1842	2.74	516	143	122
Terrace													
TP	0.015	N/A	N/A	N/A	1.10E+05	6.62E+03	N/A	N/A	N/A	N/A	255	30	31
River bed													
RS1	0.00	N/A	N/A	N/A	4.84E+04	2.14E+04	N/A	N/A	N/A	N/A	587	469	190
RS2	0.00	N/A	N/A	N/A	5.15E+04	1.15E+04	N/A	N/A	N/A	N/A	552	169	116
RS3	0.00	N/A	N/A	N/A	4.12E+04	6.06E+03	N/A	N/A	N/A	N/A	689	140	114

In the Xiyu conglomeratic formation (above ~500 m in thickness) the paleomagnetic sampling density was lower which yielded large uncertainties on the accumulation rates at the time of deposition. Therefore, for samples KBe10 to KBe15, we estimated their ages and erosion rates based on average accumulation rates found in the lower part of the section.
* Includes 15 at/gr due to the recent exposure at surface, N/A: non-applicable.
** Average accumulation rates.

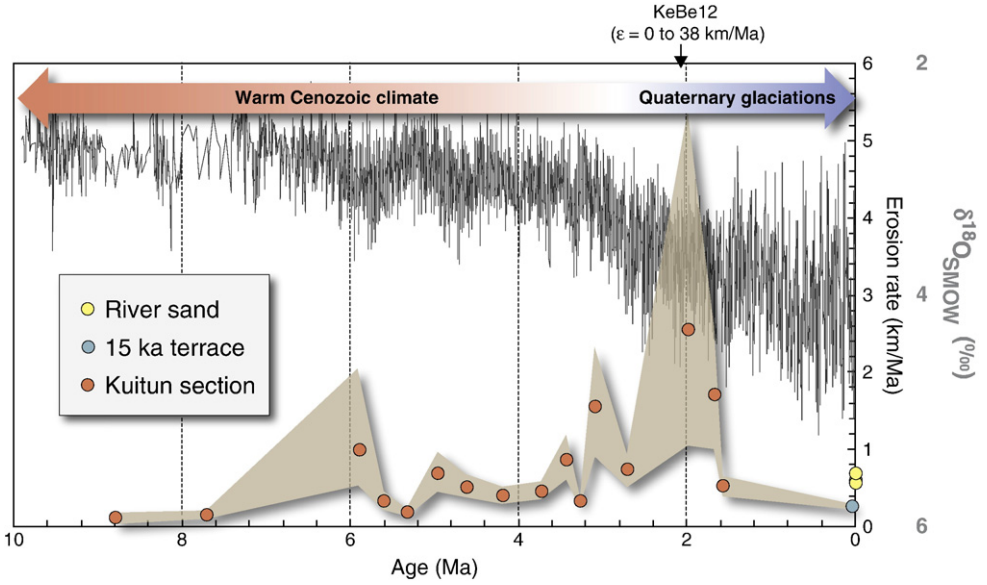

Fig. 5. Erosion rates as function of depositional age (Charreau et al., 2005) and global deep-sea oxygen isotope record (Zachos et al., 2001) over the last 10 Myr. The 1 σ uncertainty envelop is shown in gray. Sample KeBe12 is not shown because it presents very large uncertainties, but its low ^{10}Be concentration nevertheless suggests high erosion rates.

of the crust, lithosphere an asthenosphere), as well as on the erodability of exhumed rocks under fluvial and hillslope processes. Our study suggests that in the case of North Tianshan, the erosional response to the onset of Quaternary glaciations (at about 3 Ma) might thus have lasted less than 2 Ma only.

However, this scenario could also be criticized because if tectonic is constant while erosion increases, this would actually imply a reduction of the watershed altitude. This might affect the accuracy of the erosion rates that we compute here under the assumption of a constant hypsometry. However, given that the eroded material is partially balanced by isostatic and tectonic inflows, the total net altitudinal change due to enhanced erosion is probably already accounted in our uncertainties. Moreover, if true, a decreasing altitude should have lowered the production rate and yield lower cosmogenic ^{10}Be concentrations while since ~2 Ma we observe higher concentrations (Table 1). As Shuster et al. (2005), we suggest that the onset of glaciations implied a shift from fluvial to glacial erosion processes (typically V-shape to U-shape valleys) which yield to enhanced erosion. After ~2 Ma, most of the surplus material has been removed, leading to more stable U-shape glaciated valley and, then, a new equilibrium with lower erosion rates.

Finally, as this record is only focused on one single drainage basin, a limitation of this study is that the Kuitun river watershed could have been impacted by local tectonic particularities. It must also be considered that the erosion rates of Central Asia could also be partially decoupled from the global erosion rates, because of superimposed regional tectonic or local climatic particularities. Consequently, we acknowledge that the debate remains open and that this apparent transient response of erosion to climate must be tested in the future by applying this method to other localities of Central Asia and other regions of the world.

In any case our study presents a new and quite powerful approach to obtain quantitative estimates of paleo-erosion rates. It moreover provides the first record of long term erosion in a region where, as pointed out by Molnar (2004), the mass transfer is only driven by the competition between tectonics and climate and not altered by sea level changes and exposure of continental platforms.

Acknowledgements

This study was financed by the French INSU/CNRS programs SYSTER and ANR. We thank Peter Molnar and one anonymous reviewer for their very constructive comments that greatly improved the manuscript. Fruitful discussions with Jérôme Lavé and Raphaël Pik were useful for interpreting this record. Expert Jean-Pierre Valet and Yves Gallet are also thanked for their advice about the long term variations in the earth virtual magnetic moment. We are also grateful to Robert Joussemet (STEVAL mineral processing pilot plant, Lem, Nancy) for his help in separating quartz and to the ASTER team for the cosmogenic nuclide concentration measurements (M. Arnold, G. Aumaître, K. Keddadouche, L. Léanni and F. Chauvet). ASTER AMS national facility (CEREGE, Aix en Provence) is supported by the INSU/CNRS, the French Ministry of Research and Higher Education, IRD and CEA. This is CRPG contribution n° 2101.

References

Abdrakhmatov, K.Y., Aldazhanov, S.A., Hager, B.H., Hamburger, M.W., Herring, T.A., Kalabaev, K.B., Makarov, V.I., Molnar, P., Panasyuk, S.V., Prilepin, M.T., Reilinger, R.E., Sadybakasov, I.S., Souter, B.J., Trapeznikov, Y.A., Tsurkov, V.Y., Zubovich, A.V., 1996. Relatively recent construction of the Tien Shan inferred from GPS measurements crustal deformation rates. Nature 384, 450–453.

Amidon, W., Farley, K.A., 2011. Cosmogenic 3He production rates in apatite, zircon and pyroxene inferred from Bonneville flood erosional surfaces. Quaternary Geochronology 6 (1), 10–21. doi:10.1016/j.quageo.2010.03.005.

Avouac, J.-P., Burov, E.B., 1996. Erosion as a driving mechanism of intracontinental mountain growth. J. Geophys. Res. 101, 17747.

Avouac, J.-P., Tapponnier, P., Bai, P., You, M., Wang, G.A., 1993. Active thrusting and folding along the northern Tien Shan and late Cenozoic rotation of the Tarim relative to Dzungaria and Kazakhstan. J. Geophys. Res. 98, 6755–6804.

Balco, G., Stone, J.O., Lifton, N.A., Dunai, T.J., 2008. A complete and easily accessible means of calculating surface exposure ages or erosion rates from ^{10}Be and ^{26}Al measurements. Quat. Geochronol. 3, 174–195.

Berner, R.A., Lasaga, A.C., Garrels, R.M., 1983. The carbonate–silicate geochemical cycle and its effect on atmospheric carbon dioxide over the last 100 million years. Am. J. Sci. 205, 641–683.

Biggin, A.J., Strik, G.H.M.A., Langereis, C.G., 2009. The intensity of the geomagnetic field in the late-Archaean: new measurements and an analysis of the updated IAGA palaeointensity database. Earth Planet. Space 61, 9–22.

Blard, P.H., Bourles, D., Lave, J., Pik, R., 2006. Applications of ancient cosmic-ray exposures: theory, techniques and limitations. Quat. Geochronol. 1, 59–73.

Braucher, R., Bourlès, D.L., Brown, E.T., Colin, F., Muller, J.-P., Braun, J.-J., Delaune, M., Minko, A.E., Lescouet, C., Raisbeck, G.M., Yiou, F., 2000. Application of in situ-produced cosmogenic 10Be and 26Al to the study of lateritic soil development in tropical forest: theory and examples from Cameroon and Gabon. Chem. Geol. 170, 95–111.

Braucher, R., Brown, E.T., Bourlès, D.L., Colin, F., 2003. In situ produced ^{10}Be measurements at great depths: implications for production rates by fast muons. Earth Planet. Sci. Lett. 211, 251–258.

Brown, E.T., Edmond, J.M., Raisbeck, G.M., Yiou, F., Kurz, M.D., Brook, E.J., 1991. Examination of surface exposure ages of Antarctic moraines using in situ produced ^{10}Be And ^{26}Al. Geochim. Cosmochim. Acta 55, 2269–2283.

Brown, E.T., Stallard, R.F., Larsen, M.C., Raisbeck, G.M., Yiou, F., 1995. Denudation rates determined from the accumulation of in situ produced ^{10}Be in the Luquillo experimental forest, Puerto-Rico. Earth Planet. Sci. Lett. 129, 193–202.

Brown, E.T., Stallard, R.F., Larsen, M.C., Bourles, D.L., Raisbeck, G.M., Yiou, F., 1998. Determination of predevelopment denudation rates of an agricultural watershed (Cayaguas River, Puerto Rico) using in-situ-produced Be-10 in river-borne quartz. Earth Planet. Sci. Lett. 160, 723–728.

Bullen, M.E., Burbank, D.W., Garver, J.I., Abdrakhmatov, K.Y., 2001. Late Cenozoic tectonic evolution of the northwestern Tien Shan: new age estimates for the initiation of mountain building. Bull. Geol. Soc. Am. 113, 1544–1559.

Bullen, M.E., Burbank, D.W., Garver, J.I., 2003. Building the Northern Tien Shan: integrated thermal, structural, and topographic constraints. J. Geol. 111, 149–165.

Burtman, V.S., 1975. Structural geology of the Variscan Tian Shan, USSR. Am. J. Sci. 275-A, 157–186.

Chamberlain, C.P., Poage, M.A., 2000. Reconstructing the paleotopography of mountain belts from isotopic composition of authigenic minerals. Geology 28, 115–118.

Charreau, J., 2005. Tectonic evolution of the Tianshan mountains during Cenozoic time in response to the India–Asia collision: from magnetostratigraphy and U–Th/He thermochronology analysis of Neogene sediments: Orleans, Orleans.

Charreau, J., Chen, Y., Gilder, S., Dominguez, S., Avouac, J.-P., Sevket, S., Sun, D., Li, Y., Wang, W.-M., 2005. Magnetostratigraphy and rock magnetism of the Neogene Kuitun He section (northwest China): implications for Late Cenozoic uplift of the Tianshan mountains. Earth Planet. Sci. Lett. 230, 177–192.

Charreau, J., Gilder, S., Chen, Y., Dominguez, S., Avouac, J.-P., Sevket, Sen, Jolivet, M., Li, Y., Wang, W., 2006. Magnetostratigraphy of the Yaha section, Tarim Basin (China): 11 Ma acceleration in erosion and uplift of the Tianshan Mountains. Geology 34, 181–184.

Charreau, J., Avouac, J.-P., Chen, Y., Dominguez, S., Gilder, S., 2008. Miocene to present kinematics of fault-bend folding across the Huerguosi anticline, northern Tianshan (China), derived from structural, seismic, and magnetostratigraphic data. Geology 871–874.

Charreau, J., Chen, Y., Gilder, S., Barrier, L., Dominguez, S., Augier, R., Sen, S., Avouac, J.-P., Gallaud, A., Graveleau, F., Li, Y., 2009a. Neogene uplift pulses of the Tianshan mountains observed in the magnetic record of the Jingou River section (Northwest China). Tectonics 28, doi:10.1029/2007TC002137.

Charreau, J., Gumiaux, C., Avouac, J.-P., Augier, R., Chen, Y., Barrier, L., Gilder, S., Dominguez, S., Charles, N., Wang, Q., 2009b. The Neogene Xiyu Formation, a diachronous prograding gravel wedge at front of the Tianshan: climatic and tectonic implications. Earth Planet. Sci. Lett. 287, 283–310.

Charvet, J., Shu, L.S., Laurent-Charvet, S., 2007. Paleozoic structural and geodynamic evolution of eastern Tianshan (NW China): welding of the Tarim and Junggar plates. Episodes 30, 162–186.

Chmeleff, J., von Blanckenburg, F., Kossert, K., Jakob, D., 2010. Determination of the 10Be half-life by multicollector ICP-MS and liquid scintillation counting. Nucl. Instrum. Methods Phys. Res. Sect. B 268, 192–199.

Clift, P.D., 2006. Controls on the erosion of Cenozoic Asia and the flux of clastic sediment to the ocean. Earth Planet. Sci. Lett. 241, 571–580.

Dahlen, F.A., Suppe, J., 1988. Mechanics, growth, and erosion of mountain belts. In: Clark, S.P., Burchfiel, B.C., Suppe, J. (Eds.), Processes in Continental Lithospheric Deformation: Geological Society of America Special Paper, Volume 218, pp. 161–178.

Dumitru, T.A., Zhou, D., Chang, E.Z., Graham, S.A., Hendrix, M.S., Sobel, E.R., Caroll, A.R., 2001. Uplift, exhumation, and deformation in the Chinese Tian Shan. In: Hendrix, M.S., Davis, G.A. (Eds.), Paleozoic and Mesozoic Tectonic Evolution of Central Asia: From Continental Assembly to Intracontinental Deformation: Boulder: Colorado: Geological Society of America Memoir, 194, pp. 71–99.

Dunai, T.J., 2001. Influence of secular variation of the geomagnetic field on production rates of in situ produced cosmogenic nuclides. Earth Planet. Sci. Lett. 193, 197–212.

Dunne, J., Elmore, D., Muzikar, P., 1999. Scaling factors for the rates of production of cosmogenic nuclides for geometric shielding and attenuation at depth on sloped surfaces. Geomorphology 27, 3–11.

France-Lanord, C., Derry, L.A., 1997. Organic carbon burial forcing of the carbon cycle from Himalayan erosion. Nature 390, 65–75.

Galy, V., France-Lanord, C., Beyssac, O., Faure, P., Kudrass, H., Palhol, F., 2007. Efficient organic carbon burial in the Bengal fan sustained by the Himalayan erosional system. Nature 450, 407–410.

Gao, J., Li, M., Xiao, X., Tang, Y., He, G., 1998. Paleozoic tectonic evolution of the Tianshan Orogen, northwestern China. Tectonophysics 287, 213–231.

Hay, W.W., Sloan, J.L., Wold, C.N., 1988. Mass age distribution and composition of sediments on the ocean-floor and the global rate of sediment subduction. J. Geophy. Res. 93, 14933–14940.

Heermance, R.V., Chen, J., Burbank, D.W., Wang, C., 2007. Chronology and tectonic controls of Late Tertiary deposition in the southwestern Tian Shan foreland, NW China. Basin Res., doi:10.1111/j.1365-2117.2007.00339.x

Kent-Corson, M.L., Ritts, B.D., Charreau, J., Zhuang, G., Bovet, P.M., Graham, S.A., Chamberlain, P., 2008. Stable Isotopic Insights into Sedimentary Basin Evolution Along the Northern Tibetan Margin: Eos Trans. AGU, 89(53. Fall Meet. Suppl., Abstract T32A-01.

Korschinek, G., Bergmaier, A., Faestermann, T., Gerstmann, U.C., Knie, K., Rugel, G., Wallner, A., Dillmann, I., Dollinger, G., Lierse von Gosstomski, C., Kossert, K., Maiti, M., Poutivtsev, M., Remmert, A., 2010. A new value for the 10Be half-life by heavy-ion elastic recoil detection and liquid scintillation counting. Nucl. Instrum. Meth. 268, 187–191.

Lal, D., 1991. Cosmic ray labeling of erosion surfaces: in situ nuclide production rates and erosion models. Earth Planet. Sci. Lett. 104, 424–439.

Lin, W., Faure, M., Shi, Y., Wang, Q., Li, Z., 2008. Palaeozoic tectonics of the south-western Chinese Tianshan: new insights from a structural study of the high-pressure/low-temperature metamorphic belt. Int. J. Earth Sci., doi:10.1007/s00531-008-0371-7

Lourens, L., Hilgen, F., Shackleton, N.J., Laskar, J., and Wilson, D., 2004, The Neogene Period, in Felix M. Gradstein, J.G.O., and Alan G. Smith, ed., A Geological Time Scale: London, Cambridge.

Métivier, F., 2002. On the use of sedimentation rates in deciphering global change. Geophys. Res. Lett. 29.

Métivier, F., Gaudemer, Y., 1997. Mass transfer between eastern Tien Shan and adjacent basins (central Asia): constraints on regional tectonics. Geophys. J. Int. 128, 1–17.

Molnar, P., 2004. Late Cenozoic increase in accumulation rates of terrestrial sediment: how might climate change have affected erosion rates? Annu. Rev. Earth Planet. Sci. 32, 67–89.

Molnar, P., Brown, E.T., Burchfiel, B.C., Deng, Q., Feng, X., Li, J., Raisbeck, G.M., Shi, J., Wu, Z., Yiou, F., You, H., 1994. Quaternary climate change and the formation of river terraces across growing anticlines on the north flank of the Tien Shan, China. J. Geol. 102, 583–602.

Nishiizumi, K., Imamura, M., Caffee, M.W., Southon, J.R., Finkel, R.C., McAninch, J., 2007. Absolute calibration of ^{10}Be AMS standards. Nucl. Instrum. Methods Phys. Res. Sect. B 258, 403–413.

Poisson, B., Avouac, J.P., 2004. Holocene hydrological changes inferred from alluvial stream entrenchment in North Tian Shan (Northwestern China). J. Geol. 112, 231–249.

Raymo, M.E., Ruddiman, W.F., 1992. Tectonic forcing of late cenozoic climate. Nature 359, 117–122.

Refsnider, K.A., 2010, Dramatic increase in late Cenozoic alpine erosion rates recoreded by cave sediment in the southern Rocky Moutains. Earth Planet. Sci. Lett. 297, 505–511.

Reigber, C., Michel, G.W., Galas, R., Angermann, D., Klotz, J., Chen, J.Y., Papschev, A., Arslanov, R., Tzurkov, V.E., Ishanov, M.C., 2001. New space geodetic constraints on the distribution of deformation in the Central Asia. Earth Planet. Sci. Lett. 191, 157–165.

Sadler, P.M., 1999. The influence of hiatuses on sediment accumulation rates. GeoResearch Forum 5, 15–40.

Schaller, M., von Blanckenburg, F., Veldkamp, A., Tebbens, L.A., Hovius, N., Kubik, P.W., 2002. A 30 000 yr record of erosion rates from cosmogenic ^{10}Be in Middle European river terraces. Earth Planet. Sci. Lett. 204, 307–320.

Shuster, D.L., Ehlers, T.A., Rusmore, M.E., Farley, K.A., 2005. Rapid glacial erosion at 1.8 Ma revealed by 4He/3He thermochronometry. Science 310, 1668–1670.

Sobel, E.R., Dumitru, T.A., 1997. Thrusting and exhumation around the margins of the western Tarim basin during India–Asia collision. J. Geophys. Res. 102, 5043–5063.

Sobel, E., Chen, J., Heermance, R.V., 2006. Late Oligocene–Early Miocene initiation of shortening in the Southwestern Chinese Tian Shan: implications for Neogene shortening rate variations. Earth Planet. Sci. Lett. 247, 70–81.

Stone, J.O., 2000. Air pressure and cosmogenic isotope production. J. Geophys. Res. Solid Earth 105, 23753–23759.

von Blanckenburg, F., 2005. The control mechanisms of erosion and weathering at basin scale from cosmogenic nuclides in river sediment. Earth Planet. Sci. Lett. 237, 462–479.

Wang, Y., Kromhout, E., Zhang, C., Xu, Y., Parker, W., Deng, T., Qiu, Z., 2008. Stable isotopic variations in modern herbivore tooth enamel, plants and water on the Tibetan Plateau: implications of paleoclimate and paleoelevation reconstructions. Palaeogeogr. Palaeoclimatol. Palaeoecol. 260, 359–374.

Whipple, K.X., Meade, B.J., 2006. Orogen response to changes in climatic and tectonic forcing. Earth Planet. Sci. Lett. 243, 218–228.

Willenbring, J.K., von Blanckenburg, F., 2010. Long-term stability of global erosion rates and weathering during late-Cenozoic cooling. Nature 465, 211–214.

Willett, S.D., Brandon, M.T., 2002. On steady state in mountain belts. Geology 30, 175–178.

Windley, B.F., Allen, M.B., Zhang, C., Zhao, Z.-Y., Wang, G.R., 1990. Paleozoic accretion and Cenozoic deformation of the Chinese Tien Shan Range, central Asia. Geology 18, 128–131.

Yin, A., Nie, S., Craig, P., Harrison, T.M., 1998. Late Cenozoic tectonic evolution of the southern Chinese Tian Shan. Tectonics 17, 1–27.

Zachos, J., Pagani, M., Sloan, L., Thomas, E., Billups, K., 2001. Trends, rhythms, and aberrations in global climate 65 Ma to present. Science 292, 686–693.

Zeitler, P.K., Koons, P.O., Bishop, M.P., Chamberlain, C.P., Craw, D., Edwards, M.A., Hamidullah, S., Jan, M.Q., Khan, M.A., Khattak, M.U.K., Kidd, W.S.F., Mackie, R.L., Meltzer, A.S., Park, S.K., Pecher, A., Poage, M.A., Sarker, G., Schneider, D.A., Seeber, L., Shroder, J.F., 2001. Crustal reworking at Nanga Parbat, Pakistan: metamorphic consequences of thermal–mechanical coupling facilitated by erosion. Tectonics 20, 712–728.

Zhang, P., Molnar, P., Downs, W.R., 2001. Increased sedimentation rates and grain sizes 2–4 Myr ago due to the influence of climate change on erosion rates. Nature 410, 891–897.

Détermination des paléo-taux d'érosion par l'utilisation des isotopes cosmogéniques.

-

Paleo-erosion rates from cosmogenic nuclides

Mot clefs : érosion, dénudation, pliocène, pleistocène, cosmogénique, ^{10}Be, Himalaya, Tianshan.

Keywords : erosion, denudation, Pliocene, Pleistocene, cosmogenic, ^{10}Be, Himalaya, Tianshan

Résumé

L'analyse dans des dépôts anciens des isotopes cosmogéniques in-situ, déjà largement employés dans les sédiments de rivières actuelles, a le potentiel de fournir des enregistrements haute résolution, sur des échelles de temps de 10 Ma, de taux de dénudations intégrés sur des bassins versant entiers.

Nous avons étendu avec succès cette méthode à des sédiments des piedmonts du Tian-Shan (Chine) et de l'Himalaya (collines Siwaliks, Népal). Ces deux zones sont au coeur de débats sur l'évolution des relations climat/érosion/tectonique depuis ~10 Ma.

Quatre sections au Tian-Shan, couvrant ~9 Ma, et une large étendue spatiale autour de cette chaîne, ne montrent pas de brusque accélération de l'érosion il y a ~3-5 Ma. Au contraire, nous observons à l'échelle régionale une augmentation progressive (× 4 entre 9 et 4 Ma) puis une stabilisation entre 4 Ma et l'actuel. Ces résultats suggèrent une influence limitée des cycles glaciaires quaternaires sur les taux d'érosion dans cette zone.

Un enregistrement dans les sédiments himalayens ne montre également pas d'augmentation significative de l'érosion depuis ~6.5 Ma. Il est en revanche probablement le témoin de réorganisation des systèmes de drainages et d'évolutions tectoniques dans cette région.

Avec ces études, nous avons ainsi pu produire pour la première fois des enregistrements haute résolution de taux d'érosion depuis ~10 Ma, grâce aux isotopes cosmogéniques. Cette méthode étant potentiellement applicable dans de nombreux contextes géologiques et climatiques, elle permettra indubitablement des avancées importantes dans la compréhension des processus de surface actuels et passés.

Abstract

In-situ cosmogenic nuclides analysis in ancient sediment could potentially provide high-resolution records of denudation rates, integrated over whole drainage basins, and on several million-year time scales.

We successfully extended this method to sediments from the Tianshan (China), and the Himalayas (Nepal) piedmonts. These two areas are at the core of ongoing debates on climate-erosion-tectonics relationships since ~10 Ma.

Four sections in the Tianshan, covering ~9 Myr and a broad spatial extent around this range, do not display a brutal increase in denudation at 3-5 Ma. On the other hand, they show at the regional scale a progressive increase (×4 between 4-9 Ma) and a subsequent stabilization since ~4 Ma. These results suggest a limited influence of Quaternary glaciations on erosion in this region.

One section in the Himalayan piedmont (Siwaliks hills), neither display any significant increase since ~6.5 Ma that would be link to a major climatic shift. It has nevertheless probably recorded reorganizations of the drainage system and tectonics evolutions in this region.

With these studies, we were able to produce the first cosmogenic nuclides-based high resolution records of denudation rates over 10 Myr. This method being potentially applicable in many geological and climatic settings, it will indubitably allow further advances in our understanding of past and present surface processes